

**INVESTIGATION OF THE STABILITY OF METALLIC/COMPOSITE-CASED
SOLID PROPELLANT ROCKET MOTORS
UNDER EXTERNAL PRESSURE**

by
Hung-Peng Li

Dissertation submitted to the Faculty of the
Virginia Polytechnic Institute and State University
in partial fulfillment of the requirements for the degree
of
DOCTOR OF PHILOSOPHY
in
ENGINEERING MECHANICS

Approved:

Robert A. Heller, Chairman

R. H. Plaut

L. Librescu

O. H. Griffin

S. Thangjitham

September, 1998
Blacksburg, Virginia

**INVESTIGATION OF THE STABILITY OF METALLIC/COMPOSITE-CASED
SOLID PROPELLANT ROCKET MOTORS
UNDER EXTERNAL PRESSURE**

by

Hung-Peng Li

Robert A. Heller, Chairman

Engineering Science and Mechanics

(ABSTRACT)

Solid rocket motors consist of a thin metallic or composite shell filled with a soft rubbery propellant. Such motors are vulnerable and prone to buckling due to sudden external pressures produced by nearby detonation.

The stability conditions of rocket motors subjected to axisymmetric, external pressure loading are examined. The outer cases of motors are considered as isotropic (metallic) or anisotropic (composite), thin and high-strength shells, which are the main structures of interest in the stability analyses. The inner, low-strength elastic cores are modeled as linear and nonlinear elastic foundations.

A general, refined, Sanders' nonlinear shell theory, which accounts for geometric nonlinearity in the form of von Karman type of nonlinear strain-displacement relations, is used to model thin-walled, laminated, composite cylindrical shells. The first order shear deformable concept is adopted in the analysis to include the transverse shear flexibility of composites. A Winkler-type linear and nonlinear elastic foundation is applied to model the internal foundations. Pasternak-foundation constants are also chosen to modify the proposed elastic foundation model for the purpose of shear interactions. A set of displacement-based finite element codes have been formulated to determine critical buckling loads and mode shapes. The effect of initial imperfections on the structural responses are also incorporated in the formulations.

A variety of numerical examples are investigated to demonstrate the validity and efficiency of the proposed theory under various boundary conditions and loading cases. First, linear eigenvalue analysis is used to examine approximate buckling loads and buckling modes as well as symmetry conditions. An iterative solution procedure, either

Newton-Raphson or Riks-Wempner method, is employed to trace the nonlinear equilibrium paths for the cases of stress, buckling and post-buckling analyses. Both ring- and shell-type models are applied for the structural analyses with different internal elastic foundations and initial imperfections.

ACKNOWLEDGMENTS

I would like to express my sincere appreciation and thanks to my advisor Professor Robert A. Heller for his guidance, support and encouragement throughout my study towards the Ph.D. degree. Also, special thanks are due to Professors R. H. Plaut and L. Librescu for their valuable advice and help during the course of this work. I would also like to extend my thanks to Professors O. H. Griffin and S. Thangjitham for their kindness and time to serve on my graduate committee and review this dissertation.

I would like to thank my colleagues and friends whom I have met during my stay at Virginia Tech. Without their friendship and encouragement this work would not be possible. I would also like to thank the Department of Engineering Science and Mechanics for financially supporting me as a GTA during my doctoral study at VPI&SU. The experience was very precious and rewarding, and I am going to carry it for the rest of my life.

Finally, I would like to dedicate this dissertation to my parents and my families. Without their patience, understanding and support, I would have never accomplished my doctoral degree. I can never express how much their support has meant to me.

TABLE OF CONTENTS

ABSTRACT	ii
ACKNOWLEDGMENTS.....	iv
TABLE OF CONTENTS.....	v
LIST OF FIGURES	xiv
LIST OF TABLES.....	xviii
1 <u>INTRODUCTION</u>	1
1.1 Motivation	1
1.2 Objectives and Present Study	2
2 <u>REVIEW OF LITERATURE</u>	5
2.1 Buckling of Circular Arches and Rings.....	5
2.2 Shell Theories.....	6
2.2.1 Classical Shell Theories.....	6
2.2.2 Shear Deformable Shell Theories.....	7
2.2.3 Stability of Circular Cylindrical Shells.....	9
2.3 Buckling of Cylindrical Shell with Elastic Core	11
2.3.1 Elastic Buckling of Isotropic Cylindrical Shells.....	11
2.3.2 Elastic Buckling of Anisotropic Cylindrical Shells	12
2.4 Elastic Foundations.....	13

3	<u>GENERAL EQUATIONS FOR CIRCULAR ARCHES AND RINGS</u>	15
3.1	Introduction and Basic Assumptions.....	15
3.2	Displacement Fields.....	16
3.3	Kinematic (Strain-Displacement) Relations.....	18
3.3.1	Linear Formulation.....	18
3.3.2	Nonlinear Formulation.....	19
3.4	Mechanical Behavior of a Lamina.....	19
3.5	Constitutive Equations of a Laminate.....	21
3.6	Stress and Moment Resultants.....	24
3.7	Virtual Work Statement.....	28
3.8	Equilibrium Equations and Associated Boundary Conditions.....	30
3.8.1	Linear Relations.....	30
3.8.2	Nonlinear Relations.....	31
3.9	Weak Formulation and Finite Element Model.....	32
3.10	Consideration of Elastic Foundations.....	35
3.11	Linear and Nonlinear Buckling Analyses.....	38
3.11.1	Linear Eigenvalue Analysis.....	39
3.11.2	Nonlinear Buckling and Initial Post-Buckling Analysis.....	43
4	<u>GENERAL EQUATIONS FOR CIRCULAR CYLINDRICAL SHELLS</u>	46
4.1	Introduction and Basic Assumptions.....	46
4.2	Displacement Fields.....	47
4.3	Kinematic (Strain-Displacement) Relations.....	49
4.3.1	Linear Formulation.....	49
4.3.2	Nonlinear Formulation.....	51

4.4	Mechanical Behavior of a Lamina	52
4.5	Constitutive Equations of a Laminate.....	52
4.6	Stress and Moment Resultants	52
4.7	Virtual Work Statement.....	52
4.8	Equilibrium Equations and Associated Boundary Conditions.....	55
4.8.1	Linear Relations.....	55
4.8.2	Nonlinear Relations.....	56
4.9	Weak Formulation and Finite Element Model	58
4.9.1	Linear Finite Element Equations	58
4.9.2	Nonlinear Finite Element Equations.....	63
4.10	Consideration of Elastic Foundations	65
4.11	Linear and Nonlinear Buckling Analyses	69
4.11.1	Linear Eigenvalue Analysis	69
4.11.2	Nonlinear Buckling and Initial Post-Buckling Analysis.....	75
5	<u>INFLUENCE OF INITIAL IMPERFECTIONS</u>	78
5.1	Introduction.....	78
5.2	Theory for Rings with Initial Imperfections.....	79
5.2.1	Displacement Fields.....	79
5.2.2	Kinematic Relations	80
5.2.3	Virtual Work Statement.....	80
5.2.4	Equilibrium Equations and Associated Boundary Conditions.....	81
5.2.5	Weak Formulation and Finite Element Model	82
5.2.6	Nonlinear Finite Element Analysis of Imperfect Rings	85
5.3	Theory for Cylindrical Shells with Initial Imperfections.....	87

	5.3.1	Displacement Fields.....	87
	5.3.2	Kinematic Relations	88
	5.3.3	Virtual Work Statement.....	88
	5.3.4	Equilibrium Equations and Associated Boundary Conditions	90
	5.3.5	Weak Formulation and Finite Element Model	91
	5.3.6	Nonlinear Finite Element Analysis of Imperfect Cylindrical Shells	96
6		<u>NUMERICAL SOLUTION PROCEDURES</u>	99
	6.1	Introduction.....	99
	6.2	Eigenvalue Analysis	100
	6.3	Newton-Raphson Method.....	101
	6.4	Riks-Wempner Method on a Normal Plane.....	103
	6.5	Convergence Criteria	116
7		<u>EXAMPLE ANALYSES AND NUMERICAL RESULTS FOR RING MODEL</u>	118
	7.1	Introduction.....	118
	7.2	Test Examples for Arch and Ring Structures.....	119
	7.2.1	Static Analysis of an Isotropic Circular Ring Under Uniform Pressure.....	119
	7.2.2	Nonlinear, Large Deflection Analysis of a Hinged, Deep Arch under a Concentrated Load at the Apex.....	121
	7.2.3	Geometrically Nonlinear Analysis of a Clamped, Shallow, Circular Arch Subjected to a Concentrated Load at Midspan	124

7.3	Example Studies for One-Layered Isotropic or Orthotropic Arch and Ring Structures	128
7.3.1	Linearly Stability Analysis of a Uniformly Compressed, Isotropic, Circular Ring.....	128
7.3.2	Nonlinear Buckling Analysis of a Uniformly Compressed Circular Ring.....	131
7.3.3	Linear and Nonlinear Buckling Analysis of a Uniformly Compressed Circular Arch with Pinned-Pinned Ends	135
7.3.4	Stability Analysis of Isotropic Rings with Internal Elastic Foundations under Constant Directional Pressure.....	138
7.3.5	Effect of Pasternak's Constants on the Stability of an Isotropic Ring with Internal Elastic Foundation $K_0 = 2 \times 10^5$ Pa under Uniform Pressure	143
7.3.6	Effect of Nonlinear Winkler-Foundation Constant K_1 on the Stability of an Isotropic Ring with Internal Elastic Foundation $K_0 = 2 \times 10^5$ Pa under Uniform Radial Pressure.....	144
7.4	Example Studies for Multi-Layered, Composite Ring Structures.....	146
7.4.1	Stability Analysis of Uniformly Compressed, Composite Circular Rings.....	146
7.4.2	Stability Analysis of Composite Circular Rings with Internal Elastic Foundations under Uniform, Constant-Directional Pressure	148
7.5	Imperfection Sensitivity Analysis of Rings under Uniform Radial Pressure	150

7.5.1	Imperfection Sensitivity Analysis of an Isotropic Circular Ring under Uniform Radial Pressure	150
7.5.2	Imperfection Sensitivity Analysis of Composite Circular Rings under Uniform Radial Pressure	151
7.5.3	Imperfection Sensitivity Analysis of a Composite (0 / 45 / -45 / 0) Circular Ring with Internal Elastic Foundation ($K_0 = 1000$ KPa) under Uniform Radial Pressure	152
8	<u>EXAMPLE ANALYSES AND NUMERICAL RESULTS FOR CYLINDRICAL SHELL MODEL</u>	158
8.1	Introduction.....	158
8.2	Test Examples for Cylindrical Shell Structures.....	159
8.2.1	Linear Static Analysis of a Pressurized, Clamped, Cylindrical Shell	159
8.2.2	Buckling of a Simply-Supported Isotropic Cylindrical Panel Subjected to Axial Loading.....	163
8.2.3	Nonlinear Analysis of a Simply-Supported Cylindrical Roof under a Central Point Load.....	166
8.3	Example Studies for Cylindrical Shell Structures.....	171
8.3.1	Linear and Nonlinear Buckling Analysis of an Isotropic Cylindrical Shell under Uniform Radial Pressure.....	171
8.3.2	Stability Analysis of an Isotropic Cylindrical Shell with Internal Elastic Foundation under Uniform Radial Pressure	178
8.3.3	Stability Analysis of Composite Cylindrical Shells under Uniform Radial Pressure.....	179

8.3.4	Stability Analysis of Composite Cylindrical Shells with Internal Elastic Foundations under Uniform Pressure.....	181
8.3.5	Stability Analysis of an Isotropic Cylindrical Shell with a Two-Parameter Elastic Foundation under Uniform Radial Pressure	183
8.3.6	Stability Analysis of an Isotropic Cylindrical Shell with a Nonlinear Elastic Foundation under Uniform Radial Pressure.....	184
8.4	Initial Post-Buckling and Imperfection Sensitivity Analysis for Cylindrical Shell Structures.....	187
8.4.1	Imperfection Sensitivity Analysis of an Isotropic Cylindrical Shell with Simply Supported Ends under Uniform Radial Pressure	187
8.4.2	Imperfection Sensitivity Analysis of an Angle-Ply Type of Composite Cylindrical Shell with Simply Supported Edges under Radial Pressure	192
8.4.3	Imperfection Sensitivity Analysis of an Isotropic Cylindrical Shell with Simply Supported Ends and Elastic Foundation ($K_0 = 2 \times 10^8 \text{ N / m}^3$) under Uniform Radial Pressure.....	194
8.4.4	Imperfection Sensitivity Analysis of an Isotropic Cylindrical Shell with Simply Supported Ends and Elastic Foundation ($K_0 = 2 \times 10^8 \text{ N / m}^3$) under Uniform Radial Pressure.....	196
9	<u>CONCLUSIONS AND FURTHER WORK</u>	204
9.1	Summary and Conclusions.....	204
9.2	Recommendations for Further Research	207

REFERENCES.....	208	
APPENDIX A	COEFFICIENTS OF ELEMENT STIFFNESS MATRIX AND FORCE VECTOR FOR A RING ELEMENT.....	225
A.1	Coefficients of Linear Element Stiffness Matrix and Force Vector....	225
A.2	Coefficients of Nonlinear Element Stiffness Matrix	226
APPENDIX B	COEFFICIENTS OF ELEMENT TANGENT STIFFNESS MATRIX FOR A RING ELEMENT.....	229
APPENDIX C	COEFFICIENTS OF ELEMENT STIFFNESS MATRIX AND FORCE VECTOR FOR A CYLINDRICAL SHELL ELEMENT....	231
C.1	Coefficients of Linear Element Stiffness Matrix and Force Vector....	232
C.2	Coefficients of Nonlinear Element Stiffness Matrix	235
APPENDIX D	COEFFICIENTS OF ELEMENT TANGENT STIFFNESS MATRIX FOR A CYLINDRICAL SHELL ELEMENT.....	242
APPENDIX E	COEFFICIENTS OF ELEMENT STIFFNESS MATRIX FOR AN INITIALLY IMPERFECT RING ELEMENT.....	248
APPENDIX F	COEFFICIENTS OF ELEMENT TANGENT STIFFNESS MATRIX FOR A NONLINEAR RING ELEMENT WITH INITIAL IMPERFECTIONS.....	249

APPENDIX G	COEFFICIENTS OF ELEMENT STIFFNESS MATRIX FOR AN INITIALLY IMPERFECT, CYLINDRICAL SHELL ELEMENT..	252
APPENDIX H	COEFFICIENTS OF ELEMENT TANGENT STIFFNESS MATRIX FOR A NONLINEAR, CYLINDRICAL SHELL ELEMENT WITH INITIAL IMPERFECTIONS.....	256
VITA.....		266

LIST OF FIGURES

Figure 3.1	Geometry and coordinate definition of a ring.....	17
Figure 3.2	Laminae coordinate system.....	23
Figure 3.2	Geometry of an N-layered laminate.....	26
Figure 3.2	Positive directions for stress and moment resultants for a cylindrical shell element.....	27
Figure 4.1	Geometry and coordinate system of a cylindrical shell	48
Figure 6.1	Newton-Raphson method for a single degree of freedom system.....	104
Figure 6.2	Riks-Wempner method on a normal plane for a single degree of freedom system.....	106
Figure 6.3	Similar triangles for solving $\Delta \lambda_i^{(1)} \left\{ \Delta U_i^{(1)} \right\}^{(1)}$ for the Riks-Wempner method on a normal plane	110
Figure 6.4	The graph for the first iteration of the first load step in the Riks-Wempner method on a normal plane	113
Figure 6.5	Similar triangles in the first iteration of the first load step for the Riks-Wempner method on a normal plane	114
Figure 7.1	Geometry and mesh information of a circular ring.....	120
Figure 7.2	A hinged, deep, circular arch subjected to a center point load	122
Figure 7.3	Nonlinear load-deflection curve of a simply-supported, deep arch subjected to a point load at midspan.....	123
Figure 7.4	A shallow, circular arch with both fixed end conditions under a concentrated load at the apex	126

Figure 7.5	Nonlinear load-deflection curve of a fixed ended, shallow arch subjected to a concentrated load at the apex	127
Figure 7.6	Undeformed and buckled shapes of a complete circular ring subjected to uniform dead pressure.....	130
Figure 7.7(a)	Configuration of a half circular ring with a small concentrated load.....	132
Figure 7.7(b)	Configuration of a circular ring with an initially out-of-round model	132
Figure 7.8	Nonlinear load-deflection curves of a circular ring subjected to uniform dead pressure for the case of model I.....	133
Figure 7.9	Nonlinear load-deflection curves of a circular ring subjected to uniform dead pressure for the case of model II.....	134
Figure 7.10	Configuration of a circular arch under uniform dead pressure with pinned boundary conditions.....	136
Figure 7.11	Critical buckling mode of a circular arch under uniform dead pressure with pinned boundary conditions	137
Figure 7.12	Undeformed and buckled shapes ($n = 3$) of a complete circular ring with $K_0 = 2 \times 10^4$ KPa when subjected to uniform dead pressure.....	141
Figure 7.13	Undeformed and buckled shapes ($n = 5$) of a complete circular ring with $K_0 = 2 \times 10^5$ KPa when subjected to uniform dead pressure.....	142
Figure 7.14	Nonlinear load-deflection curves of an isotropic ring with various initial imperfections under uniform radial pressure.....	154
Figure 7.15	Nonlinear load-deflection curves of a cross-ply $(0/90/90/0)_s$ type of composite ring with various initial imperfections under uniform radial pressure	155

Figure 7.16	Nonlinear load-deflection curves of an angle-ply $(0/45/-45/0)_s$ type of composite ring with various initial imperfections under uniform radial pressure.....	156
Figure 7.17	Nonlinear load-deflection curves of an angle-ply $(0/45/-45/0)$ type of composite ring with internal elastic foundation ($K_0 = 1000$ KPa) with various imperfection amplitudes under uniform radial pressure.....	157
Figure 8.1	Geometry of a clamped cylindrical shell.....	161
Figure 8.2	A simply-supported cylindrical panel.....	164
Figure 8.3	Mesh and geometry information of a simply-supported cylindrical roof under a central point load.....	167
Figure 8.4	Nonlinear response of a simply-supported, orthotropic cylindrical roof under a central point load.....	168
Figure 8.5	Nonlinear response of a simply-supported, cross-ply $(0/90)$ cylindrical roof under a central point load.....	169
Figure 8.6(a)	Geometry and coordinate system of a cylindrical shell.....	173
Figure 8.6(b)	Mesh information and the corresponding boundary conditions of a simply-supported cylindrical shell.....	173
Figure 8.7(a)	First buckling mode with $q_0 = 1528$ KPa.....	176
Figure 8.7(b)	Second buckling mode with $q_0 = 2446$ KPa.....	176
Figure 8.7(c)	Third buckling mode with $q_0 = 3094$ KPa.....	177
Figure 8.8	Nonlinear load-displacement curves of isotropic cylinders with various imperfection function amplitudes.....	189
Figure 8.9	Normalized determinants versus applied loads of isotropic cylinders with various imperfection function amplitudes.....	190

Figure 8.10	Nonlinear load-displacement curves of imperfect isotropic cylinders on elastic foundation ($K_0 = 2 \times 10^8 \text{ N / m}^3$), wave parameters $m = 1$, and $n = 2$	198
Figure 8.11	Nonlinear load-displacement curves of imperfect isotropic cylinders on elastic foundation ($K_0 = 2 \times 10^8 \text{ N / m}^3$), wave parameters $m = 1$, and $n = 4$	199
Figure 8.12	Normalized determinants versus applied loads of imperfect isotropic cylinders on elastic foundation ($K_0 = 2 \times 10^8 \text{ N / m}^3$), wave parameters $m = 1$, and $n = 2$	200
Figure 8.13	Normalized determinants versus applied loads of imperfect isotropic cylinders on elastic foundation ($K_0 = 2 \times 10^8 \text{ N / m}^3$), the wave parameters $m = 1$, and $n = 4$	201
Figure 8.14	Nonlinear load-displacement curves of imperfect composite cylinders on elastic foundation ($K_0 = 1 \times 10^5 \text{ N / m}^3$), wave parameters $m = 1$, and $n = 4$	202
Figure 8.15	Normalized determinants versus applied loads of imperfect composite cylinders on elastic foundation ($K_0 = 1 \times 10^5 \text{ N / m}^3$), wave parameters $m = 1$, and $n = 4$	203

LIST OF TABLES

Table 7.1	Comparisons of critical buckling loads based on various theories	135
Table 7.2	Comparisons of first buckling loads and the associated modes of a circular ring for various elastic foundation constants	140
Table 7.3	Comparisons of the critical buckling pressures under various shear parameters	143
Table 7.4	Comparisons of the critical buckling pressures under various nonlinear elastic foundational constants	145
Table 7.5	Comparisons of the critical buckling pressures of composite rings under various lamination sequences	147
Table 7.6	Comparisons of the critical buckling pressures of two different types of composite rings with various elastic foundational constants.....	148
Table 7.7	Comparisons of the critical buckling pressures of two different types of composite rings with various initial imperfections.....	152
Table 7.8	Comparisons of the critical buckling pressures of a Composite Circular Ring with Internal Elastic Foundation ($K_0 = 1000$ KPa) under various initial imperfection amplitudes.....	153
Table 8.1	Comparisons of the midspan deflections in mm of a clamped cylinder subjected to hydrostatic pressure	162
Table 8.2	Comparison of the critical buckling loads, N_x , (N/m) of a simply-supported cylindrical panel under axial compressive loading	165
Table 8.3	Comparison of the applied loads to produce the central deflection of 2.026 inch (5.146 cm) for the case of a single-layered cylindrical roof under various studies.....	170

Table 8.4	Comparison of the applied loads to produce the central deflection of 2.222 inch (5.644 cm) for the case of a (0/90) composite cylindrical roof under various studies.....	171
Table 8.5	Comparisons of the corresponding buckling loads between the linear numerical analysis and the classical solutions based on Donnell's quasi-shallow, thin theory.....	174
Table 8.6	Comparisons of the critical buckling pressure q_0 (N/m ²) of simply-supported cylindrical shells with and without elastic foundations under uniform lateral pressure.....	179
Table 8.7	Comparisons of the critical buckling pressure q_0 (N/m ²) of simply-supported, composite cylinders with different lamination schemes under uniform lateral pressure.....	181
Table 8.8	Comparisons of the numbers of lobes of composite cylinders with different lamination schemes under uniform lateral pressure.....	181
Table 8.9	Comparisons of the critical buckling pressures q_0 (N/m ²) of simply-supported, cross-ply (0/90/90/0) type of composite cylinders with different elastic foundations under uniform lateral pressure.....	183
Table 8.10	Comparisons of the critical buckling pressures q_0 (N/m ²) of simply-supported, angle-ply (0/45/-45/0) type of composite cylinders with different elastic foundations under uniform lateral pressure.....	183
Table 8.11	Comparisons of the critical buckling pressures of simply-supported, isotropic cylindrical shells with various Pasternak elastic foundation constants under uniform lateral pressure.....	184

Table 8.12	Comparisons of the critical buckling pressures of simply-supported, isotropic cylindrical shells with various nonlinear elastic foundation constants under uniform lateral pressure	186
Table 8.13	Comparisons of the critical buckling pressure q_0 (N/m ²) of simply-supported, isotropic cylinders under uniform lateral pressure for the cases of linear, nonlinear, and imperfection sensitivity analyses	191
Table 8.14	Comparisons of the critical buckling pressure of simply-supported, angle-ply type of composite cylinders under uniform lateral pressure for the cases of imperfection sensitivity analyses	193
Table 8.15	Comparisons of the critical buckling pressure of simply-supported, isotropic cylindrical shell with elastic foundation under uniform lateral pressure for the cases of imperfection sensitivity analyses.....	195
Table 8.15	Comparisons of the critical buckling pressure of simply-supported, angle-ply type of cylindrical shell with elastic foundation under uniform lateral pressure for the cases of imperfection sensitivity analyses.....	197

CHAPTER 1

INTRODUCTION

1.1 Motivation

In recent years, fiber-reinforced composite materials have been widely used in the construction of solid-propellant rocket motors. Because of their excellent advantages of high stiffness, strength to weight ratio, and superior mechanical properties, the uses of composites have significantly improved performance of rocket motors, and the advances in fiber manufacturing technology have given an additional assist to their use. However, despite numerous advantages of composites over conventional metallic materials, there are still some areas of concern to be considered in industry, such as high cost, difficult quality control, and complicated manufacturing processes.

From the above considerations, the efficient use of these materials requires a good understanding of the structural response to external causes such as mechanical and environmental loads. In earlier researches [1, 2, 3, 4, 5], the material properties, stress, and reliability analyses of solid-propellant rocket motors under various loading conditions have been studied. These reports treated the motor case as an isotropic or orthotropic single layer or multiply-layer composite, and utilized elastic approaches, finite element stress analysis, and experimental measurements to characterize the structures.

During a war explosions in the vicinity of motors may produce high circumferential pressures. Such external pressure might cause the motors to buckle and then become

inoperational. Therefore, the stability analyses of rocket motors under external pressure becomes important for the safety consideration of such structures.

Rocket motors are modeled as long multi-layered cylinders with thin, high-strength outer cases and thick, low-strength rubber-like inner layers. In the proposed model, the case is treated as an isotropic layer, which is made of metallic materials, or as a multiply anisotropic composite. The inner layer is also treated as an elastic medium.

Other than rocket motors, such thin-walled circular rings and cylindrical tubes subjected to external pressure are commonly used in silos, water towers, oil tanks, large penstocks, aircraft fuselages, submarines, and other aerospace and underwater structures. The nonlinear response and buckling analysis are of major interest in the design of such systems.

1.2 Objectives and Present Study

The primary object of this present research is to derive specific forms of equations that govern the nonlinear structural behavior of thin, anisotropic, circular rings and cylindrical shells with internal elastic foundations as well as initial imperfections under various loading and boundary conditions. Based on the above formulations, finite element equations are developed for both linear and nonlinear analyses. It is of interest to examine the nonlinear bending, buckling and initial post-buckling behavior of the proposed rocket motor models under axisymmetric external pressure loading. The outer cases of motors are considered as isotropic (metallic) and anisotropic (composite) circular rings or

cylindrical shells. They are the main structures of interest in the stability analyses. The inner elastic core is modeled as linear and nonlinear elastic foundations.

For the purpose of reducing the mathematical difficulty and physical complexity of the general nonlinear elasticity equations in polar coordinates, a refined Sanders type, nonlinear shell theory is employed. The model accounts for small strains, and moderately large rotations about the normal to the shell mid-surface. Due to non-negligible transverse shear effects in composite materials, first order shear deformable theory is also applied to determine global response of the structures. A Winkler-type linear and nonlinear elastic foundation is used to model the internal elastic medium. Pasternak-foundation constants are also chosen to modify the proposed elastic foundation for the purpose of shear interactions.

The present theory is developed from an assumed displacement field, von Karman type of nonlinear strain-displacement relations valid for large displacements, equations of mechanics of composite materials, and the principle of virtual displacements. With the resulting equations as a starting point, the nonlinear governing equations, the associated boundary conditions, and the displacement-based finite element models are formulated by making certain simplifying assumptions.

To compare to the work of early researchers, a variety of numerical examples are investigated to demonstrate the validity and efficiency of the proposed theory and corresponding finite element programs under various boundary conditions and loading cases. Eigenvalue analysis is used to predict approximate buckling loads, mode shapes, and symmetrical conditions by solving a set of linearized, coupled equations. An iterative

solution procedure, either Newton-Raphson or Riks-Wempner method, is employed to trace the equilibrium paths for the cases of nonlinear analysis.

Several cases studies are performed numerically to determine the geometric nonlinear behavior of general ring-type and shell-type structures, anisotropic as well as isotropic, with and without the inclusion of internal elastic foundations and the effect of initial imperfections, in bending, buckling and post-buckling under various boundary conditions.

The results indicate that the stability of thin-walled cylindrical structures can be significantly improved by the application of soft, elastic liners.

CHAPTER 2

LITERATURE REVIEW

2.1 Buckling of Circular Arches and Rings

The problems of the buckling of circular arches and rings under external pressure loading have captured a great amount of attention in the design of aerospace and underwater structures. Many variations of the equilibrium and stability equations for circular rings are available in the literature.

The early classical works have been discussed by Timoshenko and Gere [6]. More contributions on the linear analysis of the structural behavior of circular rings under various types of pressure loading are made by Stevens [7], Boresi [8], and Wasserman [9]. In Smith and Simitses' [10] paper, the external pressure loadings are classified into three different categories, which are: hydrostatic ("live"); constant-directional radial ("dead"); and centrally directed pressures. The critical values of the buckling pressures of a complete circular ring are different for various pressure loading conditions. Brush and Almroth [11] summarized linear and nonlinear equilibrium and stability equations by use of Donnell's approximations. They also conducted analytical solutions of the buckling pressures of a ring on a Winkler elastic foundation. Rehfield [12] and Naschie [13] investigated the initial postbuckling behavior of circular rings under external pressures. In Katzenberger's [14] thesis, he considered the geometric nonlinearity in developing his finite elements for arches, rings and frames.

2.2 Shell Theories

2.2.1 Classical Shell Theories

In the past, a wide variety of different shell theories were proposed to discuss the mechanical responses of a thin shell structures. Love [15] is the first author who presented the foundations of linear classical theory of thin shells by applying Kirchoff's hypothesis, which assumes that the normals to the reference surface remain straight and normal during the deformation. The transverse shear strains are also neglected in his theory. Based on the Love-Kirchhoff linear theory, numerous works appeared in the literature [16-23]. Sanders [20], Budiansky and Sanders [24], Budiansky and Radkowski [25], and Koiter [26] modified Love's linear first-order theory in order to remedy some of the inconsistencies. Leissa [27] presented an excellent comparison of various theories used in linear shell analysis.

Among the great amount of research in the area of geometrically nonlinear shell theories, a simple set of nonlinear equations governing the response of cylindrical shells was first presented by Donnell [28]. Based on Love's assumptions, Vlasov [30] extended them to the Donnell-Mushtari-Vlasov (DMV) equations for the analysis of quasi-shallow shells. Novozhilov [31] presented another set of nonlinear equations for general shell problems. Donnell's [28, 29], Flugge's [32], and Sanders' [33] equations are the three most commonly employed in analysis of circular cylindrical shells. For the purpose of reducing complexities, there are significant differences in the formulations of strain-displacement (kinematics) equations and the expressions for the force and moment resultants (constitutive equations) for a thin shell structure. In the applications of the

above three shell theories, several publications are available. Marquerre [34] achieved good results on shallow cylindrical panels by using Donnell's equations. Hoff [35] presented the closed-form solutions for the linear bending response of isotropic cylinders based on both Flugge and DMV theories. The general linear theoretical solutions for anisotropic cylinders were performed by Cheng and Ho [36], Jones and Morgan [37], Jones [38], and Hennemann and Hirano [39]. Dong, Pister and Taylor [40] studied thin shell structures made of fiber composite laminates by extension of Donnell's shallow shell theory. Wu [41] and Simites, et al. [42, 43] studied the responses of laminated cylindrical shells using various theories.

2.2.2 Shear Deformable Shell Theories

The transverse shear effects have become quite significant for thick shells and certain composite structures. The Love-Kirchhoff theory usually underestimates deflections and stresses, but overestimates natural frequencies and buckling loads of shell structures [44, 45, 46]. Due to the above consideration, numerous plate and shell theories which account for transverse shear flexibility are well documented in the literature.

Reissner [47] proposed the first stress-based shear deformable shell theory. It assumed a linear distribution of normal and shear stresses through the thickness of the bodies. The transverse normal and shear stresses may be obtained by integrating the equilibrium equations which are derived from three-dimensional elasticity theory over the thickness. Basset's [48] theory describes a displacement-based shear deformable shell theory. In contrast to Reissner's theory, the displacement components are considered as linear

variations across the thickness. In the application of Basset's work, Hildebrand, Reissner and Thomas [49] proposed a first order shear deformable theory to analyze shells. The first shear deformable theory was also applied for anisotropic laminated shells by Yang, Norris and Stavsky [50]. Later on, Dong and Tso [51] also constructed their laminated orthotropic shell theory including transverse shear deformations. Reddy used the refined first-order shear theory to study moderately thick laminated shells [52]. For the first order theory, a shear correction factor is required for transverse shear terms.

To include the transverse shear deformations in the analysis of moderately thick, anisotropic composite shells, Di Sciuva [53] and Librescu and Schmidt [54] assumed a piecewise linear displacement field to satisfy the continuity of interlaminar shear stresses. In higher-order, displacement-based shear deformable shell theories, the displacement fields are interpolated in power series of the thickness coordinate and unknown generalized displacement vectors. Librescu and Khdeir [55] and Murthy [56] formulated their problems in this manner. Librescu [57] also developed a refined geometrical nonlinear shell theory for anisotropic laminated shells by expanding the displacement vectors with respect to the thickness coordinate. There are numerous higher-order refined shear deformable theories in the literature, such as third-order [58-64] and other higher-order theories [65-69].

Usually, the first order shear deformable theories provide good predictions for global response, such as eigen-frequencies and critical buckling loads. Higher-order theories generally give much more accurate results in transverse stress components and are also particularly good for special purposes of analyses, such as the determination of the interlaminar stresses, boundary effects and some delimitation problems.

2.2.3 Stability of Circular Cylindrical Shells

The stability of circular cylindrical shells has been studied since the late 1800's. However, early researchers could only solve linear buckling problems of shells by solving a set of linear differential equations. The earliest solution for circular cylinders subjected to axial compression was presented by Lorenz [70] in 1911. Southwell [71] is the first researcher to propose solutions for buckling loads of cylindrical shells under uniform lateral pressure. Flugge [72] presented a comprehensive treatment of cylindrical shell stability by providing the theory of buckling of orthotropic cylinders, including combined loading and cylinders subjected to bending. The results for cylinders under torsional load were given by Donnell [28], where a relatively simple set of equations governing the stability condition for circular cylindrical shells was suggested. Batdorf [73] reviewed the early work available for buckling of thin circular cylindrical shells and also proposed a simplified method. Ho and Cheng [74] studied the stability of heterogeneous cylinders under combined loading and arbitrary boundary conditions. Seide and Weingarten [75] assumed a linear prebuckled state, and showed that the bending buckling load of isotropic cylinders was nearly the same as the buckling load of the same cylinder under pure axial compression. Holston [76] performed a similar analysis on cylinders made of laminated composite materials. Up to this point, their works were based on the assumptions of small displacements and the Love-Kirchhoff hypothesis.

In their analysis of the buckling of thin-walled cylinders, von Karman and Tsien [77] considered nonlinear terms in the kinematic relations. Donnell [28] was the first author who pointed out that imperfections in the shape of the shell play an important role in the buckling analysis. With the limitation of small deflections, some shell theories are not

capable of solving post-buckling problems [78]. To improve the deficiencies of small displacement theories, Naghdi [79] developed a finite deflection theory for post-buckling analysis. Koiter [80] published a general theory for post-buckling behavior of shells in his dissertation. In his work, he also showed that the buckling loads are significantly reduced even for small imperfections. His theory was applied by Hutchinson [81], Budiansky and Hutchinson [82], and Arbocz and Babcock [83] to investigate imperfection sensitivity to buckling of cylindrical shells under axial or lateral compression.

The finite element method has become a very useful tool for the analyses of static, stability, and vibration problems of shells. Based on small displacement theories, Schmit and Monforton [84], Panda and Natarajan [85], Shivakumar and Krishna Murty [86], Rao [87], Seide and Chang [88], Hsu, Reddy, and Bert [89], Reddy [90], and Venkatesh and Rao [91, 92] studied the structural behavior of anisotropic laminated cylindrical shells using finite element analysis. In the stability analysis of circular cylindrical shells, a high geometrical nonlinearity is required in order to accurately predict the buckling loads. The finite element technique possesses great advantages in those problems. In the literature [93, 94, 95], the finite element method was used to analyze the nonlinear instability problems of arches and shells. Riks and Wempner [96] used the constant-arc-length method to investigate the post-buckling load versus the displacement path. Ramm [97] and Crisfield [98] gave a good study of the commonly used algorithms for shell stability analysis.

2.3 Buckling of Cylindrical Shell with Elastic Core

2.3.1 Elastic Buckling of Isotropic Cylindrical Shells

Solid propellant rocket motors were modeled as thin shells with soft elastic cores. The stability of such rocket-motors is of great interest. The elastic buckling behavior of thin-walled, isotropic cylinders with elastic cores have also been investigated by many authors under various loading configurations. Based on linear and small-deformation theory, Reissner [99], Zak and Bollard [100], Seide [101], and Yao [102] presented the stabilizing effect of cores on the buckling strength of shells under axially compressive loads. In Seide's work [101], the Winkler type of foundation [103] was used to model the soft elastic core. Yao [102] found that the radial stress of the core is the predominant stabilizing force in buckling behavior, and also indicated that the effect of the second parameter was very weak. Myint [104] used a Pasternak (two-parameter) foundation to include shear interactions.

For the problems of the stability condition under uniform radial pressure, Seide and Weingarten [105], and Herrmann and Forrestal [106] calculated the buckling pressures of circular rings (plane stress) and long cylinders (plane strain). Seide [101] investigated finite length, simply-supported cylinders by using Batdorf's modified Donnell equations and neglecting the shear stresses between the cylinder and the core. Korbut and Soksonov's [107] work included both the linear and nonlinear problems.

Other loading situations include circumferential band of pressure (Yao [108]), combined loading of axial compression and uniform radial pressure (Seide [101]; Brush and Almroth

[109]; Vlasov [110]), and combined loading of axial compression and non uniform radial pressure or circumferential band of pressure (Brush and Almroth [109]), axially varying circumferential thermal stress (Zak and Bollard [100]), bending (Yabuta [111]), and torsion (Weingarten [112]). The experimental studies can also be found in the early publications of Kachman [113], Fitzgibbon [114], and Goree and Nash [115]. Recently, Karam and Gibson [116] experimentally investigated the buckling resistance of silicon rubber shells with and without compliant cores using uniaxial compression and four point bending tests.

2.3.2 Elastic Buckling of Anisotropic Cylindrical Shells

Regarding the effect of heterogeneity and transverse shear flexibility of composite cylindrical shells, numerous studies have been made. Lemke [117] and Holston [118] performed buckling analyses of core-filled orthotropic shells. Their work considered specially orthotropic shells, but neglected shear deformable flexibility. It has, however, been shown that transverse shear flexibility is much more significant in composite materials than in homogeneous, isotropic ones [119].

Based on the Timoshenko-type hypotheses, Bert [120] determined the buckling loads of core-filled specially isotropic and orthotropic cylinders with the effect of transverse shear deformation. He also used a Winkler-type foundation to model the isotropic core. Vlasov [121] analyzed the buckling behavior of an orthotropic cylindrical composite shell strongly bonded to a solid elastic transversely isotropic core. Malyutin et. al. [122]

presented experimental and theoretical studies of the stability of cylindrical shells in axial compression.

Stability of cylindrical shells with an elastic-plastic filler under axial compression was studied by Babich and Cherevko [123]. They employed three-dimensional linearized stability theory for both the filler and the supporting shell.

2.4 Elastic Foundations

Structures supported by elastic foundations are quite important in design for engineers. The literature on the linear analysis of beams, rings, plates and shells continuously supported by one or two-parameter elastic media is extensive. In general, the analysis of structures on an elastic foundation is based on the assumption that the reaction forces of the foundation are proportional at every point to the deflection of the body at that particular point.

The simplest model of formulating an elastic foundation was proposed by Winkler [103], who assumed that the reaction force generated by an elastic base is proportional to the deflection of the footing at that point. This assumption is applied by Zimmermann [124] to study the problems of railroad tracks. Hetenyi [125, 126] developed the classical differential equations to study beams or plates on an elastic foundation. Even with the simplicity of Winkler's assumption, his work showed satisfactory results in stress analysis of beams on an elastic foundation. Pasternak [127] introduced shear interaction between the springs to improve the accuracy of Winkler's model. Vlasov and Leont'ev

[128] also included the shear interactions in the foundation and formulated their problems by using the variational method. They studied numerous problems involving beams, plates, and shells on elastic foundations. Despite the fact that a two parameter elastic foundation gives better results, it is difficult to determine an appropriate value for the second parameter. Vallabhan [129, 130] showed the determination of this value in his works.

For the nonlinear analysis of this class of structures, much less work has been covered and discussed and, in particular, very little attention has been given to structures on a nonlinear elastic foundation. The relevant publications in the literature are the works of Amazigo et al. [131], Fraser and Budiansky [132], Hui and Hansen [133], Hui [134], Keener [135], Tvergaard and Needleman [136], Mahrenholtz et al. [137] and Reissner [138, 139].

CHAPTER 3

GENERAL EQUATIONS FOR CIRCULAR ARCHES AND RINGS

3.1 Introduction and Basic Assumptions

The primary object of the presented research is to investigate the buckling and initial post-buckling behavior of rocket motors under various loading conditions. As a first step, one dimensional arches and rings are investigated. The formulation of two-dimensional elasticity theory in polar coordinates can be simplified to one-dimensional arch and ring equations by referencing about the centroidal axes for thin elastic bodies [11]. Due to the complexity and shear deformable flexibility of composite materials, the first order, shear deformable, laminate theory will be applied. Both linear and geometrically nonlinear analyses will be undertaken.

The basic assumptions that provide a reasonable description of the proposed theory for thin-walled arches and rings on elastic foundations are stated as follows:

1. Sections originally perpendicular to the reference axis of the ring will remain plane, but not necessarily normal to the deformed mid-surface because of transverse shear considerations.
2. The transverse thickness is inextensible.
3. The ring is thin so that the ratio of thickness-to-radius is small compared to unity.

- 4 Transverse normal stress is small compared to other normal stress components, and can be neglected.
- 5 Strains are small, but rotations of ring elements about the normal planes are allowed to be moderately large.
- 6 Material behavior is linearly elastic.
- 7 Only in-plane stretching and bending are considered.
- 8 There is a perfect bond between the ring and the elastic foundation.

3.2 Displacement Field

A laminated composite ring is composed of N orthotropic laminae of arbitrarily oriented fiber angles with respect to the ring coordinate system as shown in Figure 3.1. Using the assumption of first order shear deformable theory, one can define the displacement vectors for linear and nonlinear theories as follows:

$$v(y, z) = v_0(y) + z \psi_y(y) \tag{3.1}$$

$$w(y, z) = w_0(y)$$

where v and w are the total displacements in the tangential and radial directions, respectively; v_0 , and w_0 are the associated mid-surface displacements in the y and z directions; ψ_y is the rotation about the x -axis (in the yz plane).

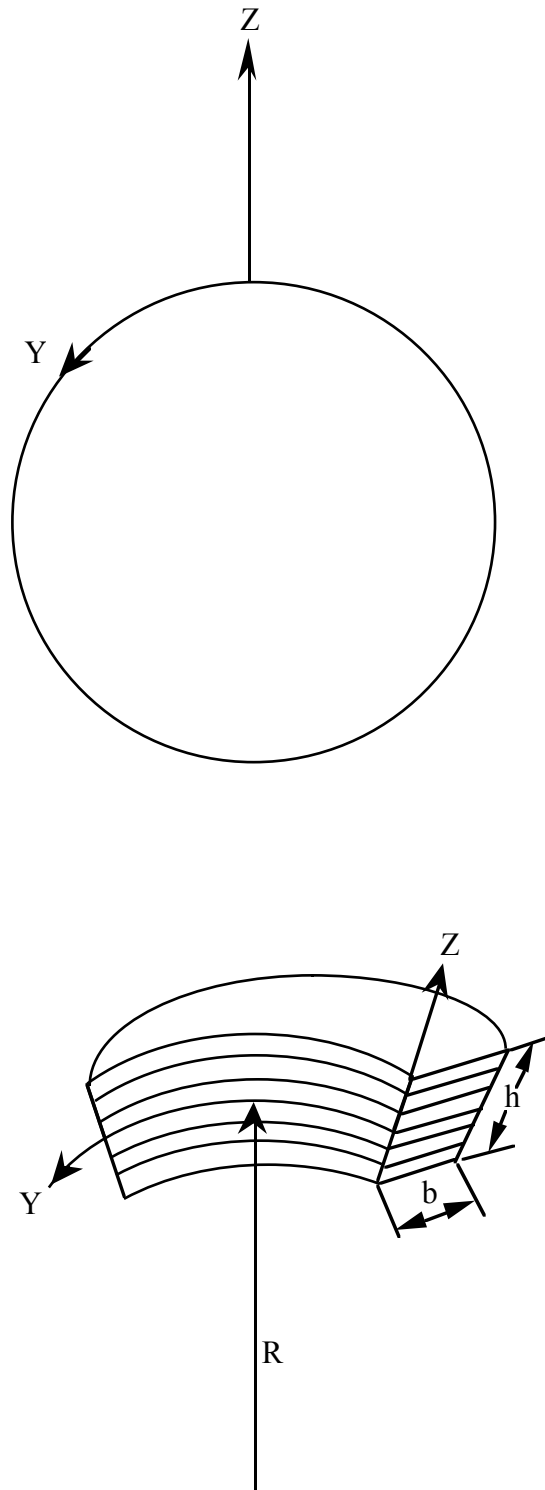


Figure 3.1- Geometry and coordinate definition of a ring

3.3 Kinematic (Strain-Displacement) Relations

3.3.1 Linear Formulation

In association with the displacement fields defined in equation (3.1), one can obtain the linear strain-displacement relations of a ring-type structure in an orthogonal ring coordinate system by specializing the corresponding expressions for polar coordinates of the Sanders kinematic relations [20] as:

$$e_x = 0$$

$$e_y = e_y^0 + z\kappa_y^0$$

$$e_z = 0 \tag{3.2}$$

$$\gamma_{yz} = \gamma_{yz}^0$$

$$\gamma_{xy} = \gamma_{xz} = 0$$

where

$$e_y^0 = \frac{dv_0}{dy} + \frac{w_0}{R}$$

$$\kappa_y^0 = \frac{d\psi_y}{dy} \tag{3.3}$$

$$\gamma_{yz}^0 = \psi_y + \frac{dw_0}{dy} - \frac{v_0}{R}$$

3.3.2 Non-linear Formulation [33, 10]

In the study of the nonlinear behavior, the von Karman theory [140], which assumes that the in-plane displacements are relatively small when compared to the transverse displacements, is applied. It is stated that all the nonlinear terms of the Green's strain tensor are negligible except for the term containing products of transverse deflections. In contrast to those of linear relations, the alternative components of strain-displacement relations in an orthogonal ring coordinate system are:

$$e_y^0 = \frac{dv_0}{dy} + \frac{w_0}{R} + \frac{1}{2} \left(\frac{dw_0}{dy} - \frac{v_0}{R} \right)^2 \quad (3.4)$$

3.4 Mechanical Behavior of a Lamina

Consider a composite laminate composed of N thin orthotropic layers, each one having constant thickness. Fibers in each layer are oriented at an arbitrary angle with respect to the ring coordinate system. Utilizing the generalized Hooke's law relating stress and strain, the general equations for a lamina of a fiber-reinforced orthotropic composite material can be obtained as follows [141, 142]:

$$\begin{Bmatrix} \sigma_{11} \\ \sigma_{22} \\ \sigma_{33} \\ \tau_{23} \\ \tau_{13} \\ \tau_{12} \end{Bmatrix} = \begin{bmatrix} Q_{11} & Q_{12} & Q_{13} & 0 & 0 & 0 \\ Q_{12} & Q_{22} & Q_{23} & 0 & 0 & 0 \\ Q_{13} & Q_{23} & Q_{33} & 0 & 0 & 0 \\ 0 & 0 & 0 & Q_{44} & 0 & 0 \\ 0 & 0 & 0 & 0 & Q_{55} & 0 \\ 0 & 0 & 0 & 0 & 0 & Q_{66} \end{bmatrix} \begin{Bmatrix} \varepsilon_1 \\ \varepsilon_2 \\ \varepsilon_3 \\ \gamma_{23} \\ \gamma_{31} \\ \gamma_{12} \end{Bmatrix} \quad (3.5)$$

where 1, 2, and 3 refer to three respective principal axes of each lamina. In the above equations, the Q_{ij} are used for stiffness quantities. Using the notation of Sloan [143], their related equations with the lamina's material properties and geometry are shown as follows:

$$Q_{11} = E_{11} (1 - \nu_{23} \nu_{32}) / \Delta,$$

$$Q_{22} = E_{22} (1 - \nu_{31} \nu_{13}) / \Delta,$$

$$Q_{33} = E_{33} (1 - \nu_{12} \nu_{21}) / \Delta,$$

$$Q_{44} = G_{23},$$

$$Q_{55} = G_{13},$$

$$Q_{66} = G_{12},$$

$$Q_{12} = E_{11} (\nu_{21} + \nu_{31} \nu_{23}) / \Delta = E_{22} (\nu_{12} + \nu_{32} \nu_{13}) / \Delta,$$

(3.6)

$$Q_{13} = E_{11} (v_{31} + v_{21} v_{32}) / \Delta = E_{22} (v_{13} + v_{12} v_{23}) / \Delta,$$

$$Q_{23} = E_{22} (v_{32} + v_{12} v_{31}) / \Delta = E_{33} (v_{23} + v_{21} v_{13}) / \Delta,$$

$$\Delta = 1 - v_{12} v_{21} - v_{23} v_{32} - v_{31} v_{13} - 2 v_{21} v_{32} v_{13}.$$

3.5 Constitutive Equations of a Laminate

The constitutive equations of each layer were defined in the preceding paragraph. Combining and relating these to the x-y-z orthogonal coordinate system, one can easily obtain a three dimensional constitutive equation of an arbitrarily oriented orthotropic lamina as [141, 142]:

$$\begin{Bmatrix} \sigma_x \\ \sigma_y \\ \sigma_z \\ \tau_{yz} \\ \tau_{xz} \\ \tau_{xy} \end{Bmatrix} = \begin{bmatrix} \bar{Q}_{11} & \bar{Q}_{12} & \bar{Q}_{13} & 0 & 0 & \bar{Q}_{16} \\ \bar{Q}_{12} & \bar{Q}_{22} & \bar{Q}_{23} & 0 & 0 & \bar{Q}_{26} \\ \bar{Q}_{13} & \bar{Q}_{23} & \bar{Q}_{33} & 0 & 0 & \bar{Q}_{36} \\ 0 & 0 & 0 & \bar{Q}_{44} & \bar{Q}_{45} & 0 \\ 0 & 0 & 0 & \bar{Q}_{45} & \bar{Q}_{55} & 0 \\ \bar{Q}_{16} & \bar{Q}_{26} & \bar{Q}_{36} & 0 & 0 & \bar{Q}_{66} \end{bmatrix} \begin{Bmatrix} e_x \\ e_y \\ e_z \\ \gamma_{yz} \\ \gamma_{xz} \\ \gamma_{xy} \end{Bmatrix} \quad (3.7)$$

where \bar{Q}_{ij} are the generalized stiffness coefficients. The relationship between \bar{Q}_{ij} and Q_{ij} is also stated in the following equations:

$$\bar{Q}_{11} = Q_{11} m^4 + 2(Q_{12} + 2Q_{66})m^2 n^2 + Q_{22} n^4$$

$$\bar{Q}_{12} = (Q_{11} + Q_{22} - 4Q_{66})m^2 n^2 + Q_{12}(m^4 + n^4)$$

$$\bar{Q}_{13} = Q_{13} m^2 + Q_{23} n^2$$

$$\bar{Q}_{16} = -mn^3 Q_{22} + m^3 n Q_{11} - mn(m^2 - n^2)(Q_{12} + 2Q_{66})$$

$$\bar{Q}_{22} = Q_{11} n^4 + 2(Q_{12} + 2Q_{66})m^2 n^2 + Q_{22} m^4$$

$$\bar{Q}_{23} = Q_{13} n^2 + Q_{23} m^2$$

$$\bar{Q}_{33} = Q_{33} \tag{3.8}$$

$$\bar{Q}_{26} = -m^3 n Q_{22} + mn^3 Q_{11} + mn(m^2 - n^2)(Q_{12} + 2Q_{66})$$

$$\bar{Q}_{36} = (Q_{13} - Q_{23})mn$$

$$\bar{Q}_{44} = Q_{44} m^2 + Q_{55} n^2$$

$$\bar{Q}_{45} = (Q_{55} - Q_{44})mn$$

$$\bar{Q}_{55} = Q_{55} m^2 + Q_{44} n^2$$

$$\bar{Q}_{66} = (Q_{11} + Q_{22} - 2Q_{12})m^2 n^2 + Q_{66}(m^2 - n^2)^2$$

where $m = \cos\theta$, $n = \sin\theta$, and θ is defined positive as shown in Figure 3.2.

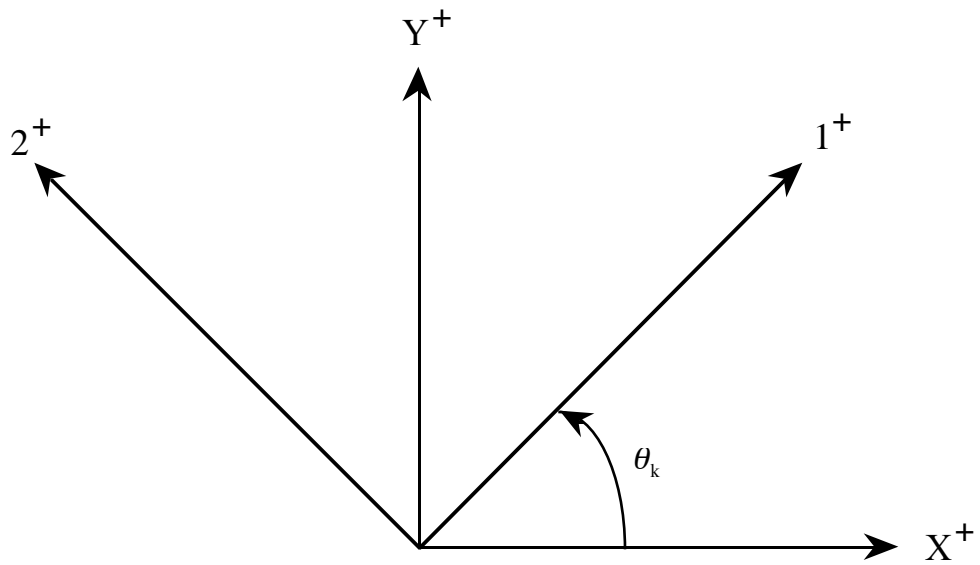


Figure 3.2 - Laminae coordinate system

The shear correlation factor K_s [144] is taken into account, so that the constitutive equations can be rewritten in another form:

$$\begin{Bmatrix} \sigma_x \\ \sigma_y \\ \sigma_z \\ \tau_{xy} \end{Bmatrix}_{(k)} = \begin{bmatrix} \bar{Q}_{11} & \bar{Q}_{12} & \bar{Q}_{13} & \bar{Q}_{16} \\ \bar{Q}_{12} & \bar{Q}_{22} & \bar{Q}_{23} & \bar{Q}_{26} \\ \bar{Q}_{13} & \bar{Q}_{23} & \bar{Q}_{33} & \bar{Q}_{36} \\ \bar{Q}_{16} & \bar{Q}_{26} & \bar{Q}_{36} & \bar{Q}_{66} \end{bmatrix}^{(k)} \begin{Bmatrix} e_x \\ e_y \\ e_z \\ \gamma_{xy} \end{Bmatrix}_{(k)} \quad (3.9)$$

$$\begin{Bmatrix} \tau_{yz} \\ \tau_{xz} \end{Bmatrix}_{(k)} = K_s \begin{bmatrix} \bar{Q}_{44} & \bar{Q}_{45} \\ \bar{Q}_{45} & \bar{Q}_{55} \end{bmatrix}^{(k)} \begin{Bmatrix} \gamma_{yz} \\ \gamma_{xz} \end{Bmatrix}_{(k)} \quad (3.10)$$

3.6 Stress and Moment Resultants

For a laminated structure, the stress and moment resultants are obtained by integration of the stress components in each layer or lamina across the laminate thickness. Since each layer has uniform properties, one can also obtain the resultant forces and moments acting on a laminate by performing the summations of the stress and moment resultants of every lamina as shown in the following relations:

$$\begin{Bmatrix} N_x \\ N_y \\ N_{xy} \end{Bmatrix} = \int_{-\frac{h}{2}}^{\frac{h}{2}} \begin{Bmatrix} \sigma_x \\ \sigma_y \\ \tau_{xy} \end{Bmatrix} \left(1 + \frac{z}{R}\right) dz = \sum_{k=1}^N \int_{h_{k-1}}^{h_k} \begin{Bmatrix} \sigma_x \\ \sigma_y \\ \tau_{xy} \end{Bmatrix} \left(1 + \frac{z}{R}\right) dz \quad (3.11)$$

$$\begin{Bmatrix} M_x \\ M_y \\ M_{xy} \end{Bmatrix} = \int_{-\frac{h}{2}}^{\frac{h}{2}} \begin{Bmatrix} \sigma_x \\ \sigma_y \\ \tau_{xy} \end{Bmatrix} z \left(1 + \frac{z}{R}\right) dz = \sum_{k=1}^N \int_{h_{k-1}}^{h_k} \begin{Bmatrix} \sigma_x \\ \sigma_y \\ \tau_{xy} \end{Bmatrix} z \left(1 + \frac{z}{R}\right) dz \quad (3.12)$$

where h_k and h_{k-1} are defined in Figure 3.3.

Similarly, the shear stress resultants are defined as:

$$\begin{Bmatrix} Q_{yz} \\ Q_{xz} \end{Bmatrix} = \int_{-\frac{h}{2}}^{\frac{h}{2}} \begin{Bmatrix} \tau_{yz} \\ \tau_{xz} \end{Bmatrix} \left(1 + \frac{z}{R}\right) dz = \sum_{k=1}^N \int_{h_{k-1}}^{h_k} \begin{Bmatrix} \tau_{yz} \\ \tau_{xz} \end{Bmatrix} \left(1 + \frac{z}{R}\right) dz \quad (3.13)$$

The positive directions of all the resultant forces (force per unit length) and couples (moment per unit length) are shown in Figure 3.4.

Since the quantity z/R is small compared to unity and may be neglected, substituting the constitutive equations into the above expressions leads to:

$$\begin{Bmatrix} N_x \\ N_y \\ N_z \end{Bmatrix} = \begin{bmatrix} A_{11} & A_{12} & A_{16} \\ A_{12} & A_{22} & A_{26} \\ A_{16} & A_{26} & A_{66} \end{bmatrix} \begin{Bmatrix} e_x^0 \\ e_y^0 \\ \gamma_{xy}^0 \end{Bmatrix} + \begin{bmatrix} B_{11} & B_{12} & B_{16} \\ B_{12} & B_{22} & B_{26} \\ B_{16} & B_{26} & B_{66} \end{bmatrix} \begin{Bmatrix} \kappa_x^0 \\ \kappa_y^0 \\ \kappa_{xy}^0 \end{Bmatrix}, \quad (3.14)$$

$$\begin{Bmatrix} M_x \\ M_y \\ M_z \end{Bmatrix} = \begin{bmatrix} B_{11} & B_{12} & B_{16} \\ B_{12} & B_{22} & B_{26} \\ B_{16} & B_{26} & B_{66} \end{bmatrix} \begin{Bmatrix} e_x^0 \\ e_y^0 \\ \gamma_{xy}^0 \end{Bmatrix} + \begin{bmatrix} D_{11} & D_{12} & D_{16} \\ D_{12} & D_{22} & D_{26} \\ D_{16} & D_{26} & D_{66} \end{bmatrix} \begin{Bmatrix} \kappa_x^0 \\ \kappa_y^0 \\ \kappa_{xy}^0 \end{Bmatrix}, \quad (3.15)$$

and

$$\begin{Bmatrix} Q_{yz} \\ Q_{xz} \end{Bmatrix} = K_S \begin{bmatrix} A_{44} & A_{45} \\ A_{45} & A_{55} \end{bmatrix} \begin{Bmatrix} \gamma_{yz} \\ \gamma_{xz} \end{Bmatrix}. \quad (3.16)$$

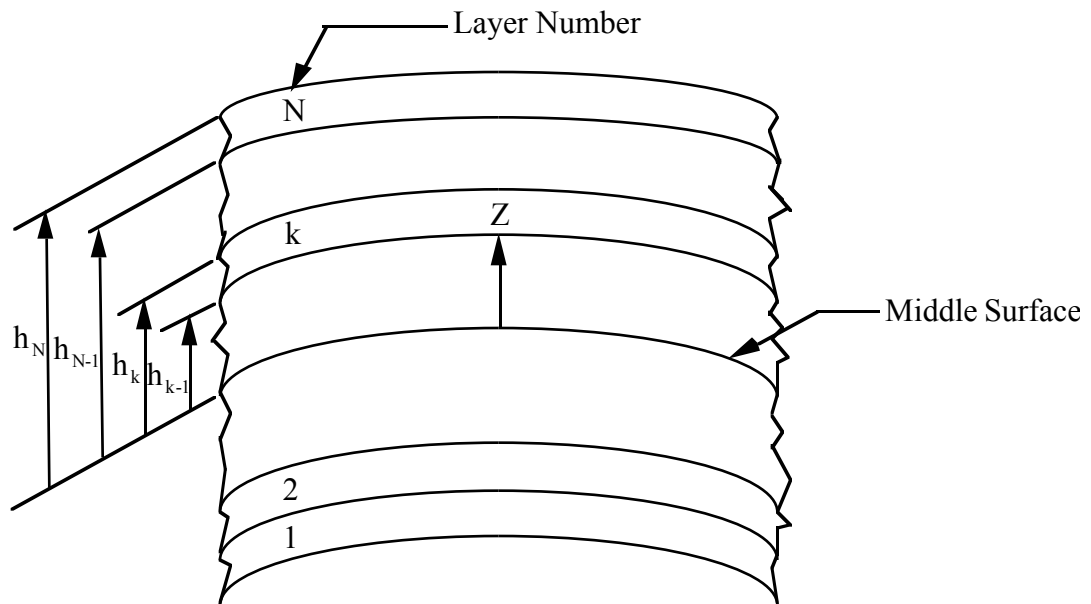


Figure 3.3 - Geometry of an N-layered laminate

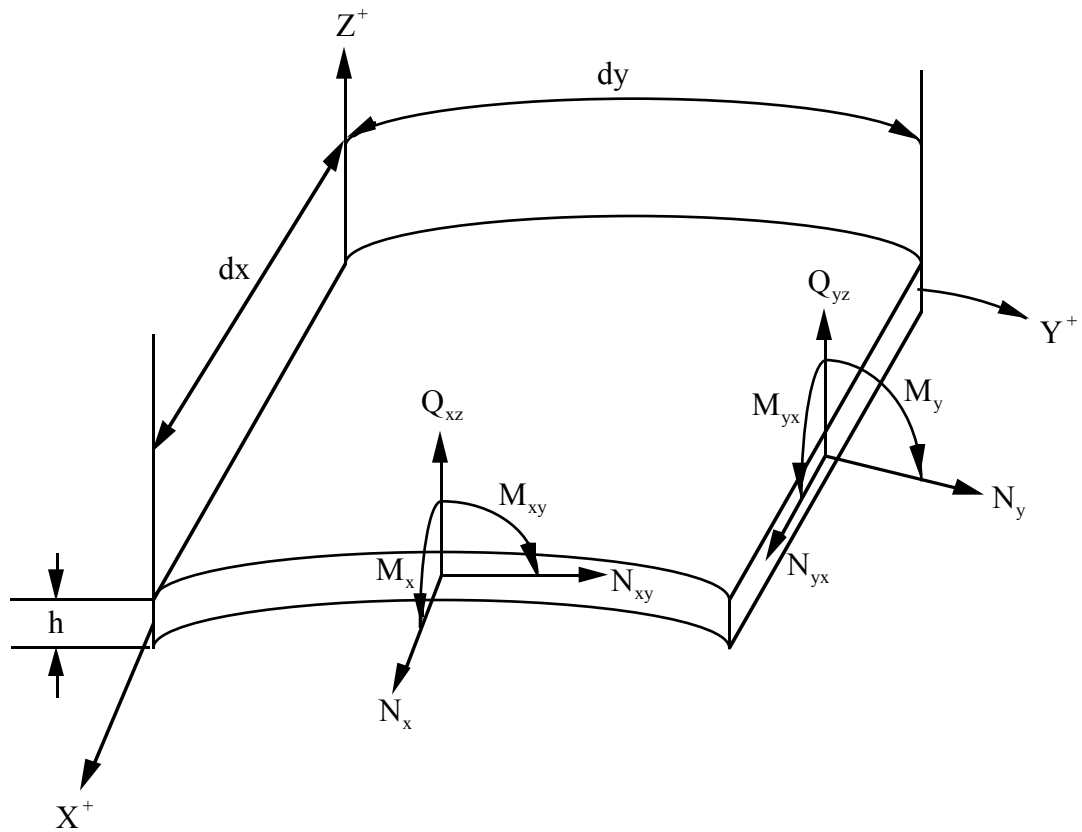


Figure 3.4 - Positive directions for stress and moment resultants
for a cylindrical shell element

where A_{ij} , B_{ij} and D_{ij} are given by

$$A_{ij} = \int_{-\frac{h}{2}}^{\frac{h}{2}} (\bar{Q}_{ij}) dz = \sum_{k=1}^N (\bar{Q}_{ij})_k [h_k - h_{k-1}], \quad [i, j = 1, 2, 4, 5, 6];$$

$$B_{ij} = \int_{-\frac{h}{2}}^{\frac{h}{2}} (\bar{Q}_{ij}) z dz = \frac{1}{2} \sum_{k=1}^N (\bar{Q}_{ij})_k [h_k^2 - h_{k-1}^2], \quad [i, j = 1, 2, 6]; \quad (3.17)$$

$$D_{ij} = \int_{-\frac{h}{2}}^{\frac{h}{2}} (\bar{Q}_{ij}) z^2 dz = \frac{1}{3} \sum_{k=1}^N (\bar{Q}_{ij})_k [h_k^3 - h_{k-1}^3], \quad [i, j = 1, 2, 6].$$

3.7 Virtual Work Statement

Using Hamilton's principle, the virtual work statement implies that minimization of total potential energy of the elastic body under the equilibrium state will become zero, which indicates that

$$\delta \Pi = \delta U + \delta V = 0, \quad (3.18)$$

where Π is the total potential energy of the elastic body; U is the total strain energy of the elastic body; V is the total potential energy of applied loads; δ denotes the variational operator.

The virtual strain energy of an elastic ring associated with internal stresses is given as:

$$\delta U = \int_{\Omega} \int_{-\frac{h}{2}}^{\frac{h}{2}} (\sigma_{yy} \delta e_{yy} + \tau_{yz} \delta \gamma_{yz}) dz dA, \quad (3.19)$$

where Ω is the cross-sectional area of the elastic body along the x-y plane.

The virtual work generated by the applied loads along the domain is of the form:

$$\delta V = - \int_{\Omega} p_{\text{total}} \cdot \delta w \, dA \quad (3.20)$$

where p_{total} is the applied radial pressure.

Substitutions of the strain-displacement relations into the total potential energy equation, utilizing also the expressions of stress and moment resultants, leads to the following weak form of the virtual work statement:

$$\begin{aligned} 0 = \delta \pi &= \int_{\Omega} (N_y \delta e_{yy}^0 + M_y \delta \kappa_y^0 + Q_{yz} \delta \gamma_{yz}^0) dA - \int_{\Omega} p_{\text{total}} \cdot \delta w_0 \, dA \\ &= \int_{y_1}^{y_2} (\bar{N}_y \delta e_{yy}^0 + \bar{M}_y \delta \kappa_y^0 + \bar{Q}_{yz} \delta \gamma_{yz}^0) dy - \int_{y_1}^{y_2} q_{\text{total}} \cdot \delta w_0 \, dA \end{aligned} \quad (3.21)$$

where $\bar{N}_y = b N_y$, $\bar{M}_y = b M_y$, $\bar{Q}_{yz} = b Q_{yz}$, $q_{\text{total}} = b p_{\text{total}}$, which denotes the applied radial force per unit circumferential length, and b is the width of the ring.

Based on the linear theory, equation (3.21) can be rewritten as:

$$0 = \int_{y_1}^{y_2} \left[\bar{N}_y \left(\frac{d\delta v_0}{dy} + \frac{\delta w_0}{R} \right) + \bar{M}_y \left(\frac{d\delta \psi_y}{dy} \right) + \bar{Q}_{yz} \left(\delta \psi_y + \frac{d\delta w_0}{dy} - \frac{\delta v_0}{R} \right) \right] dy - \int_{y_1}^{y_2} q_{total} \cdot \delta w_0 dy \quad (3.22)$$

Similarly, introduction of the nonlinear theory, equation (3.21) can be expressed as:

$$\int_{y_1}^{y_2} \left\{ \bar{N}_y \left[\frac{d\delta v_0}{dy} + \frac{\delta w_0}{R} + \left(\frac{v_0}{R} - \frac{dw_0}{dy} \right) \left(\frac{\delta v_0}{R} - \frac{d\delta w_0}{dy} \right) \right] + \bar{M}_y \left(\frac{d\delta \psi_y}{dy} \right) + \bar{Q}_{yz} \left(\delta \psi_y + \frac{d\delta w_0}{dy} - \frac{\delta v_0}{R} \right) \right\} dy - \int_{y_1}^{y_2} q_{total} \cdot \delta w_0 dy \quad (3.23)$$

3.8 Equilibrium Equations and Associated Boundary Conditions

Utilizing integration by parts on the derivatives of various displacement variables of equations (3.22) and (3.23), one can obtain the equilibrium equations and the associated boundary conditions by collecting terms involving δv_0 , δw_0 , and $\delta \psi_y$, respectively as shown in the following sub-chapter.

3.8.1 Linear Relations

Based on the linear theory as stated before, the equilibrium equations which govern the behavior of elastic arches and rings can be expressed as:

$$\delta v_0 \dots \dots \frac{d\bar{N}_y}{dy} + \frac{\bar{Q}_{yz}}{R} = 0$$

$$\delta w_0 \dots \frac{d\bar{Q}_{yz}}{dy} - \frac{\bar{N}_y}{R} + q_{\text{total}} = 0 \quad (3.24)$$

$$\delta \psi_y \dots \frac{d\bar{M}_y}{dy} - \bar{Q}_{yz} = 0$$

The geometrical and natural boundary conditions associated with the linear theory are specified as:

Geometrical		Natural
$v_0 = \hat{v}_0$		$\bar{N}_y = \hat{N}_y$
$w_0 = \hat{w}_0$	or	$\bar{Q}_{yz} = \hat{Q}_{yz}$
$\psi_y = \hat{\psi}_y$		$\bar{M}_y = \hat{M}_y$

(3.25)

3.8.2 Non-linear Relations

Similarly, applying the non-linear theory leads to the equations of equilibrium which govern the nonlinear behavior of elastic arches and rings as:

$$\delta v_0 \dots \frac{d\bar{N}_y}{dy} + \frac{\bar{Q}_{yz}}{R} + \frac{\bar{N}_y}{R} \left(\frac{dw_0}{dy} - \frac{v_0}{R} \right) = 0$$

$$\delta w_0 \dots \frac{d\bar{Q}_{yz}}{dy} - \frac{\bar{N}_y}{R} + \frac{d}{dy} \left[\bar{N}_y \left(\frac{dw_0}{dy} - \frac{v_0}{R} \right) \right] + q_{\text{total}} = 0 \quad (3.26)$$

$$\delta \psi_y \dots \frac{d\bar{M}_y}{dy} - \bar{Q}_{yz} = 0$$

The geometrical and natural boundary conditions associated with the nonlinear theory are specified as:

Geometrical

Natural

$$v_0 = \hat{v}_0$$

$$\bar{N}_y = \hat{N}_y$$

$$w_0 = \hat{w}_0$$

or

$$\bar{Q}_{yz} + \bar{N}_y \left(\frac{dw_0}{dy} - \frac{v_0}{R} \right) = \hat{Q}_{yz} \quad (3.27)$$

$$\psi_y = \hat{\psi}_y$$

$$\bar{M}_y = \hat{M}_y$$

3.9 Weak Formulation and Finite Element Model

Introduction of the equations of stress and moment resultants of a composite, which were represented by equations (3.14) to (3.16), the linear and nonlinear variational formulations of the minimum potential energy statement (equations (3.22) and (3.23)) can be rewritten in terms of displacement vectors only by using strain-displacement relations of equations (3.2), (3.3), and (3.4), as the following equations (3.28) and (3.29), respectively:

$$\begin{aligned}
0 &= \{ \delta \pi \}_{\text{Linear}} = \{ \delta U + \delta V \}_{\text{Linear}} \\
&= \int_{y_1}^{y_2} \left\{ b \left[A_{22} \left(\frac{dv_0}{dy} + \frac{w_0}{R} \right) + B_{22} \left(\frac{d\psi_y}{dy} \right) \right] \left(\frac{d\delta v_0}{dy} + \frac{\delta w_0}{R} \right) \right. \\
&\quad + b \left[B_{22} \left(\frac{dv_0}{dy} + \frac{w_0}{R} \right) + D_{22} \left(\frac{d\psi_y}{dy} \right) \right] \left(\frac{d\delta \psi_y}{dy} \right) \\
&\quad \left. + b \left[K_s A_{44} \left(\psi_y + \frac{dw_0}{dy} - \frac{v_0}{R} \right) \right] \left(\delta \psi_y + \frac{d\delta w_0}{dy} - \frac{\delta v_0}{R} \right) \right\} dy \\
&\quad + [\text{Boundary Terms}]_{y=y_1}^{y=y_2} - \int_{y_1}^{y_2} q_{\text{total}} \cdot \delta w_0 dy,
\end{aligned} \tag{3.28}$$

$$\begin{aligned}
0 &= \{ \delta \pi \}_{\text{Nonlinear}} = \{ \delta U + \delta V \}_{\text{Nonlinear}} \\
&= \int_{y_1}^{y_2} \left\{ b \left[A_{22} \left[\frac{dv_0}{dy} + \frac{w_0}{R} + \frac{1}{2} \left(\frac{v_0}{R} - \frac{dw_0}{dy} \right)^2 \right] + B_{22} \left(\frac{d\psi_y}{dy} \right) \right] \right. \\
&\quad \left[\frac{d\delta v_0}{dy} + \frac{\delta w_0}{R} + \left(\frac{v_0}{R} - \frac{dw_0}{dy} \right) \left(\frac{\delta v_0}{R} - \frac{d\delta w_0}{dy} \right) \right] \\
&\quad + b \left[B_{22} \left[\frac{dv_0}{dy} + \frac{w_0}{R} + \frac{1}{2} \left(\frac{v_0}{R} - \frac{dw_0}{dy} \right)^2 \right] + D_{22} \left(\frac{d\psi_y}{dy} \right) \right] \left(\frac{d\delta \psi_y}{dy} \right) \\
&\quad \left. + b \left[K_s A_{44} \left(\psi_y + \frac{dw_0}{dy} - \frac{v_0}{R} \right) \right] \left(\delta \psi_y + \frac{d\delta w_0}{dy} - \frac{\delta v_0}{R} \right) \right\} dy \\
&\quad + [\text{Boundary Terms}]_{y=y_1}^{y=y_2} - \int_{y_1}^{y_2} q_{\text{total}} \cdot \delta w_0 dy.
\end{aligned} \tag{3.29}$$

For a typical element, consider three displacement vectors, v_0 , w_0 , and ψ_y , as linear combinations of Lagrange interpolation functions in the form of

$$v_0(y) = \sum_{j=1}^l v_j \phi_j^{(1)}(y),$$

$$w_0(y) = \sum_{j=1}^m w_j \phi_j^{(2)}(y),$$

(3.30)

and

$$\psi_y(y) = \sum_{j=1}^n \psi_{yj} \phi_j^{(3)}(y).$$

where $\phi_j^{(1)}$, $\phi_j^{(2)}$, and $\phi_j^{(3)}$ are the interpolation functions of degrees l-1, m-1, and n-1, respectively; v_j , w_j , and ψ_{yj} are the nodal values of v_0 , w_0 , and ψ_y , respectively.

Substituting of equation (3.30) into (3.28), and letting $\delta v_0 = \phi_i^{(1)}$, $\delta w_0 = \phi_i^{(2)}$, and $\delta \psi_y = \phi_i^{(3)}$, leads to a typical linear finite-element equation of an arch or ring structure as follows:

$$\left[\mathbf{k}^{(e)} \right]_{\mathbb{L}} \{ \mathbf{u} \} = \{ \mathbf{f}^{(e)} \} \quad (3.31)$$

where $\{ \mathbf{u} \} = \{ \{ v_0 \}, \{ w_0 \}, \{ \psi_y \} \}^T$ is the displacement vector, $\left[\mathbf{k}^{(e)} \right]_{\mathbb{L}}$ is the linear element stiffness matrix, and $\{ \mathbf{f}^{(e)} \}$ is the force vector.

For the expressions in matrix form, one can also obtain an alternative form as:

$$\left[\begin{array}{c} \left[\mathbf{k}^{11} \right] \\ \left[\mathbf{k}^{12} \right] \\ \left[\mathbf{k}^{13} \right] \end{array} \right]_{(e)} \left[\begin{array}{c} \left[\mathbf{k}^{12} \right] \\ \left[\mathbf{k}^{22} \right] \\ \left[\mathbf{k}^{23} \right] \end{array} \right]_{(e)} \left[\begin{array}{c} \left[\mathbf{k}^{13} \right] \\ \left[\mathbf{k}^{23} \right] \\ \left[\mathbf{k}^{33} \right] \end{array} \right]_{(e)} \left\{ \begin{array}{c} \{ v_0 \} \\ \{ w_0 \} \\ \{ \psi_y \} \end{array} \right\} = \left\{ \begin{array}{c} \{ f^1 \} \\ \{ f^2 \} \\ \{ f^3 \} \end{array} \right\}_{(e)} \quad (3.32)$$

In the interest of brevity, the corresponding components of the element stiffness matrix $\left[\mathbf{k}^{(e)} \right]_{\mathbb{L}}$ and the force vector $\{ \mathbf{f}^{(e)} \}$ are included in Appendix A.1.

Utilizing similar procedures as those for a linear ring element, substitution of equation (3.30) into (3.29) yields the nonlinear finite element equations as:

$$([\mathbf{k}^{(e)}]_{\text{L}} + [\mathbf{k}^{(e)}]_{\text{NL}})\{\mathbf{u}\} = \{\mathbf{f}^{(e)}\} \quad (3.33)$$

where the components of $[\mathbf{k}^{(e)}]_{\text{L}}$ and $\{\mathbf{f}^{(e)}\}$ are the same as those shown in Appendix A.1, and those of $[\mathbf{k}^{(e)}]_{\text{NL}}$ are also detailed in Appendix A.2. Note that $[\mathbf{k}^{(e)}]_{\text{L}}$ is a symmetric matrix, and $[\mathbf{k}^{(e)}]_{\text{NL}}$ is non-symmetrical.

3.10 Consideration of Elastic Foundations

For the purpose of analyzing the buckling and initial post-buckling behavior of rocket motors, we consider them first as circular rings completely filled with a soft elastic medium. The outer surface is considered as a thin composite layer, and the inner one is treated as an infinite set of radial springs.

The nonlinear elastic foundation is used to model the inner elastic core. Both the Winkler and Pasternak foundations are chosen to formulate the model for the present research in order to account for shear interactions between individual springs. The reaction pressure between the elastic body and the foundation is described by

$$q_f = - \left(K_0 w_0 + K_1 w_0^3 - K_G \frac{d^2 w_0}{dy^2} \right) \quad (3.34)$$

where q_f is the reactive force per unit circumferential length due to the interaction between the body and the foundation, K_0 , in force per unit square length, is the linear Winkler-foundation parameter, K_1 , in force per unit length to the fourth power, is the

nonlinear Winkler-foundation parameter, and K_G , in force per unit length, is the shear parameter of a Pasternak type of foundation.

A set of concise assumptions that provide a reasonable description of the behavior of the present elastic-foundation model is stated as follows:

1. The medium is considered to be homogeneous and isotropic.
2. The medium is always in contact with the ring before and after the body deforms.

Based on the above statements and formulation, the potential energy with the nonlinear elastic foundation, defined in equation (3.34), is obtained as:

$$V_f = \int_{y_1}^{y_2} \left[\frac{1}{2} K_0 w_0^2 \delta w_0 + \frac{1}{4} K_1 w_0^4 \delta w_0 + \frac{1}{2} K_G \left(\frac{dw_0}{dy} \right)^2 \right] dy \quad (3.35)$$

The virtual strain energy associated with the elastic foundation may also be obtained as:

$$\delta V_f = \int_{y_1}^{y_2} \left[K_0 w_0 \delta w_0 + K_1 w_0^3 \delta w_0 + K_G \left(\frac{dw_0}{dy} \right) \left(\frac{d\delta w_0}{dy} \right) \right] dy \quad (3.36)$$

Using integration by parts on the derivatives of the displacement variable w_0 , equation (3.36) can be evaluated as:

$$\begin{aligned} \delta V_f = \int_{y_1}^{y_2} \left\{ \left(K_0 w_0 + K_1 w_0^3 \right) \delta w_0 - \frac{d}{dy} \left[K_G \left(\frac{dw_0}{dy} \right) \right] \delta w_0 \right\} dy \\ + \left[K_G \left(\frac{dw_0}{dy} \right) \delta w_0 \right]_{y=y_1}^{y=y_2} \end{aligned} \quad (3.37)$$

The equilibrium equation associated with δw_0 , which was expressed in equation (3.26), is altered as:

$$\delta w_0 \dots \frac{d\bar{Q}_{yz}}{dy} - \frac{\bar{N}_y}{R} + \frac{d}{dy} \left[\bar{N}_y \left(\frac{dw_0}{dy} - \frac{v_0}{R} \right) \right] + q_{\text{total}} = 0 \quad (3.38)$$

where

$$q_{\text{total}} = q_0 - \left[K_0 w_0 + K_1 w_0^3 - K_G \left(\frac{d^2 w_0}{dy^2} \right) \right] \quad (3.39)$$

The corresponding boundary conditions associated with the elastic foundation can also be obtained as:

Geometrical

Natural

$$w_0 = \hat{w}_0 \quad \text{or} \quad \bar{Q}_{yz} + \bar{N}_y \left(\frac{dw_0}{dy} - \frac{v_0}{R} \right) + K_G \left(\frac{dw_0}{dy} \right) = \hat{Q}_{yz} \quad (3.40)$$

With the additional virtual strain energy, δV_f , the variational formulation over an element, which was shown in equation (3.29), can be obtained as:

$$\int_{y_1}^{y_2} \{ \text{same as the ones of equation (3.29)} \} dy + [\text{Boundary Terms}]_{y=y_1}^{y=y_2} \quad (3.41)$$

$$- \int_{y_1}^{y_2} \{ [q_0 - (K_0 w_0 + K_1 w_0^3)] \cdot \delta w_0 - K_G \left(\frac{dw_0}{dy} \right) \left(\frac{d\delta w_0}{dy} \right) \} dy$$

The additional components of the $[k_{ij}^{22}]$ term of the finite-element equation, over an element, with the elastic foundation can be generated as follows:

$$\begin{aligned}
 [k_{ij}^{22}] &= \int_{y_1}^{y_2} \{ \text{same as the ones of equation (A.17)} \\
 &+ K_0 \phi_i^{(2)} \phi_j^{(2)} + K_1 w_0^2 \phi_i^{(2)} \phi_j^{(2)} + K_G \left(\frac{d\phi_i^{(2)}}{dy} \right) \left(\frac{d\phi_j^{(2)}}{dy} \right) \} dy
 \end{aligned}
 \tag{3.42}$$

3.11 Linear and Nonlinear Buckling Analyses

For complex, composite, curved structures and the theory of large deformations, the coupling relations between different displacement vectors sometimes produce significant pre-buckling deformations before the elastic bodies even reach the buckling stage. It is, however, also critical for design purposes to have approximate estimates of the critical buckling loads and modes by performing a linearized stability analysis.

Moreover, for post-buckling, imperfection sensitivity analysis, predictions of the buckling loads and modes become extremely important for further nonlinear buckling and post-buckling analysis. For the analysis of elastic bodies on elastic foundations, the estimated results of eigenvalues and vectors will provide the tendency of the deformable behavior and the symmetric conditions before and after buckling occurs. One can reduce the computational effort and expense for nonlinear analysis by applying symmetry as much as possible.

In general, there are two major types of buckling phenomena: the bifurcation point and limit point types of buckling. For the determination of the bifurcation points, linear eigenvalue analysis will be selected. But, in most of the general cases, including the imperfection sensitivity analysis, loss of stability occurs at a limit point rather than at a bifurcation point. In such cases the critical buckling load must be evaluated through solutions of a set of nonlinear equations of equilibrium for the purpose of accuracy. The following sub-chapters are to explain the theories of linear and nonlinear analyses of elastic rings.

3.11.1 Linear Eigenvalue Analysis

Under the external loading of uniform radial pressure q_0 (force per unit length), the circumferential normal stress $b \sigma_y$ generated in the ring body can be expressed as

$$\bar{N}_y^0 = b h \sigma_y = R(q_0) \quad (3.43)$$

where R is the radius, and h is the thickness of the ring.

The potential energy associated with an initially circumferential compressive load \bar{N}_y^0 is given as

$$V_p = \int_{y_1}^{y_2} \left[\frac{1}{2} \bar{N}_y^0 \left(\frac{dw_0}{dy} - \frac{v_0}{R} \right)^2 \right] dy \quad (3.44)$$

where \bar{N}_y^0 has a positive sign for a tensile load, and negative sign for a compressive one.

The virtual work done by an initially circumferential compressive load \bar{N}_y^0 is also given as

$$\delta V_p = \int_{y_1}^{y_2} \left[\bar{N}_y^0 \left(\frac{dw_0}{dy} - \frac{v_0}{R} \right) \left(\frac{d\delta w_0}{dy} - \frac{\delta v_0}{R} \right) \right] dy \quad (3.45)$$

Integration by parts on the derivative of the displacement variable w_0 of equation (3.45) leads to

$$\begin{aligned} \delta V_p = & \int_{y_1}^{y_2} \left\{ -\frac{d}{dy} \left[\bar{N}_y^0 \left(\frac{dw_0}{dy} - \frac{v_0}{R} \right) \right] \delta w_0 \right\} dy - \int_{y_1}^{y_2} \left\{ \left[\bar{N}_y^0 \left(\frac{dw_0}{dy} - \frac{v_0}{R} \right) \right] \frac{\delta v_0}{R} \right\} dy \\ & + \left[\bar{N}_y^0 \left(\frac{dw_0}{dy} - \frac{v_0}{R} \right) \delta w_0 \right]_{y=y_1}^{y=y_2} \end{aligned} \quad (3.46)$$

In association with δv_0 and δw_0 , respectively, the equilibrium equations governing the stability of an elastic ring may be obtained as:

$$\delta v_0 \dots \dots \frac{d\bar{N}_y}{dy} + \frac{\bar{Q}_{yz}}{R} + \frac{\bar{N}_y^0}{R} \left(\frac{dw_0}{dy} - \frac{v_0}{R} \right) = 0 \quad (3.47)$$

$$\delta w_0 \dots \dots \frac{d\bar{Q}_{yz}}{dy} - \frac{\bar{N}_y}{R} + q_f + \frac{d}{dy} \left[\bar{N}_y^0 \left(\frac{dw_0}{dy} - \frac{v_0}{R} \right) \right] = 0 \quad (3.48)$$

where q_f is the pressure (force per unit circumferential length) generated by the reaction from the linear Pasternak-elastic-foundation.

The corresponding boundary conditions can also obtained as:

Geometrical

Natural

$$w_0 = \widehat{w}_0 \quad \text{or} \quad \bar{Q}_{yz} + \bar{N}_y^0 \left(\frac{dw_0}{dy} - \frac{v_0}{R} \right) + K_G \left(\frac{dw_0}{dy} \right) = \widehat{Q}_{yz} \quad (3.49)$$

The additional components of the $[k_{ij}^{mn}]$ terms of the finite-element equations, over an element, can be generated as follows:

$$\begin{aligned} [k_{ij}^{11}] &= \int_{y_1}^{y_2} \{ \text{same as the ones of equation (A.1)} \\ &+ \frac{\bar{N}_y^0}{R^2} \phi_i^{(1)} \phi_j^{(1)} \} dy \end{aligned} \quad (3.50)$$

$$\begin{aligned} [k_{ij}^{12}] &= \int_{y_1}^{y_2} \{ \text{same as the ones of equation (A.2)} \\ &- \frac{\bar{N}_y^0}{R} \phi_i^{(1)} \frac{d\phi_j^{(2)}}{dy} \} dy \end{aligned} \quad (3.51)$$

$$\begin{aligned} [k_{ij}^{21}] &= \int_{y_1}^{y_2} \{ \text{same as the ones of equation (A.4)} \\ &- \frac{\bar{N}_y^0}{R} \frac{d\phi_i^{(2)}}{dy} \phi_j^{(1)} \} dy \end{aligned} \quad (3.52)$$

$$\begin{aligned} [k_{ij}^{22}] &= \int_{y_1}^{y_2} \{ \text{same as the ones of equation (A.5)} \\ &+ K_0 \phi_i^{(2)} \phi_j^{(2)} + K_G \left(\frac{d\phi_i^{(2)}}{dy} \right) \left(\frac{d\phi_j^{(2)}}{dy} \right) + \bar{N}_y^0 \left(\frac{d\phi_i^{(2)}}{dy} \right) \left(\frac{d\phi_j^{(2)}}{dy} \right) \} dy \end{aligned} \quad (3.53)$$

Substituting equations (3.50) to (3.53) into equation (3.32), for the eigenvalue analysis, the finite element model takes the form:

$$\begin{bmatrix} \begin{bmatrix} k^{11} \\ k^{12} \\ k^{13} \end{bmatrix} \\ \begin{bmatrix} k^{12} \\ k^{22} \\ k^{23} \end{bmatrix} \\ \begin{bmatrix} k^{13} \\ k^{23} \\ k^{33} \end{bmatrix} \end{bmatrix}_{(e)} \begin{Bmatrix} \{v_0\} \\ \{w_0\} \\ \{\psi_y\} \end{Bmatrix} = (\lambda) \begin{bmatrix} \begin{bmatrix} S^{11} \\ S^{21} \\ 0 \end{bmatrix} \\ \begin{bmatrix} S^{12} \\ S^{22} \\ 0 \end{bmatrix} \\ \begin{bmatrix} 0 \\ 0 \\ S^{33} \end{bmatrix} \end{bmatrix}_{(e)} \quad (3.54)$$

where the components of k_{ij}^{mn} ($m, n = 1, 2, 3$) were defined in Appendix A.1 and equation (3.42), which is associated with the elastic foundations,

$$S_{ij}^{13} = S_{ij}^{23} = S_{ij}^{31} = S_{ij}^{32} = S_{ij}^{33} = 0, \quad (3.55)$$

and

$$[S_{ij}^{11}] = \int_{y_1}^{y_2} \left\{ \frac{1}{R^2} \phi_i^{(1)} \phi_j^{(1)} \right\} dy. \quad (3.56)$$

$$[S_{ij}^{12}] = \int_{y_1}^{y_2} \left\{ -\frac{1}{R} \phi_i^{(1)} \frac{d\phi_j^{(2)}}{dy} \right\} dy. \quad (3.57)$$

$$[S_{ij}^{21}] = \int_{y_1}^{y_2} \left\{ -\frac{1}{R} \frac{d\phi_i^{(2)}}{dy} \phi_j^{(1)} \right\} dy. \quad (3.58)$$

$$[S_{ij}^{22}] = \int_{y_1}^{y_2} \left\{ \left(\frac{d\phi_i^{(2)}}{dy} \right) \left(\frac{d\phi_j^{(2)}}{dy} \right) \right\} dy. \quad (3.59)$$

Solving the eigenvalue problem defined by equations (3.54) to (3.59), one can obtain a set of eigenvalues and the corresponding eigenvectors. The minimum eigenvalue and the

corresponding eigenvector provide the information of the critical buckling load and mode. Similarly, the critical buckling pressure can also be evaluated by using the relation shown in equation (3.43).

3.11.2 Nonlinear Buckling and Initial Post-Buckling Analysis

Note that the solutions of the eigenvalue analysis only provide an approximate estimate of buckling loads. In the present study, the behavior of buckling and initial post-buckling of elastic arches and rings is governed by a set of nonlinear partial differential equations, which were modeled as the finite element equations defined in equation (3.33). Introducing the nonlinear elastic foundations and geometrical nonlinearity, the accuracy of the results of the linear buckling analysis may be far different from the real ones. So, some numerically nonlinear schemes should be applied for solving the problems by using incremental iterative processes. The Newton-Raphson and Riks-Wempner methods will be applied. The detailed descriptions and algorithms of these schemes will be introduced in Chapter 6.

In order to use these schemes, the tangent stiffness matrix for a nonlinear ring, apart from equation (3.33), needs to be determined first. The procedure of determining the tangent stiffness matrix is shown as follows:

Let

$$R_i = \sum_{j=1}^1 k_{ij}^{11} v_j + \sum_{j=1}^m k_{ij}^{12} w_j + \sum_{j=1}^1 k_{ij}^{13} \psi_{yj} - F_i^1, \quad (3.60)$$

$$R_2 = \sum_{j=1}^l k_{ij}^{21} v_j + \sum_{j=1}^m k_{ij}^{22} w_j + \sum_{j=1}^l k_{ij}^{23} \psi_{yj} - F_i^2, \quad (3.61)$$

and

$$R_3 = \sum_{j=1}^l k_{ij}^{31} v_j + \sum_{j=1}^m k_{ij}^{32} w_j + \sum_{j=1}^l k_{ij}^{33} \psi_{yj} - F_i^3. \quad (3.62)$$

where R_1 , R_2 , and R_3 are the residual force vectors associated with three different directions, separately; the other components of the equations (3.60) to (3.62) are defined in Appendix A.2.

From the definition of the tangent stiffness matrix, one obtains

$$(k_T)_{ij}^{pq} = \frac{\partial R_p}{\partial U_q} = k_{ij}^{pq} + \sum_{k=1}^3 \frac{\partial k_{ij}^{pq}}{\partial U_k} U_k \quad (3.63)$$

where

$$R_p = (k_{ij}^{pq}) U_q - F_p \quad (p, q = 1, 2, 3) \quad (3.64)$$

Introducing equations (3.60) to (3.64), the element tangent stiffness matrix, over an element, can be generated as:

$$[k_T]_{(e)} = \left[\begin{array}{c} [k^{11}] \\ [k^{12}] \\ [k^{13}] \end{array} \left[\begin{array}{c} [k^{12}] \\ [k^{22}] \\ [k^{23}] \end{array} \right] \left[\begin{array}{c} [k^{13}] \\ [k^{23}] \\ [k^{33}] \end{array} \right] \right]_{(e)} \quad (3.65)$$

The coefficients of the element tangent stiffness matrix are included in Appendix B. Note that the tangent stiffness matrix is symmetric.

CHAPTER 4

GENERAL EQUATIONS FOR CIRCULAR CYLINDRICAL SHELLS

4.1 Introduction and Basic Assumptions

It is quite difficult to solve the buckling and post-buckling problems through a direct application of the general nonlinear theory of elasticity, owing to mathematical and physical complexities. The fundamental equations of three-dimensional elasticity theory can be simplified and approximated into a two-dimensional formulation for thin-walled, flexible bodies. In contrast to the counterparts stated in Chapter 3, the formulation of a general two-dimensional model for cylindrical shells based on Sanders' thin shell theory [20, 33] will be reviewed.

Unlike the traditional classical theory, known as Love's first approximation theory [15], the present formulation is based on the first order shear deformable theory. It takes into account the transverse shear flexibility of layered anisotropic composites. To account for the parabolic distribution of transverse shear stresses, shear correction factors are used.

Using an extension of Sanders' shell theory, a displacement-based finite element model, for both linear and nonlinear analyses, is developed and is shown in the following sub-chapters. For the portion of geometrical nonlinearity, the von Karman nonlinear strains [140] are incorporated.

The major assumptions for supporting the present theory of thin cylindrical shells on elastic foundations are:

1. Sections originally perpendicular to the reference axis of the ring will remain plane, but not necessarily normal to the deformed mid-surface because of transverse shears.
2. The shell is sufficiently thin so that the thickness is small compared to other dimensions.
3. The transverse thickness is considered to be inextensible.
4. Transverse normal stress is small compared to other normal stress components, and can be neglected.
5. Strains are sufficiently small, and Hooke's law applies; in other words, material behavior is within the linearly elastic range.
6. Rotations of shell elements about the normal planes are allowed to be moderately large so that, in the second order terms, the derivatives of in-plane displacements are small compared to the derivatives of the out-of-plane displacements (the von Karman theory holds).
7. There is a perfect bond between the shell and the elastic foundation.

4.2 Displacement Field

The laminated cylindrical shell under consideration is composed of a finite number of orthotropic laminae of arbitrarily oriented fiber angles with respect to the shell coordinate system, as shown in Figure 4.1. Based on the first order shear deformable theory, one can

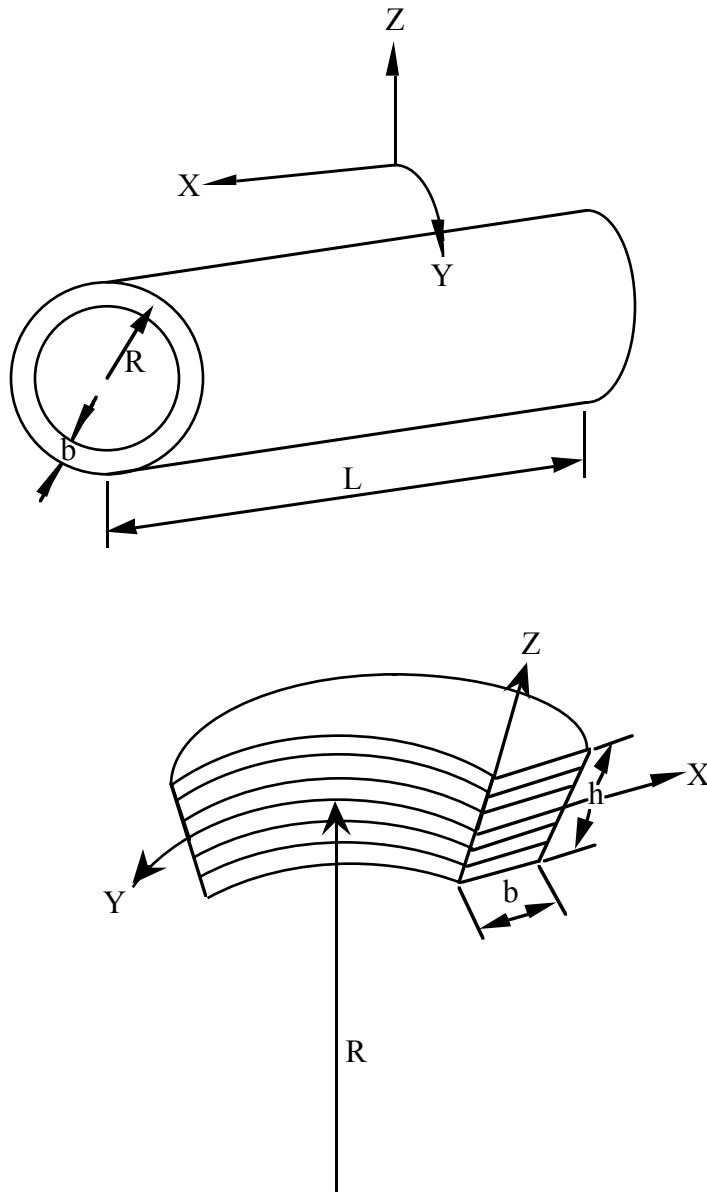


Figure 4.1 - Geometry and coordinate system of a cylindrical shell

assume the displacement vectors at a generic point (x, y, z) in the body, for both linear and nonlinear theories, to be of the following form:

$$u(x, y, z) = u_0(x, y) + z \psi_x(x, y)$$

$$v(x, y, z) = v_0(x, y) + z \psi_y(x, y) \tag{4.1}$$

$$w(x, y, z) = w_0(x, y)$$

where u , v , and w are the total displacements, and u_0 , v_0 , and w_0 are the associated mid-surface displacements in the x , y , and z directions, respectively; ψ_x is the rotation about the y -axis (in the xz plane); ψ_y is the rotation about the x -axis (in the yz plane).

4.3 Kinematic (Strain-Displacement) Relations

4.3.1 Linear Formulation

With the displacement fields defined in equation (4.1) and the assumptions stated in Chapter 4.1, the linear strain-displacement relations of a cylinder in an orthogonal cylindrical coordinate system are shown as [20, 145, 146]:

$$e_x = e_x^0 + z \kappa_x^0 \tag{4.2}$$

$$e_y = e_y^0 + z \kappa_y^0$$

$$e_z = 0$$

$$\gamma_{yz} = \gamma_{yz}^0$$

$$\gamma_{xz} = \gamma_{xz}^0$$

$$\gamma_{xy} = \gamma_{xy}^0 + z\kappa_{xy}^0$$

(4.2)

where

$$e_x^0 = \frac{\partial u_0}{\partial x}$$

$$e_y^0 = \frac{\partial v_0}{\partial y} + \frac{w_0}{R}$$

$$\gamma_{xy}^0 = \frac{\partial u_0}{\partial y} + \frac{\partial v_0}{\partial x}$$

$$\kappa_x^0 = \frac{\partial \psi_x}{\partial x}$$

$$\kappa_y^0 = \frac{\partial \psi_y}{\partial y}$$

(4.3)

$$\kappa_{xy}^0 = \frac{\partial \psi_x}{\partial y} + \frac{\partial \psi_y}{\partial x} - C_0 \left(\frac{\partial v_0}{\partial x} - \frac{\partial u_0}{\partial y} \right)$$

$$\gamma_{yz}^0 = \psi_y + \frac{\partial w_0}{\partial y} - \frac{v_0}{R}$$

$$\gamma_{xz}^0 = \psi_x + \frac{\partial w_0}{\partial x}$$

$$C_0 = -\frac{1}{2R}$$

in which the C_0 term is introduced by Sanders [20] and accounts for the condition of zero strain for rigid body motion.

4.3.2 Non-linear Formulation

Under the assumptions of small strains and moderate rotations about the reference surface of the shell, the von Karman type of nonlinear strains are considered in the study of nonlinear behavior. The rotation components with respect to the normal to the shell reference surface are negligible when thin walled structures are considered; where the ratio of thickness-to-radius is relatively small compared to unity. The nonlinear strain-displacement relations in an orthogonal cylindrical coordinate system are:

$$e_x^0 = \frac{\partial u_0}{\partial x} + \frac{1}{2} \left(\frac{\partial w_0}{\partial x} \right)^2$$

$$e_y^0 = \frac{\partial v_0}{\partial y} + \frac{w_0}{R} + \frac{1}{2} \left(\frac{v_0}{R} - \frac{\partial w_0}{\partial y} \right)^2 \quad (4.4)$$

$$\gamma_{xy}^0 = \frac{\partial u_0}{\partial y} + \frac{\partial v_0}{\partial x} + \left(\frac{\partial w_0}{\partial x} \right) \left(\frac{\partial w_0}{\partial y} - \frac{v_0}{R} \right)$$

where the relations of the remaining strain components are the same as the corresponding ones of the linear theory.

4.4 Mechanical Behavior of a Lamina

It is the same as those stated in Chapter 3.4.

4.5 Constitutive Equations of a Laminate

It is the same as those stated in Chapter 3.5.

4.6 Stress and Moment Resultants

It is the same as those stated in Chapter 3.6

4.7 Virtual Work Statement

The principle of minimization of total potential energy for the present problem implies that

$$\delta \Pi = \delta U + \delta V = 0 \tag{4.5}$$

where Π is the total potential energy, U is the total strain energy of the elastic body; V is the total potential energy of applied loads; δ denotes the variational operator.

The virtual strain energy of a cylindrical shell associated with internal stresses is given as:

$$\delta U = \int_{\Omega} \int_{-\frac{h}{2}}^{\frac{h}{2}} (\sigma_{xx} \delta e_{xx} + \sigma_{yy} \delta e_{yy} + \tau_{xy} \delta \gamma_{xy} + \tau_{yz} \delta \gamma_{yz} + \tau_{xz} \delta \gamma_{xz}) dz dA, \quad (4.6)$$

where Ω is the cross-sectional area of the elastic body along the x-y plane.

The virtual work generated by the applied loads along the domain is of the form:

$$\delta V = - \int_{\Omega} p_{\text{total}} \cdot \delta w \, dA \quad (4.7)$$

where p_{total} is the applied radial pressure (force per unit area).

Substitutions of the strain-displacement relations into the total potential energy equation, utilizing also the expressions of stress and moment resultants, leads to the following weak form of the virtual work statement:

$$\begin{aligned} 0 = \int_{\Omega} (N_x \delta e_{xx}^0 + N_y \delta e_{yy}^0 + N_{xy} \delta \gamma_{xy}^0 + M_x \delta \kappa_x^0 + M_y \delta \kappa_y^0 + M_{xy} \delta \kappa_{xy}^0 \\ + Q_{yz} \delta \gamma_{yz}^0 + Q_{xz} \delta \gamma_{xz}^0) dA - \int_{\Omega} p_{\text{total}} \cdot \delta w_0 \, dA \end{aligned} \quad (4.8)$$

where the components of N , M , and Q are defined in Chapter 3.6.

Introduction of equations (4.2) and (4.3), equation (4.8) can be expressed as the linear version of weak formulation:

$$\begin{aligned}
0 = & \int_{\Omega} \left[N_x \left(\frac{\partial \delta u_0}{\partial x} \right) + N_y \left(\frac{\partial \delta v_0}{\partial y} + \frac{\delta w_0}{R} \right) + N_{xy} \left(\frac{\partial \delta u_0}{\partial y} + \frac{\partial \delta v_0}{\partial x} \right) \right. \\
& + M_x \left(\frac{\partial \delta \psi_x}{\partial x} \right) + M_y \left(\frac{\partial \delta \psi_y}{\partial y} \right) + M_{xy} \left[\frac{\partial \delta \psi_x}{\partial y} + \frac{\partial \delta \psi_y}{\partial x} - C_0 \left(\frac{\partial \delta v_0}{\partial x} - \frac{\partial \delta u_0}{\partial y} \right) \right] \\
& + Q_{yz} \left(\delta \psi_y + \frac{\partial \delta w_0}{\partial y} - \frac{\delta v_0}{R} \right) + Q_{xz} \left(\delta \psi_x + \frac{\partial \delta w_0}{\partial x} \right) \left. \right] dA \\
& - \int_{\Omega} p_{\text{total}} \cdot \delta w_0 dA
\end{aligned} \tag{4.9}$$

Similarly, introduction of the nonlinear strain-displacement equations (4.2), (4.3), and (4.4) leads to the nonlinear weak form:

$$\begin{aligned}
0 = & \int_{\Omega} \left\{ N_x \left[\frac{\partial \delta u_0}{\partial x} + \left(\frac{\partial w_0}{\partial x} \right) \left(\frac{\partial \delta w_0}{\partial x} \right) \right] \right. \\
& + N_y \left[\frac{\partial \delta v_0}{\partial y} + \frac{\delta w_0}{R} + \left(\frac{\partial w_0}{\partial y} - \frac{v_0}{R} \right) \left(\frac{\partial \delta w_0}{\partial y} - \frac{\delta v_0}{R} \right) \right] \\
& + N_{xy} \left[\frac{\partial \delta u_0}{\partial y} + \frac{\partial \delta v_0}{\partial x} + \left(\frac{\partial \delta w_0}{\partial x} \right) \left(\frac{\partial w_0}{\partial y} - \frac{v_0}{R} \right) + \left(\frac{\partial w_0}{\partial x} \right) \left(\frac{\partial \delta w_0}{\partial y} - \frac{\delta v_0}{R} \right) \right] \\
& + M_x \left(\frac{\partial \delta \psi_x}{\partial x} \right) + M_y \left(\frac{\partial \delta \psi_y}{\partial y} \right) + M_{xy} \left[\frac{\partial \delta \psi_x}{\partial y} + \frac{\partial \delta \psi_y}{\partial x} - C_0 \left(\frac{\partial \delta v_0}{\partial x} - \frac{\partial \delta u_0}{\partial y} \right) \right] \\
& + Q_{yz} \left(\delta \psi_y + \frac{\partial \delta w_0}{\partial y} - \frac{\delta v_0}{R} \right) + Q_{xz} \left(\delta \psi_x + \frac{\partial \delta w_0}{\partial x} \right) \left. \right\} dA \\
& - \int_{\Omega} p_{\text{total}} \cdot \delta w_0 dA
\end{aligned} \tag{4.10}$$

4.8 Equilibrium Equations and the Associated Boundary Conditions

Utilizing integration by parts on the derivatives of various displacement variables of equations (4.9) and (4.10), one can obtain the equilibrium equations and the associated boundary conditions by collecting terms involving δu_0 , δv_0 , δw_0 , $\delta \psi_x$ and $\delta \psi_y$, respectively, as shown in the following sub-chapter:

4.8.1 Linear Relations

Based on the linear equations of strain-displacement relations as stated before, the equilibrium equations which govern the behavior of elastic cylindrical shells can be expressed as:

$$\begin{aligned}
 \delta u_0 \dots \frac{\partial N_x}{\partial x} + \frac{\partial N_{xy}}{\partial y} + C_0 \frac{\partial M_{xy}}{\partial y} &= 0 \\
 \delta v_0 \dots \frac{\partial N_{xy}}{\partial x} + \frac{\partial N_y}{\partial y} - C_0 \frac{\partial M_{xy}}{\partial x} + \frac{Q_{yz}}{R} &= 0 \\
 \delta w_0 \dots \frac{\partial Q_{xz}}{\partial x} + \frac{\partial Q_{yz}}{\partial y} - \frac{N_y}{R} + p_{\text{total}} &= 0 \\
 \delta \psi_x \dots \frac{\partial M_x}{\partial x} + \frac{\partial M_{xy}}{\partial y} - Q_{xz} &= 0
 \end{aligned} \tag{4.11}$$

$$\delta\psi_y \dots \frac{\partial M_{xy}}{\partial x} + \frac{\partial M_y}{\partial y} - Q_{yz} = 0$$

The associated geometric and natural boundary conditions are specified as:

Geometric

Natural

$$u_0 = \hat{u}_0$$

$$N_n = n_x N_x + n_y (N_{xy} + C_0 M_{xy}) = \hat{N}_n$$

$$v_0 = \hat{v}_0$$

$$N_t = n_x (N_{xy} - C_0 M_{xy}) + n_y N_y = \hat{N}_t$$

$$w_0 = \hat{w}_0$$

or

$$P_n = n_x Q_{xz} + n_y Q_{yz} = \hat{P}_n \quad (4.12)$$

$$\psi_x = \hat{\psi}_x$$

$$M_n = n_x M_x + n_y M_{xy} = \hat{M}_n$$

$$\psi_y = \hat{\psi}_y$$

$$M_t = n_x M_{xy} + n_y M_y = \hat{M}_t$$

where (n_x, n_y) denote the components of the unit outward normal vector on the boundary.

4.8.2 Non-linear Relations

Similarly, applying the non-linear equations of strain-displacement relations leads to a set of nonlinear governing differential equations of elastic cylindrical shells as:

$$\begin{aligned}
\delta u_0 \dots \frac{\partial N_x}{\partial x} + \frac{\partial N_{xy}}{\partial y} + C_0 \frac{\partial M_{xy}}{\partial y} &= 0 \\
\delta v_0 \dots \frac{\partial N_{xy}}{\partial x} + \frac{\partial N_y}{\partial y} - C_0 \frac{\partial M_{xy}}{\partial x} + \frac{Q_{yz}}{R} + \frac{N_{xy}}{R} \left(\frac{\partial w_0}{\partial x} \right) + \frac{N_y}{R} \left(\frac{\partial w_0}{\partial y} - \frac{v_0}{R} \right) &= 0 \\
\delta w_0 \dots \frac{\partial}{\partial x} \left[N_x \left(\frac{\partial w_0}{\partial x} \right) + N_{xy} \left(\frac{\partial w_0}{\partial y} - \frac{v_0}{R} \right) \right] + \frac{\partial}{\partial y} \left[N_{xy} \left(\frac{\partial w_0}{\partial x} \right) + N_y \left(\frac{\partial w_0}{\partial y} - \frac{v_0}{R} \right) \right] \\
\frac{\partial Q_{xz}}{\partial x} + \frac{\partial Q_{yz}}{\partial y} - \frac{N_y}{R} + p_{\text{total}} &= 0 \\
\delta \psi_x \dots \frac{\partial M_x}{\partial x} + \frac{\partial M_{xy}}{\partial y} - Q_{xz} &= 0 \\
\delta \psi_y \dots \frac{\partial M_{xy}}{\partial x} + \frac{\partial M_y}{\partial y} - Q_{yz} &= 0
\end{aligned} \tag{4.13}$$

The geometric and natural boundary conditions associated with the nonlinear theory are specified as:

Geometric

Natural

$$u_0 = \hat{u}_0$$

$$N_n = n_x N_x + n_y (N_{xy} + C_0 M_{xy}) = \hat{N}_n$$

$$v_0 = \hat{v}_0$$

$$N_t = n_x (N_{xy} - C_0 M_{xy}) + n_y N_y = \hat{N}_t$$

$$\begin{aligned}
w_0 = \widehat{w}_0 \quad \text{or} \quad P_n &= n_x \left[N_x \left(\frac{\partial w_0}{\partial x} \right) + N_{xy} \left(\frac{\partial w_0}{\partial y} - \frac{v_0}{R} \right) \right] \\
&+ n_y \left[N_{xy} \left(\frac{\partial w_0}{\partial x} \right) + N_y \left(\frac{\partial w_0}{\partial y} - \frac{v_0}{R} \right) \right] \\
&+ n_x Q_{xz} + n_y Q_{yz} = \widehat{P}_n
\end{aligned} \tag{4.14}$$

$$\psi_x = \widehat{\psi}_x \quad M_n = n_x M_x + n_y M_{xy} = \widehat{M}_n$$

$$\psi_y = \widehat{\psi}_y \quad M_t = n_x M_{xy} + n_y M_y = \widehat{M}_t$$

4.9 Weak Formulation and Finite Element Model

4.9.1 Linear Finite Element Equations

Introduction of the equations of stress and moment resultants of a composite, which were represented by equations (3.14) to (3.16), the linear variational formulations of the minimum potential energy statement (equations (4.9)) can be rewritten in terms of displacement vectors only by using the strain-displacement relations of equations (4.2) and (4.3) as follows:

$$\begin{aligned}
0 &= \{ \delta \Pi \}_{\text{Linear}} = \{ \delta U + \delta V \}_{\text{Linear}} \\
&= \{ \delta U_s + \delta U_b + \delta U_{bs} + \delta U_T + \delta V \}_{\text{Linear}}
\end{aligned} \tag{4.15}$$

where $\{ \delta U_s \}_{\text{Linear}}$ is the variational strain energy term caused by in-plane stretching alone,

$$\begin{aligned}
\{\delta U_s\}_{\text{Linear}} = \int_{\Omega} \{ & A_{11} \left(\frac{\partial u_0}{\partial x} \right) \left(\frac{\partial \delta u_0}{\partial x} \right) + A_{22} \left(\frac{\partial v_0}{\partial y} + \frac{w_0}{R} \right) \left(\frac{\partial \delta v_0}{\partial y} + \frac{\delta w_0}{R} \right) \\
& + A_{66} \left(\frac{\partial u_0}{\partial y} + \frac{\partial v_0}{\partial x} \right) \left(\frac{\partial \delta u_0}{\partial y} + \frac{\partial \delta v_0}{\partial x} \right) + A_{12} \left(\frac{\partial v_0}{\partial y} + \frac{w_0}{R} \right) \left(\frac{\partial \delta u_0}{\partial x} \right) \\
& + A_{12} \left(\frac{\partial u_0}{\partial x} \right) \left(\frac{\partial \delta v_0}{\partial y} + \frac{\delta w_0}{R} \right) + A_{16} \left(\frac{\partial u_0}{\partial y} + \frac{\partial v_0}{\partial x} \right) \left(\frac{\partial \delta u_0}{\partial x} \right) \\
& + A_{16} \left(\frac{\partial u_0}{\partial x} \right) \left(\frac{\partial \delta u_0}{\partial y} + \frac{\partial \delta v_0}{\partial x} \right) + A_{26} \left(\frac{\partial u_0}{\partial y} + \frac{\partial v_0}{\partial x} \right) \left(\frac{\partial \delta v_0}{\partial y} + \frac{\delta w_0}{R} \right) \\
& + A_{26} \left(\frac{\partial v_0}{\partial y} + \frac{w_0}{R} \right) \left(\frac{\partial \delta u_0}{\partial y} + \frac{\partial \delta v_0}{\partial x} \right) \} dA,
\end{aligned} \tag{4.16}$$

$\{\delta U_b\}_{\text{Linear}}$ is the variational strain energy term caused by bending alone,

$$\begin{aligned}
\{\delta U_b\}_{\text{Linear}} = \int_{\Omega} \{ & D_{11} \left(\frac{\partial \psi_x}{\partial x} \right) \left(\frac{\partial \delta \psi_x}{\partial x} \right) + D_{22} \left(\frac{\partial \psi_y}{\partial y} \right) \left(\frac{\partial \delta \psi_y}{\partial y} \right) \\
& + D_{66} \left(\frac{\partial \psi_y}{\partial x} + \frac{\partial \psi_x}{\partial y} \right) \left[\frac{\partial \delta \psi_x}{\partial y} + \frac{\partial \delta \psi_y}{\partial x} - C_0 \left(\frac{\partial \delta v_0}{\partial x} - \frac{\partial \delta u_0}{\partial y} \right) \right] \\
& + D_{12} \left(\frac{\partial \psi_x}{\partial x} \right) \left(\frac{\partial \delta \psi_y}{\partial y} \right) + D_{12} \left(\frac{\partial \psi_y}{\partial y} \right) \left(\frac{\partial \delta \psi_x}{\partial x} \right) \\
& + D_{16} \left[\frac{\partial \psi_x}{\partial y} + \frac{\partial \psi_y}{\partial x} - C_0 \left(\frac{\partial v_0}{\partial x} - \frac{\partial u_0}{\partial y} \right) \right] \left(\frac{\partial \delta \psi_x}{\partial x} \right) \\
& + D_{16} \left(\frac{\partial \psi_x}{\partial x} \right) \left[\frac{\partial \delta \psi_x}{\partial y} + \frac{\partial \delta \psi_y}{\partial x} - C_0 \left(\frac{\partial \delta v_0}{\partial x} - \frac{\partial \delta u_0}{\partial y} \right) \right] \\
& + D_{26} \left[\frac{\partial \psi_x}{\partial y} + \frac{\partial \psi_y}{\partial x} - C_0 \left(\frac{\partial v_0}{\partial x} - \frac{\partial u_0}{\partial y} \right) \right] \left(\frac{\partial \delta \psi_y}{\partial y} \right) \\
& + D_{26} \left(\frac{\partial \psi_y}{\partial y} \right) \left[\frac{\partial \delta \psi_x}{\partial y} + \frac{\partial \delta \psi_y}{\partial x} - C_0 \left(\frac{\partial \delta v_0}{\partial x} - \frac{\partial \delta u_0}{\partial y} \right) \right] \} dA,
\end{aligned} \tag{4.17}$$

$\{\delta U_{bs}\}_{\text{Linear}}$ is the variational strain energy term caused by bending-stretching coupling alone,

$$\begin{aligned}
\{\delta U_{bs}\}_{\text{Linear}} = & \int_{\Omega} \left\{ B_{11} \left(\frac{\partial \psi_x}{\partial x} \right) \left(\frac{\partial \delta u_0}{\partial x} \right) + B_{11} \left(\frac{\partial u_0}{\partial x} \right) \left(\frac{\partial \delta \psi_x}{\partial x} \right) \right. \\
& + B_{22} \left(\frac{\partial v_0}{\partial y} + \frac{w_0}{R} \right) \left(\frac{\partial \delta \psi_y}{\partial y} \right) + B_{22} \left(\frac{\partial \psi_y}{\partial y} \right) \left(\frac{\partial \delta v_0}{\partial y} + \frac{\delta w_0}{R} \right) \\
& + B_{66} \left(\frac{\partial u_0}{\partial y} + \frac{\partial v_0}{\partial x} \right) \left[\frac{\partial \delta \psi_x}{\partial y} + \frac{\partial \delta \psi_y}{\partial x} - C_0 \left(\frac{\partial \delta v_0}{\partial x} - \frac{\partial \delta u_0}{\partial y} \right) \right] \\
& + B_{66} \left[\frac{\partial \psi_x}{\partial y} + \frac{\partial \psi_y}{\partial x} - C_0 \left(\frac{\partial v_0}{\partial x} - \frac{\partial u_0}{\partial y} \right) \right] \left(\frac{\partial \delta u_0}{\partial y} + \frac{\partial \delta v_0}{\partial x} \right) \\
& + B_{12} \left(\frac{\partial \psi_x}{\partial x} \right) \left(\frac{\partial \delta u_0}{\partial x} \right) + B_{12} \left(\frac{\partial u_0}{\partial x} \right) \left(\frac{\partial \delta \psi_y}{\partial y} \right) \\
& + B_{12} \left(\frac{\partial \psi_y}{\partial y} \right) \left(\frac{\partial \delta v_0}{\partial y} + \frac{\delta w_0}{R} \right) + B_{12} \left(\frac{\partial v_0}{\partial y} + \frac{w_0}{R} \right) \left(\frac{\partial \delta \psi_x}{\partial x} \right) \\
& + B_{16} \left[\frac{\partial \psi_x}{\partial y} + \frac{\partial \psi_y}{\partial x} - C_0 \left(\frac{\partial v_0}{\partial x} - \frac{\partial u_0}{\partial y} \right) \right] \left(\frac{\partial \delta u_0}{\partial x} \right) \\
& + B_{16} \left(\frac{\partial u_0}{\partial x} \right) \left[\frac{\partial \delta \psi_x}{\partial y} + \frac{\partial \delta \psi_y}{\partial x} - C_0 \left(\frac{\partial \delta v_0}{\partial x} - \frac{\partial \delta u_0}{\partial y} \right) \right] \\
& + B_{16} \left(\frac{\partial \psi_x}{\partial x} \right) \left(\frac{\partial \delta u_0}{\partial y} + \frac{\partial \delta v_0}{\partial x} \right) + B_{16} \left(\frac{\partial u_0}{\partial y} + \frac{\partial v_0}{\partial x} \right) \left(\frac{\partial \delta \psi_x}{\partial x} \right) \\
& + B_{26} \left(\frac{\partial v_0}{\partial y} + \frac{w_0}{R} \right) \left[\frac{\partial \delta \psi_x}{\partial y} + \frac{\partial \delta \psi_y}{\partial x} - C_0 \left(\frac{\partial \delta v_0}{\partial x} - \frac{\partial \delta u_0}{\partial y} \right) \right] \\
& + B_{26} \left[\frac{\partial \psi_x}{\partial y} + \frac{\partial \psi_y}{\partial x} - C_0 \left(\frac{\partial v_0}{\partial x} - \frac{\partial u_0}{\partial y} \right) \right] \left(\frac{\partial \delta v_0}{\partial y} + \frac{\delta w_0}{R} \right) \\
& \left. + B_{26} \left(\frac{\partial \psi_y}{\partial y} \right) \left(\frac{\partial \delta u_0}{\partial y} + \frac{\partial \delta v_0}{\partial x} \right) + B_{26} \left(\frac{\partial u_0}{\partial y} + \frac{\partial v_0}{\partial x} \right) \left(\frac{\partial \delta \psi_y}{\partial y} \right) \right\} dA,
\end{aligned} \tag{4.18}$$

$\{\delta U_T\}_{\text{Linear}}$ denotes the variational strain energy term resulting from transverse shear deformations,

$$\begin{aligned}
\{\delta U_T\}_{\text{Linear}} = & \int_{\Omega} \left\{ K_s A_{44} \left(\psi_y + \frac{\partial w_0}{\partial y} - \frac{v_0}{R} \right) \left(\delta \psi_y + \frac{\partial \delta w_0}{\partial y} - \frac{\delta v_0}{R} \right) \right. \\
& + K_s A_{55} \left(\psi_x + \frac{\partial w_0}{\partial x} \right) \left(\delta \psi_x + \frac{\partial \delta w_0}{\partial x} \right) \\
& + K_s A_{45} \left(\psi_x + \frac{\partial w_0}{\partial x} \right) \left(\delta \psi_y + \frac{\partial \delta w_0}{\partial y} - \frac{\delta v_0}{R} \right) \\
& \left. + K_s A_{45} \left(\psi_y + \frac{\partial w_0}{\partial y} - \frac{v_0}{R} \right) \left(\delta \psi_x + \frac{\partial \delta w_0}{\partial x} \right) \right\} dA,
\end{aligned} \tag{4.19}$$

and $\{\delta V\}_{\text{Linear}}$ denotes the variational potential energy term due to applied loads,

$$\{\delta V\}_{\text{Linear}} = \int_{\Omega} \{ \mathbf{p}_{\text{total}} \cdot \delta \mathbf{w}_0 \} dA. \tag{4.20}$$

For a typical linear shell element, the generalized displacement vectors, \mathbf{u}_0 , \mathbf{v}_0 , w_0 , ψ_x and ψ_y , are interpolated by Lagrange interpolation functions of the form of

$$\begin{aligned}
\mathbf{u}_0(x, y) &= \sum_{j=1}^l \mathbf{u}_j \phi_j^{(1)}(\xi_1, \xi_2), \\
\mathbf{v}_0(x, y) &= \sum_{j=1}^m \mathbf{v}_j \phi_j^{(2)}(\xi_1, \xi_2), \\
w_0(x, y) &= \sum_{j=1}^n w_j \phi_j^{(3)}(\xi_1, \xi_2), \\
\psi_x(x, y) &= \sum_{j=1}^p \psi_{xj} \phi_j^{(4)}(\xi_1, \xi_2),
\end{aligned} \tag{4.21}$$

and

$$\psi_y(x, y) = \sum_{j=1}^q \psi_{yj} \phi_j^{(5)}(\xi_1, \xi_2),$$

where $\phi_j^{(1)}$, $\phi_j^{(2)}$, $\phi_j^{(3)}$, $\phi_j^{(4)}$, and $\phi_j^{(5)}$ are the interpolation functions of degrees l-1, m-1, n-1, p-1 and q-1 respectively; u_j , v_j , w_j , ψ_{xj} and ψ_{yj} are the nodal values of u_0 , v_0 , w_0 , ψ_x and ψ_y , respectively.

Substituting equation (4.21) into (4.15), and letting $\delta u_0 = \phi_i^{(1)}$, $\delta v_0 = \phi_i^{(2)}$, $\delta w_0 = \phi_i^{(3)}$, $\delta \psi_x = \phi_i^{(4)}$ and $\delta \psi_y = \phi_i^{(5)}$, leads to a typical linear finite-element equation of a cylindrical shell element as follows:

$$[k^{(e)}]_{\mathbb{L}} \{\Delta\} = \{f^{(e)}\} \quad (4.22)$$

where $\{\Delta\} = \{\{u_0\}, \{v_0\}, \{w_0\}, \{\psi_x\}, \{\psi_y\}\}^T$ is the generalized displacement vector, $[k^{(e)}]_{\mathbb{L}}$ is the linear element stiffness matrix, and $\{f^{(e)}\}$ is the element force vector.

One can also obtain an alternative expression in matrix form as:

$$\begin{bmatrix} [k^{11}] \\ [k^{21}] \\ [k^{31}] \\ [k^{41}] \\ [k^{51}] \end{bmatrix} \begin{bmatrix} [k^{12}] \\ [k^{22}] \\ [k^{32}] \\ [k^{42}] \\ [k^{52}] \end{bmatrix} \begin{bmatrix} [k^{13}] \\ [k^{23}] \\ [k^{33}] \\ [k^{43}] \\ [k^{53}] \end{bmatrix} \begin{bmatrix} [k^{14}] \\ [k^{24}] \\ [k^{34}] \\ [k^{44}] \\ [k^{54}] \end{bmatrix} \begin{bmatrix} [k^{15}] \\ [k^{25}] \\ [k^{35}] \\ [k^{45}] \\ [k^{55}] \end{bmatrix} \begin{Bmatrix} \{u_0\} \\ \{v_0\} \\ \{w_0\} \\ \{\psi_x\} \\ \{\psi_y\} \end{Bmatrix} = \begin{Bmatrix} \{f^1\} \\ \{f^2\} \\ \{f^3\} \\ \{f^4\} \\ \{f^5\} \end{Bmatrix} \quad (4.23)$$

In the interest of brevity, the corresponding components of the element stiffness matrix $[k^{(e)}]_{\mathbb{L}}$ and the force vector $\{f^{(e)}\}$ are included in Appendix C.1.

4.9.2 Non-linear Finite Element Equations

Utilizing similar procedures as those for a linear shell element, the nonlinear variational formulations of the minimum potential energy statement (equations (4.10)) can be expressed in terms of displacement vectors only by using the nonlinear strain-displacement relations of equations (4.2), (4.3) and (4.4) as follows:

$$\begin{aligned}
 0 &= \{ \delta \Pi \}_{\text{Linear}} + \{ \delta \Pi \}_{\text{Nonlinear}} \\
 &= \{ \delta U + \delta V \}_{\text{Linear}} + \{ \delta U \}_{\text{Nonlinear}} \quad (4.24) \\
 &= \{ \delta U_s + \delta U_b + \delta U_{bs} + \delta U_T + \delta V \}_{\text{Linear}} + \{ \delta U \}_{\text{Nonlinear}}
 \end{aligned}$$

where $\{ \delta U + \delta V \}_{\text{Linear}}$ is the variational energy, which is defined in Chapter 4.9.1, resulting from the linear theory.

The variational form of the total potential energy associated with nonlinear terms is obtained as:

$$\begin{aligned}
 \{ \delta U \}_{\text{Nonlinear}} &= \int_{\Omega} \{ A_{11} \left[\frac{\partial u_0}{\partial x} + \frac{1}{2} \left(\frac{\partial w_0}{\partial x} \right)^2 \right] \left(\frac{\partial w_0}{\partial x} \right) \left(\frac{\partial \delta w_0}{\partial x} \right) \right. \\
 &+ A_{12} \left[\frac{\partial v_0}{\partial y} + \frac{w_0}{R} + \frac{1}{2} \left(\frac{\partial w_0}{\partial y} - \frac{v_0}{R} \right)^2 \right] \left(\frac{\partial w_0}{\partial x} \right) \left(\frac{\partial \delta w_0}{\partial x} \right) \\
 &+ A_{16} \left[\frac{\partial u_0}{\partial y} + \frac{\partial v_0}{\partial x} + \left(\frac{\partial w_0}{\partial x} \right) \left(\frac{\partial w_0}{\partial y} - \frac{v_0}{R} \right) \right] \left(\frac{\partial w_0}{\partial x} \right) \left(\frac{\partial \delta w_0}{\partial x} \right) \\
 &+ B_{11} \left(\frac{\partial \psi_x}{\partial x} \right) \left(\frac{\partial w_0}{\partial x} \right) \left(\frac{\partial \delta w_0}{\partial x} \right) + B_{12} \left(\frac{\partial \psi_y}{\partial y} \right) \left(\frac{\partial w_0}{\partial x} \right) \left(\frac{\partial \delta w_0}{\partial x} \right) \\
 &\left. + B_{16} \left[\frac{\partial \psi_x}{\partial y} + \frac{\partial \psi_y}{\partial x} - C_0 \left(\frac{\partial v_0}{\partial x} - \frac{\partial u_0}{\partial y} \right) \right] \left(\frac{\partial w_0}{\partial x} \right) \left(\frac{\partial \delta w_0}{\partial x} \right) \right\}
 \end{aligned}$$

$$\begin{aligned}
& + \left[\frac{B_{11}}{2} \left(\frac{\partial w_0}{\partial x} \right)^2 + \frac{B_{12}}{2} \left(\frac{\partial w_0}{\partial y} - \frac{v_0}{R} \right)^2 + B_{16} \left(\frac{\partial w_0}{\partial x} \right) \left(\frac{\partial w_0}{\partial y} - \frac{v_0}{R} \right) \right] \left(\frac{\partial \delta \psi_x}{\partial x} \right) \\
& + \left[\frac{B_{12}}{2} \left(\frac{\partial w_0}{\partial x} \right)^2 + \frac{B_{22}}{2} \left(\frac{\partial w_0}{\partial y} - \frac{v_0}{R} \right)^2 + B_{26} \left(\frac{\partial w_0}{\partial x} \right) \left(\frac{\partial w_0}{\partial y} - \frac{v_0}{R} \right) \right] \left(\frac{\partial \delta \psi_y}{\partial y} \right) \\
& + \left[\frac{B_{16}}{2} \left(\frac{\partial w_0}{\partial x} \right)^2 + \frac{B_{26}}{2} \left(\frac{\partial w_0}{\partial y} - \frac{v_0}{R} \right)^2 + B_{66} \left(\frac{\partial w_0}{\partial x} \right) \left(\frac{\partial w_0}{\partial y} - \frac{v_0}{R} \right) \right] \\
& \left[\frac{\partial \delta \psi_x}{\partial y} + \frac{\partial \delta \psi_y}{\partial x} - C_0 \left(\frac{\partial \delta v_0}{\partial x} - \frac{\partial \delta u_0}{\partial y} \right) \right] \} dA
\end{aligned}$$

Using similar procedures as those for obtaining a linear finite element equation, substitution of equation (4.21) into (4.25) yields the nonlinear finite element equations over a typical cylindrical shell element as:

$$\left(\left[\mathbf{k}^{(e)} \right]_{\text{L}} + \left[\mathbf{k}^{(e)} \right]_{\text{NL}} \right) \{ \Delta \} = \{ \mathbf{f}^{(e)} \} \quad (4.26)$$

where the components of $\left[\mathbf{k}^{(e)} \right]_{\text{L}}$ and $\{ \mathbf{f}^{(e)} \}$ are the same as those shown in Appendix C.1, and those of $\left[\mathbf{k}^{(e)} \right]_{\text{NL}}$ are also detailed in Appendix C.2. Note that $\left[\mathbf{k}^{(e)} \right]_{\text{L}}$ is a symmetric matrix, and $\left[\mathbf{k}^{(e)} \right]_{\text{NL}}$ is non-symmetric.

4.10 Consideration of Elastic Foundations

In this chapter, a solid propellant rocket motor is modeled as a thin-walled circular cylindrical shell with inner, soft, elastic core. As stated in Chapter 3.10, the outer case is also treated as a layered composite cylinder.

The Winkler-type nonlinear elastic foundation is used to model the inner elastic medium. The Pasternak-foundation constants are also chosen to modify the present model for the purpose of accounting for shear interactions. The reaction pressure between the elastic shell and the proposed foundation is mathematically described by

$$p_f = - [k_0 w_0 + k_1 w_0^3 - k_G \left(\frac{\partial^2 w_0}{\partial x^2} + \frac{\partial^2 w_0}{\partial y^2} \right)] \quad (4.27)$$

where p_f is the reactive force per unit area resulting from the interaction between the body and the foundation, k_0 , in force per unit volume, is the linear Winkler-foundation parameter, k_1 , in force per unit length to the fifth power, is the nonlinear Winkler-foundation parameter, and k_G , in force per unit area, is the shear parameter of a Pasternak type of foundation.

The assumptions that support this proposed elastic-foundation model are the same as the ones stated in Chapter 3.10.

According to the preceding statements and formulation, the potential energy generated by the nonlinear elastic foundation is obtained as:

$$V_f = \int_{\Omega} \left[\frac{1}{2} k_0 w_0^2 + \frac{1}{4} k_1 w_0^4 + \frac{1}{2} k_G \left(\frac{\partial w_0}{\partial x} \right)^2 + \frac{1}{2} k_G \left(\frac{\partial w_0}{\partial y} \right)^2 \right] dA \quad (4.28)$$

The virtual strain energy associated with the elastic foundation may also be obtained as:

$$\delta V_f = \int_{\Omega} \left[k_0 w_0 \delta w_0 + k_1 w_0^3 \delta w_0 + k_G \left(\frac{\partial w_0}{\partial x} \right) \left(\frac{\partial \delta w_0}{\partial x} \right) + k_G \left(\frac{\partial w_0}{\partial y} \right) \left(\frac{\partial \delta w_0}{\partial y} \right) \right] dA \quad (4.29)$$

Integrating by parts on the derivatives of the mid-surface displacement variable w_0 , equation (4.29) can be rewritten as:

$$\begin{aligned} \delta V_f = & \int_{\Omega} \left\{ (k_0 w_0 + k_I w_0^3) - \frac{\partial}{\partial x} \left[k_G \left(\frac{\partial w_0}{\partial x} \right) \right] - \frac{\partial}{\partial y} \left[k_G \left(\frac{\partial w_0}{\partial y} \right) \right] \right\} \delta w_0 dA \\ & + \int_{\Gamma} \left[n_x \cdot k_G \left(\frac{\partial w_0}{\partial x} \right) + n_y \cdot k_G \left(\frac{\partial w_0}{\partial y} \right) \right] \delta w_0 dS \end{aligned} \quad (4.30)$$

Due to the presence of the elastic foundation, the nonlinear equilibrium equation associated with δw_0 , which was expressed in equation (4.13), is rewritten as:

$$\begin{aligned} \delta w_0 \dots \dots \frac{\partial}{\partial x} \left[N_x \left(\frac{\partial w_0}{\partial x} \right) + N_{xy} \left(\frac{\partial w_0}{\partial y} \right) \right] + \frac{\partial}{\partial y} \left[N_{xy} \left(\frac{\partial w_0}{\partial x} \right) + N_y \left(\frac{\partial w_0}{\partial y} \right) \right] \\ \frac{\partial Q_{xz}}{\partial x} + \frac{\partial Q_{yz}}{\partial y} - \frac{N_y}{R} + p_{\text{total}} = 0 \end{aligned} \quad (4.31)$$

where

$$p_{\text{total}} = p_0 - \left[k_0 w_0 + k_I w_0^3 - k_G \left(\frac{\partial^2 w_0}{\partial x^2} + \frac{\partial^2 w_0}{\partial y^2} \right) \right] \quad (4.32)$$

The corresponding boundary conditions associated with the elastic foundation can also be obtained as:

Geometric

Natural

$$w_0 = \widehat{w}_0$$

or

$$\begin{aligned} \mathbf{P}_n &= \mathbf{n}_x \left[N_x \left(\frac{\partial w_0}{\partial x} \right) + N_{xy} \left(\frac{\partial w_0}{\partial y} \right) \right] \\ &+ \mathbf{n}_y \left[N_{xy} \left(\frac{\partial w_0}{\partial x} \right) + N_y \left(\frac{\partial w_0}{\partial y} \right) \right] \\ &+ \mathbf{n}_x Q_{xz} + \mathbf{n}_y Q_{yz} \\ &+ \mathbf{n}_x \cdot \mathbf{k}_G \left(\frac{\partial w_0}{\partial x} \right) + \mathbf{n}_y \cdot \mathbf{k}_G \left(\frac{\partial w_0}{\partial y} \right) \\ &= \widehat{\mathbf{P}}_n \end{aligned} \quad (4.33)$$

With the additional virtual strain energy terms, the variational formulation over an element, which was previously shown in equation (4.24), can be altered as:

$$\begin{aligned} 0 &= \int_{\Omega} \{ \text{same as the ones of equation (4.24)} \} dA \\ &+ \int_{\Gamma} \{ \text{Boundary Terms} \} dS \\ &+ \int_{\Omega} \{ [(k_0 w_0 + k_1 w_0^3)] \cdot \delta w_0 - k_G \left(\frac{\partial w_0}{\partial x} \right) \left(\frac{\partial \delta w_0}{\partial x} \right) - k_G \left(\frac{\partial w_0}{\partial y} \right) \left(\frac{\partial \delta w_0}{\partial y} \right) \} dA \end{aligned} \quad (4.34)$$

Over a typical shell element, the additional components of the $[k_{ij}^{33}]$ term of the finite-element equation with the existence of the nonlinear elastic foundation can, therefore, be generated as follows:

$$\begin{aligned} [k_{ij}^{33}] &= \int_{\Omega} \{ \text{same as the ones of equation (C.13)} + \text{equation (C.43)} \\ &+ k_0 \phi_i^{(3)} \phi_j^{(3)} + k_1 w_0^2 \phi_i^{(3)} \phi_j^{(3)} + k_G \left(\frac{\partial \phi_i^{(3)}}{\partial x} \right) \left(\frac{\partial \phi_j^{(3)}}{\partial x} \right) + k_G \left(\frac{\partial \phi_i^{(3)}}{\partial y} \right) \left(\frac{\partial \phi_j^{(3)}}{\partial y} \right) \} dA \end{aligned} \quad (4.35)$$

4.11 Linear and Nonlinear Buckling Analyses

The major objective of the study is to determine the buckling loads and modes of a general anisotropic cylinder on elastic foundation under various loading conditions. As stated in Chapter 3.11, the linear eigenvalue analysis is applied for obtaining estimated values of the critical buckling loads and modes. Furthermore, more accurate results can be achieved by performing the nonlinear stability analysis. The supporting theories for the present research are stated in the following sub-chapters.

4.11.1 Linear Eigenvalue Analysis

In determining the state of stresses in the cylinder prior to buckling it is assumed that the end effects can be neglected. For the pre-buckling stage, the stresses are considered to be pure in a membrane state. Under uniform radial pressure p_0 (force per unit area), the circumferential normal stress σ_y produced in the body can be expressed as

$$\bar{N}_y^0 = h \sigma_y = R(p_0) \quad (4.36)$$

where R is the radius, h is the thickness of the cylinder.

The potential energy associated with an initially circumferential compressive load \bar{N}_y^0 is given as

$$V_{py} = \int_{\Omega} \left[\frac{1}{2} \bar{N}_y^0 \left(\frac{\partial w_0}{\partial y} - \frac{v_0}{R} \right)^2 \right] dA \quad (4.37)$$

where \bar{N}_y^0 has a positive sign for a tensile load, and negative sign for a compressive one.

Similarly, the potential energy of the cylinder resulting from an initially axial compressive load \bar{N}_x^0 is also given by

$$V_{px} = \int_{\Omega} \left[\frac{1}{2} \bar{N}_x^0 \left(\frac{\partial w_0}{\partial x} \right)^2 \right] dA \quad (4.38)$$

The virtual work done by these prebuckling stresses can be written as:

$$\begin{aligned} \delta V_p &= \delta (V_{px} + V_{py}) \\ &= \int_{\Omega} \left[\bar{N}_x^0 \left(\frac{\partial w_0}{\partial x} \right) \left(\frac{\partial \delta w_0}{\partial x} \right) + \bar{N}_y^0 \left(\frac{\partial w_0}{\partial y} - \frac{v_0}{R} \right) \left(\frac{\partial \delta w_0}{\partial y} - \frac{\delta v_0}{R} \right) \right] dA \end{aligned} \quad (4.39)$$

Integration by parts on the derivatives of the displacement variable w_0 of equation (4.39) leads to

$$\begin{aligned} \delta V_p &= \int_{\Omega} \left\{ - \frac{\partial}{\partial x} \left[\bar{N}_x^0 \left(\frac{\partial w_0}{\partial x} \right) \right] \delta w_0 \right\} dA + \int_{\Gamma} \left[n_x \cdot \left(\bar{N}_x^0 \left(\frac{\partial w_0}{\partial x} \right) \right) \delta w_0 \right] dS \\ &+ \int_{\Omega} \left\{ - \frac{\partial}{\partial y} \left[\bar{N}_y^0 \left(\frac{\partial w_0}{\partial y} - \frac{v_0}{R} \right) \right] \delta w_0 \right\} dA - \int_{\Omega} \left\{ \left[\bar{N}_y^0 \left(\frac{\partial w_0}{\partial y} - \frac{v_0}{R} \right) \right] \frac{\delta v_0}{R} \right\} dA \\ &+ \int_{\Gamma} \left[n_y \cdot \left(\bar{N}_y^0 \left(\frac{\partial w_0}{\partial y} - \frac{v_0}{R} \right) \right) \delta w_0 \right] dS \end{aligned} \quad (4.40)$$

In association with δv_0 and δw_0 , the equilibrium equations governing the stability of an elastic cylindrical shell may be obtained as:

$$\delta v_0 \dots \frac{\partial N_{xy}}{\partial x} + \frac{\partial N_y}{\partial y} - C_0 \frac{\partial M_{xy}}{\partial x} + \frac{Q_{yz}}{R} + \frac{(\bar{N}_y)^0}{R} \left(\frac{\partial w_0}{\partial y} - \frac{v_0}{R} \right) = 0 \quad (4.41)$$

$$\delta w_0 \dots \frac{\partial Q_{xz}}{\partial x} + \frac{\partial Q_{yz}}{\partial y} - \frac{N_y}{R} + \frac{\partial}{\partial x} [\bar{N}_x^0 \left(\frac{\partial w_0}{\partial x} \right)] + \frac{\partial}{\partial y} [\bar{N}_y^0 \left(\frac{\partial w_0}{\partial y} - \frac{v_0}{R} \right)] + p_f = 0 \quad (4.42)$$

where p_f is the pressure resulting from the interaction between the elastic cylinder and the linear Pasternak-elastic-foundation.

The corresponding boundary conditions can also obtained as:

Geometric

Natural

$$\begin{aligned}
 P_n &= n_x Q_{xz} + n_y Q_{yz} \\
 &+ K_s \left[n_x \left(\frac{\partial w_0}{\partial x} \right) + n_y \left(\frac{\partial w_0}{\partial y} \right) \right] \\
 &+ n_x \left[\bar{N}_x^0 \left(\frac{\partial w_0}{\partial x} \right) \right] \\
 w_0 = \hat{w}_0 \quad \quad \quad \text{or} \quad \quad \quad &+ n_y \left[\bar{N}_y^0 \left(\frac{\partial w_0}{\partial y} - \frac{v_0}{R} \right) \right] \\
 &= \hat{P}_n
 \end{aligned} \quad (4.43)$$

The corresponding $[k_{ij}^{mn}]$ terms of the finite-element equations, over an element, associated with the pre-buckling stresses may be obtained as follows:

$$\begin{aligned}
\left[k_{ij}^{22} \right] &= \int_{\Omega} \left\{ \text{same as the ones of equation (C.7)} \right. \\
&\quad \left. + \frac{\bar{N}_y^0}{R^2} \phi_i^{(2)} \phi_j^{(2)} \right\} dA
\end{aligned} \tag{4.44}$$

$$\begin{aligned}
\left[k_{ij}^{23} \right] &= \int_{\Omega} \left\{ \text{same as the ones of equation (C.8)} \right. \\
&\quad \left. - \left(\frac{\bar{N}_y^0}{R} \right) \phi_i^{(2)} \frac{\partial \phi_j^{(3)}}{\partial y} \right\} dA
\end{aligned} \tag{4.45}$$

$$\begin{aligned}
\left[k_{ij}^{32} \right] &= \int_{\Omega} \left\{ \text{same as the ones of equation (C.12)} \right. \\
&\quad \left. - \left(\frac{\bar{N}_y^0}{R} \right) \frac{\partial \phi_i^{(3)}}{\partial y} \phi_j^{(2)} \right\} dA
\end{aligned} \tag{4.46}$$

$$\begin{aligned}
\left[k_{ij}^{33} \right] &= \int_{\Omega} \left\{ \text{same as the ones of equation (C.13)} \right. \\
&\quad + K_0 \phi_i^{(3)} \phi_j^{(3)} + K_G \left(\frac{\partial \phi_i^{(3)}}{\partial x} \right) \left(\frac{\partial \phi_j^{(3)}}{\partial x} \right) + K_G \left(\frac{\partial \phi_i^{(3)}}{\partial y} \right) \left(\frac{\partial \phi_j^{(3)}}{\partial y} \right) \\
&\quad \left. + \bar{N}_x^0 \left(\frac{\partial \phi_i^{(3)}}{\partial x} \right) \left(\frac{\partial \phi_j^{(3)}}{\partial x} \right) + \bar{N}_y^0 \left(\frac{\partial \phi_i^{(3)}}{\partial y} \right) \left(\frac{\partial \phi_j^{(3)}}{\partial y} \right) \right\} dA
\end{aligned} \tag{4.47}$$

Substituting equations (4.44) to (4.47) into the linear finite element equation (4.23), the finite element model takes the form for eigenvalue analysis as:

$$\begin{bmatrix} \left[\begin{matrix} k^{11} \\ k^{21} \\ k^{31} \\ k^{41} \\ k^{51} \end{matrix} \right] & \left[\begin{matrix} k^{12} \\ k^{22} \\ k^{32} \\ k^{42} \\ k^{52} \end{matrix} \right] & \left[\begin{matrix} k^{13} \\ k^{23} \\ k^{33} \\ k^{43} \\ k^{53} \end{matrix} \right] & \left[\begin{matrix} k^{14} \\ k^{24} \\ k^{34} \\ k^{44} \\ k^{54} \end{matrix} \right] & \left[\begin{matrix} k^{15} \\ k^{25} \\ k^{35} \\ k^{45} \\ k^{55} \end{matrix} \right] \end{bmatrix}_{(e)} \begin{Bmatrix} \left\{ \begin{matrix} u_0 \\ v_0 \\ w_0 \end{matrix} \right\} \\ \left\{ \begin{matrix} \psi_x \\ \psi_y \end{matrix} \right\} \end{Bmatrix} = (\lambda) \begin{bmatrix} \left[S^{11} \right] & 0 & 0 & 0 & 0 \\ 0 & \left[S^{22} \right] & \left[S^{23} \right] & 0 & 0 \\ 0 & \left[S^{32} \right] & \left[S^{33} \right] & 0 & 0 \\ 0 & 0 & 0 & \left[S^{44} \right] & 0 \\ 0 & 0 & 0 & 0 & \left[S^{55} \right] \end{bmatrix}_{(e)} \quad (4.48)$$

where the components of k_{ij}^{mn} ($m, n = 1, 2, 3, 4, 5$) were defined in Appendix C.1 and equations (4.44) to (4.47), which account for the existence of linear elastic foundations; the values of S_{ij} are shown as

$$\begin{aligned}
S_{ij}^{11} &= S_{ij}^{12} = S_{ij}^{13} = S_{ij}^{14} = S_{ij}^{15} = S_{ij}^{21} = S_{ij}^{24} = S_{ij}^{25} \\
&= S_{ij}^{31} = S_{ij}^{34} = S_{ij}^{35} = S_{ij}^{41} = S_{ij}^{42} = S_{ij}^{43} = S_{ij}^{44} \\
&= S_{ij}^{45} = S_{ij}^{51} = S_{ij}^{52} = S_{ij}^{53} = S_{ij}^{54} = S_{ij}^{55} = 0.
\end{aligned} \quad (4.49)$$

For the case of axial compression only, one can obtain the nonzero factors of the S matrix as:

$$\left[S_{ij}^{22} \right] = \int_{\Omega} \left\{ \frac{1}{R^2} \phi_i^{(2)} \phi_j^{(2)} \right\} dA, \quad (4.50)$$

$$\left[S_{ij}^{23} \right] = \int_{\Omega} \left\{ -\left(\frac{1}{R} \right) \phi_i^{(2)} \frac{\partial \phi_j^{(3)}}{\partial y} \right\} dA, \quad (4.51)$$

$$[S_{ij}^{32}] = \int_{\Omega} \left\{ -\left(\frac{1}{R}\right) \frac{\partial \phi_i^{(3)}}{\partial y} \phi_j^{(2)} \right\} dA, \quad (4.52)$$

$$[S_{ij}^{33}] = \int_{\Omega} \left\{ \left(\frac{\partial \phi_i^{(3)}}{\partial x}\right) \left(\frac{\partial \phi_j^{(3)}}{\partial x}\right) \right\} dA. \quad (4.53)$$

For the case of radial (lateral) compression only, one can also obtain the distinct nonzero factor, apart from the case of axial compression, of the S matrix as

$$[S_{ij}^{33}] = \int_{\Omega} \left\{ \left(\frac{\partial \phi_i^{(3)}}{\partial y}\right) \left(\frac{\partial \phi_j^{(3)}}{\partial y}\right) \right\} dA. \quad (4.54)$$

Similarly, for the case of both axial and lateral compression, one may obtain the different nonzero component as

$$[S_{ij}^{33}] = \int_{\Omega} \left\{ \left(\frac{\partial \phi_i^{(3)}}{\partial x}\right) \left(\frac{\partial \phi_j^{(3)}}{\partial x}\right) + f_0 \left(\frac{\partial \phi_i^{(3)}}{\partial y}\right) \left(\frac{\partial \phi_j^{(3)}}{\partial y}\right) \right\} dA, \quad (4.55)$$

where f_0 , a fraction factor between \bar{N}_x^0 and \bar{N}_y^0 , is described by the following relation:

$$\bar{N}_y^0 = f_0 \bar{N}_x^0 \quad (4.56)$$

Based on equations (4.48) to (4.56), one can obtain a set of eigenvalues and the corresponding eigenvectors for various loading cases. The minimum eigenvalue and the corresponding eigenvector provide the information of the critical buckling load and mode.

4.11.2 Nonlinear Buckling and Initial Post-Buckling Analysis

With the additional terms caused by the nonlinear elastic foundations, which were shown in equation (4.26), the behavior of buckling and post-buckling of elastic cylindrical shells is purely nonlinear and could be described by a set of nonlinear partial differential equations, which were modeled as the finite element equations (4.26). Some nonlinear finite element solution procedures have to be applied in order to solve the problems by using incremental iterative processes. For the present research, the Newton-Raphson and Riks-Wempner methods will be chosen. The theories and algorithms of using these numerical procedures will be mentioned, in detail, in Chapter 6.

The first step in applying these schemes is to determine the tangent stiffness matrix for a nonlinear cylindrical shell element. Similarly to the ones stated in Chapter 3.11.2, the procedure of obtaining the tangent stiffness matrix is shown as follows.

Let

$$R_1 = \sum_{j=1}^l k_{ij}^{11} u_j + \sum_{j=1}^m k_{ij}^{12} v_j + \sum_{j=1}^n k_{ij}^{13} w_j + \sum_{j=1}^p k_{ij}^{14} \psi_{xj} + \sum_{j=1}^q k_{ij}^{15} \psi_{yj} - F_i^1, \quad (4.57)$$

$$R_2 = \sum_{j=1}^l k_{ij}^{21} u_j + \sum_{j=1}^m k_{ij}^{22} v_j + \sum_{j=1}^n k_{ij}^{23} w_j + \sum_{j=1}^p k_{ij}^{24} \psi_{xj} + \sum_{j=1}^q k_{ij}^{25} \psi_{yj} - F_i^2, \quad (4.58)$$

$$R_3 = \sum_{j=1}^l k_{ij}^{31} u_j + \sum_{j=1}^m k_{ij}^{32} v_j + \sum_{j=1}^n k_{ij}^{33} w_j + \sum_{j=1}^p k_{ij}^{34} \psi_{xj} + \sum_{j=1}^q k_{ij}^{35} \psi_{yj} - F_i^3, \quad (4.59)$$

$$R_4 = \sum_{j=1}^l k_{ij}^{41} u_j + \sum_{j=1}^m k_{ij}^{42} v_j + \sum_{j=1}^n k_{ij}^{43} w_j + \sum_{j=1}^p k_{ij}^{44} \psi_{xj} + \sum_{j=1}^q k_{ij}^{45} \psi_{yj} - F_i^4, \quad (4.60)$$

and

$$R_5 = \sum_{j=1}^l k_{ij}^{51} u_j + \sum_{j=1}^m k_{ij}^{52} v_j + \sum_{j=1}^n k_{ij}^{53} w_j + \sum_{j=1}^p k_{ij}^{54} \psi_{xj} + \sum_{j=1}^q k_{ij}^{55} \psi_{yj} - F_i^5. \quad (4.61)$$

where R_1, R_2, R_3, R_4 and R_5 are the residual force vectors associated with five different directions, separately; the components of the element stiffness matrix are included in Appendix C.2.

Evaluating the tangent stiffness matrix, one obtains

$$(k_T)_{ij}^{rs} = \frac{\partial R_r}{\partial U_s} = k_{ij}^{rs} + \sum_{k=1}^5 \frac{\partial k_{ij}^{rs}}{\partial U_s} U_k \quad (4.62)$$

where

$$R_r = (k_{ij}^{rs}) U_s - F_r \quad (r, s = 1, 2, 3, 4, 5) \quad (4.63)$$

Introducing equations (4.57) to (4.63), the element tangent stiffness matrix, over a shell element, can be generated as:

$$\left[\mathbf{k}_T \right]_{(e)} = \begin{bmatrix} \left[\begin{matrix} k_T^{11} \\ k_T^{12} \\ k_T^{13} \\ k_T^{14} \\ k_T^{15} \end{matrix} \right] & \left[\begin{matrix} k_T^{12} \\ k_T^{22} \\ k_T^{23} \\ k_T^{24} \\ k_T^{25} \end{matrix} \right] & \left[\begin{matrix} k_T^{13} \\ k_T^{23} \\ k_T^{33} \\ k_T^{34} \\ k_T^{35} \end{matrix} \right] & \left[\begin{matrix} k_T^{14} \\ k_T^{24} \\ k_T^{34} \\ k_T^{44} \\ k_T^{45} \end{matrix} \right] & \left[\begin{matrix} k_T^{15} \\ k_T^{25} \\ k_T^{35} \\ k_T^{45} \\ k_T^{55} \end{matrix} \right] \\ \left[\begin{matrix} k_T^{12} \\ k_T^{22} \\ k_T^{23} \\ k_T^{24} \\ k_T^{25} \end{matrix} \right] & \left[\begin{matrix} k_T^{22} \\ k_T^{32} \\ k_T^{42} \\ k_T^{52} \end{matrix} \right] & \left[\begin{matrix} k_T^{23} \\ k_T^{32} \\ k_T^{43} \\ k_T^{53} \end{matrix} \right] & \left[\begin{matrix} k_T^{24} \\ k_T^{34} \\ k_T^{43} \\ k_T^{54} \end{matrix} \right] & \left[\begin{matrix} k_T^{25} \\ k_T^{35} \\ k_T^{45} \\ k_T^{54} \end{matrix} \right] \\ \left[\begin{matrix} k_T^{13} \\ k_T^{23} \\ k_T^{33} \\ k_T^{34} \\ k_T^{35} \end{matrix} \right] & \left[\begin{matrix} k_T^{32} \\ k_T^{33} \\ k_T^{43} \\ k_T^{53} \end{matrix} \right] & \left[\begin{matrix} k_T^{33} \\ k_T^{43} \\ k_T^{53} \end{matrix} \right] & \left[\begin{matrix} k_T^{34} \\ k_T^{43} \\ k_T^{54} \end{matrix} \right] & \left[\begin{matrix} k_T^{35} \\ k_T^{45} \\ k_T^{54} \end{matrix} \right] \\ \left[\begin{matrix} k_T^{14} \\ k_T^{24} \\ k_T^{34} \\ k_T^{44} \\ k_T^{45} \end{matrix} \right] & \left[\begin{matrix} k_T^{24} \\ k_T^{34} \\ k_T^{43} \\ k_T^{44} \\ k_T^{54} \end{matrix} \right] & \left[\begin{matrix} k_T^{34} \\ k_T^{43} \\ k_T^{54} \end{matrix} \right] & \left[\begin{matrix} k_T^{44} \\ k_T^{54} \end{matrix} \right] & \left[\begin{matrix} k_T^{45} \\ k_T^{54} \end{matrix} \right] \\ \left[\begin{matrix} k_T^{15} \\ k_T^{25} \\ k_T^{35} \\ k_T^{45} \\ k_T^{55} \end{matrix} \right] & \left[\begin{matrix} k_T^{25} \\ k_T^{35} \\ k_T^{45} \\ k_T^{54} \end{matrix} \right] & \left[\begin{matrix} k_T^{35} \\ k_T^{45} \\ k_T^{54} \end{matrix} \right] & \left[\begin{matrix} k_T^{45} \\ k_T^{54} \end{matrix} \right] & \left[\begin{matrix} k_T^{55} \end{matrix} \right] \end{bmatrix}_{(e)} \quad (4.64)$$

The coefficients of the element tangent stiffness matrix are included in Appendix D. Note that the tangent stiffness matrix is symmetric.

CHAPTER 5

INFLUENCE OF INITIAL IMPERFECTIONS

5.1 Introduction

In the preceding chapters the geometries of elastic rings and cylindrical shells were considered to be perfectly round along the circumferential and straight along the axial directions before applying any mechanical loads. Of course, no structures are perfectly round or straight in our real world. Initial imperfections were included to describe small deviations from the assumed perfect shape of the body. It was shown in the literature [80, 11] that the existence of initial imperfections causes significant reduction in the critical buckling loads for some particular structures when theoretical results are compared with experimental ones. In 1941, Von Karman and Tsien [77] performed an analysis of the post-buckling equilibrium of axially compressed cylinders. It has been pointed out that the secondary equilibrium path, which plays a very important role in governing the load-displacement curve beyond the buckling point, drops sharply downward from the bifurcation point. The consideration of initial imperfections becomes critical for the determination of the stability condition and the analysis of post-buckling behavior.

Let an imperfection function describe a known, small, imperfection. The main assumptions for applying this function in further derivation of the theory are:

- 1 An imperfection function is defined as a slight deviation of the centroidal (or middle) surface from a perfect structure.

- 2 The elastic body with an initial imperfection is assumed to be stress-free before applying any external loading.
- 3 The magnitude of an initial imperfect function is also assumed to be a small fraction of the ring- or shell-wall thickness.

In this chapter, the theories for rings and cylindrical shells involving small imperfections are developed. The finite element equations based on the assumed initially imperfect models will also be derived and stated in the following sections.

5.2 Theory for Rings with Initial Imperfections

As an example of initial imperfection analysis, we consider the slight imperfection along the circumferential direction of an elastic ring. Introducing an initial imperfection function, which is expressed as $\bar{w}_0(y)$, one can define the amplitude of small deviations of the undeformed, imperfect ring mid-surface, from a perfectly circular shape.

5.2.1 Displacement Fields

With the addition of the initial imperfection function $\bar{w}_0(y)$, the displacement fields, which were expressed by equation (3.1), can be rewritten as

$$v(y, z) = v_0(y) + z \psi_y(y) \tag{5.1}$$

$$w(y, z) = w_0(y) + \bar{w}_0(y)$$

where v , w , v_0 , w_0 and ψ_y were defined in Chapter 3.2.

5.2.2 Kinematic (Strain-Displacement) Relations

Introducing the initial imperfection function, the strain-displacement relation, previously defined in equations (3.3) and (3.4), is replaced by the following form:

$$e_y^0 = \frac{d v_0}{d y} + \frac{w_0}{R} + \frac{1}{2} \left(\frac{d w_0}{d y} - \frac{v_0}{R} \right)^2 + \left(\frac{d w_0}{d y} - \frac{v_0}{R} \right) \left(\frac{d \bar{w}_0}{d y} \right) \quad (5.2)$$

where γ_{yz}^0 and κ_y^0 remain the same as those defined in equation (3.3).

5.2.3 Virtual Work Statement

The principle of virtual work for an imperfect ring was already stated and defined through equations (3.18) to (3.20). Introduction of the newly derived equation of displacement fields, equation (5.1), and strain-displacement relations, equation (5.2), the weak form of the virtual statement associated with the initially imperfect ring can be derived and is obtained as follows:

$$0 = \delta \Pi = \delta U + \delta V$$

$$\begin{aligned}
&= \int_{y_1}^{y_2} (\bar{N}_y \delta e_{yy}^0 + \bar{M}_y \delta \kappa_y^0 + \bar{Q}_{yz} \delta \gamma_{yz}^0) dy - \int_{y_1}^{y_2} \mathbf{q}_{\text{total}} \cdot \delta \mathbf{w} dA \\
&= \int_{y_1}^{y_2} \left\{ \bar{N}_y \left[\frac{dv_0}{dy} + \frac{w_0}{R} + \frac{1}{2} \left(\frac{dw_0}{dy} - \frac{v_0}{R} \right)^2 + \left(\frac{dw_0}{dy} - \frac{v_0}{R} \right) \left(\frac{d\bar{w}_0}{dy} \right) \right] \right. \\
&\quad \left. + \bar{M}_y \left(\frac{d\delta\psi_y}{dy} \right) + \bar{Q}_{yz} \left(\delta\psi_y + \frac{d\delta w_0}{dy} - \frac{\delta v_0}{R} \right) \right\} dy - \int_{y_1}^{y_2} \mathbf{q}_{\text{total}} \cdot \delta \mathbf{w}_0 dA
\end{aligned} \tag{5.3}$$

Using integration by parts on the displacement variables separately, one can obtain three new equilibrium equations and the corresponding boundary conditions by collecting terms involving δv_0 , δw_0 , and $\delta \psi_y$, respectively, as shown in the following sub-chapter.

5.2.4 Equilibrium Equations and Associated Boundary Conditions

Based on the principle of the minimum potential energy, as stated in the previous paragraph, the equilibrium equations which govern the behavior of imperfect, elastic arches and rings can be given by:

$$\begin{aligned}
\delta v_0 \dots \dots \frac{d\bar{N}_y}{dy} + \frac{\bar{Q}_{yz}}{R} + \frac{\bar{N}_y}{R} \left(\frac{dw_0}{dy} - \frac{v_0}{R} \right) + \frac{\bar{N}_y}{R} \left(\frac{d\bar{w}_0}{dy} \right) &= 0 \\
\delta w_0 \dots \dots \frac{d\bar{Q}_{yz}}{dy} - \frac{\bar{N}_y}{R} + \frac{d}{dy} \left[\bar{N}_y \left(\frac{dw_0}{dy} - \frac{v_0}{R} \right) \right] + \frac{d}{dy} \left[\bar{N}_y \left(\frac{d\bar{w}_0}{dy} \right) \right] + \mathbf{q}_{\text{total}} &= 0 \\
\delta \psi_y \dots \dots \frac{d\bar{M}_y}{dy} - \bar{Q}_{yz} &= 0
\end{aligned} \tag{5.4}$$

The geometric and natural boundary conditions associated with the linear theory are specified as:

Geometrical		Natural
$v_0 = \widehat{v}_0$		$\bar{N}_y = \widehat{N}_y$
$w_0 = \widehat{w}_0$	or	$\bar{Q}_{yz} + \bar{N}_y \left[\frac{d(w_0 + \bar{w}_0)}{dy} - \frac{v_0}{R} \right] = \widehat{Q}_{yz} \quad (5.5)$
$\psi_y = \widehat{\psi}_y$		$\bar{M}_y = \widehat{M}_y$

5.2.5 Weak Formulation and Finite Element Model

Introduction of the principle of virtual work statement, expressed in equation (5.3), combined with the equations of stress and moment resultants of a composite, which were shown on equations (3.14) to (3.16), and the equations of strain-displacement relations, which are written as equations (3.2), (3.3) and (5.2), one obtains the variational weak-form of a nonlinear elastic ring with initial imperfections over an element as:

$$0 = \delta \Pi = \delta U + \delta V$$

$$= \int_{y_1}^{y_2} \left\{ b \left[A_{22} \left[\frac{dv_0}{dy} + \frac{w_0}{R} + \frac{1}{2} \left(\frac{dw_0}{dy} - \frac{v_0}{R} \right)^2 + \left(\frac{dw_0}{dy} - \frac{v_0}{R} \right) \left(\frac{d\bar{w}_0}{dy} \right) \right] + B_{22} \left(\frac{d\psi_y}{dy} \right) \right]$$

$$\left[\frac{d\delta v_0}{dy} + \frac{\delta w_0}{R} + \left(\frac{dw_0}{dy} - \frac{v_0}{R} \right) \left(\frac{d\delta w_0}{dy} - \frac{\delta v_0}{R} \right) + \left(\frac{d\delta w_0}{dy} - \frac{\delta v_0}{R} \right) \left(\frac{d\bar{w}_0}{dy} \right) \right]$$

$$\begin{aligned}
& + b \left[B_{22} \left[\frac{d v_0}{d y} + \frac{w_0}{R} + \frac{1}{2} \left(\frac{d w_0}{d y} - \frac{v_0}{R} \right)^2 + \left(\frac{d w_0}{d y} - \frac{v_0}{R} \right) \left(\frac{d \bar{w}_0}{d y} \right) \right] \right. \\
& + D_{22} \left(\frac{d \psi_y}{d y} \right) \left(\frac{d \delta \psi_y}{d y} \right) + b \left[K_s A_{44} \left(\psi_y + \frac{d w_0}{d y} - \frac{v_0}{R} \right) \right] \left(\delta \psi_y + \frac{d \delta w_0}{d y} - \frac{\delta v_0}{R} \right) \left. \right\} dy \\
& + [\text{Boundary Terms}]_{y=y_1}^{y=y_2} - \int_{y_1}^{y_2} q_{\text{total}} \cdot \delta w_0 dy
\end{aligned} \tag{5.6}$$

Let four displacement vectors, v_0 , w_0 , ψ_y , and \bar{w}_0 , be represented in terms of Lagrange interpolation functions in the forms of

$$\begin{aligned}
v_0(y) &= \sum_{j=1}^l v_j \phi_j^{(1)}(y), \\
w_0(y) &= \sum_{j=1}^m w_j \phi_j^{(2)}(y), \\
\psi_y(y) &= \sum_{j=1}^n \psi_{yj} \phi_j^{(3)}(y),
\end{aligned} \tag{5.7}$$

and

$$\bar{w}_0(y) = \sum_{j=1}^p \bar{w}_j \phi_j^{(4)}(y).$$

where $\phi_j^{(1)}$, $\phi_j^{(2)}$, $\phi_j^{(3)}$, and $\phi_j^{(4)}$ are the interpolation functions of degrees $l-1$, $m-1$, $n-1$, and $p-1$, respectively.

Substitution of equation (5.7) into (5.6), and letting $\delta v_0 = \phi_i^{(1)}$, $\delta w_0 = \phi_i^{(2)}$, and $\delta \psi_y = \phi_i^{(3)}$ leads to a typical finite-element equation of initially imperfect arch or ring structures, over an element, as follows:

$$\left[\mathbf{k}^{(e)} \right]_{\text{Imperfect}} \{ \mathbf{u} \} = \{ \mathbf{f}^{(e)} \} \quad (5.8)$$

where $\{ \mathbf{u} \} = \{ \{ v_0 \}, \{ w_0 \}, \{ \psi_y \}, \{ \bar{w}_0 \} \}^T$ is the displacement vector, $\left[\mathbf{k}^{(e)} \right]_{\text{Imperfect}}$ is the element stiffness matrix, and $\{ \mathbf{f}^{(e)} \}$ is the element nodal force vector.

Equation (5.8) can also be expressed in matrix form as follows:

$$\left[\begin{array}{cccc} \left[\mathbf{k}^{11} \right] & \left[\mathbf{k}^{12} \right] & \left[\mathbf{k}^{13} \right] & \left[\mathbf{k}^{14} \right] \\ \left[\mathbf{k}^{21} \right] & \left[\mathbf{k}^{22} \right] & \left[\mathbf{k}^{23} \right] & \left[\mathbf{k}^{24} \right] \\ \left[\mathbf{k}^{31} \right] & \left[\mathbf{k}^{32} \right] & \left[\mathbf{k}^{33} \right] & \left[\mathbf{k}^{34} \right] \\ \left[\mathbf{k}^{41} \right] & \left[\mathbf{k}^{42} \right] & \left[\mathbf{k}^{43} \right] & \left[\mathbf{k}^{44} \right] \end{array} \right]_{(e)} \left\{ \begin{array}{c} \{ v_0 \} \\ \{ w_0 \} \\ \{ \psi_y \} \\ \{ \bar{w}_0 \} \end{array} \right\} = \left\{ \begin{array}{c} \{ f^1 \} \\ \{ f^2 \} \\ \{ f^3 \} \\ \{ f^4 \} \end{array} \right\}_{(e)} \quad (5.9)$$

The additional components of the element stiffness matrix $\left[\mathbf{k}^{(e)} \right]_{\text{Imperfect}}$ and the force vector $\{ \mathbf{f}^{(e)} \}$ are stated in Appendix E. All the other coefficients are the same as the ones defined in Appendix A.2. Note that the presence of the imperfection function introduces the additional terms corresponding to the the fourth row and column.

Since the initial imperfection over the entire domain is prescribed, the terms associated with \bar{w}_0 can be considered and entered as boundary terms, and moved to the right-hand side vector of equation (5.9). The equation of the finite element model of an initially imperfect ring is, therefore, rewritten as:

$$\left\{ \begin{matrix} \left[\begin{matrix} k^{11} \\ k^{21} \\ k^{31} \end{matrix} \right] \\ \left[\begin{matrix} k^{12} \\ k^{22} \\ k^{32} \end{matrix} \right] \\ \left[\begin{matrix} k^{13} \\ k^{23} \\ k^{33} \end{matrix} \right] \end{matrix} \right\}_{(e)} \left\{ \begin{matrix} \{v_0\} \\ \{w_0\} \\ \{\psi_y\} \end{matrix} \right\} = \left\{ \begin{matrix} \{f^1\} - \left[\begin{matrix} k^{14} \\ k^{24} \\ k^{34} \end{matrix} \right] \{ \bar{w}_0 \} \\ \{f^2\} - \left[\begin{matrix} k^{14} \\ k^{24} \\ k^{34} \end{matrix} \right] \{ \bar{w}_0 \} \\ \{f^3\} - \left[\begin{matrix} k^{14} \\ k^{24} \\ k^{34} \end{matrix} \right] \{ \bar{w}_0 \} \end{matrix} \right\}_{(e)} \quad (5.10)$$

where the components of equation (5.10) are identical to those of equation (5.9).

5.2.6 Nonlinear Finite Element Analysis of Imperfect Rings

For the purpose of solving the nonlinear behavior and stability condition of imperfect ring structures, which are governed by equation (5.9) and (5.10), some iterative nonlinear methods will be required. Similarly, as stated in Chapter 3.11.2, the determination of the element tangent stiffness matrix will be the priority step for applying these nonlinear schemes. The procedures are stated as follows:

Let

$$R_1 = \sum_{j=1}^l k_{ij}^{11} v_j + \sum_{j=1}^m k_{ij}^{12} w_j + \sum_{j=1}^l k_{ij}^{13} \psi_{yj} - F_i^1 + \sum_{j=1}^p k_{ij}^{14} \bar{w}_j, \quad (5.11)$$

$$R_2 = \sum_{j=1}^l k_{ij}^{21} v_j + \sum_{j=1}^m k_{ij}^{22} w_j + \sum_{j=1}^l k_{ij}^{23} \psi_{yj} - F_i^2 + \sum_{j=1}^p k_{ij}^{24} \bar{w}_j, \quad (5.12)$$

and

$$R_3 = \sum_{j=1}^l k_{ij}^{31} v_j + \sum_{j=1}^m k_{ij}^{32} w_j + \sum_{j=1}^l k_{ij}^{33} \psi_{yj} - F_i^3 + \sum_{j=1}^p k_{ij}^{34} \bar{w}_j. \quad (5.13)$$

where R_1 , R_2 , and R_3 are the residual force vectors associated with three different directions, respectively; the other components of equations (5.11) to (5.13) are defined in Appendix E.

From the definition of the tangent stiffness matrix, one obtains

$$(k_T)_{ij}^{pq} = \frac{\partial R_p}{\partial U_q} = k_{ij}^{pq} + \sum_{q=1}^3 \frac{\partial k_{ij}^{pq}}{\partial U_q} U_q + \frac{\partial k_{ij}^{p4}}{\partial U_q} U_4 \quad (5.14)$$

where

$$R_p = (k_{ij}^{pq}) U_q + (k_{ij}^{p4}) U_4 - F_p \quad (p, q = 1, 2, 3) \quad (5.15)$$

Introducing equations (5.11) into (5.15), the element tangent stiffness matrix can be generated as:

$$\left[k_T^{(e)} \right]_{\text{Imperfect}} = \left[\begin{array}{c} \left[k_T^{11} \right] \\ \left[k_T^{12} \right] \\ \left[k_T^{13} \right] \\ \left[k_T^{22} \right] \\ \left[k_T^{23} \right] \\ \left[k_T^{33} \right] \end{array} \right]_{(e)} \quad (5.16)$$

The coefficients of the element tangent stiffness matrix are included in Appendix F.

5.3 Theory for Cylindrical Shells with Initial Imperfections

For the purpose of analysis of an initially imperfect cylinder, an initial imperfection function $\bar{w}_0(x, y)$ is chosen as a known function to represent small deviations from a perfectly circular cylindrical shape. Based on the existence of an initial imperfection function, the refined theory and finite element model, apart from those stated in Chapter 4, are determined and derived in the following sub-chapters.

5.3.1 Displacement Fields

With the additional terms caused by the presence of the initial imperfection function $\bar{w}_0(x, y)$, the displacement fields can be rewritten as

$$u(x, y, z) = u_0(x, y) + z \psi_x(x, y)$$

$$v(x, y, z) = v_0(x, y) + z \psi_y(x, y) \tag{5.17}$$

$$w(x, y, z) = w_0(x, y) + \bar{w}_0(x, y)$$

where u , v , w , u_0 , v_0 , w_0 , ψ_x and ψ_y were defined in Chapter 4.2.

5.3.2 Kinematic (Strain-Displacement) Relations

Introducing an initial imperfection function, the strain-displacement relations, previously defined in equation (4.4) for a perfect cylindrical shell, are replaced by the following forms:

$$\begin{aligned}
 e_x^0 &= \frac{\partial u_0}{\partial x} + \frac{1}{2} \left(\frac{\partial w_0}{\partial x} \right)^2 + \left(\frac{\partial w_0}{\partial x} \right) \left(\frac{\partial \bar{w}_0}{\partial x} \right) \\
 e_y^0 &= \frac{\partial v_0}{\partial y} + \frac{w_0}{R} + \frac{1}{2} \left(\frac{\partial w_0}{\partial y} - \frac{v_0}{R} \right)^2 + \left(\frac{\partial w_0}{\partial y} - \frac{v_0}{R} \right) \left(\frac{\partial \bar{w}_0}{\partial y} \right) \\
 \gamma_{xy}^0 &= \frac{\partial u_0}{\partial y} + \frac{\partial v_0}{\partial x} + \left(\frac{\partial w_0}{\partial x} \right) \left(\frac{\partial w_0}{\partial y} - \frac{v_0}{R} \right) + \left(\frac{\partial w_0}{\partial x} \right) \left(\frac{\partial \bar{w}_0}{\partial y} \right) + \left(\frac{\partial w_0}{\partial y} - \frac{v_0}{R} \right) \left(\frac{\partial \bar{w}_0}{\partial x} \right)
 \end{aligned} \tag{5.18}$$

The rest of the strain-displacement relations remain the same as those defined in equations (4.2) and (4.3).

5.3.3 Virtual Work Statement

Introducing newly derived equations of displacement fields (equation (5.17)) and strain-displacement relations (equation (5.18)) for an imperfect, nonlinear cylindrical shell, the weak form derived from the principle of the virtual work can be obtained as follows:

$$0 = \delta \Pi = \delta U + \delta V$$

$$\begin{aligned}
&= \int_{\Omega} (N_x \delta e_{xx}^0 + N_y \delta e_{yy}^0 + N_{xy} \delta \gamma_{xy}^0 + M_x \delta \kappa_x^0 + M_y \delta \kappa_y^0 + M_{xy} \delta \kappa_{xy}^0 \\
&\quad + Q_{yz} \delta \gamma_{yz}^0 + Q_{xz} \delta \gamma_{xz}^0) dA - \int_{\Omega} p_{\text{total}} \cdot \delta w_0 dA \\
&= \int_{\Omega} \left\{ N_x \left[\frac{\partial \delta u_0}{\partial x} + \left(\frac{\partial w_0}{\partial x} \right) \left(\frac{\partial \delta w_0}{\partial x} \right) + \left(\frac{\partial \delta w_0}{\partial x} \right) \left(\frac{\partial \bar{w}_0}{\partial x} \right) \right] \right. \\
&\quad + N_y \left[\frac{\partial \delta v_0}{\partial y} + \frac{\delta w_0}{R} + \left(\frac{\partial w_0}{\partial y} - \frac{v_0}{R} \right) \left(\frac{\partial \delta w_0}{\partial y} - \frac{\delta v_0}{R} \right) + \left(\frac{\partial \delta w_0}{\partial y} - \frac{\delta v_0}{R} \right) \left(\frac{\partial \bar{w}_0}{\partial y} \right) \right] \\
&\quad + N_{xy} \left[\frac{\partial \delta u_0}{\partial y} + \frac{\partial \delta v_0}{\partial x} + \left(\frac{\partial \delta w_0}{\partial x} \right) \left(\frac{\partial w_0}{\partial y} - \frac{v_0}{R} \right) + \left(\frac{\partial w_0}{\partial x} \right) \left(\frac{\partial \delta w_0}{\partial y} - \frac{\delta v_0}{R} \right) \right. \\
&\quad \left. + \left(\frac{\partial \delta w_0}{\partial x} \right) \left(\frac{\partial \bar{w}_0}{\partial y} \right) + \left(\frac{\partial \delta w_0}{\partial y} - \frac{\delta v_0}{R} \right) \left(\frac{\partial \bar{w}_0}{\partial x} \right) \right] \\
&\quad + M_x \left(\frac{\partial \delta \psi_x}{\partial x} \right) + M_y \left(\frac{\partial \delta \psi_y}{\partial y} \right) + M_{xy} \left[\frac{\partial \delta \psi_x}{\partial y} + \frac{\partial \delta \psi_y}{\partial x} - C_0 \left(\frac{\partial \delta v_0}{\partial x} - \frac{\partial \delta u_0}{\partial y} \right) \right] \\
&\quad \left. + Q_{yz} \left(\delta \psi_y + \frac{\partial \delta w_0}{\partial y} - \frac{\delta v_0}{R} \right) + Q_{xz} \left(\delta \psi_x + \frac{\partial \delta w_0}{\partial x} \right) \right\} dA \\
&\quad - \int_{\Omega} p_{\text{total}} \cdot \delta w_0 dA
\end{aligned} \tag{5.19}$$

Using integration by parts on various displacement variables individually and also applying the Gauss identity theory, one can obtain five new equilibrium equations and the corresponding boundary conditions which govern the nonlinear behavior of an initially imperfect cylindrical shell by collecting terms involving δu_0 , δv_0 , δw_0 , $\delta \psi_x$ and $\delta \psi_y$, respectively. The newly derived equations of equilibrium and boundary conditions are stated in Chapter 5.3.4.

5.3.4 Equilibrium Equations and Associated Boundary Conditions

According to the statement of the minimum potential energy theory and the procedures stated in the preceding sub-chapter, the refined equilibrium equations which govern the behavior of imperfect, elastic cylindrical shells are obtained as:

$$\begin{aligned}
 \delta u_0 \dots \frac{\partial N_x}{\partial x} + \frac{\partial N_{xy}}{\partial y} + C_0 \frac{\partial M_{xy}}{\partial y} &= 0 \\
 \delta v_0 \dots \frac{\partial N_{xy}}{\partial x} + \frac{\partial N_y}{\partial y} - C_0 \frac{\partial M_{xy}}{\partial x} + \frac{Q_{yz}}{R} + \frac{N_{xy}}{R} \left(\frac{\partial w_0}{\partial x} + \frac{\partial \bar{w}_0}{\partial x} \right) \\
 + \frac{N_y}{R} \left(\frac{\partial w_0}{\partial y} + \frac{\partial \bar{w}_0}{\partial y} - \frac{v_0}{R} \right) &= 0 \\
 \delta w_0 \dots \frac{\partial}{\partial x} \left[N_x \left(\frac{\partial w_0}{\partial x} + \frac{\partial \bar{w}_0}{\partial x} \right) + N_{xy} \left(\frac{\partial w_0}{\partial y} + \frac{\partial \bar{w}_0}{\partial y} - \frac{v_0}{R} \right) \right] \\
 + \frac{\partial}{\partial y} \left[N_{xy} \left(\frac{\partial w_0}{\partial x} + \frac{\partial \bar{w}_0}{\partial x} \right) + N_y \left(\frac{\partial w_0}{\partial y} + \frac{\partial \bar{w}_0}{\partial y} - \frac{v_0}{R} \right) \right] \\
 \frac{\partial Q_{xz}}{\partial x} + \frac{\partial Q_{yz}}{\partial y} - \frac{N_y}{R} + p_{\text{total}} &= 0 \tag{5.20} \\
 \delta \psi_x \dots \frac{\partial M_x}{\partial x} + \frac{\partial M_{xy}}{\partial y} - Q_{xz} &= 0 \\
 \delta \psi_y \dots \frac{\partial M_{xy}}{\partial x} + \frac{\partial M_y}{\partial y} - Q_{yz} &= 0
 \end{aligned}$$

The geometrical and natural boundary conditions related to the initial imperfection theory are specified as:

Geometric

$$u_0 = \hat{u}_0$$

$$v_0 = \hat{v}_0$$

$$w_0 = \hat{w}_0$$

$$\psi_x = \hat{\psi}_x$$

$$\psi_y = \hat{\psi}_y$$

Natural

$$N_n = n_x N_x + n_y (N_{xy} + C_0 M_{xy}) = \hat{N}_n$$

$$N_t = n_x (N_{xy} - C_0 M_{xy}) + n_y N_y = \hat{N}_t$$

$$\begin{aligned} P_n = n_x [& N_x \left(\frac{\partial w_0}{\partial x} + \frac{\partial \bar{w}_0}{\partial x} \right) \\ & + N_{xy} \left(\frac{\partial w_0}{\partial y} + \frac{\partial \bar{w}_0}{\partial y} - \frac{v_0}{R} \right)] \\ & + n_y [N_{xy} \left(\frac{\partial w_0}{\partial x} + \frac{\partial \bar{w}_0}{\partial x} \right) \\ & + N_y \left(\frac{\partial w_0}{\partial y} + \frac{\partial \bar{w}_0}{\partial y} - \frac{v_0}{R} \right)] \\ & + n_x Q_{xz} + n_y Q_{yz} = \hat{P}_n \end{aligned} \quad (5.21)$$

$$M_n = n_x M_x + n_y M_{xy} = \hat{M}_n$$

$$M_t = n_x M_{xy} + n_y M_y = \hat{M}_t$$

5.3.5 Weak Formulation and Finite Element Model

Introducing the principle of virtual work statement, expressed in equation (5.19), combined with the equations of stress and moment resultants of a composite, shown in equations (3.14) to (3.16), and the equations of strain-displacement relations, stated in equations (4.2), (4.3) and (5.18), the displacement-based, variational weak-form of a

nonlinear, elastic cylindrical shell involving initial imperfections over an element result in the following equations:

$$\begin{aligned}
0 &= \{ \delta \Pi \}_{\text{Perfect}} + \{ \delta \Pi \}_{\text{Imperfect}} \\
&= \{ \delta U + \delta V \}_{\text{Perfect}} + \{ \delta U \}_{\text{Imperfect}} \quad (5.22) \\
&= \{ \delta U_s + \delta U_b + \delta U_{bs} + \delta U_T + \delta V \}_{\text{Perfect}} + \{ \delta U \}_{\text{Imperfect}}
\end{aligned}$$

where $\{ \delta U + \delta V \}_{\text{Perfect}}$ is the variational energy resulting from the theory for a perfectly circular cylindrical shell, and is also defined in Chapter 4.

The variational form of the total potential energy related to initially imperfect terms is given as follows:

$$\begin{aligned}
\{ \delta U \}_{\text{Imperfect}} &= \int_{\Omega} \left\{ \left\{ A_{11} \left[\frac{\partial u_0}{\partial x} + \frac{1}{2} \left(\frac{\partial w_0}{\partial x} \right)^2 + \left(\frac{\partial w_0}{\partial x} \right) \left(\frac{\partial \bar{w}_0}{\partial x} \right) \right] \right. \right. \\
&+ A_{12} \left[\frac{\partial v_0}{\partial y} + \frac{w_0}{R} + \frac{1}{2} \left(\frac{\partial w_0}{\partial y} - \frac{v_0}{R} \right)^2 + \left(\frac{\partial w_0}{\partial y} - \frac{v_0}{R} \right) \left(\frac{\partial \bar{w}_0}{\partial y} \right) \right] \\
&+ A_{16} \left[\frac{\partial u_0}{\partial y} + \frac{\partial v_0}{\partial x} + \left(\frac{\partial w_0}{\partial x} \right) \left(\frac{\partial w_0}{\partial y} - \frac{v_0}{R} \right) + \left(\frac{\partial w_0}{\partial x} \right) \left(\frac{\partial \bar{w}_0}{\partial y} \right) + \left(\frac{\partial w_0}{\partial y} - \frac{v_0}{R} \right) \left(\frac{\partial \bar{w}_0}{\partial x} \right) \right] \\
&+ B_{11} \left(\frac{\partial \psi_x}{\partial x} \right) + B_{12} \left(\frac{\partial \psi_y}{\partial y} \right) + B_{16} \left[\frac{\partial \psi_x}{\partial y} + \frac{\partial \psi_y}{\partial x} - C_0 \left(\frac{\partial v_0}{\partial x} - \frac{\partial u_0}{\partial y} \right) \right] \left. \right\} \left(\frac{\partial \delta w_0}{\partial x} \right) \left(\frac{\partial \bar{w}_0}{\partial x} \right) \\
&+ \left\{ A_{12} \left[\frac{\partial u_0}{\partial x} + \frac{1}{2} \left(\frac{\partial w_0}{\partial x} \right)^2 + \left(\frac{\partial w_0}{\partial x} \right) \left(\frac{\partial \bar{w}_0}{\partial x} \right) \right] \right. \\
&+ A_{22} \left[\frac{\partial v_0}{\partial y} + \frac{w_0}{R} + \frac{1}{2} \left(\frac{\partial w_0}{\partial y} - \frac{v_0}{R} \right)^2 + \left(\frac{\partial w_0}{\partial y} - \frac{v_0}{R} \right) \left(\frac{\partial \bar{w}_0}{\partial y} \right) \right] \\
&+ A_{26} \left[\frac{\partial u_0}{\partial y} + \frac{\partial v_0}{\partial x} + \left(\frac{\partial w_0}{\partial x} \right) \left(\frac{\partial w_0}{\partial y} - \frac{v_0}{R} \right) + \left(\frac{\partial w_0}{\partial x} \right) \left(\frac{\partial \bar{w}_0}{\partial y} \right) + \left(\frac{\partial w_0}{\partial y} - \frac{v_0}{R} \right) \left(\frac{\partial \bar{w}_0}{\partial x} \right) \right] \\
&+ B_{12} \left(\frac{\partial \psi_x}{\partial x} \right) + B_{22} \left(\frac{\partial \psi_y}{\partial y} \right) + B_{26} \left[\frac{\partial \psi_x}{\partial y} + \frac{\partial \psi_y}{\partial x} - C_0 \left(\frac{\partial v_0}{\partial x} - \frac{\partial u_0}{\partial y} \right) \right] \left. \right\}
\end{aligned}$$

$$\begin{aligned}
& + B_{66} \left(\left(\frac{\partial w_0}{\partial x} \right) \left(\frac{\partial \bar{w}_0}{\partial y} \right) + \left(\frac{\partial w_0}{\partial y} - \frac{v_0}{R} \right) \left(\frac{\partial \bar{w}_0}{\partial x} \right) \right)] \\
& \left[\frac{\partial \delta \psi_x}{\partial y} + \frac{\partial \delta \psi_y}{\partial x} - C_0 \left(\frac{\partial \delta v_0}{\partial x} - \frac{\partial \delta u_0}{\partial y} \right) \right] \} dA
\end{aligned} \tag{5.23}$$

As in the case of perfect cylindrical shells, the mid-surface displacements (u_0 , v_0 , w_0 , ψ_x , ψ_y , \bar{w}_0) over an element are expanded as linear combinations of the two dimensional Lagrange interpolation functions in the forms of

$$u_0(x, y) = \sum_{j=1}^l u_j \phi_j^{(1)}(\xi_1, \xi_2),$$

$$v_0(x, y) = \sum_{j=1}^m v_j \phi_j^{(2)}(\xi_1, \xi_2),$$

$$w_0(x, y) = \sum_{j=1}^n w_j \phi_j^{(3)}(\xi_1, \xi_2),$$

$$\psi_x(x, y) = \sum_{j=1}^p \psi_{xj} \phi_j^{(4)}(\xi_1, \xi_2),$$

$$\psi_y(x, y) = \sum_{j=1}^q \psi_{yj} \phi_j^{(5)}(\xi_1, \xi_2),$$

and

$$\bar{w}_0(x, y) = \sum_{j=1}^r \bar{w}_j \phi_j^{(6)}(\xi_1, \xi_2).$$

where $\phi_j^{(1)}$, $\phi_j^{(2)}$, $\phi_j^{(3)}$, $\phi_j^{(4)}$, $\phi_j^{(5)}$ and $\phi_j^{(6)}$ are the interpolation functions of degrees 1-1, m-1, n-1, p-1 q-1 and r-1, respectively; u_j , v_j , w_j , ψ_{xj} , ψ_{yj} , and \bar{w}_j are the nodal values.

Substituting equation (5.24) into equation (5.23), and letting $\delta u_0 = \phi_i^{(1)}$, $\delta v_0 = \phi_i^{(2)}$, $\delta w_0 = \phi_i^{(3)}$, $\delta \psi_x = \phi_i^{(4)}$ and $\delta \psi_y = \phi_i^{(5)}$, leads to a typical finite-element equation of an initially imperfect cylindrical shell over an element as follows:

$$\left[\mathbf{k}^{(e)} \right]_{\text{Imperfect}} \{ \Delta \} = \{ \mathbf{f}^{(e)} \} \quad (5.25)$$

where $\{ \Delta \} = \{ \{ u_0 \}, \{ v_0 \}, \{ w_0 \}, \{ \psi_x \}, \{ \psi_y \} \}^T$ is the generalized displacement vector, $\left[\mathbf{k}^{(e)} \right]_{\text{Imperfect}}$ is an element stiffness matrix, and $\{ \mathbf{f}^{(e)} \}$ is the element nodal force vector,

which is defined in Chapter 4.

For the convenience of computer code implementation, equation (5.25) can be rewritten in matrix form as:

$$\left[\begin{array}{c} \left[\begin{array}{c} k^{11} \\ k^{21} \\ k^{31} \\ k^{41} \\ k^{51} \\ k^{61} \end{array} \right] \left[\begin{array}{c} k^{12} \\ k^{22} \\ k^{32} \\ k^{42} \\ k^{52} \\ k^{62} \end{array} \right] \left[\begin{array}{c} k^{13} \\ k^{23} \\ k^{33} \\ k^{43} \\ k^{53} \\ k^{63} \end{array} \right] \left[\begin{array}{c} k^{14} \\ k^{24} \\ k^{34} \\ k^{44} \\ k^{54} \\ k^{64} \end{array} \right] \left[\begin{array}{c} k^{15} \\ k^{25} \\ k^{35} \\ k^{45} \\ k^{55} \\ k^{65} \end{array} \right] \left[\begin{array}{c} k^{16} \\ k^{26} \\ k^{36} \\ k^{46} \\ k^{56} \\ k^{66} \end{array} \right] \\ \left[\begin{array}{c} k^{11} \\ k^{21} \\ k^{31} \\ k^{41} \\ k^{51} \\ k^{61} \end{array} \right] \left[\begin{array}{c} k^{12} \\ k^{22} \\ k^{32} \\ k^{42} \\ k^{52} \\ k^{62} \end{array} \right] \left[\begin{array}{c} k^{13} \\ k^{23} \\ k^{33} \\ k^{43} \\ k^{53} \\ k^{63} \end{array} \right] \left[\begin{array}{c} k^{14} \\ k^{24} \\ k^{34} \\ k^{44} \\ k^{54} \\ k^{64} \end{array} \right] \left[\begin{array}{c} k^{15} \\ k^{25} \\ k^{35} \\ k^{45} \\ k^{55} \\ k^{65} \end{array} \right] \left[\begin{array}{c} k^{16} \\ k^{26} \\ k^{36} \\ k^{46} \\ k^{56} \\ k^{66} \end{array} \right] \end{array} \right]_{(e)} \left\{ \begin{array}{c} u_0 \\ v_0 \\ w_0 \\ \psi_x \\ \psi_y \\ \bar{w}_0 \end{array} \right\} = \left\{ \begin{array}{c} f^1 \\ f^2 \\ f^3 \\ f^4 \\ f^5 \\ f^6 \end{array} \right\}_{(e)} \quad (5.26)$$

The additional components of the element stiffness matrix $\left[\mathbf{k}^{(e)} \right]_{\text{Imperfect}}$ and the force vector $\{ \mathbf{f}^{(e)} \}$ are stated in Appendix G. All the other coefficients are the same as the

ones defined in Appendix C.2. Note that the presence of the imperfection function introduces the additional terms corresponding to the sixth row and column.

Since the initial imperfection over the entire domain is prescribed, the terms associated with \bar{w}_0 can be considered and entered as boundary terms, and moved to the right-hand side vector of equation (5.26). The equation of the finite element model of an initially imperfect cylindrical shell is, therefore, rewritten as:

$$\begin{bmatrix} \begin{bmatrix} k^{11} \\ k^{21} \\ k^{31} \\ k^{41} \\ k^{51} \end{bmatrix} & \begin{bmatrix} k^{12} \\ k^{22} \\ k^{32} \\ k^{42} \\ k^{52} \end{bmatrix} & \begin{bmatrix} k^{13} \\ k^{23} \\ k^{33} \\ k^{43} \\ k^{53} \end{bmatrix} & \begin{bmatrix} k^{14} \\ k^{24} \\ k^{34} \\ k^{44} \\ k^{54} \end{bmatrix} & \begin{bmatrix} k^{15} \\ k^{25} \\ k^{35} \\ k^{45} \\ k^{55} \end{bmatrix} & \begin{bmatrix} k^{16} \\ k^{26} \\ k^{36} \\ k^{46} \\ k^{56} \end{bmatrix} \end{bmatrix}_{(e)} \begin{Bmatrix} \{u_0\} \\ \{v_0\} \\ \{w_0\} \\ \{\psi_x\} \\ \{\psi_y\} \end{Bmatrix} = \begin{Bmatrix} \{f^1\} - \begin{bmatrix} k^{16} \\ k^{26} \\ k^{36} \\ k^{46} \\ k^{56} \end{bmatrix} \{\bar{w}_0\} \\ \{f^2\} - \begin{bmatrix} k^{16} \\ k^{26} \\ k^{36} \\ k^{46} \\ k^{56} \end{bmatrix} \{\bar{w}_0\} \\ \{f^3\} - \begin{bmatrix} k^{16} \\ k^{26} \\ k^{36} \\ k^{46} \\ k^{56} \end{bmatrix} \{\bar{w}_0\} \\ \{f^4\} - \begin{bmatrix} k^{16} \\ k^{26} \\ k^{36} \\ k^{46} \\ k^{56} \end{bmatrix} \{\bar{w}_0\} \\ \{f^5\} - \begin{bmatrix} k^{16} \\ k^{26} \\ k^{36} \\ k^{46} \\ k^{56} \end{bmatrix} \{\bar{w}_0\} \end{Bmatrix}_{(e)} \quad (5.27)$$

where the components of equation (5.27) are exactly the same as those shown in equation (5.26).

5.3.6 Nonlinear Finite Element Analysis of Imperfect Cylindrical Shells

For the purpose of solving the nonlinear behavior and stability condition of imperfect cylindrical shell types of structures, governed by equation (5.26) and (5.27), some nonlinear methods will be required to perform the iterative solution procedures. As stated in Chapter 4.11.2, the determination of the element tangent stiffness matrix will be the first step for applying these nonlinear schemes. The procedures are shown as follows.

Let

$$R_1 = \sum_{j=1}^l k_{ij}^{11} u_j + \sum_{j=1}^m k_{ij}^{12} v_j + \sum_{j=1}^n k_{ij}^{13} w_j + \sum_{j=1}^p k_{ij}^{14} \psi_{xj} + \sum_{j=1}^q k_{ij}^{15} \psi_{yj} - F_i^1 + \sum_{j=1}^r k_{ij}^{16} \bar{w}_j, \quad (5.28)$$

$$R_2 = \sum_{j=1}^l k_{ij}^{21} u_j + \sum_{j=1}^m k_{ij}^{22} v_j + \sum_{j=1}^n k_{ij}^{23} w_j + \sum_{j=1}^p k_{ij}^{24} \psi_{xj} + \sum_{j=1}^q k_{ij}^{25} \psi_{yj} - F_i^2 + \sum_{j=1}^r k_{ij}^{26} \bar{w}_j, \quad (5.29)$$

$$R_3 = \sum_{j=1}^l k_{ij}^{31} u_j + \sum_{j=1}^m k_{ij}^{32} v_j + \sum_{j=1}^n k_{ij}^{33} w_j + \sum_{j=1}^p k_{ij}^{34} \psi_{xj} + \sum_{j=1}^q k_{ij}^{35} \psi_{yj} - F_i^3 + \sum_{j=1}^r k_{ij}^{36} \bar{w}_j, \quad (5.30)$$

$$R_4 = \sum_{j=1}^l k_{ij}^{41} u_j + \sum_{j=1}^m k_{ij}^{42} v_j + \sum_{j=1}^n k_{ij}^{43} w_j + \sum_{j=1}^p k_{ij}^{44} \psi_{xj} + \sum_{j=1}^q k_{ij}^{45} \psi_{yj} - F_i^4 + \sum_{j=1}^r k_{ij}^{46} \bar{w}_j, \quad (5.31)$$

and

$$R_5 = \sum_{j=1}^l k_{ij}^{51} u_j + \sum_{j=1}^m k_{ij}^{52} v_j + \sum_{j=1}^n k_{ij}^{53} w_j + \sum_{j=1}^p k_{ij}^{54} \psi_{xj} + \sum_{j=1}^q k_{ij}^{55} \psi_{yj} - F_i^5 + \sum_{j=1}^r k_{ij}^{56} \bar{w}_j. \quad (5.32)$$

where R_1, R_2, R_3, R_4 and R_5 are the residual force vectors associated with five different directions, separately; the components of equations (5.28) to (5.32) are included in Appendix G.

From the definition of the tangent stiffness matrix, one obtains

$$(k_T)_{ij}^{rs} = \frac{\partial R_r}{\partial U_s} = k_{ij}^{rs} + \sum_{k=1}^5 \frac{\partial k_{ij}^{rs}}{\partial U_s} U_k + \frac{\partial k_{ij}^{r6}}{\partial U_s} U_6 \quad (5.33)$$

where

$$R_r = (k_{ij}^{rs}) U_s + (k_{ij}^{r6}) U_6 - F_r \quad (r, s = 1, 2, 3, 4, 5) \quad (5.34)$$

Introducing equations (5.28) to (5.34), the element tangent stiffness matrix can be obtained as:

$$\left[k_T^{(e)} \right]_{\text{Imperfect}} = \begin{bmatrix} \left[k_T^{11} \right] & \left[k_T^{12} \right] & \left[k_T^{13} \right] & \left[k_T^{14} \right] & \left[k_T^{15} \right] \\ \left[k_T^{12} \right] & \left[k_T^{22} \right] & \left[k_T^{23} \right] & \left[k_T^{24} \right] & \left[k_T^{25} \right] \\ \left[k_T^{13} \right] & \left[k_T^{23} \right] & \left[k_T^{33} \right] & \left[k_T^{34} \right] & \left[k_T^{35} \right] \\ \left[k_T^{14} \right] & \left[k_T^{24} \right] & \left[k_T^{34} \right] & \left[k_T^{44} \right] & \left[k_T^{45} \right] \\ \left[k_T^{15} \right] & \left[k_T^{25} \right] & \left[k_T^{35} \right] & \left[k_T^{45} \right] & \left[k_T^{55} \right] \end{bmatrix}_{(e)} \quad (5.35)$$

The coefficients of the element tangent stiffness matrix are included in Appendix H.

CHAPTER 6

NUMERICAL SOLUTION PROCEDURES

6.1 Introduction

In the preceding Chapters 3, 4 and 5, the finite element equations are formulated by use of the principle of virtual displacements of the total potential energy generated from the deformations of entire elastic bodies and all the external loads, including the effects of elastic foundations and initial imperfections. The formulations lead to a set of algebraic equations for each element of the finite element mesh. After assembling element stiffness matrices and load vectors into global ones, the boundary conditions are then applied. The next important step is to try to solve the linear and nonlinear systems of equations numerically.

For the linear static and stability problems, the generalized displacement vectors and the corresponding buckling loads could be determined by means of solving a set of linear algebraic equations and the linear eigenvalue problems, respectively. Because the global stiffness matrices are constants at all times, in other words, they are independent of displacement or load vectors, the equation can be solved easily.

However, in general cases one has to deal with nonlinear static and stability problems by solving a set of coupled, nonlinear finite element equations. In order to solve those nonlinear problems, iterative schemes are often used. Most numerical schemes are incremental iterative processes that use a series of linear solutions to approximate the

nonlinear solutions. The linear solutions are achieved by expanding the nonlinear equations in terms of small incremental values of the unknowns about some known solutions. In the finite element analysis of structural mechanics, the major objective is to trace the nonlinear equilibrium path for a given structure and the associated environment.

The most basic nonlinear iterative method is based on the load control technique where prescribed load increments are applied to the system and the resulting displacements are to be calculated to satisfy the equilibrium points. The most popular load control method is the Newton-Raphson scheme. The limitation of the Newton-Raphson method is that it is not able to trace nonlinear load-displacement curves with negative slopes or non-positive determinants of the total stiffness matrices. Therefore, more complicated solution procedures are applied to overcome these problems where the methods treat both the incremental loads and resulting displacements as unknowns in the analysis. They are referred to as arc length methods. The most popular arc length schemes are derived from the Riks-Wempner method. They will be explicitly described in the following sub-chapters [147].

6.2 Eigenvalue Analysis

Linear stability analysis of elastic bodies under uniform pressure requires the solution of the eigenvalues and the associated eigenvectors of a system of linear finite element equations. The eigenvalues and eigenvectors of the global stiffness matrices are referred to as buckling loads and modes, respectively. An eigenvalue and eigenvector solver is

required for the present analysis. The DVGLRG subroutine in the IMSL library has been used.

6.3 Newton-Raphson Method

Consider a nonlinear set of finite element equations which has the form:

$$[K(u_i)] \{u_i\} = \{F_i\}, \quad i = 1, 2, \dots, n \quad (6.1)$$

or

$$\{R(u_i)\} = \{F_i\} - [K(u_i)] \{u_i\} = 0, \quad i = 1, 2, \dots, n \quad (6.2)$$

where $[K(u)]$ is the global secant stiffness matrix, $\{u\}$ is the generalized displacement vector, $\{F\}$ is the global force vector, and $\{R\}$ is the out-of-balance force vector (so-called residual force vector). Expanding $R(u)$ about the known solution $u^{(r-1)}$ in Taylor's series, neglecting the second and higher order terms in δu , one can obtain

$$\begin{aligned} \{\delta u\} &= - [K_T(u^{(r-1)})]^{-1} \cdot \{R(u^{(r-1)})\} \\ &= - [K_T(u^{(r-1)})]^{-1} \cdot [F - K(u^{(r-1)}) \cdot u^{(r-1)}] \end{aligned} \quad (6.3)$$

where δu is the increment, which can be expressed as

$$\delta u = u^{(r)} - u^{(r-1)}, \quad (6.4)$$

and K_T is the slope (tangent) of the curve $R(u)$ at the equilibrium point of $u^{(r-1)}$, which may be given as:

$$K_T = \left(\frac{\partial R}{\partial u} \right) \Big|_{u^{(r-1)}} \quad (6.5)$$

The new equilibrium solution at the end of the r -th iteration is updated as:

$$u^{(r)} = u^{(r-1)} + \delta u \quad (6.6)$$

The residual or imbalance force, $R(u^{(r-1)})$, is gradually reduced to zero if the procedure is repeated. The iteration is continued until a specified convergence criterion is satisfied.

The algorithm for the Newton-Raphson scheme may be summarized as follows.

For each load step (with a specified load increment), the method starts at a known point ($r-1$) on the equilibrium path as shown in Figure 6.1. Then, the following computational steps should be followed:

- Step 1. Evaluate element matrices $[k^{(e)}]$ and $\{F^{(e)}\}$, and also compute $[k_T^{(e)}]$ and $\{R^{(e)}\}$ for each element.
- Step 2. Assemble element matrices $[k_T^{(e)}]$ and $\{R^{(e)}\}$ into global matrices.
- Step 3. Apply the boundary conditions on the assembled set of nonlinear equations.
- Step 4. Solve the assembled equations.
- Step 5. Update the obtained solution vector $\{u^{(r)}\}$.
- Step 6. Check for convergence.

- Step 7. If the convergence criterion is satisfied, increase the load by adding another load increment, initialize the iteration counter, and repeat steps 1 through 6.
- Step 8. If the convergence criterion is not satisfied, check if the maximum allowed number of iterations is exceeded. If it is not exceeded, go back to step 1 and repeat those steps. If it exceeds the maximum iteration number, then stop the computational procedure.

6.4 Riks-Wempner on a Normal Plane Method

The assembled equations to be solved are of the form,

$$[K(U)]\{U\} = \{Q\} \quad (6.7)$$

where

$[K]_{n \times n}$ is the assembled stiffness matrix,

$\{U\}_{n \times 1}$ is the column vector of nodal displacements of an elastic body,

$\{Q\}_{n \times 1}$ is the column vector of external nodal forces,

and n is the total number of degrees of freedom included in the mesh.

Introduction of a load factor λ , which is a number between zero and one, as an independent variable, one may obtain

$$\{Q\}_{n \times 1} = \lambda \{\bar{Q}\}_{n \times 1} \quad (6.8)$$

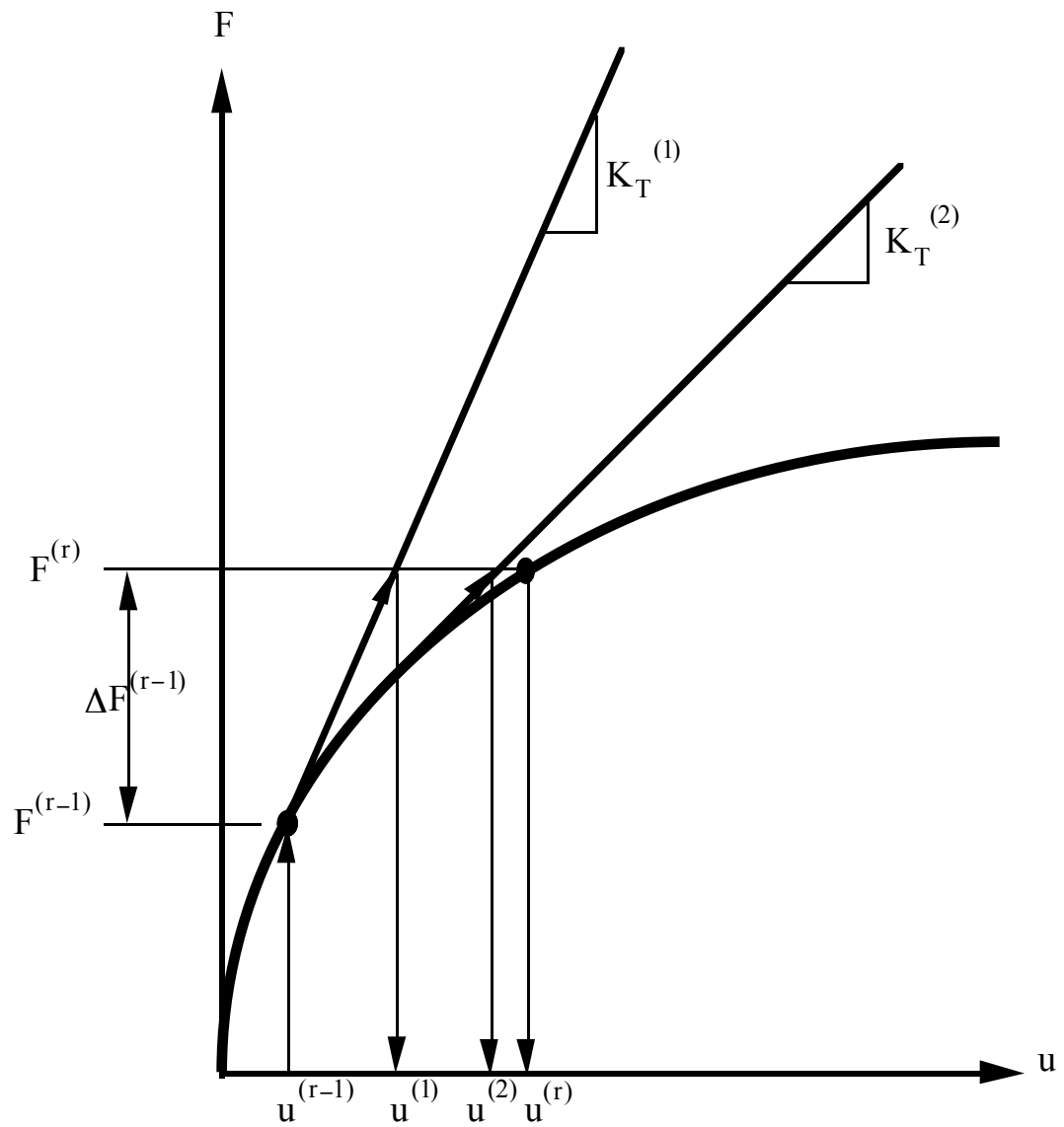


Figure 6.1 - Newton-Raphson method for a single degree of freedom system

where $\{\bar{Q}\}_{n \times 1}$ is a specified constant load vector.

Combining with equation (6.8), equation (6.7) can be rewritten as:

$$\{R(\{U\}, \lambda)\} = [K]\{U\} - \lambda \{\bar{Q}\}_{n \times 1} \quad (6.9)$$

where $\{R\}$ is a residual vector associated with both λ and $\{U\}$.

The Riks-Wempner solution technique treats both the load vector λ and displacement vector $\{U\}$ as unknowns, which are independent of each other, in the analysis. The process of solving equation (6.9) is prescribed as follows.

As shown in Figure 6.2, iteration begins at point i on the load-displacement curve, and the solution of the equilibrium point i , which is $(\{U_i\}, \lambda_i)$, is assumed to be known or determined for the i -th load step. Let t_i be a vector which is tangent to the equilibrium path at point i , and is defined as

$$t_i = \begin{bmatrix} \{\Delta U_i^{(0)}\} \\ \Delta \lambda_i^{(0)} \end{bmatrix} \quad (6.10)$$

where the scalar $\Delta \lambda_i^{(0)}$ is the load increment at point i and the vector $\{\Delta U_i^{(0)}\}$ is the displacement increment at point i , which can be obtained by solving

$$[K_{Ti}^{(0)}]\{\Delta U_i^{(0)}\} = \Delta \lambda_i^{(0)} \{\bar{Q}\} \quad (6.11)$$

where $[K_{Ti}^{(0)}]$ is the assembled global tangent stiffness matrix at the equilibrium point i .

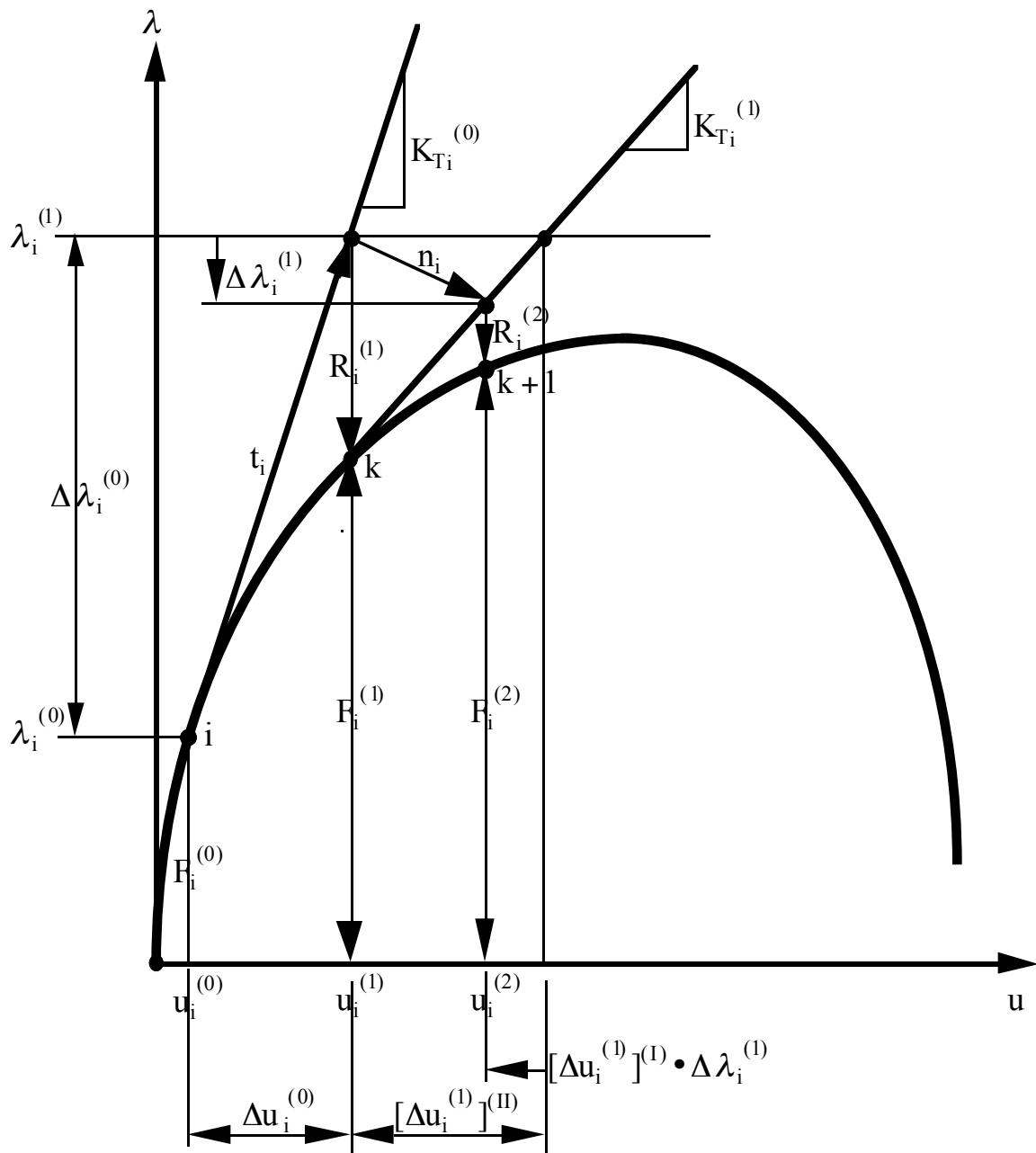


Figure 6.2 - Riks-Wempner method on a normal plane for a single degree of freedom system

The objective of this method is to iterate along a normal to the tangent vector t_i until the new equilibrium point is found. The normal n_i , which is also shown in Figure 6.2, is referred to as

$$n_i = \begin{bmatrix} \{\Delta U_i^{(1)}\} \\ \Delta \lambda_i^{(1)} \end{bmatrix} \quad (6.12)$$

where the vector $\{\Delta U_i^{(1)}\}$ is an unknown displacement vector from point k to the intersection point between the normal vector n_i and the tangent from point k. The scalar $\Delta \lambda_i^{(1)}$ is an unknown load increment from $\lambda_i^{(1)}$ down to the point where n_i intersects with the tangent from point k.

It is required that the inner product between t_i and n_i be equal to zero in order to constrain the iterative process to a normal plane. It is also implied mathematically that

$$t_i \bullet n_i = 0 \quad (6.13)$$

Substitution of equations (6.10) and (6.12) into equation (6.13) leads to

$$\{\Delta U_i^{(0)}\}^T \{\Delta U_i^{(1)}\} + \Delta \lambda_i^{(0)} \Delta \lambda_i^{(1)} = 0 \quad (6.14)$$

From equation (6.9), expanding the residual vector $\{R\}$, which is a function of λ and $\{U\}$, in Taylor's series about the previous equilibrium point k, one has

$$R(\{U_i^{(2)}\}, \lambda_i^{(2)}) = R(\{U_i^{(1)}\}, \lambda_i^{(1)}) + \left(\frac{\partial R}{\partial \lambda}\right)_k + \left(\frac{\partial R}{\partial \{U\}}\right)_k \{\Delta U_i^{(1)}\} + \text{H.O.T.} = \{0\} \quad (6.15)$$

Omitting the higher order terms involving the increments $\Delta\lambda_i^{(1)}$ and $\{\Delta U_i^{(1)}\}$, rearrangement of equation (6.15) gives

$$\{0\} = -\Delta\lambda_i \{\bar{Q}\} + [K_{Ti}^{(1)}] \{\Delta U_i^{(1)}\} + \{R_i^{(1)}\} \quad (6.16)$$

where $\{\bar{Q}\} = -(\frac{\partial R}{\partial \lambda})_k$ is a constant load vector, and $[K_{Ti}^{(1)}] = (\frac{\partial R}{\partial \{U\}})_k$ indicates the tangent stiffness matrix at the given point k.

Based on equation (6.16), the incremental solution at the current point k of the i-th load step is given by

$$\{\Delta U_i^{(1)}\} = \Delta\lambda_i^{(1)} [K_{Ti}^{(1)}]^{-1} \{\bar{Q}\} - [K_{Ti}^{(1)}]^{-1} \{R_i^{(1)}\} \quad (6.17)$$

So, the vector $\{\Delta U_i^{(1)}\}$ can be split into two parts [97, 98]:

$$\{\Delta U_i^{(1)}\} = \{\Delta U_i^{(1)}\}^{(II)} + \Delta\lambda_i^{(1)} \{\Delta U_i^{(1)}\}^{(I)} \quad (6.18)$$

where the vector $\{\Delta U_i^{(1)}\}^{(II)}$ results from solving

$$\{\Delta U_i^{(1)}\}^{(II)} = -[K_{Ti}^{(1)}]^{-1} \{R_i^{(1)}\} \quad (6.19)$$

and the vector $\{\Delta U_i^{(1)}\}^{(I)}$ results from the equation

$$\{\Delta U_i^{(1)}\}^{(I)} = [K_{Ti}^{(1)}]^{-1} \{\bar{Q}\} \quad (6.20)$$

The vector $\Delta \lambda_i^{(1)} \{ \Delta U_i^{(1)} \}^{(1)}$ also results from the similar triangles shown in Figure 6.3. Introducing an intermediate quantity $\{ \Delta U_i^{(1)} \}^*$, the similar triangles relationship can be expressed as

$$\frac{\Delta \lambda_i^{(1)}}{\{ \Delta U_i^{(1)} \}^*} = \frac{1}{\{ \Delta U_i^{(1)} \}^{(1)}} \quad (6.21)$$

Since the direction of $\Delta \lambda_i^{(1)}$ is going downward, as shown in Figure 6.2, so $\{ \Delta U_i^{(1)} \}^*$ will also be going downward, and can be represented as

$$\{ \Delta U_i^{(1)} \}^* = \Delta \lambda_i^{(1)} \{ \Delta U_i^{(1)} \}^{(1)} \quad (6.22)$$

Substituting the expression for $\{ \Delta U_i^{(1)} \}$, which is shown in equation (6.18), into the constraint equation (6.14) gives

$$\{ \Delta U_i^{(0)} \}^T \left(\{ \Delta U_i^{(1)} \}^{(II)} + \Delta \lambda_i^{(1)} \{ \Delta U_i^{(1)} \}^{(I)} \right) + \Delta \lambda_i^{(0)} \Delta \lambda_i^{(1)} = 0 \quad (6.23)$$

Expanding the above equation and solving for $\Delta \lambda_i^{(1)}$ yields

$$\Delta \lambda_i^{(1)} = - \frac{\{ \Delta U_i^{(0)} \}^T \{ \Delta U_i^{(1)} \}^{(II)}}{\Delta \lambda_i^{(0)} + \{ \Delta U_i^{(0)} \}^T \{ \Delta U_i^{(1)} \}^{(I)}} \quad (6.24)$$

When $\Delta \lambda_i^{(1)}$ is determined, the load increment may be updated by the expression

$$\lambda_i^{(2)} = \lambda_i^{(1)} + \Delta \lambda_i^{(1)} \quad (6.25)$$

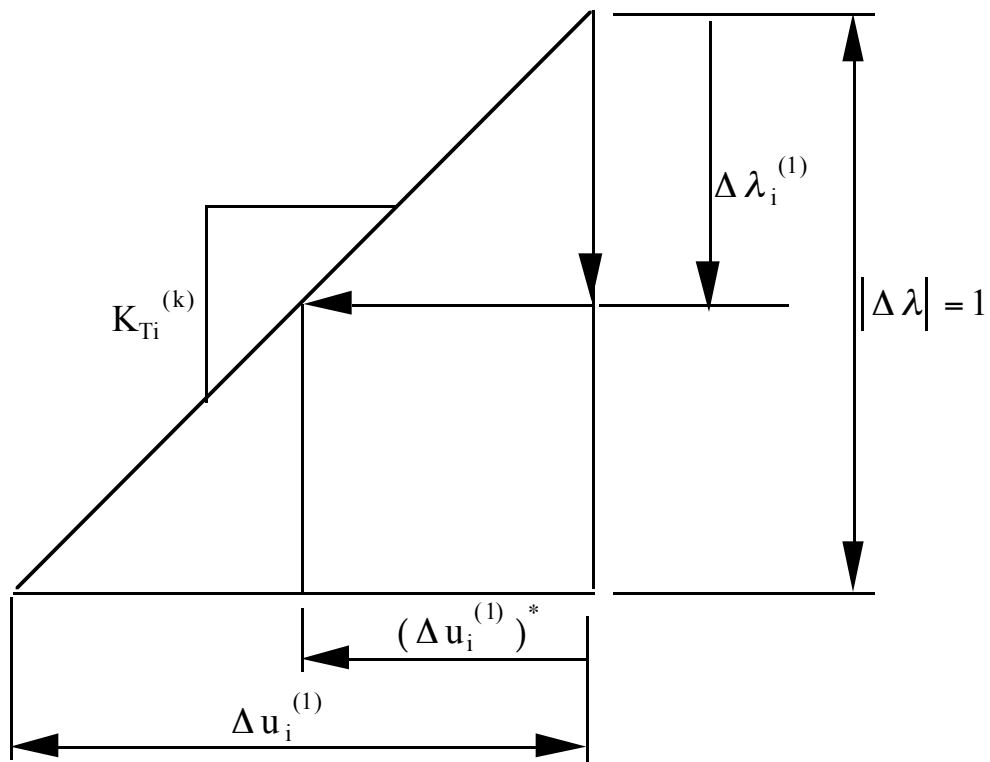


Figure 6.3 - Similar triangles for solving $\Delta \lambda_i^{(1)} \{ \Delta U_i^{(1)} \}^{(1)}$ for the Riks-Wempner method

on a normal plane

and the nodal displacement vector at point k+1 may also be updated as

$$\{U_i^{(2)}\} = \{U_i^{(1)}\} + \{\Delta U_i^{(1)}\} \quad (6.26)$$

or in the form of

$$\{U_i^{(2)}\} = \{U_i^{(1)}\} + \left(\{\Delta U_i^{(1)}\}^{(II)} + \Delta \lambda_i^{(1)} \{\Delta U_i^{(1)}\}^{(I)} \right) \quad (6.27)$$

For the first iteration of the first load step, as shown in Figure 6.4, one usually starts with a specific load increment $\Delta \lambda_0$, which is a fraction of the total external load applied to the structure. It is also often assumed that the initial starting point is the origin, which implies $\{U_0\} = \{0\}$.

Then the displacement vector $\{\Delta U_0\}$ and the length ΔS_0 of the initial tangent vector can be evaluated by using the load increment $\Delta \lambda_0$. The displacement vector $\{\Delta U_0\}$ is evaluated using the similar triangles relation shown in Figure 6.5. The vector $\{\Delta U_0\}$ is computed from the relation

$$\frac{\Delta \lambda_0}{\Delta u_0} = \frac{1}{\Delta u_{\text{total}}}, \quad \text{or} \quad \Delta u_0 = \Delta \lambda_0 \cdot \Delta u_{\text{total}}. \quad (6.28)$$

The vector $\{\Delta U_{\text{total}}\}$ is calculated from the expression

$$[K_{T_0}] \{\Delta U_{\text{total}}\} = \lambda \{\bar{Q}\} \quad (6.29)$$

where the load factor λ is equal to one, and $[K_{T_0}]$ is the assembled tangent stiffness matrix measured from the starting point O.

Since the vector $\{\Delta U_0\}$ can be determined by using equations (6.28) and (6.29), the length of t_0 , which is ΔS_0 , can also be calculated by

$$\Delta S_0 = |t_0 \cdot t_0| = \sqrt{(\Delta \lambda_0)^2 + \{\Delta U_0\}^T \{\Delta U_0\}} \quad (6.30)$$

Using equation (6.28), one could obtain the alternate form of ΔS_0 as

$$\Delta S_0 = \Delta \lambda_0 \sqrt{1 + \{\Delta U_{\text{total}}\}^T \{\Delta U_{\text{total}}\}} \quad (6.31)$$

The scalar ΔS_0 is often referred to as the arc length along the equilibrium path from the equilibrium point O. The arc length for subsequent iterations is usually held as a constant or is scaled using the relation

$$\Delta S_i = \Delta S_{i-1} \left(\frac{I_{\text{des}}}{I_{i-1}} \right)^{\frac{1}{2}} \quad (6.32)$$

The scalar ΔS_{i-1} is the current arc length, while I_{i-1} is the number of iterations required for convergence to the current equilibrium point and I_{des} is the desired number of iterations which is usually chosen as a small number approximately equal to 3. A maximum value for ΔS_i is usually specified as

$$\Delta S_{\text{max}} = 2 \cdot \Delta S_0 \quad (6.33)$$

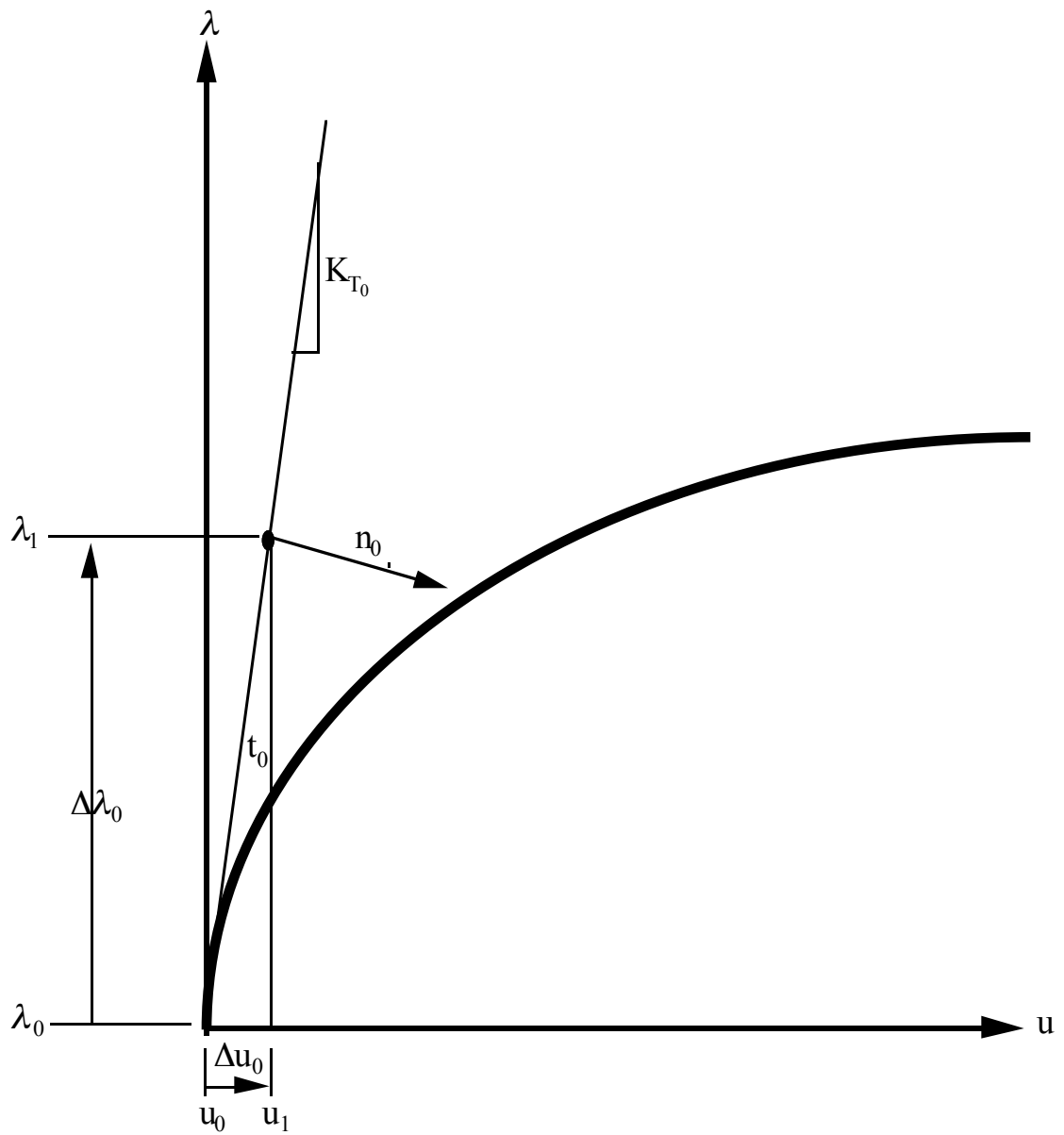


Figure 6.4 - The graph for the first iteration of the first load step in the Riks-Wempner method on a normal plane

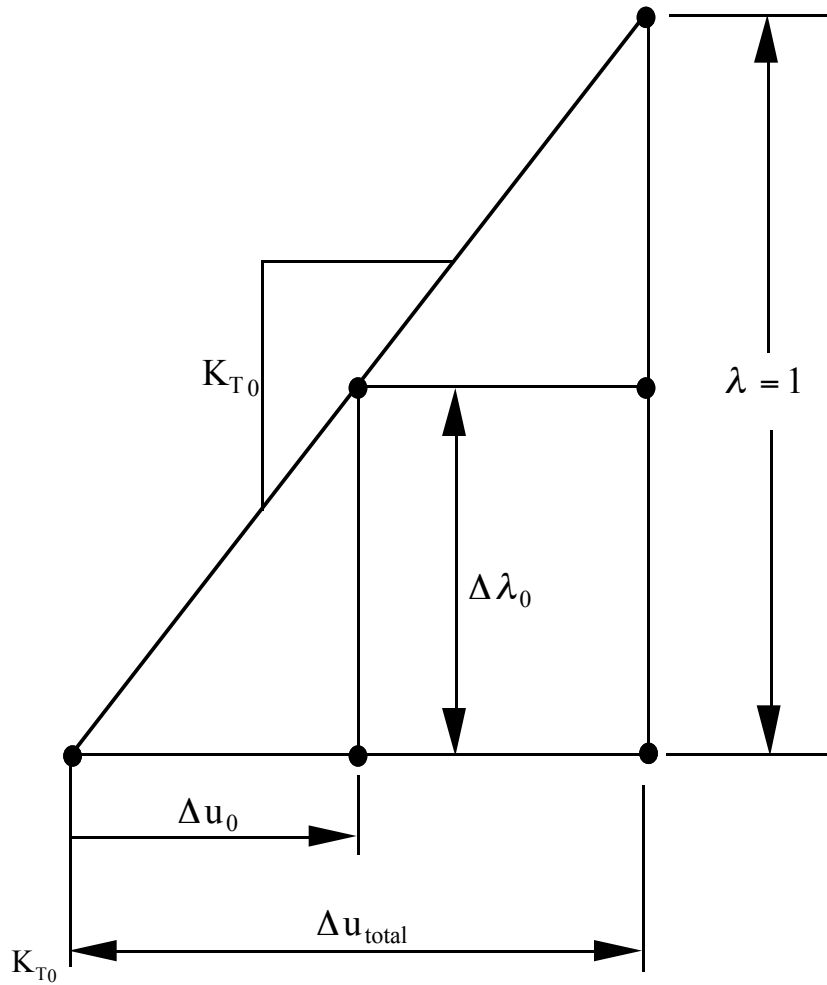


Figure 6.5 - Similar triangles in the first iteration of the first load step for the Riks-Wempner method on a normal plane

The value of ΔS_i is used to compute the value of $\Delta \lambda_i$ which is required to begin the next iteration. The load increment $\Delta \lambda_i$ is computed from equation (6.31) as

$$\Delta \lambda_i = \frac{\pm \Delta S_i}{\sqrt{1 + \{\Delta U_{\text{total}}\}_i^T \{\Delta U_{\text{total}}\}_i}} \quad (6.34)$$

where the vector $\{\Delta U_{\text{total}}\}_i$ can be evaluated from

$$\{\Delta U_{\text{total}}\}_i = [K_{Ti}]^{-1} \{\bar{Q}\} \quad (6.35)$$

The sign ambiguity in equation (6.34) results from the fact that the quantity ΔS_i is simply a length along the path whose direction is uncertain. The correct sign for $\Delta \lambda_i$ is found by looking at the projection of the hypothetical tangent vector t_i on the initial tangent vector for the previous iteration, t_{i-1} . Introducing of equation (6.10), combined with equation (6.28), the partitioned tangent vector t_i becomes

$$t_i = \begin{bmatrix} \Delta \lambda_i \{\Delta U_{\text{total}}\}_i \\ \Delta \lambda_i \end{bmatrix} \quad (6.36)$$

The vector t_i is termed hypothetical because the correct sign of $\Delta \lambda_i$ is not yet known. The projection of t_i on t_{i-1} is

$$t_i \bullet t_{i-1} = \Delta \lambda_i \{\Delta U_{\text{total}}\}_i^T \{\Delta U_{i-1}\} + \Delta \lambda_i \Delta \lambda_{i-1} \quad (6.37)$$

which reduces to

$$\mathbf{t}_i \cdot \mathbf{t}_{i-1} = \Delta \lambda_i \left(\{\Delta \mathbf{U}_{\text{total}}\}_i^T \{\Delta \mathbf{U}_{i-1}\} + \Delta \lambda_{i-1} \right) \quad (6.38)$$

If the projection of \mathbf{t}_i on \mathbf{t}_{i-1} is negative then the slope of the equilibrium path at i is negative and the load parameter $\Delta \lambda_i$ should be negative so that the external load on the structure is reduced, thereby producing an unloading effect. If the projection of \mathbf{t}_i on \mathbf{t}_{i-1} is positive, then the slope of the equilibrium path at i is positive and $\Delta \lambda_i$ should be positive, indicating that the external load is increasing.

6.5 Convergence Criteria

During the process of nonlinear iterative methods as described in the previous sections, a specified convergence criterion is applied for checking the required accuracy of the obtained solutions. This will also prevent the divergence of the solution procedures. In the analysis of nonlinear finite element schemes, two types of convergence criteria are usually used.

The first criterion ensures that the incremental displacements are relatively small. In other words, the criterion indicates that the "norm" of the incremental displacement $\{\Delta \mathbf{U}_i\}$ is small compared to the total displacement $\{\mathbf{U}_{i+1}\}$. The criterion states that

$$\frac{\|\{\Delta \mathbf{U}_i\}^T \{\Delta \mathbf{U}_i\}\|}{\|\{\mathbf{U}_{i+1}\}^T \{\mathbf{U}_{i+1}\}\|} \leq \beta_d \quad (6.39)$$

where β_d is a small, user specified tolerance on the order of 10^{-3} .

The second convergence criterion involves the residual (or out-of-balance) forces $\mathbf{R}_i^{(k+1)}$. The idea behind this criterion is to ensure that the imbalance forces themselves, or that the norm of the vector $\{\mathbf{R}_i^{(k+1)}\}$ is small. For the finite element models with rotational variables, additional problems arise because the residual vector contains both forces and moments. Therefore, when computing the norm of $\{\mathbf{R}_i^{(k+1)}\}$, quantities with different units must be added together. Because of the units involved in the analysis, the moments are generally much larger than the forces and therefore contribute much more to the calculation of the norm of $\{\mathbf{R}_i^{(k+1)}\}$. This problem can cause convergence of the solution to be obtained based solely on the moments rather than on the combination of both forces and moments. To solve this problem, scaling of the residual force vector is recommended [98, 148, 149].

The convergence criterion for checking the out-of-balance forces is

$$\frac{\sqrt{\{\mathbf{R}_i^{(k+1)}\}^T [\mathbf{S}_i] \{\mathbf{R}_i^{(k+1)}\}}}{\lambda_i^{(k+1)} \sqrt{\{\bar{\mathbf{Q}}\}^T [\mathbf{S}_i] \{\bar{\mathbf{Q}}\}}} \leq \beta_f \quad (6.40)$$

where $[\mathbf{S}_i]$ is a diagonal scaling matrix that contains the inverse of the diagonal elements of the tangent stiffness matrix $[\mathbf{K}_{Ti}]$, $\{\bar{\mathbf{Q}}\}$ is a constant external load vector, and $\lambda_i^{(k+1)}$ is the current load increment. The quantity β_d is a small, user specified tolerance on the order of 10^{-4} .

CHAPTER 7

EXAMPLE ANALYSES AND NUMERICAL RESULTS FOR RING MODEL

7.1 Introduction

Using the proposed linear and nonlinear theories for arch and ring structures, and the corresponding finite element models which are developed and detailed in Chapter 3, a wide variety of examples are investigated. As the first step, the accuracy and efficiency of the theory and finite element codes are tested. Both linear and nonlinear static and buckling analyses are performed using the prescribed finite element equations. The computational results are also compared with analytical or numerical results which are obtained from the literature, as shown in Section 7.2.

In Section 7.3, linear and nonlinear stability analyses of isotropic circular rings under uniform, constant-directional pressure are examined. The examples include a complete circular ring and a circular arch with pinned-pinned ends. An internal elastic foundation is also taken into account. Comparisons of corresponding buckling loads and modes are also made and described in this section. Utilizing the same analysis procedures, the stability of composite rings with and without elastic foundations under uniform dead pressure are investigated and included in Section 7.4. Several types of lamination stacking sequences are also considered. In section 7.5, the imperfection sensitivities of isotropic and composite rings under uniform pressure are examined. One of the studies also includes the effect of internal elastic foundations.

7.2 Test Examples for Arch and Ring Structures

7.2.1 Static Analysis of an Isotropic Circular Ring under Uniform Pressure

The first example used to verify the validity of the linear theory and the finite element model derived in Chapter 3 is to determine the radial displacements of a circular ring when subjected to uniform external pressure. The material properties, geometry and loading condition, as shown in Figure 7.1, are:

$$\begin{aligned} E &= 200 \text{ GPa} \\ G &= 77 \text{ GPa} \\ \nu &= 0.3 \\ R &= 250 \text{ mm} \\ h &= 5 \text{ mm (thickness)} \\ b &= 1 \text{ m (width)} \\ q_0 &= 5000 \text{ N / m} \end{aligned} \tag{7.1}$$

Due to axisymmetry in both loading and geometry, only one quarter of the ring was chosen to model and to create a mesh. Convergence was also achieved using four quadratic, three-node elements. The mesh details are also given in Figure 7.1.

The numerical result obtained using the present model is $w_0 = 3.125 \times 10^{-7}$ m, which is identical to that of Reference [11] and is given as:

$$w_0 = -\frac{R^2}{EA}(q_0) \tag{7.2}$$

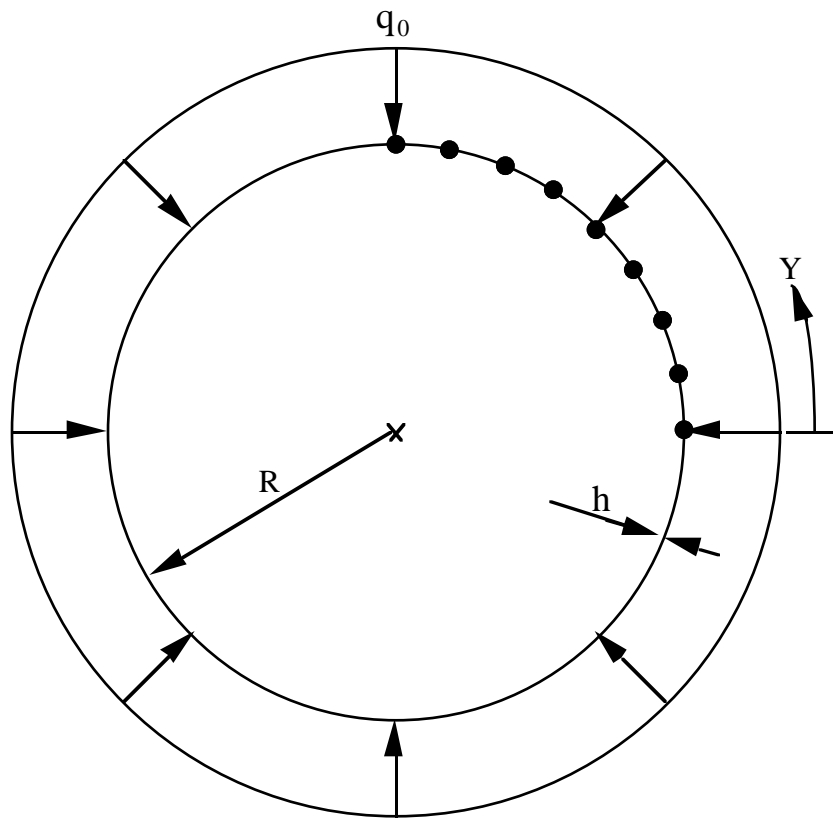


Figure 7.1 - Geometry and mesh information of a circular ring

7.2.2 Nonlinear, Large Deflection Analysis of a Hinged, Deep Arch under a Concentrated Load at the Apex

This example studies the nonlinear response of a deep, circular arch under a point load at midspan, shown in Figure 7.2. It is used to test the large radial deflection capability of the present nonlinear theory and the corresponding finite element model. For the hinged-end boundary conditions, the arch exhibits critical buckling associated with bifurcation phenomena.

The material properties and geometry information used for the present example are:

$$\begin{aligned}EA &= 1.0 \times 10^6 \text{ lb} (4.448 \times 10^6 \text{ N}), \\GA &= 1.0 \times 10^6 \text{ lb} (4.448 \times 10^6 \text{ N}), \\EI &= 1.0 \times 10^6 \text{ lb} \cdot \text{in}^2 (2.870 \text{ KN} \cdot \text{m}^2), \\R &= 100 \text{ inches}, \\\phi &= 215^\circ.\end{aligned}\tag{7.3}$$

The arch has been discretized by twenty equally-spaced, three-noded, quadratic ring elements to meet the convergence requirement. The comparisons of the load-deflection curves between the present element and a plane beam formulation, previously employed by Wriggers and Simo [150], are given in Figure 7.3. The first bifurcation point is 329 pounds predicted by the present solution, and is 335 pounds in the result of Wriggers and Simo [150]. The major differences are caused by the distinct element types and kinematics relations. For the range of moderately large rotations, it clearly shows the differences for large deflection behavior.

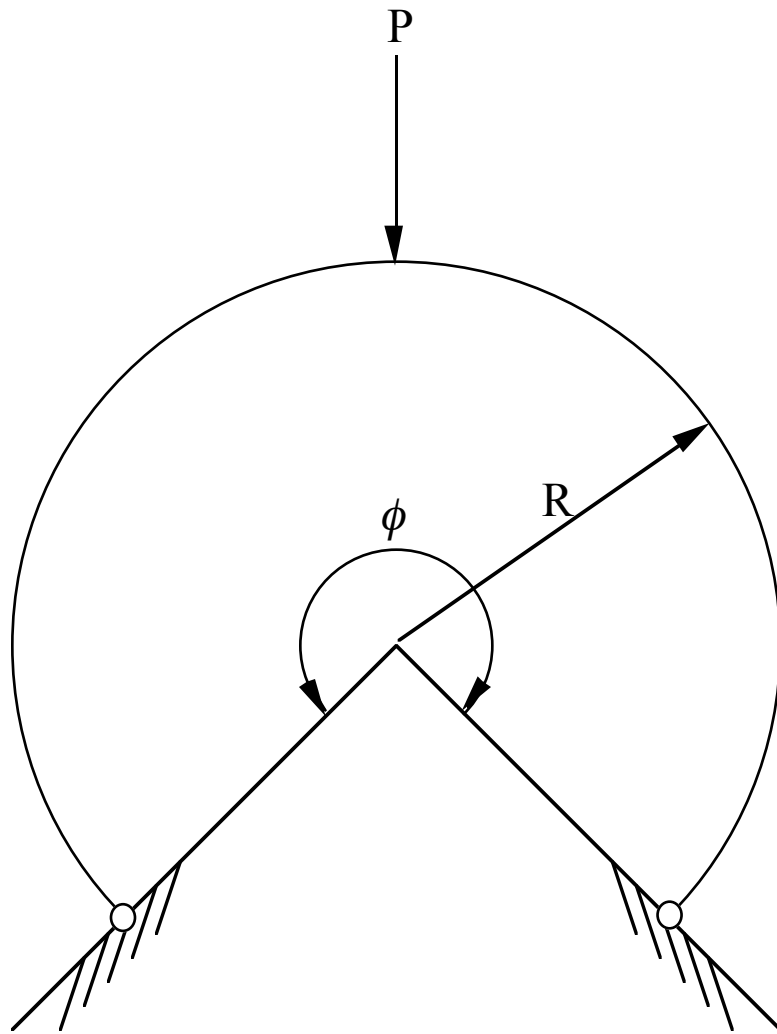


Figure 7.2 - A hinged, deep, circular arch subjected to a center point load

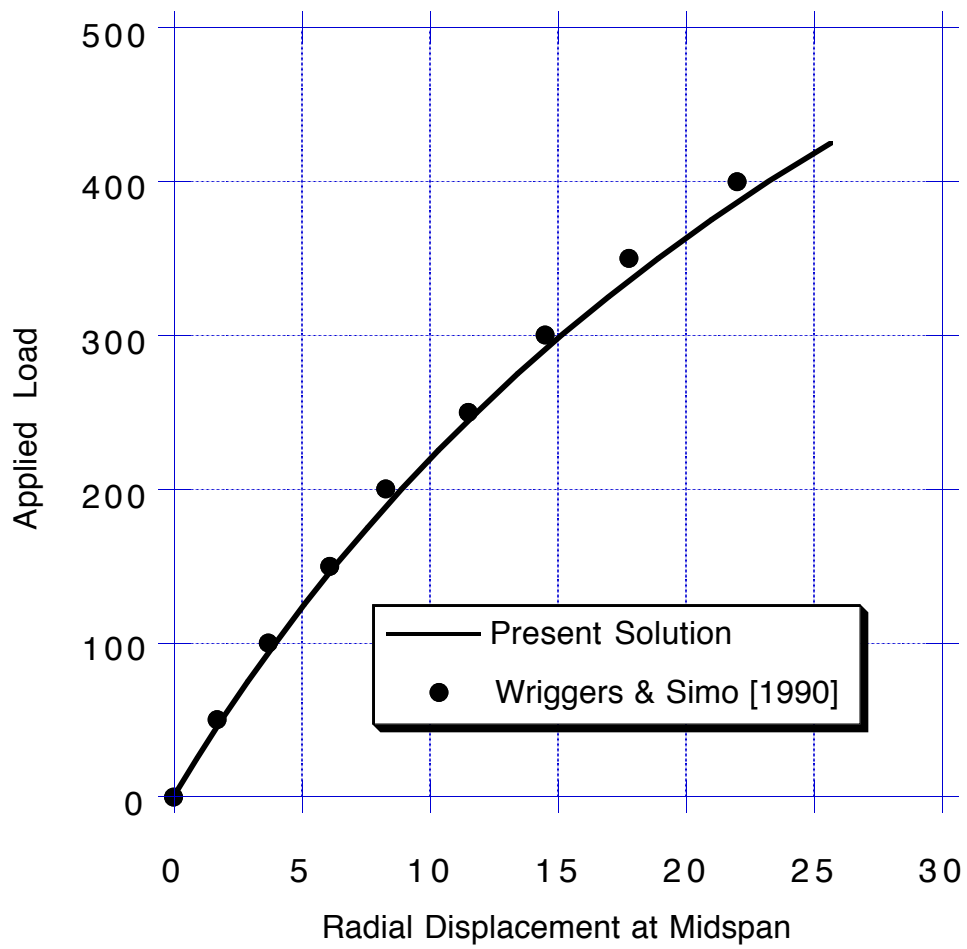


Figure 7.3 - Nonlinear load-deflection curve of a simply-supported, deep arch subjected to a point load at midspan

7.2.3 Geometrically Nonlinear Analysis of a Clamped, Shallow, Circular Arch Subjected to a Concentrated Load at Midspan

A shallow circular arch with fixed end boundary conditions is considered. A point load is applied at midspan as shown in Figure 7.4. The shell geometry is also shown in Figure 7.4. The material properties and geometry information used for the present example are:

$$\begin{aligned} E &= 10.0 \times 10^6 \text{ psi,} \\ \nu &= 0.2, \\ b &= 1.0 \text{ inch (width),} \\ R &= 133.114 \text{ inches,} \\ h &= 3/16 \text{ inch (thickness),} \\ R &= 34.0 \text{ inches,} \\ \beta &= 7.337^\circ. \end{aligned} \tag{7.4}$$

The arch was modeled with twelve equally-spaced, three-noded, quadratic ring elements to reach the accurate results. For the fixed-end boundary conditions, the load-displacement curve will exhibit a limit-point type of nonlinear response. The present numerical results are retained by using one dimensional ring elements, based on the assumptions of small strains, large deflections and moderate rotations, are plotted in Figure 7.5. The critical buckling load which corresponds to the first limit point is 34.07 pounds. As shown in Figure 7.5, it is also compared with the nonlinear finite element solutions employed by Sorem and Surana [151]. The numerical results proposed by Sorem and Surana are obtained by using a p-version geometrically nonlinear formulation based on the total Lagrangian approach for a nine node three dimensional curved shell

element. From the load-displacement graph, a fairly good agreement between the two approaches is shown.

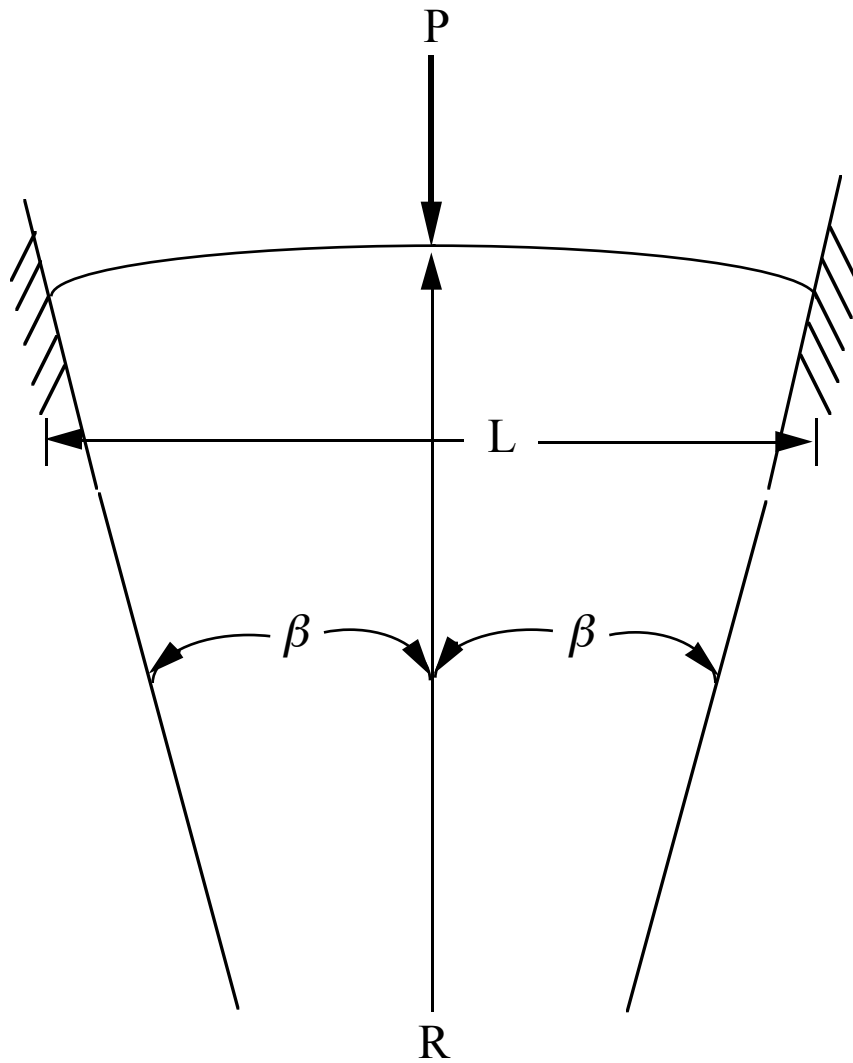


Figure 7.4 - A shallow, circular arch with both fixed end conditions under a concentrated load at the apex

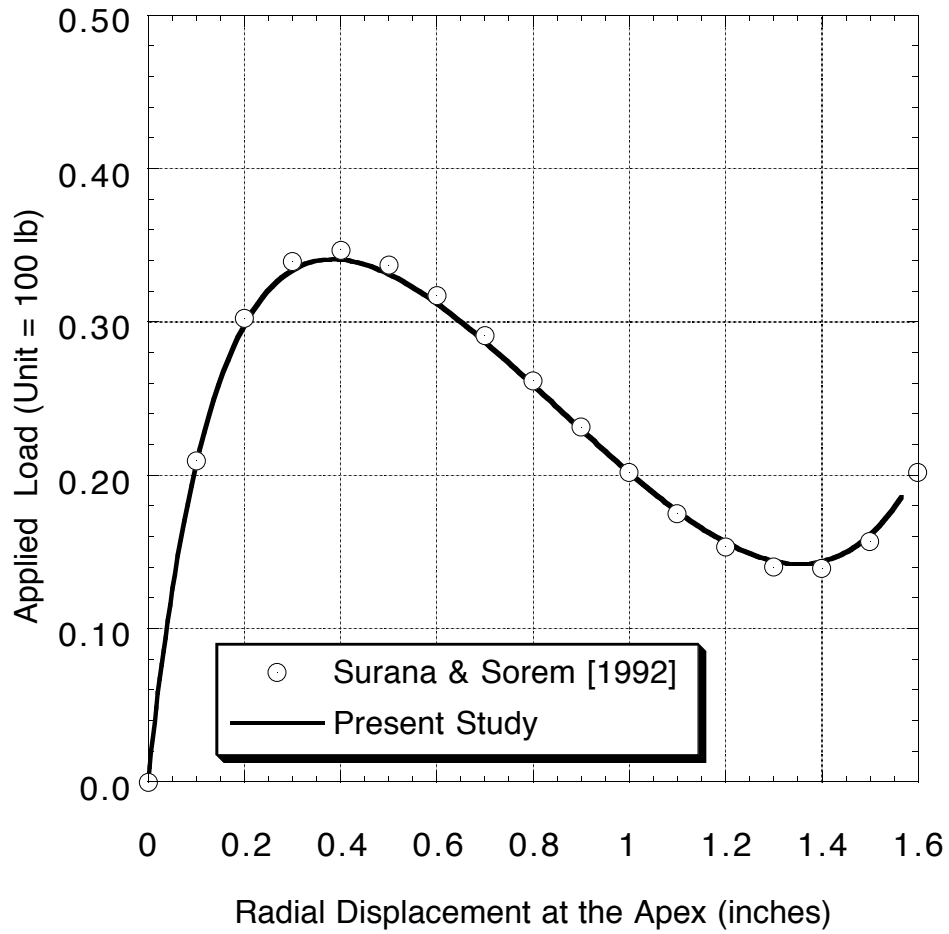


Figure 7.5 - Nonlinear load-deflection curve of a fixed ended, shallow arch subjected to a concentrated load at the apex

7.3 Example Studies for One-Layered Isotropic or Orthotropic Arch and Ring Structures

In this section, linear and nonlinear buckling analyses of single-layered, complete circular rings and arches with prescribed boundary conditions under uniformly constant-directional, hydrostatic pressure are examined. Stability analyses of circular rings with various internal elastic foundations are also compared and discussed in the following subchapters.

7.3.1 Linear Stability Analysis of a Uniformly Compressed, Isotropic, Circular Ring

Linear eigenvalue analysis is used to study the stability condition of a one-layered isotropic, complete, circular ring under uniform dead pressure. The arch and ring elements based on the linear theory which is derived in Chapter 3 were utilized to formulate the isotropic ring model. The configuration of the loading, geometry and coordinate system of a circular ring is shown in Figure 7.1. The material and geometric properties of a steel ring are:

$$\begin{aligned} E &= 200 \text{ GPa} \\ G &= 77 \text{ GPa} \\ \nu &= 0.3 \\ R &= 250 \text{ mm} \\ h &= 5 \text{ mm (thickness)} \end{aligned} \tag{7.5}$$

$b = 1 \text{ m (width)}$

Since there is axisymmetry in both loading and geometry, only half of a circular ring is used to model and mesh. For the convergence test, ten equally spaced three-nodded quadratic elements can reach a very good result. Uniformly reduced integration rule is also applied during the finite element procedures in order to eliminate membrane and transverse shear locking problems.

The numerical value for the buckling load, $(N_y)_{\text{critical}}$, under dead, hydrostatic pressure is 1.3330×10^5 Newtons. The corresponding critical buckling mode is shown in Figure 7.6. The ring buckled into a two-wave pattern ($n=2$) in the circumferential direction. For the case of dead pressure loading, the classical buckling solution may be evaluated from equation (7.6) as follows [152]:

$$(N_y)_{\text{critical}} = \frac{4EI}{R^2} \quad (7.6)$$

which provides the critical buckling load as 1.3333×10^5 Newtons. The results of the classical and the present numerical solutions are almost identical. For the case of thin-walled, isotropic rings, the effect of the transverse shear terms on the buckling loads is not very significant [10], as indicated by the present solution for this example.

----- Undeformed Shape
—— First Buckling Mode

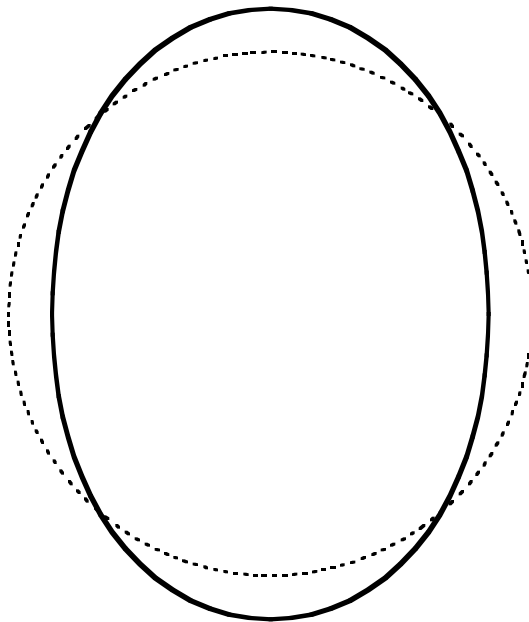


Figure 7.6 - Undeformed and buckled shapes of a complete circular ring subjected to uniform dead pressure

7.3.2 Nonlinear Buckling Analysis of a Uniformly Compressed Circular Ring

In this section, nonlinear finite element analysis is applied to examine the buckling behavior of a one-layered, isotropic ring under uniform radial pressure. The conditions of the loading, geometry, material properties and coordinate system of a circular ring are the same as those of example 7.3.1. Since a perfect ring under perfectly uniform pressure deforms in uniform contraction, a small concentrated load or an initially imperfect model is necessary to induce buckling. As shown in Figure 7.7(a), a small force with the magnitude of 100 Newtons is applied to initiate the imperfect model (model I) for the preloading stage. The other method to initiate buckling is to prescribe a slightly out-of-round model (model II) before applying any external loading. Referring to Figure 7.7(b), the radius r of the out-of-round ring is chosen as

$$r = R + 0.0000195R \cos(2\theta) \quad (7.7)$$

The Newton-Raphson method is used to trace the nonlinear load-displacement path for the present example. The normalized determinants of the corresponding tangent stiffness matrices at each equilibrium point are evaluated in order to check the stability condition of the structure under uniform load increments.

Figure 7.8 is a plot showing external radial pressure versus the radial deflections at points A and B for the case of model I, whereas Figure 7.9 corresponds to those of model II. The buckled configurations for both models are identical to the one of the linear solutions. Nonlinear numerical solution of the critical buckling pressure gives 5.330×10^5 N/m, which is very close to the linear buckling pressure 5.332×10^5 N/m.

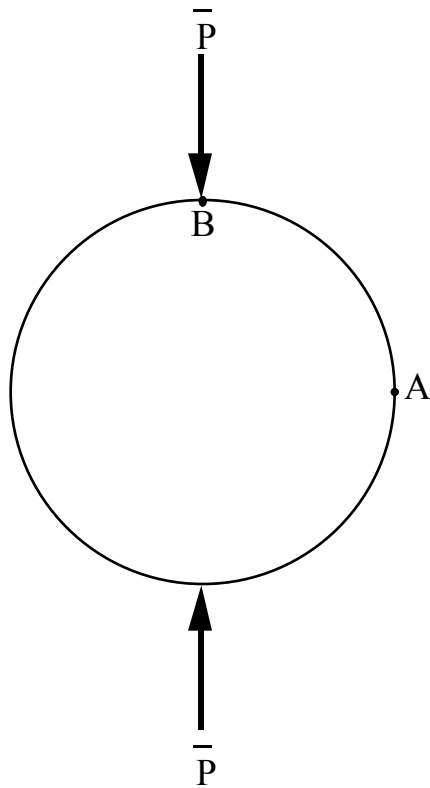


Figure 7.7 (a) - Configuration of a half circular ring with a small concentrated load

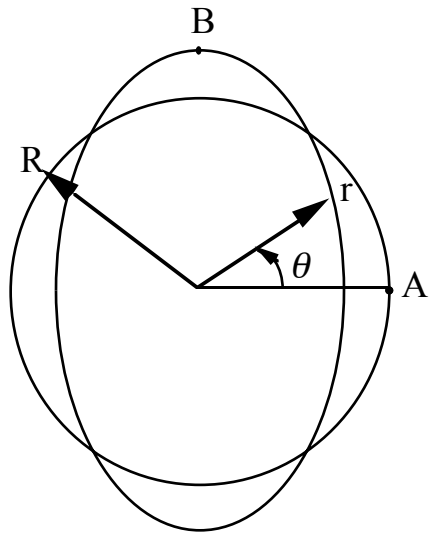


Figure 7.7 (b) - Configuration of a circular ring with an initially out-of-round model

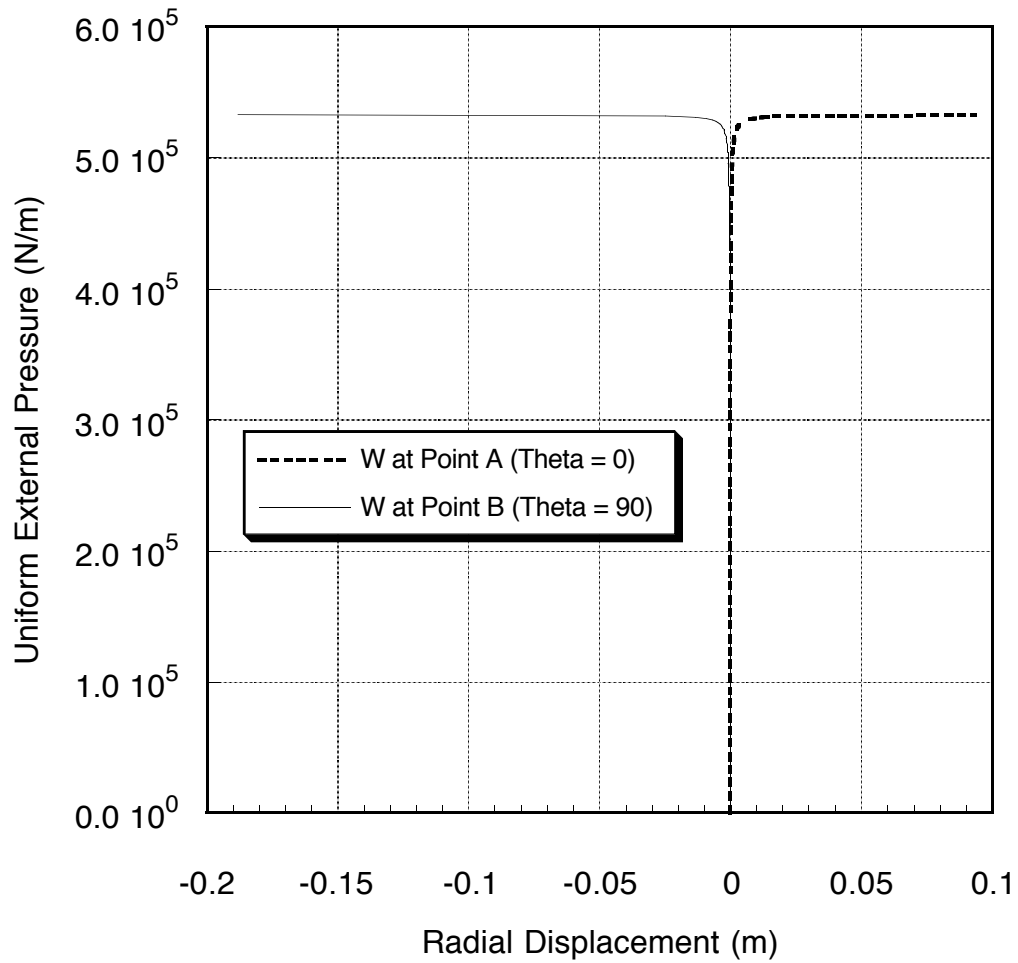


Figure 7.8 - Nonlinear load-deflection curves of a circular ring subjected to uniform dead pressure for the case of model I

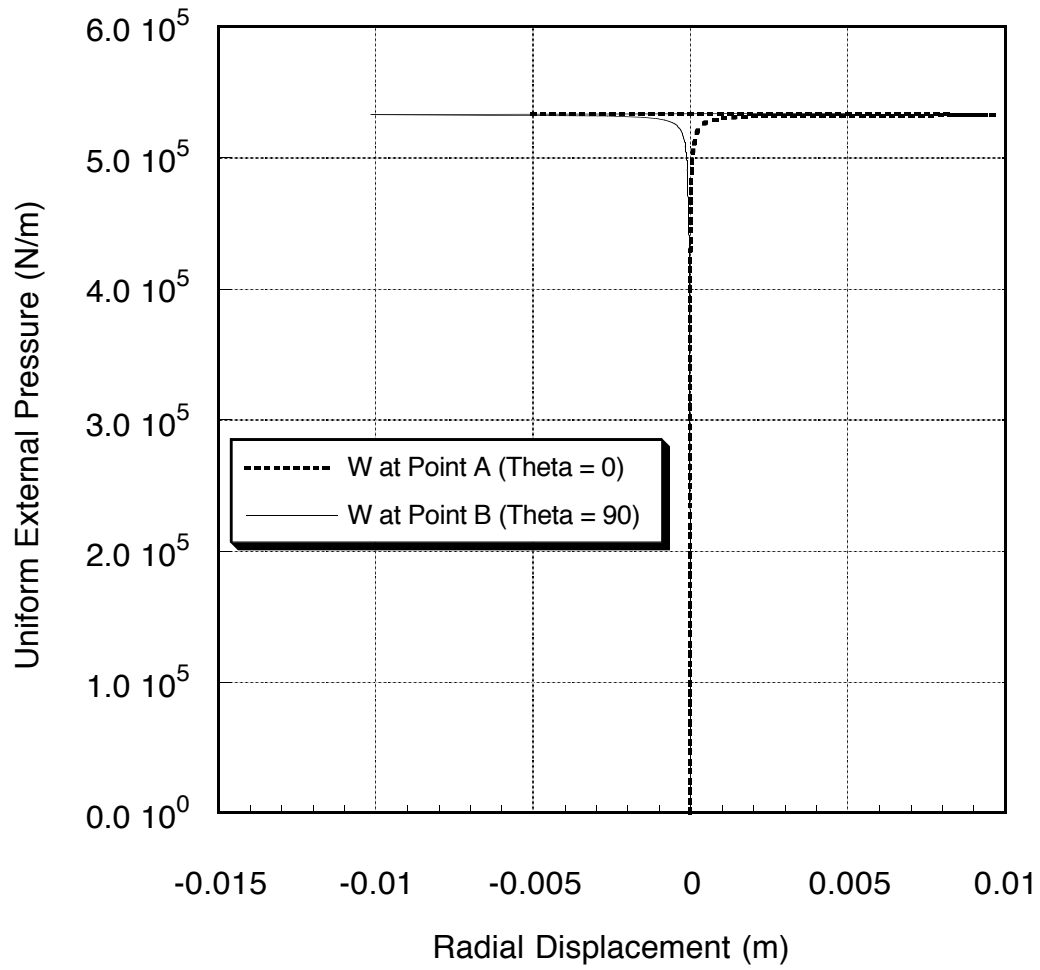


Figure 7.9 - Nonlinear load-deflection curves of a circular ring subjected to uniform dead pressure for the case of model II

7.3.3 Linear and Nonlinear Buckling Analysis of a Uniformly Compressed Circular Arch with Pinned-Pinned Ends

In this section, a half circular arch with pinned-pinned end conditions under uniform dead pressure is studied. The purpose of the present example is to understand the structural response of arch structures under various boundary conditions. The configuration of the structure, loading and boundary conditions are shown on Figure 7.10. The dimension of the arch and the material properties are the same as in the previous example. Utilizing the linear and nonlinear finite element schemes which are derived in Chapter 3, one can conclude the corresponding critical buckling loads based on various theories in the following table:

Table 7.1 - Comparisons of critical buckling loads based on various theories

Critical Buckling Pressure $(q_0)_{\text{Critical}}$ (N/m)	
Linear Solution	4.361×10^5
Nonlinear Solution	4.360×10^5
$(q_0)_{\text{Critical}} = (3.2712) EI / R^3$ Dym [153]	4.362×10^5

It is shown that there is no major difference between the above theories. The associated critical buckling mode is also plotted in Figure 7.11.

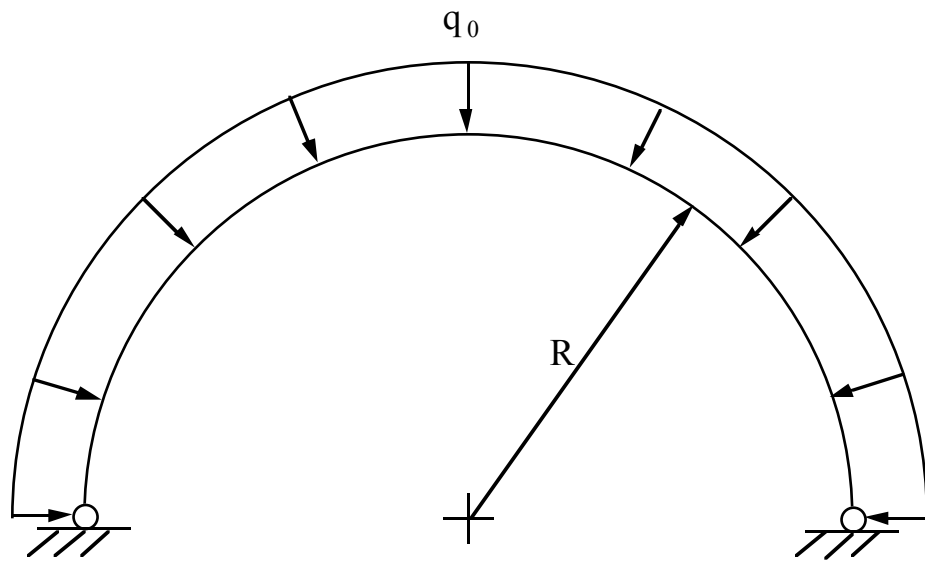


Figure 7.10 - Configuration of a circular arch under uniform dead pressure with pinned boundary conditions

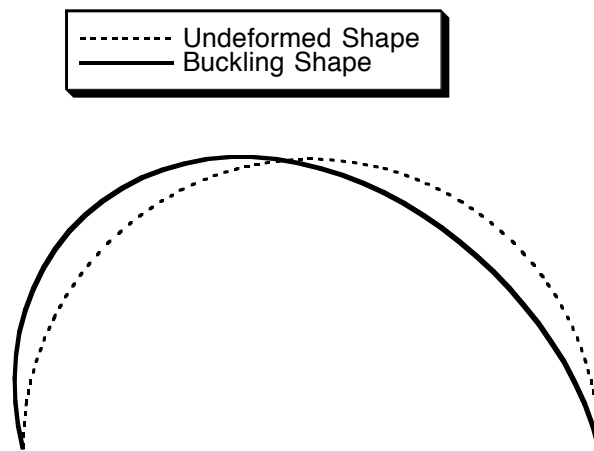


Figure 7.11 - Critical buckling mode of a circular arch under uniform dead pressure with pinned boundary conditions

7.3.4 Stability Analysis of Isotropic Rings with Internal Elastic Foundations under Constant Directional Pressure

For ring structures with elastic foundations, the internal pressure generated by internal elastic foundations through the deformation of the ring under external lateral pressure is included in the global stiffness of the solid outer layer. The effects of elastic foundations are included in the linear and nonlinear finite element formulations for the determination of the stability conditions.

The material properties and other information for the input data are the same as in example 7.3.1. In order to obtain a very good convergent solution, twenty equally-spaced, quadratic elements are chosen to mesh a half ring model. For the purpose of simulating soft elastic foundations when compared to the stiffness (200 GPa) of the outer layer, which is made of steel, the elastic foundation constants are selected in the range of 2×10^5 to 2×10^8 Pa. Linear eigenvalue and nonlinear solutions give the associated first buckling loads and modes in Table 7.1. Linear analytical results of the buckling pressures of circular rings with linear elastic foundations under uniform dead pressure loading [11], which are determined by the following equation (7.8), are also provided in Table 7.1 to make comparisons with the obtained numerical results:

$$q = (n^2) \frac{EI}{R^3} + \frac{n^2}{(n^2 - 1)^2} K_0 R, \quad n = 2, 3, 4, \dots \quad (7.8)$$

Numbers of lobes (n) represent the wavelength parameter in the circumferential direction, which characterize the buckled configurations associated with various buckling loads.

As the results will attest, the critical buckling loads are not varying much for softer elastic foundations ($K_0 = 2 \times 10^5$ and 2×10^6 Pa) and without elastic foundation. In the other cases, buckling loads tend to increase a lot with moderately hard elastic media ($K_0 = 2 \times 10^7$ and 2×10^8 Pa). The associated buckling modes also have the tendency to deform into higher numbers of wave patterns when the elastic media become more influential. The corresponding buckling shapes for the wavelength parameter n of two, three, and five are shown in Figures 7.6, 7.12, and 7.13, respectively.

Table 7.2 - Comparisons of first buckling loads and the associated modes of a circular ring for various elastic foundation constants

Critical Buckling Pressure (q_0) _{critical} : (N/m)					
K_0 (KPa)	0	2×10^2	2×10^3	2×10^4	2×10^5
Linear Solutions	5.3332×10^5	5.552×10^5	7.552×10^5	19.02×10^5	54.96×10^5
Nonlinear Solutions	5.3300×10^5	5.544×10^5	7.540×10^5	19.01×10^5	54.80×10^5
Analytical Solutions	5.3333×10^5	5.556×10^5	7.556×10^5	19.03×10^5	55.04×10^5
Number of Lobes (n)	2	2	2	3	5

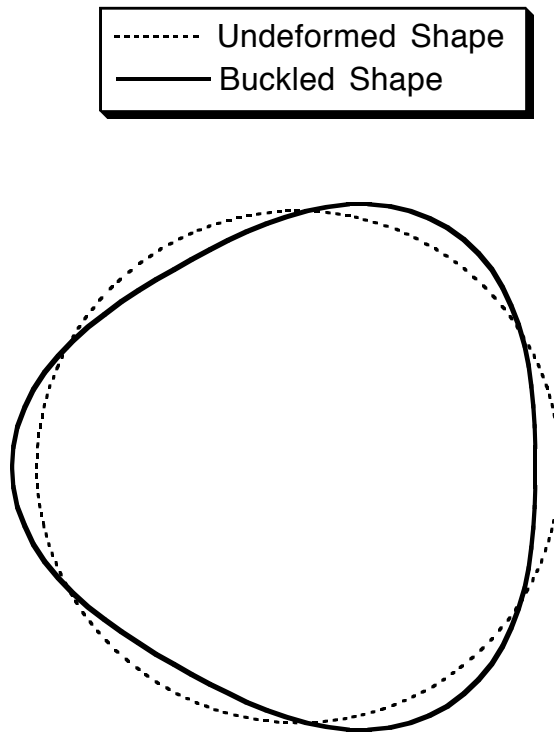


Figure 7.12 - Undeformed and buckled shapes ($n = 3$) of a complete circular ring with $K_0 = 2 \times 10^4$ KPa when subjected to uniform dead pressure

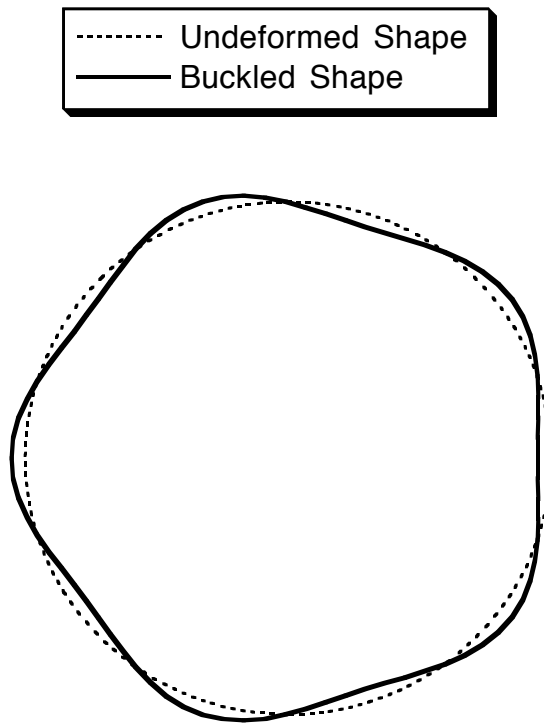


Figure 7.13 - Undeformed and buckled shapes ($n = 5$) of a complete circular ring with $K_0 = 2 \times 10^5$ KPa when subjected to uniform dead pressure

7.3.5 Effect of Pasternak's Constants on the Stability of an Isotropic Ring with Internal Elastic Foundation $K_0 = 2 \times 10^5$ Pa under Uniform Pressure

In the real phenomenon of the resulting pressure caused by an internal elastic medium, the shear interactions between individual springs should be considered. This example is to study the buckling behavior of an isotropic ring structure on a two-parameter elastic foundation under external loading of uniform pressure. Pasternak's type of shear parameter is included in the theory and the associated finite element model. Choosing the linear elastic foundation constant to be 2×10^5 Pa for the present study, the effect of the shear parameter on the buckling of an isotropic ring is examined.

In order to make comparisons with the results of section 7.3.4, the input information is set to be the same except for the values of the Pasternak constant K_s . The numerical solutions resulting from the changing of the shear parameter values are concluded in the following table.

Table 7.3 - Comparisons of the critical buckling pressures under various shear parameters

Pasternak constant K_s (N).	$(q_0)_{\text{Critical}}: (X 10^5 \text{ N/ m})$
0	5.5520
1×10^3	5.5935
2×10^3	5.6335
3×10^3	5.6735
4×10^3	5.7135

From the literature, the Pasternak's parameter is related to the elastic, shear modulus and thickness of elastic medium. For the shear parameter in the range from 1×10^3 to 4×10^3 N, the corresponding critical buckling loads could arise from 0.75 to 2.9 % when compared to that of Winkler's linear elastic foundation. The present numerical results show no significant changes of the corresponding buckling loads with the consideration of shear interactions of internal elastic foundations. With the existence of moderately large Pasternak's constants, the critical buckling loads will be much larger than the ones without considering the shear effect of internal elastic foundations.

7.3.6 Effect of Nonlinear Winkler-Foundation Constant K_1 on the Stability of an Isotropic Ring with Internal Elastic Foundation $K_0 = 2 \times 10^5$ Pa under Uniform Radial Pressure

Similar to the shear parameter study for the previous case, the effect of nonlinear foundation constants on the stability of circular rings on elastic foundations is examined. The numerical results are obtained by the nonlinear finite element analysis which includes the potential energy generated by the nonlinear elastic foundation terms. The following table contains the associated critical buckling loads under various values of nonlinear constants.

Table 7.4 Comparisons of the critical buckling pressures under various nonlinear elastic foundational constants

Nonlinear Winkler constant K_1 (N / m ⁴)	$(q_0)_{\text{Critical}}$: (X 10 ⁶ N / m)
0 - 1 X 10 ¹²	0.554
1 X 10 ¹³	0.558
2 X 10 ¹⁴	0.602

Since the radial displacements before the buckling stage are relative small, the effect of nonlinear constants on the stability conditions is not very significant. As shown in the table of this section, the critical buckling load only increases about 8.66 percent even with the inclusion of a very large value of nonlinear elastic foundation constant 2×10^{14} N / m⁴. So, one can conclude that the effect of the nonlinear elastic foundation on the stability condition is not very crucial except for the cases of post-buckling analysis with a very large value of nonlinear elastic foundation constant.

7.4 Example Studies for Multi-Layered, Composite Ring Structures

In this section, stability of multiple-layered, complete circular rings under uniformly constant-directional, hydrostatic pressure are studied. Both cross-ply $(0/90/90/0)_S$ and angle-ply $(0/45/-45/0)_S$ types of composite rings will be taken into consideration. Buckling analysis of circular rings with various internal elastic foundations is also treated in this chapter.

7.4.1 Stability Analysis of Uniformly Compressed, Composite Circular Rings

Linear eigenvalue and nonlinear finite element analyses are used to study the stability condition of multiply-layered, circular rings under uniform radial pressure. These analyses are based on linear and nonlinear theories and the associated finite element equations which are proposed in Chapter 3. The configuration of the loading, geometry and coordinate system of a composite ring is the same as the one described in Section 7.3. The composite material used for the present study is T300/5280 Graphite Epoxy and the properties are:

$$\begin{aligned} E_{11} &= 145 \text{ GPa} \\ E_{22} &= 11.7 \text{ GPa} \\ G_{12} &= G_{13} = 4.5 \text{ GPa} \\ G_{23} &= 3.0 \text{ GPa} \\ \nu_{12} &= 0.21 \end{aligned} \tag{7.9}$$

Due to axisymmetry in both loading and geometry, twenty equally spaced three-noded quadratic elements are used to model and mesh a half circular ring. Two different types of composite rings, one with $(0/90/90/0)_s$ lamination sequence and the other with $(0/45/-45/0)_s$ stacking lay-up are used to study the stability conditions. The numerical results of critical buckling pressure are listed in the following table:

Table 7.5 - Comparisons of the critical buckling pressures of composite rings under various lamination sequences

Critical Buckling Pressure $(q_0)_{\text{Critical}}$ ($\times 10^5$ N/m)		
	$(0/90/90/0)_s$ lamination	$(0/45/-45/0)_s$ lamination
Linear Solution	5.00500	4.61952
Nonlinear Solution	5.00399	4.61943
Number of Lobes (n)	2	2

From the above results, one can see that the linear and nonlinear solutions for composite rings under uniform pressure are almost identical. The buckling shapes in both cases are the same as the one for an isotropic ring, which buckled into a two wave pattern in the circumferential direction. The determination of the critical buckling pressures depends on the material properties, geometry of the structures, and lamination stacking sequences of the composites.

7.4.2 Stability Analysis of Composite Circular Rings with Internal Elastic Foundations under Uniform, Constant-Directional Pressure

By running similar tests as those of Example 7.4.1, using the same conditions and including a number of internal elastic foundation constants, the results may be compared as follows:

Table 7.6 - Comparisons of the critical buckling pressures of two different types of composite rings with various elastic foundational constants

Critical Buckling Pressure $(q_0)_{\text{Critical}}$ ($\times 10^5$ N/m) for $(0/90/90/0)_S$ Lamination						
K_0 (KPa)	0	1×10^2	1×10^3	1×10^4	1×10^5	1×10^6
Numerical Solutions	5.005	5.116	6.116	14.68	37.372	109.32
Numbers of Lobes	2	2	2	3	4	7
Critical Buckling Pressure $(q_0)_{\text{Critical}}$ ($\times 10^5$ N/m) for $(0/45/-45/0)_S$ Lamination						
K_0 (KPa)	0	1×10^2	1×10^3	1×10^4	1×10^5	1×10^6
Numerical Solutions	4.6195	4.7306	5.7306	13.8044	35.8093	104.9372
Number of Lobes	2	2	2	3	4	7

The above table shows the details of the corresponding critical buckling pressures for two different types of composite rings with various elastic foundations. Similarly to the

structural responses of isotropic rings with elastic foundations, the buckling resistance becomes much greater as elastic foundation constants become larger. The associated buckled shapes of the deformed rings have the tendency to be multiple wave patterns instead of two wave pattern (buckling modes for relatively soft or no elastic foundation cases) along the circumferential direction. The critical buckling pressures and modes become functions of the elastic foundations as the internal foundations become moderately large.

7.5 Imperfection Sensitivity Analysis of Rings under Uniform Radial Pressure

In order to induce buckling of a circular ring when subjected to uniform pressure, a slightly imperfect shape with a very small amplitude was prescribed. In this section, imperfection sensitivity analysis of the buckling behavior of complete circular rings under uniform constant-directional pressure is examined. Both isotropic and composite rings will be taken into consideration. Imperfection sensitivity analysis of rings with internal elastic foundations will also be included and compared in this chapter.

7.5.1 Imperfection Sensitivity Analysis of an Isotropic Circular Ring under Uniform Radial Pressure

This example is used to examine the nonlinear behavior and the critical buckling load of an isotropic ring when subjected to uniform radial pressure (so-called dead pressure). The nonlinear theory and the associated finite element equations for ring structures with prescribed imperfections are detailed in Chapter 5.2. From the results of the previous examples, the first buckling mode of an isotropic ring under uniform pressure is a two wave shape along the circumferential direction. So, for the reason of convenience, an initial imperfection function is assumed to be:

$$\bar{w}_0(y) = \Delta \cos\left(\frac{n y}{R}\right) \quad (7.10)$$

where n is the number of waves in the y direction, which is prescribed to be two in this example, and Δ denotes the imperfection amplitude, set as a small fraction of the ring radius. Varying the values of amplitude from 1.95×10^{-5} to 1.95×10^{-2} times R , one may obtain the corresponding nonlinear load-displacement relations shown in Figure 7.14. The critical buckling pressure remains 533,000 N/m, which is identical to the numerical result generated from the nonlinear analysis of a perfect ring. The associated buckling modes are also the same as those of the perfect structure. Buckling of isotropic rings is evidently not sensitive to initial imperfections, though the load deflection curves are significantly different.

7.5.2 Imperfection Sensitivity Analysis of Composite Circular Rings under Uniform Radial Pressure

It is of interest to examine the imperfection sensitivity of composite rings subjected to uniform dead pressure. Both cross-ply $(0/90/90/0)_s$ and angle-ply $(0/45/-45/0)_s$ types of composite rings were selected. Using the same imperfection amplitudes as in the previous example, the nonlinear behavior and the corresponding first buckling loads are given in the following table and in Figures 7.15 and 7.16, respectively.

Table 7.7 - Comparisons of the critical buckling pressures of two different types of composite rings with various initial imperfections

Critical Buckling Pressure (1×10^5 N/m)		
Δ / R	(0 / 90 / 90 / 0) _s type of composite ring	(0 / 45 / -45 / 0) _s type of composite ring
0	5.004	4.61952
1.95×10^{-5}	5.00399	4.61943
1.95×10^{-4}	5.00396	4.61940
1.95×10^{-3}	4.99210	4.60850
1.95×10^{-2}	4.9200	4.52072

As the above results indicate, the corresponding critical buckling loads drop by 1.68% and 2.14% only, respectively, even with the imperfection amplitude up to the value of 1.95×10^{-2} times the radius. It is safe to say that the buckling behavior of composite rings is not sensitive to the effect of initial imperfections but their deflection behavior is sensitive.

7.5.3 Imperfection Sensitivity Analysis of a Composite (0 / 45 / -45 / 0) Circular Ring with Internal Elastic Foundation ($K_0 = 1000$ KPa) under Uniform Radial Pressure

The effect of initial imperfections on the nonlinear behavior and critical buckling pressure of rings with internal elastic foundations under uniform pressure is studied in this section.

A composite ring containing the lamination of (0 / 45 / -45 / 0) on an internal elastic foundation with $K_0 = 1000$ KPa is chosen to test the imperfection sensitivity. The initial imperfection function before loading is assumed to be the same one used in Section 7.5.2. The wavelength parameter n is set to be three in this case. After performing the nonlinear finite element analysis, the associated buckling pressures under various imperfection amplitudes are shown in the following table, and the nonlinear load-displacement relations are shown in Figure 7.17. The results prove to be non-sensitive to initial imperfections in the presence of internal elastic foundations though their load-deflection curves differ.

Table 7.8 - Comparisons of the critical buckling pressures of a Composite Circular Ring with Internal Elastic Foundation ($K_0 = 1000$ KPa) under various initial imperfection amplitudes

Δ / R	1.95×10^{-5}	1.95×10^{-4}	1.95×10^{-3}	1.95×10^{-2}
$(q_0)_{\text{Critical}}$ ($\times 10^5$ N / m)	6.420	6.420	6.420	6.390

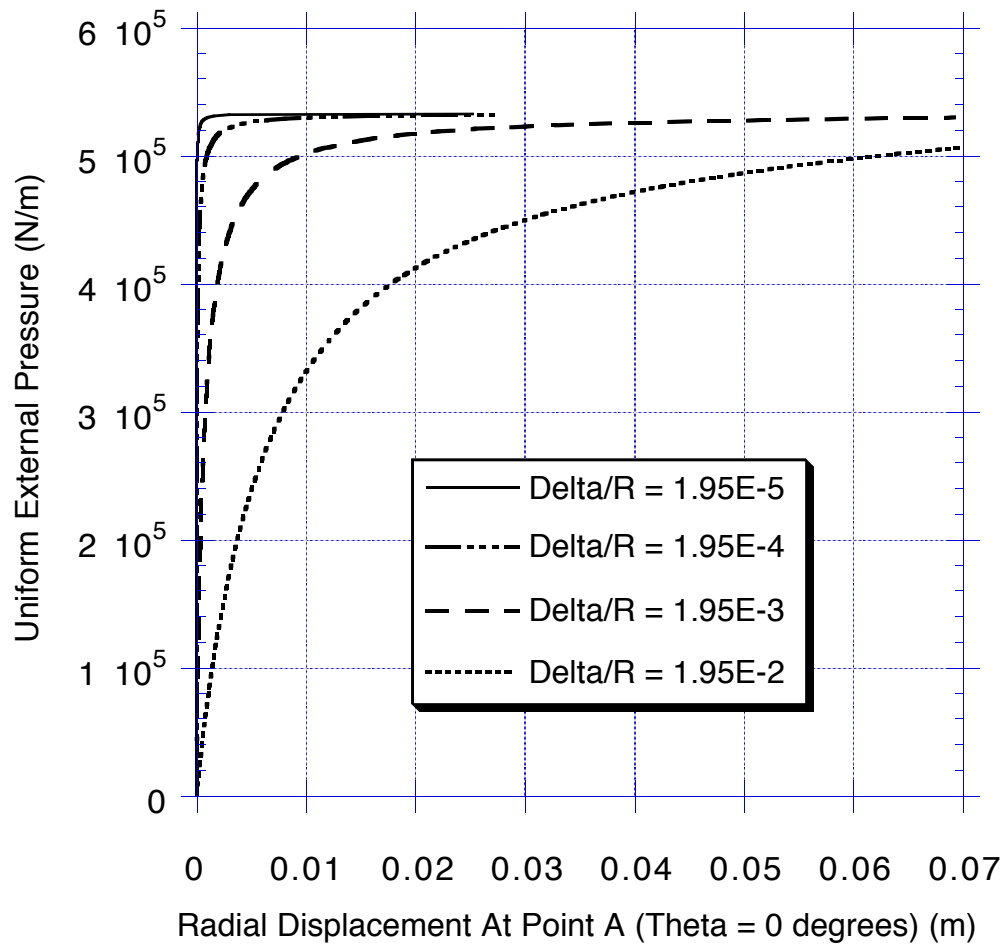


Figure 7.14 - Nonlinear load-deflection curves of an isotropic ring with various initial imperfections under uniform radial pressure

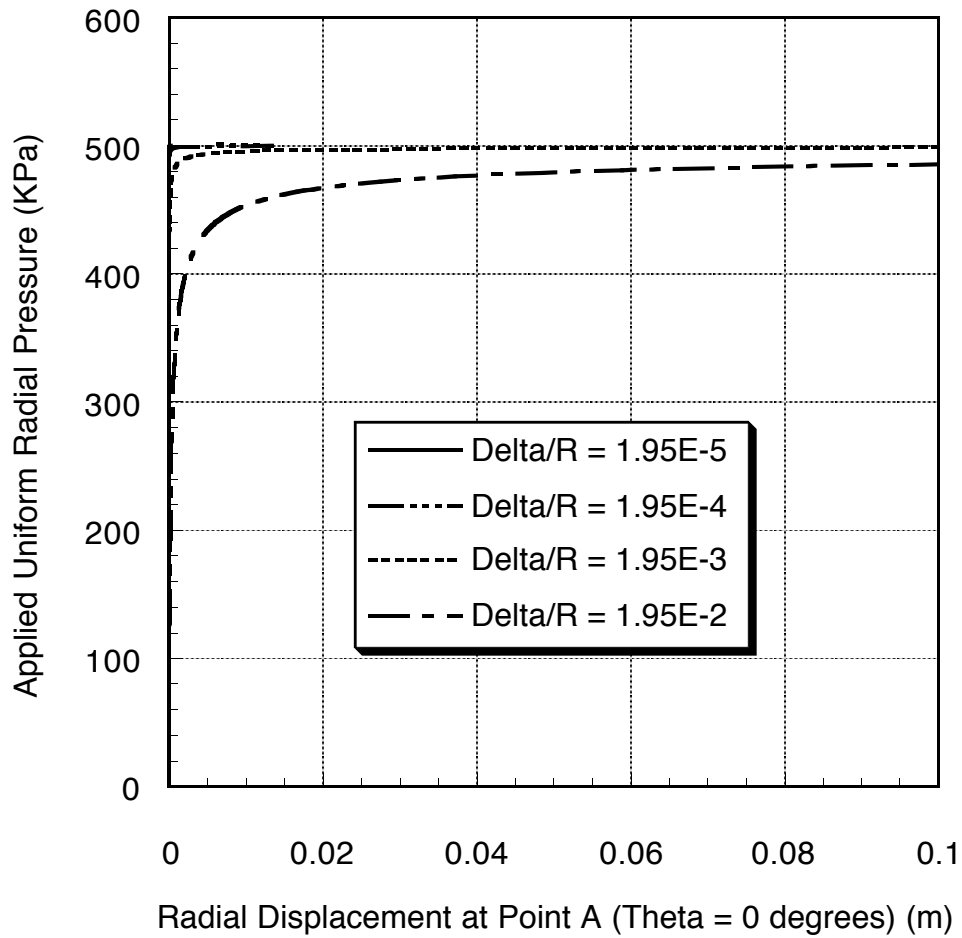


Figure 7.15 - Nonlinear load-deflection curves of a cross-ply $(0/90/90/0)_s$ type of composite ring with various initial imperfections under uniform radial pressure

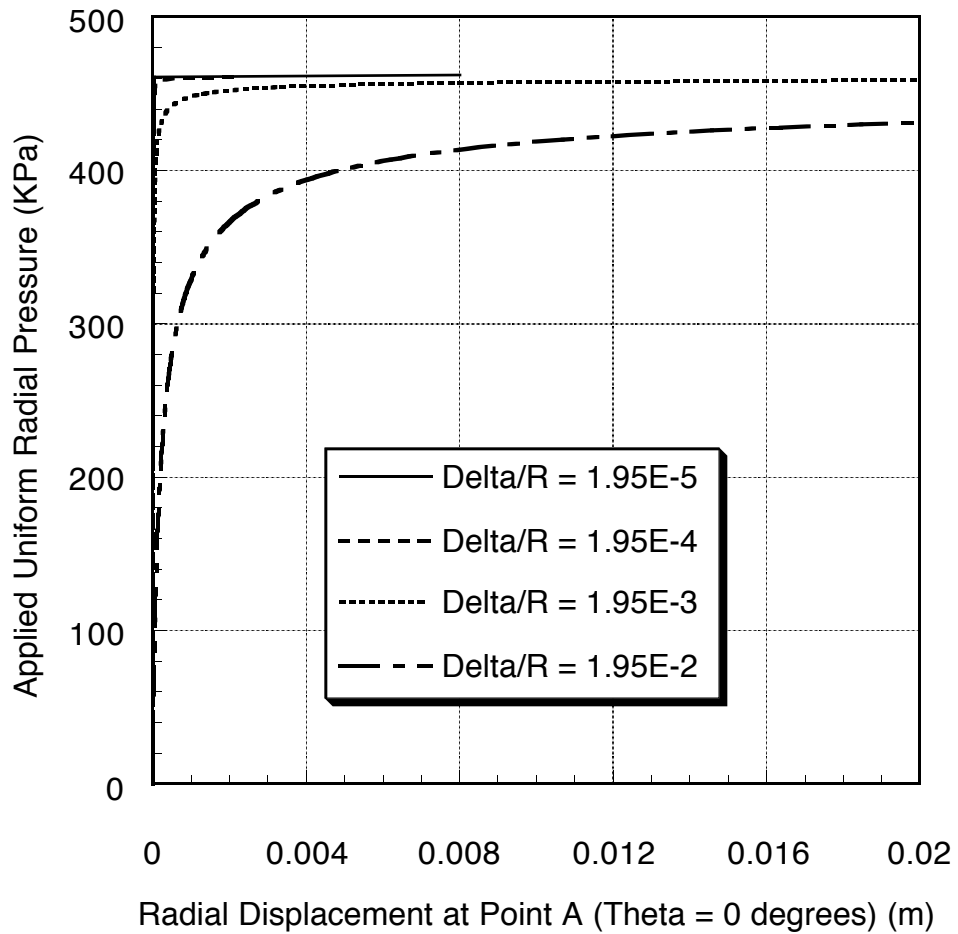


Figure 7.16 - Nonlinear load-deflection curves of an angle-ply $(0/45/-45/0)_s$ type of composite ring with various initial imperfections under uniform radial pressure

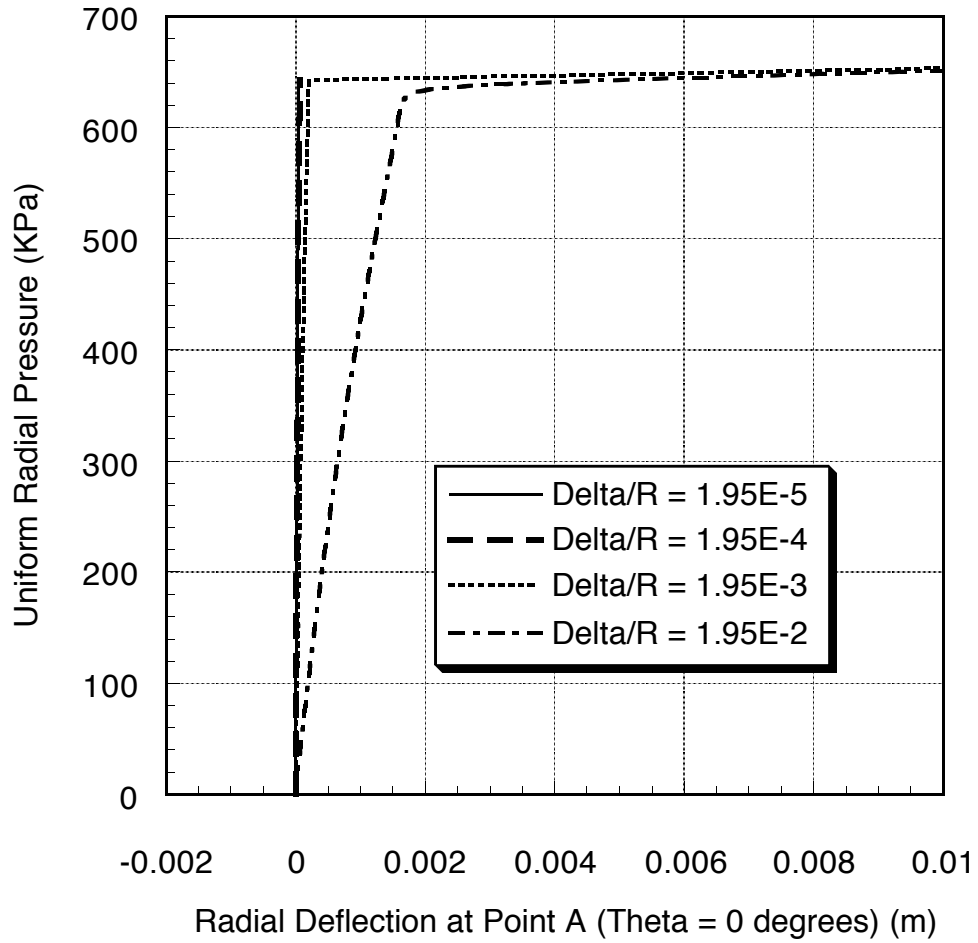


Figure 7.17 - Nonlinear load-deflection curves of an angle-ply (0/45/-45/0) type of composite ring with internal elastic foundation ($K_0 = 1000$ KPa) with various imperfection amplitudes under uniform radial pressure

CHAPTER 8

EXAMPLE ANALYSES AND NUMERICAL RESULTS FOR CYLINDRICAL SHELL MODEL

8.1 Introduction

In Chapter 4, linear and nonlinear formulations for cylindrical shells with and without elastic foundations are derived. The finite element models are also developed based on both theories. The initial imperfection functions are taken into consideration for the principle of virtual displacements and the associated finite element equations used for the analysis in this section are formulated in Chapter 5. With the above formulations and finite element models, the static, buckling, and post-buckling analyses of cylindrical shells under various conditions are applied in this chapter.

In order to verify the proposed theories and finite element programs, several examples which include static and buckling analyses of isotropic and anisotropic cylindrical panels and shells under various loading and boundary conditions are presented and the results are compared with some early research works. They are shown in Section 8.2. In Section 8.3, the linear and nonlinear stability analyses of isotropic cylinders with or without the effect of internal elastic foundations are performed. The effect of Pasternak's and nonlinear elastic foundational constants on the buckling loads are also investigated in this section. Similarly, the stability analysis of multiply-layered composite cylinders are examined and described in Section 8.3. The imperfection sensitivity analysis for

cylindrical shells with and without elastic foundations under uniform radial pressures are shown in Section 8.4.

8.2 Test Examples for Cylindrical Shell Structures

8.2.1 Linear Static Analysis of a Pressurized, Clamped, Cylindrical Shell

Calculation of the radial deflection of a thin-walled cylinder under hydrostatic pressure is used to verify the linear shell element developed in Chapter 4. Figure 8.1 presents the geometry of the shell. The material properties of an orthotropic layer (glass-epoxy composite) are given as follows:

$$E_{11} = 7.5 \times 10^6 \text{ psi } (52.90\text{GPA}),$$

$$E_{22} = E_{33} = 2.0 \times 10^6 \text{ psi } (13.79\text{GPA}),$$

$$G_{12} = G_{13} = G_{23} = 1.25 \times 10^6 \text{ psi } (8.62\text{GPA}),$$

$$\nu_{12} = \nu_{13} = 0.25, \quad \nu_{23} = 0.24, \tag{8.1}$$

$$R = 20 \text{ inches } (50.8\text{cm}),$$

$$h = 1 \text{ inch } (2.54\text{cm}),$$

$$L = 20 \text{ inches (50.8cm)},$$

$$q_0 = \frac{6.41}{\pi} \text{ psi} \left(\frac{44.20}{\pi} \text{ KPA} \right)$$

Due to axisymmetry in both loading and geometry, only an octant of the cylinder is used. The comparisons of midspan displacements for different element types and numbers are listed in Table 8.1. They show the convergence and validity conditions.

As indicated in the Table, the numerical results provide excellent agreement with those of References[146, 154, 155].

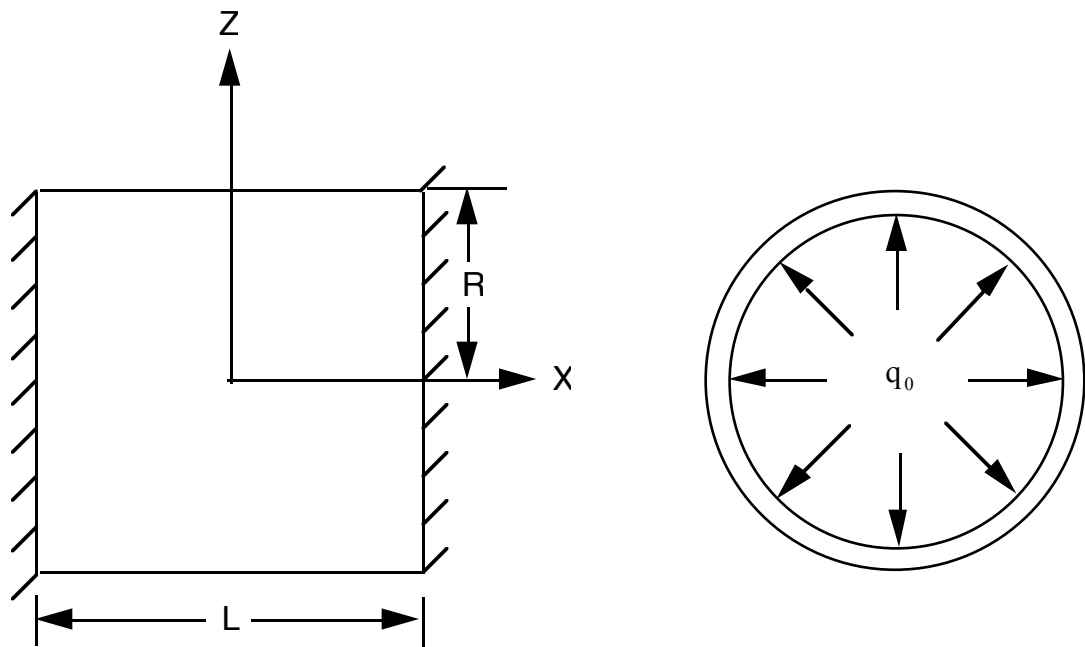


Figure 8.1 - Geometry of a clamped cylindrical shell

Table 8.1 - Comparisons of the midspan deflections in mm of a clamped cylinder subjected to hydrostatic pressure

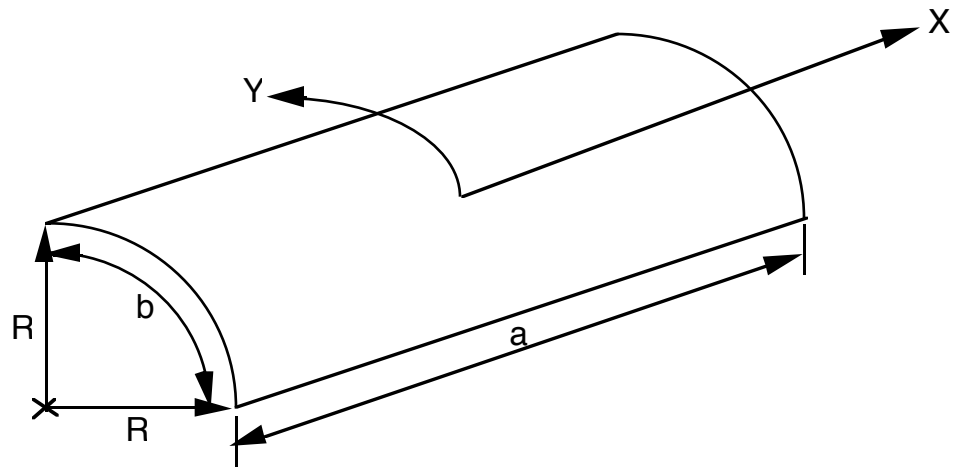
Present Solutions ($q_0 = \frac{6.41}{\pi}$ psi $\left(\frac{44.20}{\pi}$ KPa)		
Element Type & Number	Single Layer (0)	Multiple Layers (0/90)
2 L4	97.536×10^{-4}	55.651×10^{-4}
4 L4	95.504×10^{-4}	47.574×10^{-4}
6 L4	94.844×10^{-4}	46.533×10^{-4}
8 L4	94.615×10^{-4}	46.203×10^{-4}
2 Q9	94.818×10^{-4}	45.872×10^{-4}
4 Q9	94.336×10^{-4}	45.822×10^{-4}
Reddy [146]		
4 L4	95.352×10^{-4}	47.498×10^{-4}
2 Q9	94.666×10^{-4}	45.796×10^{-4}
Other References		
Rao [154]	93.116×10^{-4}	
Timoshenko & Woinowsky- Krieger [155]	93.218×10^{-4}	

8.2.2 Buckling of a Simply-Supported Isotropic Cylindrical Panel Subjected to Axial Loading

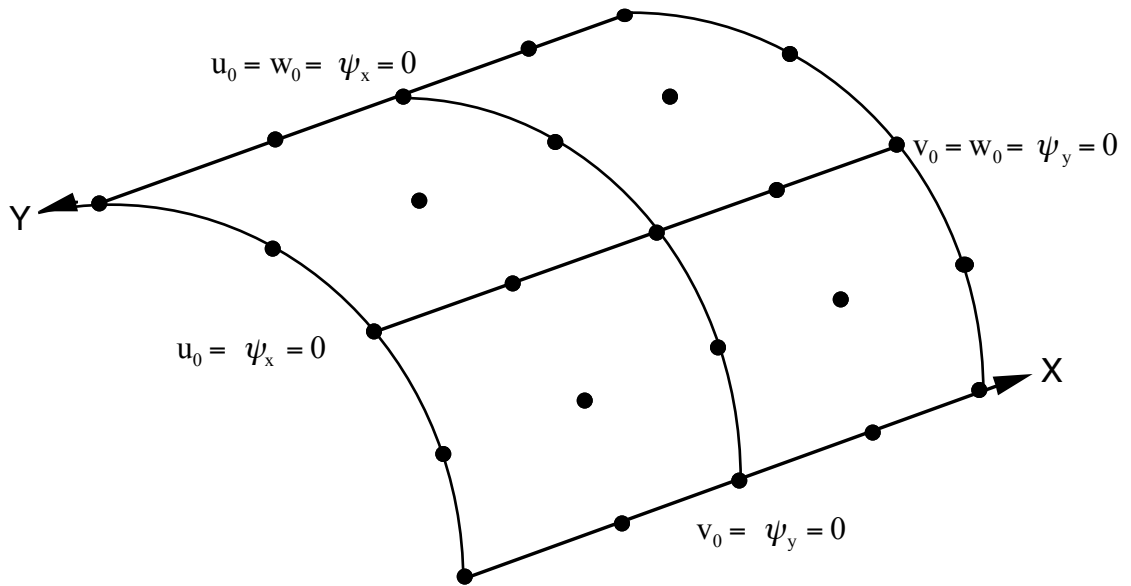
A thin-walled, isotropic cylindrical panel under axial compressive loading is analyzed to determine the critical buckling load. Figure 8.2 presents the geometry, coordinate system and boundary conditions for this problem. The material properties and panel sizes are as follows:

$$\begin{aligned} E &= 179.27 \text{ GPa}, \\ G &= 68.95 \text{ GPa}, \\ \nu &= 0.3, \\ R &= 50.8 \text{ cm}, \\ h &= 0.2 \text{ cm}, \\ a &= 12.7 \text{ cm}, \\ b &= 13.36 \text{ cm}. \end{aligned} \tag{8.2}$$

Under conditions of axisymmetry, a quarter of the panel is used for the analysis. A 2x2 mesh of nine-noded quadratic elements, as shown in Figure 8.2, is used to obtain a convergent result. Eigenvalue analysis is performed by using the proposed finite element equations, as stated in Chapter 4, and the corresponding simply-supported boundary conditions. Table 8.2 contains the comparisons of the critical buckling load of the present result with those of some early researchers [156, 157, 6].



(a) Geometry of a cylindrical panel



(b) Representative quarter model and the corresponding boundary conditions

Figure 8.2 - A simply-supported cylindrical panel

Table 8.2 - Comparison of the critical buckling loads, N_x , (N/m) of a simply-supported cylindrical panel under axial compressive loading

Critical buckling load in axial direction (N/m)	
Present Solution	0.8617×10^6
Rao & Tripathy [156]	0.8616×10^6
Kassegne [157]	0.8800×10^6
Timoshenko & Gere [6]	0.8609×10^6

8.2.3 Nonlinear Analysis of a Simply-Supported Cylindrical Roof under a Central Point Load

In the preceding examples, linear static and buckling analyses were performed in order to test the linear finite element model obtained in Chapter 4. A simply-supported cylindrical roof subjected to a central point load is studied for nonlinear structural response with two different laminate sequences. The geometry and boundary conditions are shown in Figure 8.3. The material properties and geometry information are as follows:

$$\begin{aligned} E_{11} &= 4.0 \times 10^7 \text{ psi (280GPA)}, \\ E_{22} &= E_{33} = 1.0 \times 10^6 \text{ psi (6.90GPA)}, \\ G_{12} &= G_{13} = 0.6 \times 10^6 \text{ psi (4.14GPA)}, \quad G_{23} = 0.5 \times 10^6 \text{ psi (3.45GPA)} \\ \nu_{12} &= \nu_{13} = \nu_{23} = 0.25, \\ R &= 100 \text{ inches (254cm)}, \\ h &= 1 \text{ inch (2.54cm)}, \\ a &= 20 \text{ inches (50.8cm)}, \\ b &= 20 \text{ inches (50.8cm)}. \end{aligned} \tag{8.3}$$

A quarter model with 2x2 mesh of nine-noded quadratic elements is used because of the symmetry in both loading and geometry, as shown in Figure 8.3. A convergence test was also performed.. The nonlinear load-maximum radial displacement curve is shown in Figure 8.4 for the case of a single-layered orthotropic roof, whereas Figure 8.5 contains the nonlinear response of a cross-ply (0/90) composite cylindrical roof.

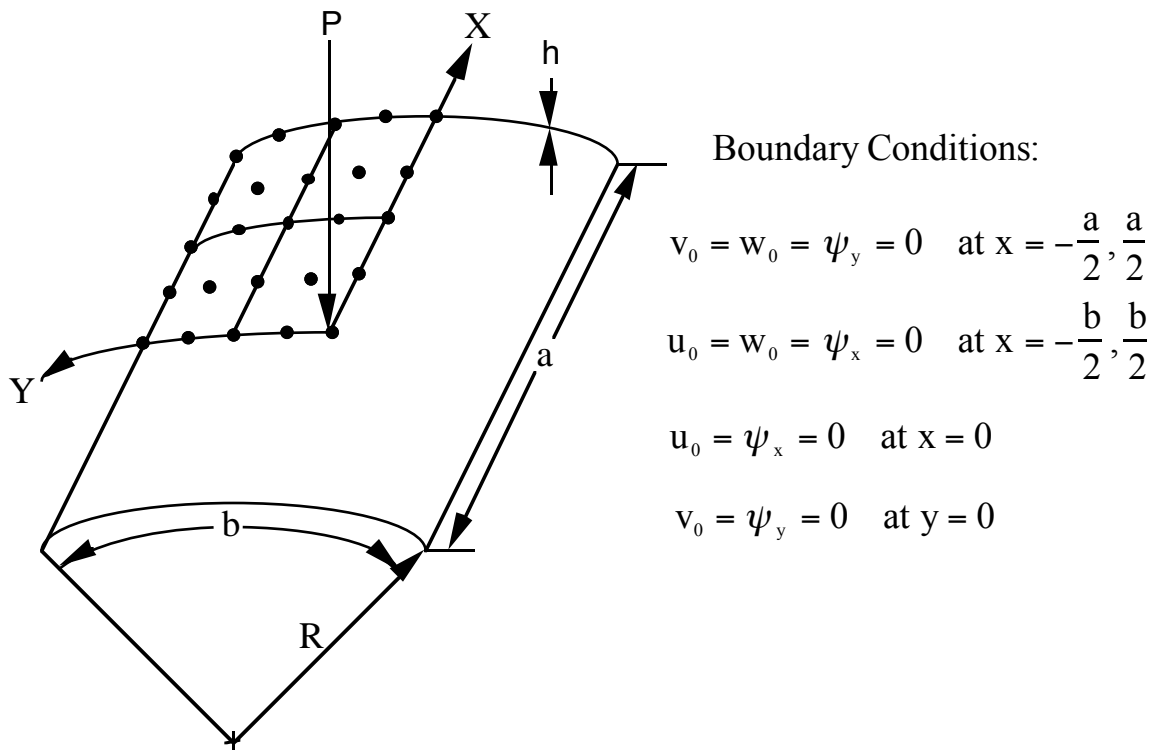


Figure 8.3 - Mesh and geometry information of a simply-supported cylindrical roof under a central point load

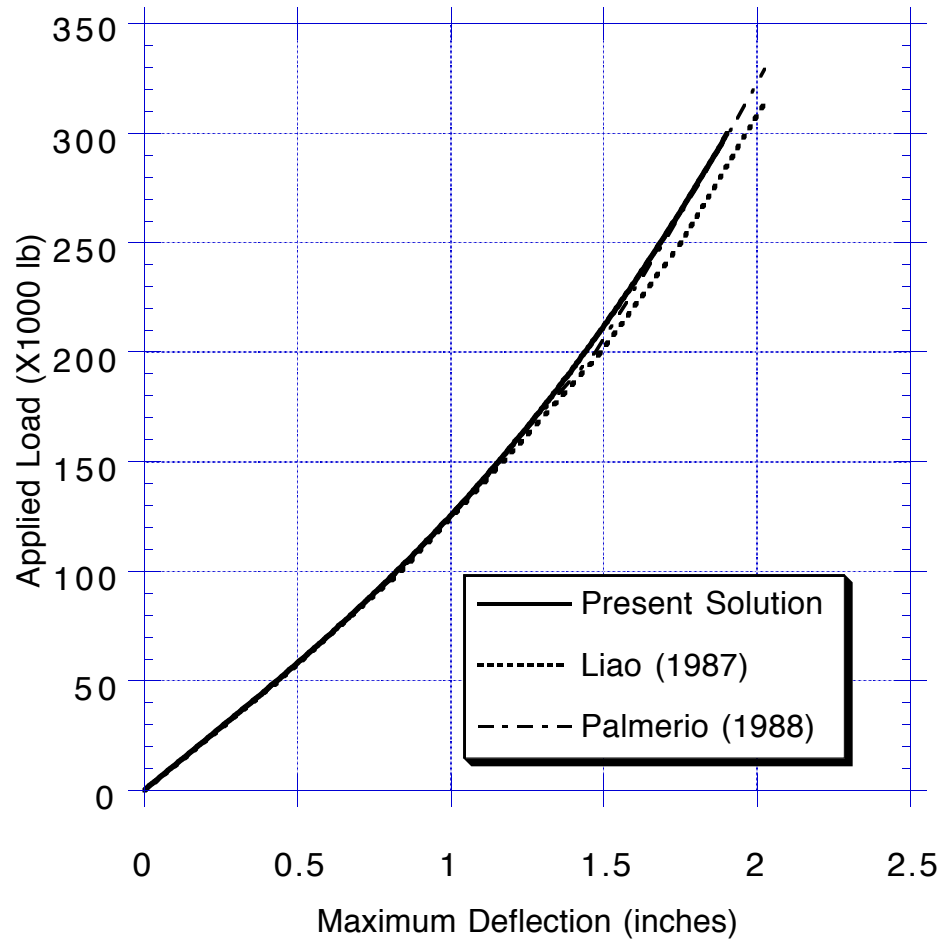


Figure 8.4 - Nonlinear response of a simply-supported, orthotropic cylindrical roof under a central point load

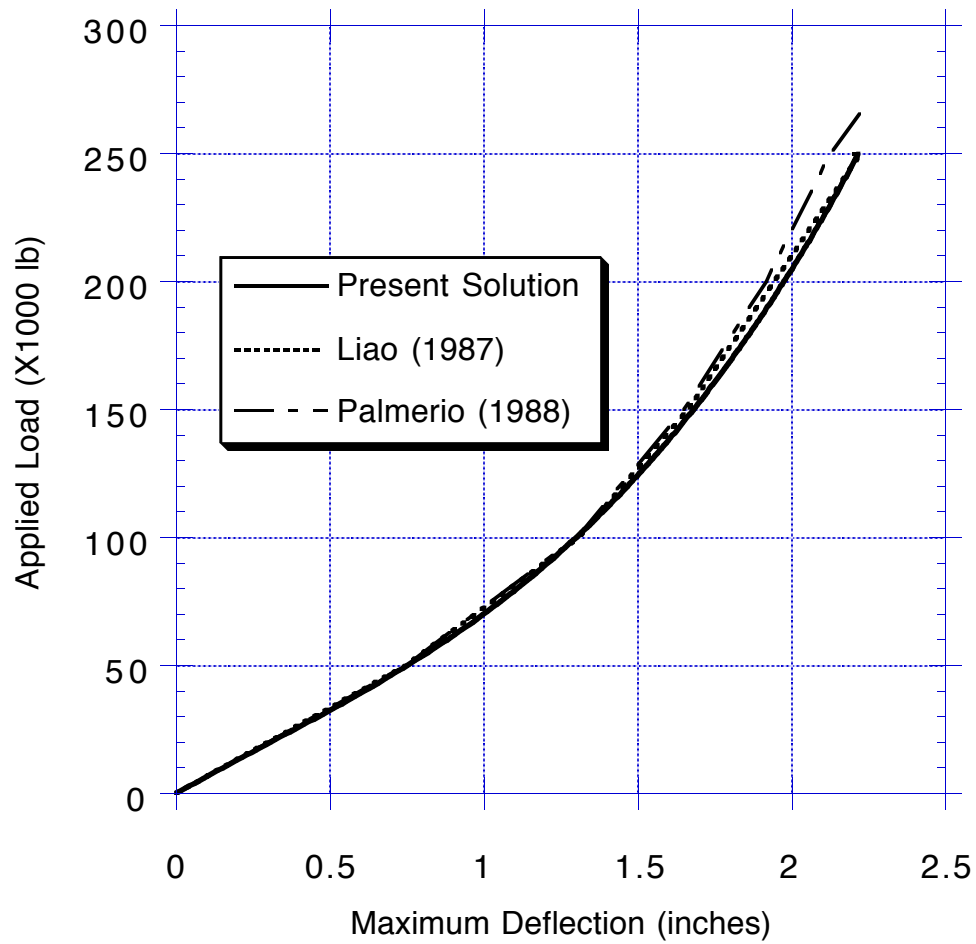


Figure 8.5- Nonlinear response of a simply-supported, cross-ply (0/90) cylindrical roof under a central point load

The present numerical results are based on the derived nonlinear equations from Chapter 4. The comparisons with other references are shown as follows.

For the case of a single-layered cylindrical roof, the corresponding applied loads to produce the central deflection of 2.026 inch (5.146 cm) in various studies are summarized as:

Table 8.3 - Comparison of the applied loads to produce the central deflection of 2.026 inch (5.146 cm) for the case of a single-layered cylindrical roof under various studies

	Applied Point Load (KN)
Present Solution	365.6
Liao [158]	348.8
MRT, Palmerio [159]	366.1
RVK, Palmerio [159]	358.7

For the other case, of a (0/90) composite cylindrical roof, the corresponding applied loads to produce a maximum deflection of 2.222 inch (5.644 cm) in various studies are also compared as:

Table 8.4 - Comparison of the applied loads to produce the central deflection of 2.222 inch (5.644 cm) for the case of a (0/90) composite cylindrical roof under various studies

	Applied Point Load (KN)
Present Solution	279.5
Liao [158]	277.4
MRT, Palmerio [159]	295.4
RVK, Palmerio [159]	283.3

8.3 Example Studies for Cylindrical Shell Structures

In this section, a number of examples are analyzed for linear and nonlinear buckling behavior of circular cylindrical shells under uniform external lateral pressure. Both isotropic and composite cylinders are considered. Comparisons of the structural responses with various internal elastic foundations are also illustrated in the following sub-chapters.

8.3.1 Linear and Nonlinear Buckling Analysis of an Isotropic Cylindrical Shell under Uniform Radial Pressure

The first example is used to study the stability conditions of an isotropic cylinder with simply-supported edges under uniform hydrostatic pressure. The finite element equations derived in Chapter 4 are used to model the present cylindrical structure and

loading conditions. The geometry and the coordinate system for the present study are included in Figure 8.6 (a).

As the first step, the linear eigenvalue analysis is applied for the determination of buckling points and the symmetry conditions. The mesh information and the corresponding boundary conditions for this problem are also shown in Figure 8.6 (b). Due to the symmetry in both loading and geometry, only a quarter model is used in order to reduce the complexity of the model and to save computational time. A 4 X 8 mesh with nine-noded quadratic elements was used to meet the convergence requirement.

The material and geometric properties used as input data for the finite element programs are:

$$\begin{aligned} E &= 200 \text{ GPa}, \\ G &= 77 \text{ GPa}, \\ \nu &= 0.3, \\ R &= 25 \text{ cm}, \\ h &= 0.5 \text{ cm}, \\ L &= 2 \text{ m}. \end{aligned} \tag{8.4}$$

The numerical results for linear buckling analysis of an isotropic, circular cylindrical shell subjected to uniform lateral pressure are listed in the following table. As shown in the table, the corresponding classical solutions based on Donnell's quasi-shallow, thin shell theory [11] are also included and compared with the present numerical solutions.

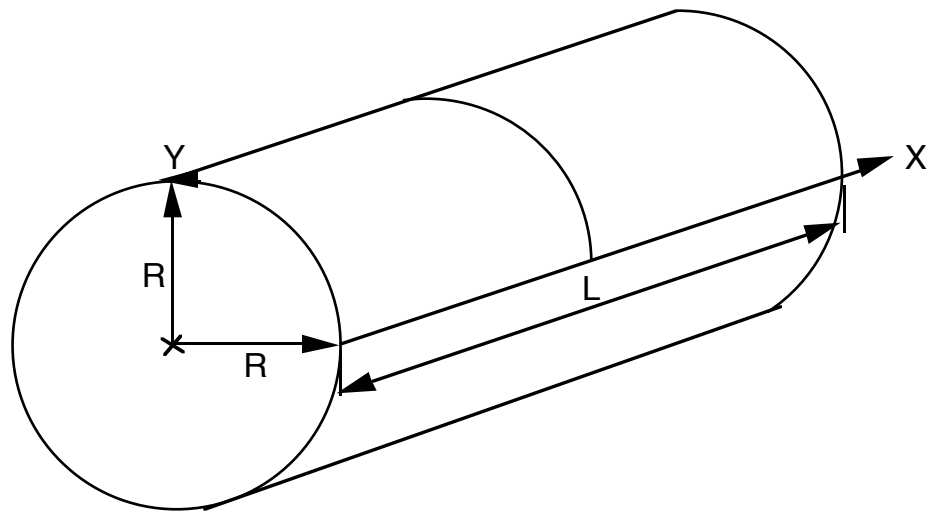
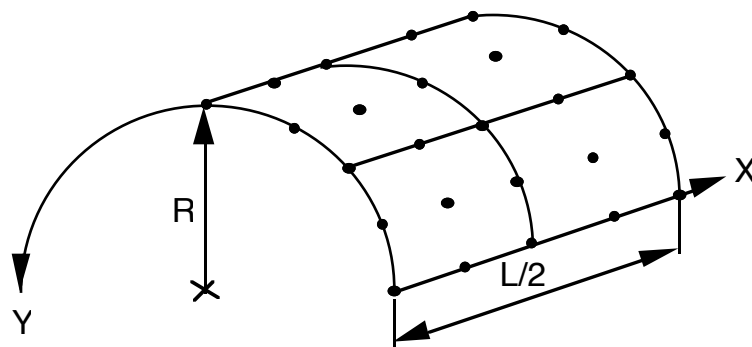


Figure 8.6 (a) - Geometry and coordinate system of a cylindrical shell



Boundary conditions:

$$\begin{aligned}
 v_0 = w_0 = \psi_y = 0 & \quad \text{at } X = 0 \\
 u_0 = \psi_x = 0 & \quad \text{at } X = \frac{L}{2} \\
 v_0 = \psi_y = 0 & \quad \text{at } Y = 0 \\
 v_0 = \psi_y = 0 & \quad \text{at } Y = \pi R
 \end{aligned}$$

Figure 8.6 (b) - Mesh information and the corresponding boundary conditions of a simply-supported cylindrical shell

Table 8.5 - Comparisons of the corresponding buckling loads between the linear numerical analysis and the classical solutions based on Donnell's quasi-shallow, thin theory

q_0 (KPa)	Critical	Second	Third
Present Solutions	1528	2446	3094
Classical Solutions	1490	2010	2413
Number of Lobes	3	2	4

The critical, second, and third buckling modes, which are evaluated by the corresponding eigenvectors, are shown in Figure 8.7(a), (b), and (c), respectively. The present numerical solutions based on Sanders' nonshallow, thin shell theory produce higher buckling load values when compared with classical results. One of the important reasons for the differences is that the cylinder is under constant directional pressure (so-called "dead load") for the present theory instead of the hydrostatic pressure (so-called "live load") for the classical solutions. The second reason is the inclusion of the v/R term in Equation (3.4). This is also the major difference between Sanders' and Donnell's theories. On the other hand, the associated buckled shapes are identical.

The nonlinear finite element analysis is also performed. The geometry, material properties, mesh information and boundary conditions are identical to those used in the linear analysis. Iterative nonlinear schemes, such as Newton-Raphson and Riks-Wempner methods, are used to trace nonlinear load-displacement curves. The normalized determinant values of the stiffness matrices at each equilibrium point are also evaluated

for the determination of the stability condition. The nonlinear numerical solutions differ only by a very small quantity from the linear ones. Since the buckling behavior for the present example undergoes a bifurcation type of phenomenon, the numerical solutions from the nonlinear finite element equations almost match the linear ones. The buckling shapes resulting from the nonlinear analysis are exactly the same as those of the linear solutions.

----- Undeformed Shape
—— First Buckling Mode

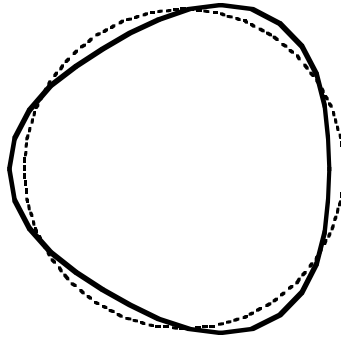


Figure 8.7(a) - First buckling mode with $q_0 = 1528$ KPa

----- Undeformed Shape
—— Second Buckling Mode

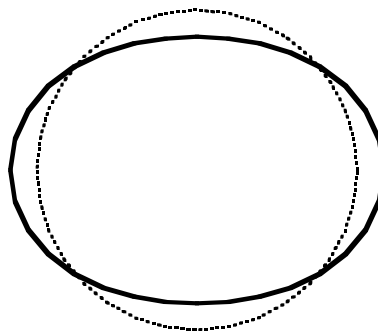


Figure 8.7(b) - Second buckling mode with $q_0 = 2446$ KPa

----- Undeformed Shape
—— Third Buckling Mode

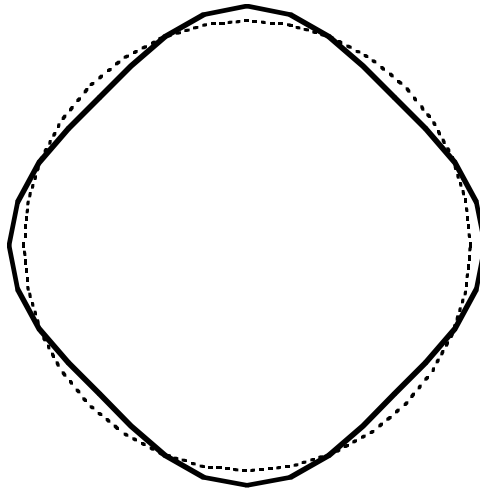


Figure 8.7(c) - Third buckling mode with $q_0 = 3094$ KPa

8.3.2 Stability Analysis of an Isotropic Cylindrical Shell with Internal Elastic Foundation under Uniform Radial Pressure

The influence of internal elastic foundations on the buckling behavior of metallic cylinders is examined. The edges of the shell are also hinged, and the applied external loads remain constant-directional radial pressure. The geometry and material properties are the same as in Chapter 8.3.1. A quarter cylindrical shell containing four by eight nine-node elements is also applied in the study.

Using both linear eigenvalue and nonlinear analyses, numerous critical buckling pressures are determined for various constants of elastic foundations. The numerical results and the corresponding buckling modes are compared in Table 8.3. It is seen from the table that the critical buckling loads for soft elastic foundations do not differ much from the case without a foundation. As the elastic-foundation constants become larger and larger, the resistance to buckling becomes much stronger. The entire stiffness is much enhanced due to the existence of the stiffer elastic medium. The pattern of the critical buckling modes is also altered to higher numbers of waves.

With internal elastic foundations, the stability is still the bifurcation type. Nonlinear solutions give somewhat more conservative results but do not vary much from the linear buckling pressures. The influence of initial imperfections on the nonlinear response and critical buckling loads of the shells with and without internal elastic foundations will be detailed in the next sub-chapter.

Table 8.6 - Comparisons of the critical buckling pressure q_0 (N/ m²) of simply-supported cylindrical shells with and without elastic foundations under uniform lateral pressure

K_0 (N/ m ³)	$(q_0)_{\text{Critical}}$ (X 10 ⁶ N/ m ²)	Number of Lobes (N)
0	1.5284	3
2×10^5	1.5355	3
2×10^6	1.5984	3
2×10^7	2.2280	3
2×10^8	5.9226	4

8.3.3 Stability Analysis of Composite Cylindrical Shells under Uniform Radial Pressure

Linear stability analyses of composite cylinders with hinged ends when subjected to uniform constant radial pressure are studied. The geometry, mesh scheme and corresponding boundary conditions for this study are illustrated in Figure 8.6 (a) and (b). The properties of the Graphite Epoxy (GY70/339) shell used in equation (8.5), are as follows:

$$\begin{aligned} E_{11} &= 289 \text{ GPa}, E_{22} = E_{33} = 6.063 \text{ GPa}, \\ \nu_{12} &= \nu_{13} = \nu_{23} = 0.31, \\ G_{12} &= G_{13} = G_{23} = 4.134 \text{ GPa}. \end{aligned} \tag{8.5}$$
$$\begin{aligned} R &= 25 \text{ cm}, \\ h &= 0.5 \text{ cm}, \\ L &= 2 \text{ m}. \end{aligned}$$

Two types of lamination schemes are examined in this section. One is a composite cylinder with cross-ply (0/90/90/0) laminate sequences, the other is an angle-ply (0/45/-45/0) type of lamination. Similarly to the procedures stated in Section 8.3.1, the linear eigenvalues and the associated eigenvectors of composite cylindrical shells are determined and are shown in Table 8.4 . Table 8.5 also contains the number of lobes of the corresponding buckling modes for the two different types of lamination schemes. Distinct buckling modes (numbers of complete cosine waves in the circumferential direction) are also presented. Performing the nonlinear finite element analysis of both cross-ply and angle-ply types of composite cylinders, the buckling pressures are 326.57

Table 8.7 - Comparisons of the critical buckling pressure q_0 (N/ m²) of simply-supported, composite cylinders with different lamination schemes under uniform lateral pressure

q_0 (KPa)		
Number of Buckling Load	(0/90/90/0) Composite Cylinder	(0/45/-45/0) Composite Cylinder
Critical	326.75	122.99
Second	462.84	169.41
Third	714.70	180.61

Table 8.8 - Comparisons of the numbers of lobes of composite cylinders with different lamination schemes under uniform lateral pressure

Number of Lobes (N) in the Circumferential Direction		
Number of Buckling Load	(0/90/90/0) Composite Cylinder	(0/45/-45/0) Composite Cylinder
Critical	3	4
Second	4	3
Third	2	5

and 122.27 KPa, respectively, whereas the corresponding linear solutions are 326.75, and 122.99 KPa, respectively.

8.3.4 Stability Analysis of Composite Cylindrical Shells with Internal Elastic Foundations under Uniform Pressure

The study of the buckling phenomenon of composite shells is extended in this section by including internal elastic foundations. The geometry, mesh scheme, corresponding boundary conditions and stacking sequences of composite cylinders were stated in Section 8.3.3. With increasing values of the elastic foundation constant K_0 , one can obtain the associated critical buckling points by using eigenvalue analysis and running the finite element program.

Table 8.6 presents the numerical results of critical buckling loads and modes for a series of elastic foundation constants, for the case of a cross-ply (0/90/90/0) composite cylinder. Similarly, Table 8.7 summarizes the results and comparisons for the case of an angle-ply (0.45/-45/0) type of composite cylindrical shell.

As one can see from the results of these two tables, the buckling loads of the soft elastic foundations do not vary much from the one without a foundation. Once the elastic foundations become stiffer, the buckling loads increase. On the other hand, the lowest buckling modes have the tendency to deform into more wave patterns when compared to those without elastic foundation and with softer elastic medium, as shown in Table 8.6 and 8.7.

Table 8.9 - Comparisons of the critical buckling pressures q_0 (N/m²) of simply-supported, cross-ply (0/90/90/0) type of composite cylinders with different elastic foundations under uniform lateral pressure

K_0 (N/m ³)	$(q_0)_{\text{Critical}}$ (X 10 ⁵ N/m ²)	Number of Lobes (N)
0	3.2675	3
1 x 10 ⁵	3.3024	3
1 x 10 ⁶	3.6169	3
1 x 10 ⁷	6.3763	3
1 x 10 ⁸	17.3719	5

Table 8.10 - Comparisons of the critical buckling pressures q_0 (N/m²) of simply-supported, angle-ply (0/45/-45/0) type of composite cylinders with different elastic foundations under uniform lateral pressure

K_0 (N/m ³)	$(q_0)_{\text{Critical}}$ (X 10 ⁵ N/m ²)	Number of Lobes (N)
0	1.2300	4
1 x 10 ⁵	1.2476	4
1 x 10 ⁶	1.4060	4
1 x 10 ⁷	2.7361	5
1 x 10 ⁸	8.1426	7

8.3.5 Stability Analysis of an Isotropic Cylindrical Shells with a Two-Parameter Elastic Foundation under Uniform Radial Pressure

In Section 7.3.5, the effect of Pasternak's constants on the stability of an isotropic ring with an internal elastic foundation was observed for the purpose of consideration of the shear interactions between individual springs. Similarly, the buckling analysis of an isotropic cylinder with internal elastic foundation under uniform external pressure is studied here by including various values of Pasternak's constants. The linear Winkler elastic foundation constant is chosen as $K_0 = 2 \times 10^6 \text{ N/m}^3$. The formulation and the finite element equations which include the terms of the Pasternak foundation are derived in Chapter 4.10. Based on those equations, the critical buckling pressures under different Pasternak's constants are detailed in the following table.

Table 8.11 - Comparisons of the critical buckling pressures of simply-supported, Isotropic Cylindrical Shells with various Pasternak Elastic Foundation Constants under uniform lateral pressure

Pasternak Elastic Foundation Constants $K_s \text{ (N/m}^2\text{)}$	$(q_0)_{\text{Critical}} \text{ : (KPa)}$
0	1598.412
1×10^4	1649.892
2×10^4	1701.372
3×10^4	1752.852
4×10^4	1804.332

According to the numerical results shown in the above table, the critical buckling pressures will rise from 3.22% to 12.88% as the values of K_s rise from 1×10^4 to 4×10^4 when compared to the one without Pasternak's constant.

8.3.6 Stability Analysis of Isotropic Cylindrical Shells with a Nonlinear Elastic Foundation under Uniform Radial Pressure

This example is to test the effect of nonlinear elastic foundation constants on the stability of isotropic cylinders under uniform radial pressure. The critical buckling pressures is compared with those of the linear Winkler elastic foundation model ($K_0 = 2 \times 10^6 \text{ N / m}^3$). An nonlinear finite element model with linear and nonlinear Winkler elastic foundations is used to determine the first buckling loads. The following table includes the numerical results of stability analyses under various nonlinear elastic foundational constants.

Table 8.12 - Comparisons of the critical buckling pressures of simply-supported, Isotropic cylindrical shells with various nonlinear elastic foundation constants under uniform lateral pressure

Nonlinear Winkler Elastic Foundation Constants K_1 (N/ m ⁵)	$(q_0)_{\text{Critical}}$: (KPa)	% increase of $(q_0)_{\text{Critical}}$ Compared with that of Linear Winkler Model
0 - 2×10^{11}	1528	-----
2×10^{12}	1530	0.131 %
1×10^{13}	1536	0.524 %
2×10^{13}	1546	1.178 %
5×10^{13}	1578	3.272 %
2×10^{14}	1792	17.28 %

As one can see from the above table, the critical buckling pressures remain almost the same even though the nonlinear constant K_1 reaches a large value of 2×10^{11} N/ m⁵. With a very large elastic foundation constant of 2×10^{14} N/ m⁵, the critical buckling pressure will increase up to 17 percent. In general, the nonlinear elastic foundation constants become more effective only when one deals with post-buckling behavior or when the value of nonlinear elastic foundation constant is very large.

8.4 Initial Post-Buckling and Imperfection Sensitivity Analysis for Cylindrical Shell Structures

In contrast to the examples of Chapter 8.3, the nonlinear responses of both isotropic and composite cylindrical shells with initial imperfections under uniform radial pressure are studied in this section. Comparisons of the buckling points and the nonlinear load-deflection behavior of cylindrical shells with and without elastic foundations are also included.

8.4.1 Imperfection Sensitivity Analysis of an Isotropic Cylindrical Shell with Simply Supported Ends under Uniform Radial Pressure

In Section 8.3.1, the linear and nonlinear analyses of an initially perfect, isotropic cylinder under external uniform pressure were performed. For the specified material and geometry, the thin shell has a first bifurcation point which corresponds to the critical buckling point. Mathematically, the bifurcation point is the intersection between the primary and secondary load-displacement curves. Before the entire structure loses its stability, the shell will contract uniformly due to uniform pressure. In other words, the equilibrium path is followed until it reaches the bifurcation point, which is also the buckling point, and then turn into the secondary path. That's the explanation for the fact of extremely close, numerically predicted values by both linear and nonlinear analyses.

In the literature cited in Chapter 5, the existence of the initial imperfection will not only change the behavior of the structure, but also dramatically reduce its buckling resistance,

especially for shell type of structures. In this example, the stability of an isotropic cylindrical shell with initial imperfections is studied. The imperfection function is assumed to be:

$$\bar{w}_0(x, y) = \Delta \sin\left(\frac{m \pi x}{L}\right) \cos\left(\frac{n y}{R}\right) \quad (8.6)$$

where \bar{w}_0 denotes the imperfection function, Δ is the imperfection amplitude, which is considered as a small fraction of the wall thickness, and m and n indicate the numbers of half sine waves in the axial direction and complete cosine waves in the circumferential direction, respectively. Using the same mesh and loading condition, one may apply the nonlinear theory associated with the initial imperfection function and the corresponding finite element program derived in Chapter 5 to characterize the nonlinear response and the first buckling point. The Riks-Wempner nonlinear scheme is used to trace the load-displacement curve, iteratively.

Let m be equal to one, and n be three, which represents the first buckled shape, as the wavelength parameters. Imperfection amplitudes were chosen to be 0.01, 0.1, and 0.2 of the shell thickness. The nonlinear responses under this imperfection function with various amplitudes are presented in Figure 8.8. Figure 8.9 also shows the normalized determinants versus the applied external loading. As one can see in Figure 8.8, the structural behavior becomes a limit-point type of equilibrium configuration. As the amplitude increases, the corresponding buckling loads drop gradually. The numerical results of critical buckling loads under various initial imperfections are contained in Table 8.8. The linear and nonlinear results of a perfect cylinder are also included in Table 8.8 to

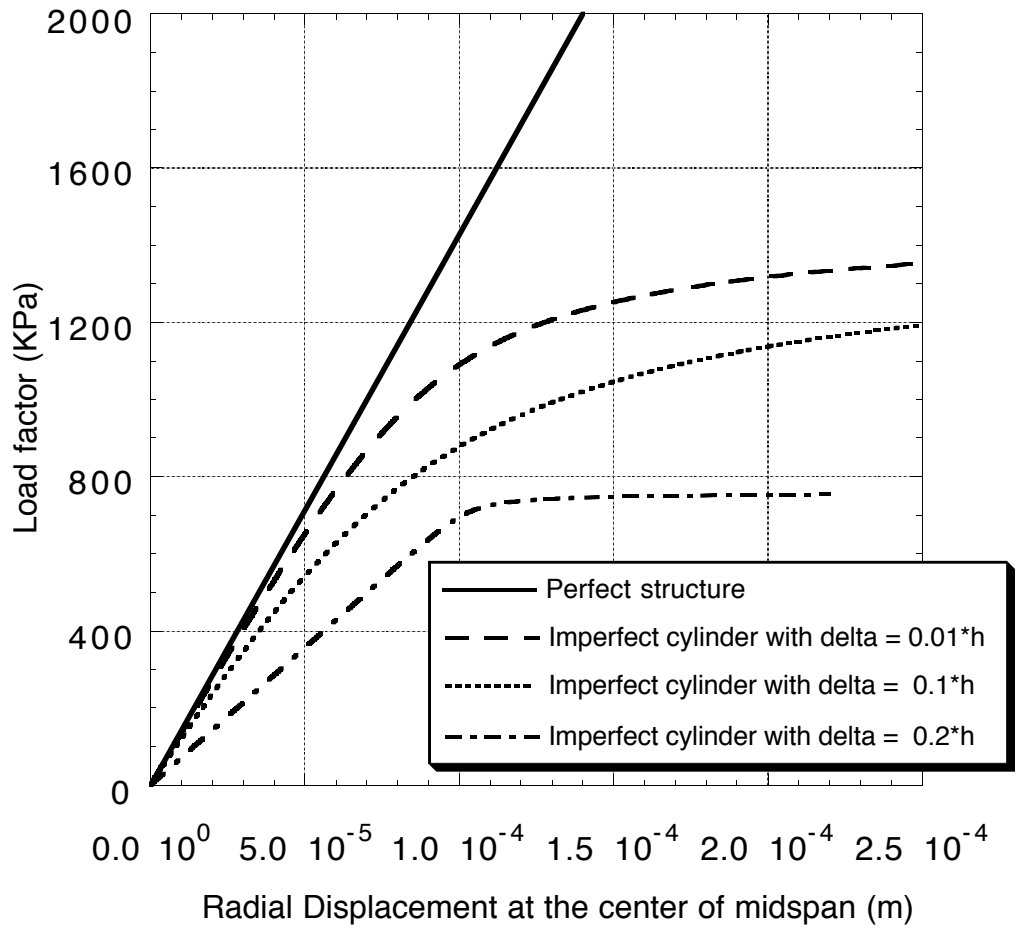


Figure 8.8 - Nonlinear load-displacement curves of isotropic cylinders with various imperfection function amplitudes

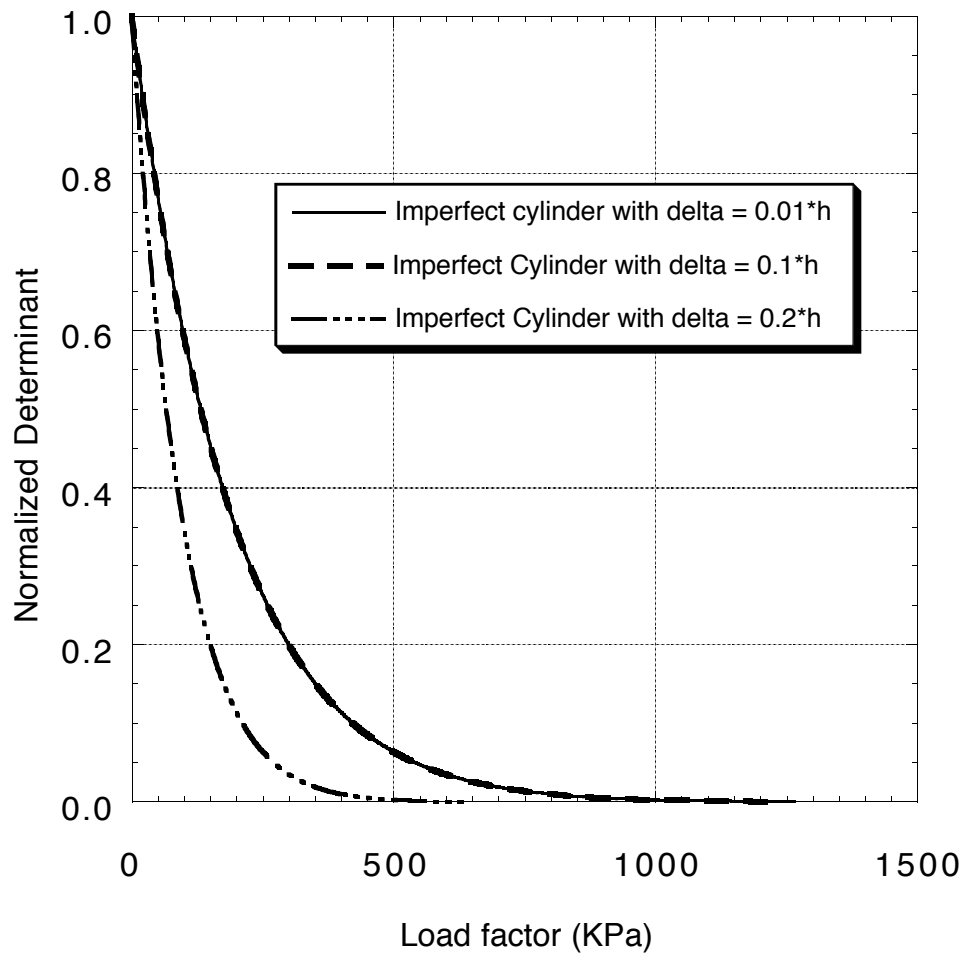


Figure 8.9 - Normalized determinants versus applied loads of isotropic cylinders with various imperfection function amplitudes

Table 8.13 - Comparisons of the critical buckling pressure q_0 (N/m²) of simply-supported, isotropic cylinders under uniform lateral pressure for the cases of linear, nonlinear, and imperfection sensitivity analyses

	Critical Buckling Pressure q_0 (KPa)
Linear Solution	1528.4
Nonlinear Solution	1527.9
Imperfection Sensivity Analysis (m = 1, n = 3)	
$\Delta = 0.01$ *thickness	1498
$\Delta = 0.1$ *thickness	1427
$\Delta = 0.2$ *thickness	1373

make comparisons. The buckling loads become 98%, 93%, and 89% of that of a perfect structure as Δ increases from 0.01, 0.1, and 0.2 of the shell thickness.

8.4.2 Imperfection Sensitivity Analysis of an Angle-Ply Type of Composite Cylindrical Shell with Simply Supported Edges under Uniform Radial Pressure

In this section, the nonlinear structural responses and the corresponding critical buckling pressures of a composite cylinder with the effect of various initial imperfections under external uniform pressure are examined. An angle-ply type of composite cylindrical shell with the lamination of (0/45/-45/0) is selected for the present example. The imperfection function is assumed to be the same one which is shown in equation (8.6). Performing the wave parameter (m and n) studies, the corresponding critical buckling pressures under various imperfection conditions are shown in the following table. The numerical solutions obtained from linear and nonlinear finite element analyses of a perfect cylindrical shell under uniform pressure are also included in the following table for comparisons.

Table 8.14 - Comparisons of the critical buckling pressure of simply-supported, angle-ply type of composite cylinders under uniform lateral pressure for the cases of imperfection sensitivity analyses

	$(q_0)_{\text{Critical}} : (\text{KPa})$
Linear Solution	123.00
Nonlinear Solution	122.27
Imperfect Cylinder with $m = 1$, and $n = 2$	
$\Delta = 0.01 * \text{thickness}$	122.25
$\Delta = 0.02 * \text{thickness}$	122.20
$\Delta = 0.05 * \text{thickness}$	121.93
Imperfect Cylinder with $m = 1$, and $n = 3$	
$\Delta = 0.01 * \text{thickness}$	121.67
Imperfect Cylinder with $m = 1$, and $n = 4$	
$\Delta = 0.01 * \text{thickness}$	120.91
$\Delta = 0.02 * \text{thickness}$	117.13

Due to the convergence difficulty of the numerical procedures, only small imperfection amplitudes are listed here. As the results indicated, the associated buckling pressures

drop as the imperfection amplitudes become larger. The critical buckling pressures also vary with a variety of the imperfection functions.

8.4.3 Imperfection Sensitivity Analysis of an Isotropic Cylindrical Shell with Simply Supported Ends and Elastic Foundation ($K_0 = 2 \times 10^8 \text{ N / m}^3$) under Uniform Radial Pressure

In contrast to the examples of imperfection sensitivity analyses of rings on elastic foundations as shown in Chapter 7.5.3, this example is to examine the nonlinear structural responses and the corresponding critical buckling loads of imperfect cylinders with internal elastic foundations under various initial imperfection conditions. The loading condition, geometry and material properties are chosen the same as those in Section 8.3.2 in order to make comparisons. The internal elastic foundation is selected as the one with $K_0 = 2 \times 10^8 \text{ N / m}^3$, which is a relatively stiff elastic medium.

A nonlinear finite element program including the terms associated with the imperfection functions is applied to determine the nonlinear load-displacement relations and also to evaluate the normalized determinants at each equilibrium point to check for stability conditions. Two types of wave parameters are selected to form the assumed imperfection functions, one with $m = 1$ and $n = 2$, and the other one with $m = 1$ and $n = 4$. With various imperfection amplitudes, the numerical results of critical buckling loads are shown in the following table. Linear and nonlinear solutions of a perfect cylinder are also provided in the table. Figures 8.10 and 8.11 represent the nonlinear solutions of imperfect, isotropic cylinders with various amplitudes under uniform radial pressure,

whereas Figures 8.12 and 8.13 also show the graphs of normalized determinants versus applied pressures, respectively.

Critical Buckling Pressure (q_0) _{Critical} : KPa	
Linear Buckling Analysis	5922.6
Nonlinear Buckling Analysis	5920
Imperfect Cylinder with $m = 1$ and $n = 2$	
$\Delta = 0.01 \cdot h$	5918
$\Delta = 0.1 \cdot h$	5918
$\Delta = 0.2 \cdot h$	5916
$\Delta = 0.5 \cdot h$	5913
Imperfect Cylinder with $m = 1$ and $n = 4$	
$\Delta = 0.01 \cdot h$	-----
$\Delta = 0.1 \cdot h$	-----
$\Delta = 0.2 \cdot h$	-----

From the computational results of the case of a perfect isotropic cylinder with internal elastic foundation under uniform pressure, which were shown in Section 8.3.2, the first buckled shape is the one with four lobes in the circumferential direction, which implies

the value of n to be four. For the case of an isotropic cylinder with a relatively stiff elastic foundation, the normalized determinant does not reach zero since the cylinder already reached the buckled shape for the case of $m = 1$ and $n = 4$. It also shown in Figure 8.11 that the radial deflections will converge as the applied pressure reaches approximately 7000 KPa. But, in the other case of $m = 1$ and $n = 2$, the critical buckling loads are not sensitive to increasing imperfection amplitudes with the inclusion of internal elastic foundation $K_0 = 2 \times 10^8 \text{ N/m}^3$, though the nonlinear load-displacement curves behave quite differently as shown in Figure 8.10.

8.4.4 Imperfection Sensitivity Analysis of an Angle-Ply Type of Composite Cylinder with Simply Supported Edges and Elastic Foundation ($K_0 = 1 \times 10^5 \text{ N/m}^3$) under Uniform Radial Pressure

In this section, the imperfection sensitivity analysis of a composite cylinder with (0/45/-45/0) stacking sequence on a relatively soft elastic foundation ($K_0 = 1 \times 10^5 \text{ N/m}^3$) under uniform radial pressure is examined. For a specified initial imperfection function, the corresponding wavelength parameters with $m = 1$ and $n = 4$ are assumed. The linear buckling pressures of a perfect cylinder along with the associated critical buckling pressures of imperfect cylinders under the consideration of various imperfection amplitudes are listed in the following table:

Table 8.15 - Comparisons of the critical buckling pressure of simply-supported, angle-ply type of cylindrical shell with elastic foundation under uniform lateral pressure for the cases of imperfection sensitivity analyses

Δ / h	0.01	0.02	0.05	0.1
$(q_0)_{\text{Critical}}$: KPa	124.03	123.98	123.73	123.25
Linear Buckling Pressure of a Perfect Cylinder = 124.76 KPa				

The nonlinear relationship of load and radial displacement are illustrated in Figure 8.14. Figure 8.15 also shows the graph of normalized determinants versus applied uniform radial pressures. Since the critical buckling loads only drop a little with the increasing of imperfection amplitudes, it can be said that the composite cylinder with a relatively soft elastic foundation ($K_0 = 1 \times 10^5 \text{ N/m}^3$) is not sensitive to initial imperfections. The structural responses with various imperfection amplitudes do not differ much. This behavior is completely different from the case of an isotropic cylinder with a relatively stiff elastic foundation ($K_0 = 2 \times 10^8 \text{ N/m}^3$).

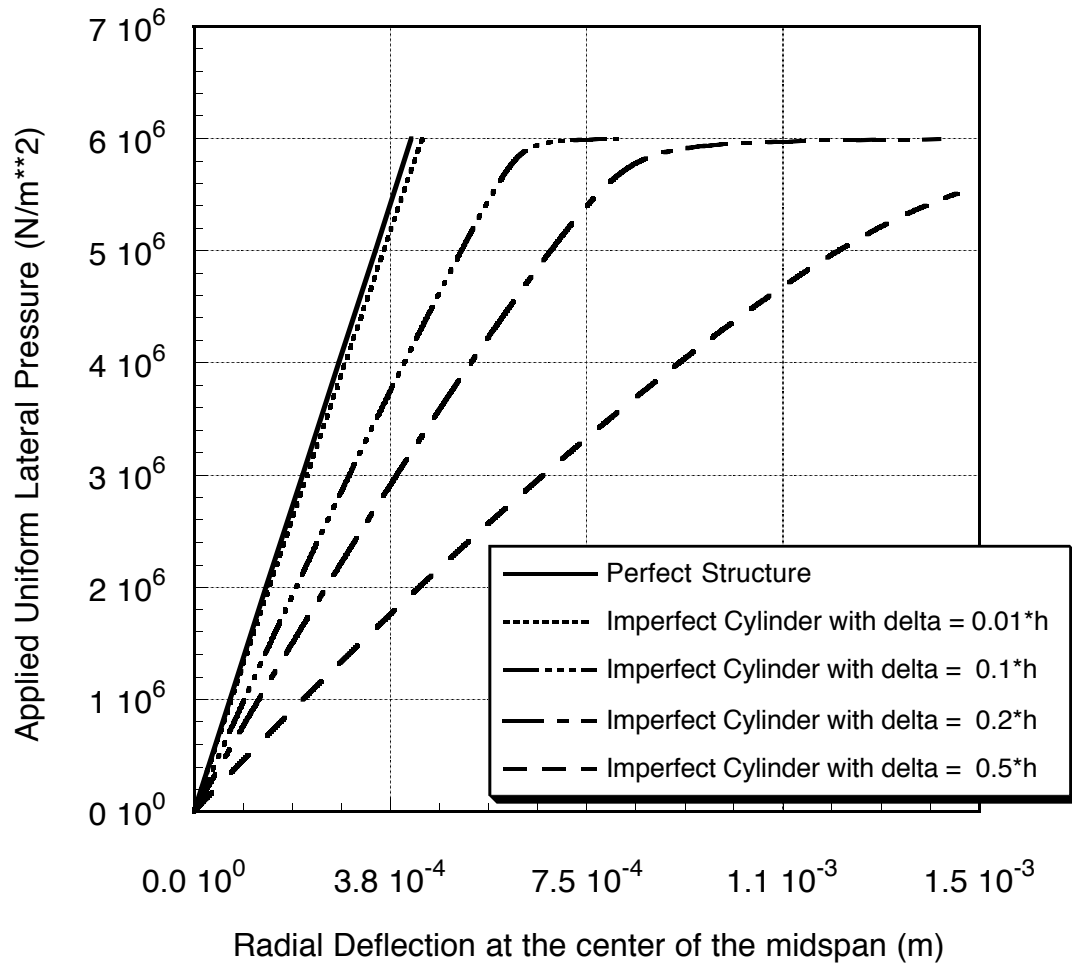


Figure 8.10 - Nonlinear load-displacement curves of imperfect isotropic cylinders on elastic foundation ($K_0 = 2 \times 10^8 \text{ N/m}^3$), wave parameters $m = 1$, and $n = 2$

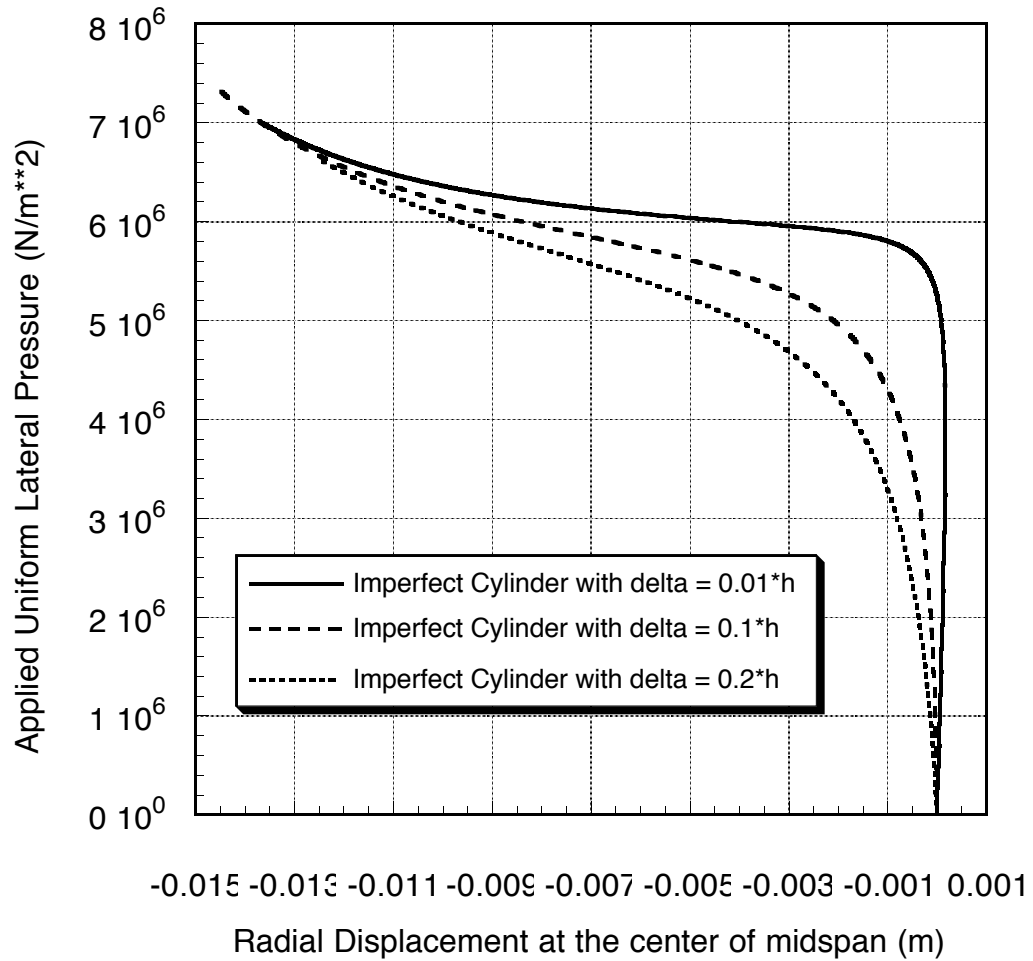


Figure 8.11 - Nonlinear load-displacement curves of imperfect isotropic cylinders on elastic foundation ($K_0 = 2 \times 10^8 \text{ N/m}^3$), wave parameters $m = 1$, and $n = 4$

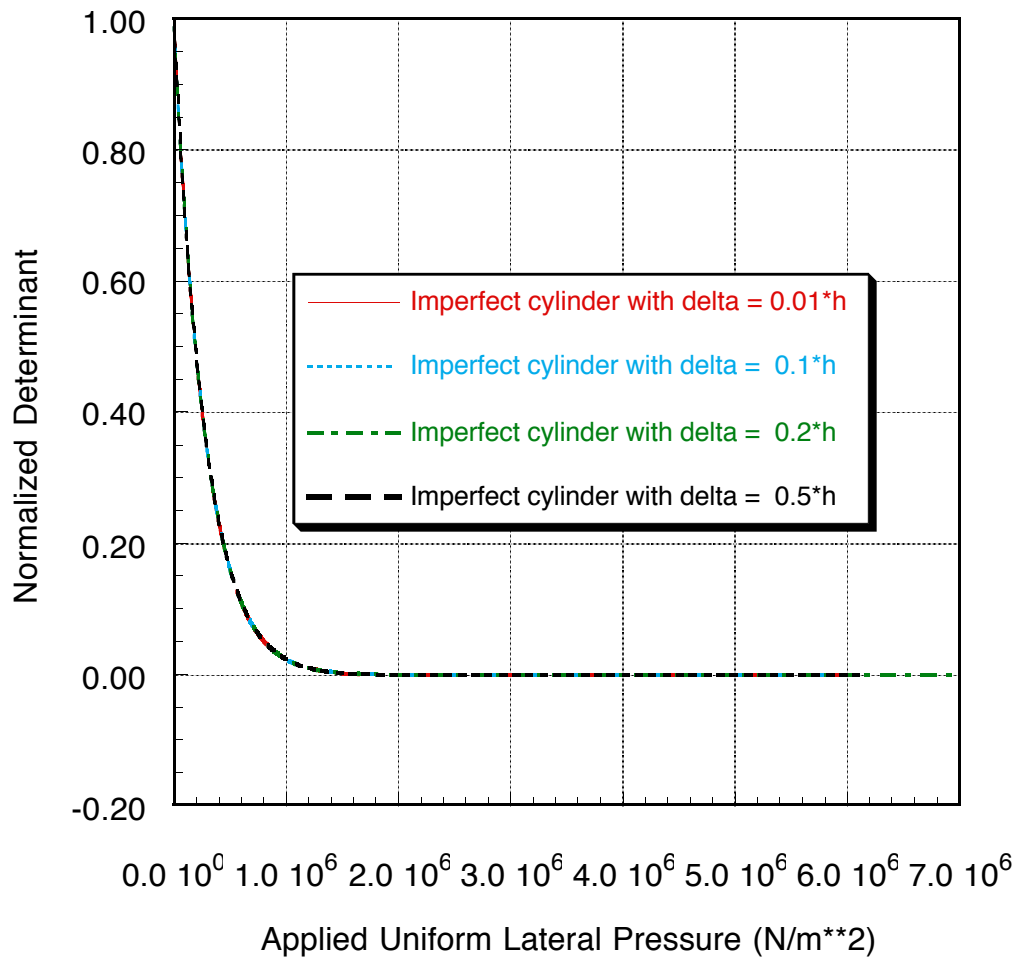


Figure 8.12 - Normalized determinants versus applied loads of imperfect isotropic cylinders on elastic foundation ($K_0 = 2 \times 10^8 \text{ N / m}^3$), wave parameters $m = 1$, and $n = 2$

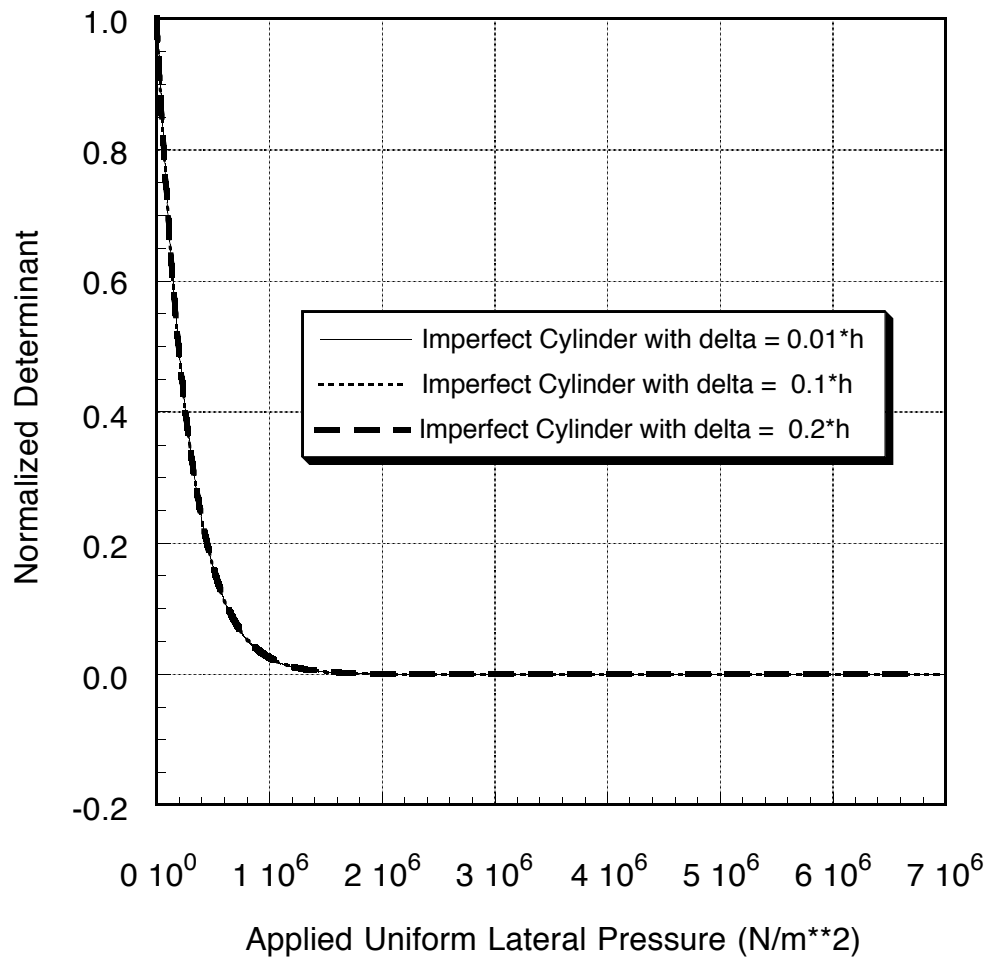


Figure 8.13 - Normalized determinants versus applied loads of imperfect isotropic cylinders on elastic foundation ($K_0 = 2 \times 10^8 \text{ N/m}^3$), the wave parameters $m = 1$, and $n = 4$

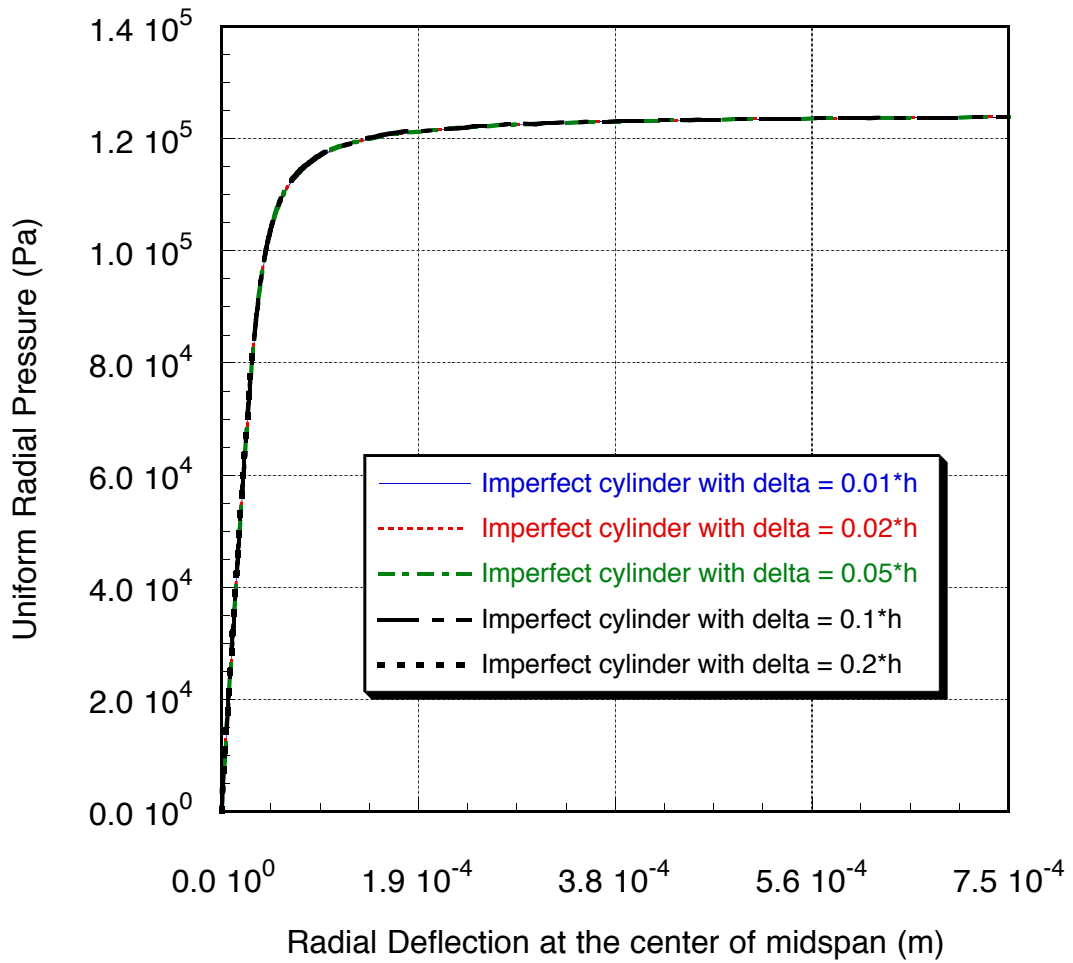


Figure 8.14 - Nonlinear load-displacement curves of imperfect composite cylinders on elastic foundation ($K_0 = 1 \times 10^5 \text{ N / m}^3$), wave parameters $m = 1$, and $n = 4$

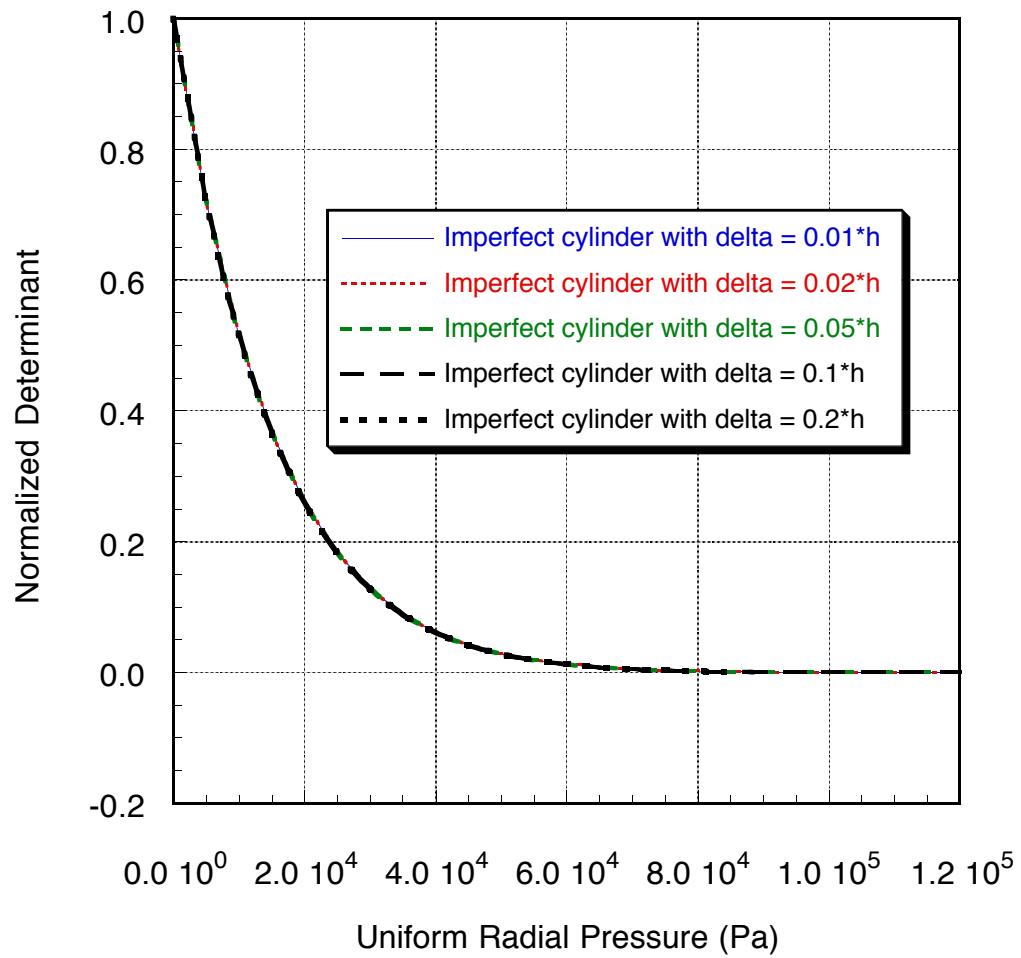


Figure 8.15 - Normalized determinants versus applied loads of imperfect composite cylinders on elastic foundation ($K_0 = 1 \times 10^5 \text{ N / m}^3$), wave parameters $m = 1$, and $n = 4$

CHAPTER 9

CONCLUSIONS AND FURTHER WORK

9.1 Summary and Conclusions

A refined Sanders theory which includes the von Karman type of geometric nonlinearity and first order shear deformable flexibility was used to develop both two-dimensional cylindrical shell and one-dimensional ring elements for the displacement-based finite element models. The proposed elements were tested in order to investigate their validity and efficiency on a variety of examples involving static, buckling and post-buckling analyses under various boundary and loading conditions.

Linear and nonlinear elastic-foundation models were applied to simulate an inner, soft, elastic medium. Pasternak-elastic constants were also chosen to modify the proposed elastic foundation model to include shear interactions between individual springs. Initial imperfections were also incorporated in the formulation of the finite element equations for both thin-walled ring and shell elements for nonlinear buckling and imperfection sensitivity analyses.

In this work, the stability analysis of arches and complete rings under uniform constant-directional radial pressure was presented in Chapter 7, whereas the buckling analysis of cylinders was shown in Chapter 8. Both isotropic and anisotropic materials were applied for the outer, thin layered structures. As the first step, linear eigenvalue analysis was performed to obtain the approximate buckling pressures and the associated buckling

modes as well as the symmetry conditions. Iterative nonlinear schemes, such as Newton-Raphson and Riks-Wempner methods, were used to solve a system of nonlinear finite element equations. Both linear and nonlinear buckling analyses of ring and cylindrical shell structures with internal elastic foundations under uniform pressure were also investigated and compared with their counterparts without elastic foundations. A slightly initially imperfect ring model was used to induce the nonlinear buckling behavior. The results show (Chapter 7) that the inclusion of initial imperfection functions does not change the critical buckling pressures. The imperfection sensitivity of rings and shells with internal elastic foundations was examined, too. Parameter studies under various imperfection amplitudes were also included in this research.

Based on the study of various examples carried out in this work, a number of conclusions are made as follows:

- The present research is based on Sanders' nonlinear theory and the first order shear deformable theory. Unlike the conventional Donnell's theory, the numerical results show much improved accuracy in dealing with global structural responses (such as the displacement field in the mid-surface or buckling loads) of complete rings, cylinders and nonshallow circular structures. It also provides the capability of including the effect of transverse shear of composites.
- Under the range of small strains and moderate rotations (less than 30 degrees), the numerical results of the test examples in Chapter 7 and 8 present reasonable coincidence when compared with studies in the literature, which use various nonlinear ring and shell theories.

- The lowest buckling modes for plane cylinders are not necessarily those with the lowest number of lobes along the circumferential direction. For both ring and shell structures with relatively stiff elastic foundations, the lowest modes are functions of the foundation stiffness.
- The existence of internal elastic foundations is beneficial to the buckling resistance of thin-walled rings and cylindrical shells.
- As the obtained results attest, the examples shown in Chapters 7 and 8 exhibit bifurcation type of buckling phenomena. With either isotropic or composite circular structures, the linear and nonlinear solutions are almost identical.
- Distinct nonlinear load-displacement relations of a cylindrical shell without elastic foundation under various initial imperfection amplitudes are observed. The critical buckling pressures drop quite a lot compared to perfect cylinders.
- The initially out-of-round model is prescribed to induce the buckling of rings in the nonlinear analysis. Numerical results in Chapter 7 show that the buckling behavior of rings is not sensitive to initial imperfections although the load-displacement curves are significantly different.
- With internal elastic foundations, especially stiffer foundations, the critical buckling pressures are not sensitive to the initial imperfection functions. However, for various values of elastic-foundation constants, the load-radial deflection relations vary from case to case.

9.2 Recommendations for Further Research

The following list of research areas might be followed in the applications of the present theories and finite element models:

- The external loading could be extended to uniform hydrostatic (so called "live"), nonuniform, constant-directional pressures, and in-plane concentrated loads.
- The proposed Sanders' theory can also be extended to shells of any general geometry such as spherical and conical shells.
- The stability of cylindrical shells with and without elastic foundations under axial pressures may be investigated. Imperfection sensitivity analyses may also be examined and compared with perfect structures under the same circumstances.
- Instead of using first order shear deformation theory, some higher order theory may be applied to accurately characterize the interlaminar displacement and stress field of the entire composite structure. Some defects or delaminations could also be considered in order to simulate the real situation.

REFERENCES

- 1 Thanjitham, S. ,Heller, R. A., "Test and Evaluation of Dynamic Properties of Solid-Propellant Rocket Motors," Volume I - Service Life of Rocket Motors, Technical Report CR-RD-86-8, U. S. Army Missile Command, Redstone Arsenal, Alabama, October, 1986.
- 2 Heller, R. A. and Heller, T. G., "Test Methods for the Characterization of Composite Cases," Technical Report CR-RD-PR-89-8, U. S. Army Missile Command, Redstone Arsenal, Alabama, September, 1989.
- 3 Lin, Y. T. and Heller, R. A., "Stress Analysis of Rocket Motors by a Mixed Finite Element Model," Technical Report CR-RD-PR-89-6, U. S. Army Missile Command, Redstone Arsenal, Alabama, September, 1989.
- 4 Heller, R. A., Janajreh, I. M., "The Reliability of Rocket Motors Subjected to Static and Dynamic loads," Technical Report CR-RD-PR-92, U. S. Army Missile Command, Redstone Arsenal, Alabama, April, 1992.
- 5 Heller, R. A., Thanjitham, S., and Wang, X., "Stress and Reliability analysis of composite Cased Rocket Motors Under Asymmetric loads," Technical Report CR-RD-PR-92, U. S. Army Missile Command, Redstone Arsenal, Alabama, October, 1992.
- 6 Timoshenko, S. P. and Gere, J. M., "Theory of Elastic Stability," Second Edition, Chapter 7, MacGraw -Hill, New York, 1961, pp. 287-297.
- 7 Stevens, G. W. H., "The Stability of a Compressed Elastic Ring and a Flexible Heavy Structure Spread by a System of Elastic Rings," Quarterly Journal of Mechanics and Applied Mathematics, Vol. 5, Pt. 2, 1952, pp. 221-236.

- 8 Boresi, A. P., "A Refinement of the Theory of Buckling of Rings under Uniform Pressure," *Journal of Applied Mechanics*, Vol. 22, No. 1, March 1955, pp. 95-102.
- 9 Wasserman, E. B., "The Effect of the Behavior of the Load on the Frequency of the Free Vibrations of a Ring," TT F-52, Jan. 1961, NASA.
- 10 Smith, C. V. Jr. and Simitzes, G. J., "Effect of Shear and Load Behavior on Ring Stability," *Journal of the Engineering Mechanics Division, Proceedings of the American Society of Civil Engineering*, Vol. 95, No. EM3, June, 1969.
- 11 Brush, D. O. and Almroth, B. O., "Buckling of Bars, Plates, and Shells," MacGraw-Hill, New York, 1975.
- 12 Rehfield, L. W., "Initial Postbuckling of Circular Rings under Pressure Loads," *AIAA Journal*, Vol. 10, No. 10, 1972, pp. 1358-1359.
- 13 Naschie, M. S., "The Initial Post-Buckling of an Extensional Ring under External Pressure," *International Journal of Mechanical Sciences*, Vol. 17, 1975, pp. 387-388.
- 14 Katzenberger, G. S., "Geometrically Nonlinear Analysis of Pressure-Loaded Arches, Rings, and Frames Using a Follower Force Algorithm," Master Thesis, VPI, August, 1983.
- 15 Love, A. E. H., "On the Small Free Vibrations and Deformations of the Elastic Shells," *Phil. Transaction of Royal Society (London), Serial A*, Vol 17, 1888, pp. 491-549.
- 16 Love, A. E. H., "A Treatise on the Mathematical Theory of Elasticity," Dover Publications, New York, 1944.

- 17 Donnell, L. H., "A Discussion of Thin Shell Theory," Proceedings of the 5th International Congress of Applied Mechanics, John Wiley, New York, 1938, pp. 66-70.
- 18 Reissner, E., "Stress and Displacement of Shallow Spherical Shells," Journal of Mathematical Physics 25, 1946, pp. 80-85.
- 19 Vlasov, A. S., "General Theory of Shells and its Application in Engineering," Gostekhizdat, Moscow, 1949.
- 20 Sanders, J. L., "An Improved Thin Shell Theory," NASA TR-R 24, 1959.
- 21 Timoshenko, S., "Theory of Plates and Shells," McGraw-Hill, New York, 1959.
- 22 Flugge, W., "Stress in Shells," Springer-Verlag, Berlin, 1962.
- 23 Naghdi, P. M. and Berry, J. G., "On the Equations of Motion of Cylindrical Shells", Journal of Applied Mechanics Z1, 1964, pp. 160-166.
- 24 Budiansky, B. and Sanders, J. L., "On the 'Best' First Order Linear Shell Theory," Progress in Applied Mechanics, MacMillan, New York, 1963.
- 25 Budiansky, B. and Radkowski, P. P., "Numerical Analysis of Unsymmetrical Bending of Shells of Revolution," AIAA Journal, Vol 1, 1963, pp. 1833-1842.
- 26 Koiter, W. T., "A Consistent First Approximation in the General Theory of Thin Shells," Theory of Thin Elastic Shells, North Holland, Amsterdam, 1960, pp. 12-33.
- 27 Leissa, A. W., "Vibration of Shells," NASA SP-288, 1960.
- 28 Donnell, L. H., "Stability of Thin-walled Tubes Under Torsion," NACA, Report 479, 1933.
- 29 Donnell, L. H., "A New Theory For Buckling Of Thin Cylinders Under Axial Compression and Bending," Trans. ASME, Vol. 56, Nov., 1934, pp. 795-806.

- 30 Vlasov, V. Z., "Allgemeine Schalen Theorie und ihre Anwendung in der Technik," Akademie-Verlag, Berlin, 1958.
- 31 Novozhilov, V. V., "Foundations of the Nonlinear Theory of Elasticity," Greylock Press, Rochester, New York, 1953.
- 32 Flugge W., "Die Stabilitat der Kreiszyinderschale," Ingenieur-Archiv, Bd 3, 1932, pp. 463-506.
- 33 Sanders, J. L., "Nonlinear Theories For Thin Shells," Quarterly of Applied Mathematics, Vol. 21, April 1963, pp. 21-36.
- 34 Marguerre, K., "Zur Theorie Der Gerkrumnten Plattern Mit Grosser Form-
anderung," Proceedings of the 5th International Congress on Applied Mechanics, 1938, pp. 93-101.
- 35 Hoff, N. J., "The Accuracy of Donnell's Equations," Journal of Applied Mechanics, Vol. 22, Sept. 1955, pp. 329-334.
- 36 Cheng, S. and Ho, B. P. C., "Stability of Heterogeneous Aeolotropic Cylindrical Shells Under Combined Loading," AIAA Journal, Vol. 1, 1963, pp. 892-898.
- 37 Jones, R. M., and Morgan, H. S., "Buckling and Vibration of Cross-Ply Laminated Circular Cylindrical Shells, " AIAA Journal, Vol. 5, No. 8, 1967, pp. 1463.
- 38 Jones, R. M., "Buckling of Circular Cylindrical Shells with Multiple Orthotropic Layers and Eccentric Stiffners, " AIAA Journal, Vol. 6, 1968, pp. 2301-2305.
- 39 Hennemann, J. and Hirano, T."Allgemeine Schalen Theorie und ihre Anwendung in der Technik," Akademie-Verlag, Berlin, 1958.
- 40 Dong, S. B., Pister, K. S., and Taylor, R. L., "On the Theory of Laminated Anisotropic Shells and Plates," Journal of the Aerospace Science, Vol. 29, Aug. 1962, pp. 969-975.

- 41 Wu, C. H., "Buckling of Anisotropic Circular Cylindrical Shells," Ph.D. Dissertation, Case Western Reserve Univ., June 1971.
- 42 Simitses, G. J., Shaw, D., and Sheinman, I., "Stability of Cylindrical Shells by Various Nonlinear Shell Theories," ZAMM Z. Angew. Math. u. Mech., Vol. 65, 1985, pp. 159-166.
- 43 Simitses, G. J., Sheinman, I., and Shaw, D., "The Accuracy of Donnell's Equations for Axially Loaded, Imperfect Orthotropic Cylinders," Computers and Structures, Vol. 20, 1985, pp. 939-945.
- 44 Soldatos, K. P., "A Comparison of Some Theories Used for the Dynamic Analysis of Cross-ply Laminated Circular Cylindrical Panels," Journal of Sound and Vibration, Vol. 97, 1984, pp. 305-319.
- 45 Soldatos, K. P., "On the Theories Used for the Wave Propagation in Laminated Composite Thin Elastic Shells," ZAMP, Vol. 36, 1985, pp. 120-133.
- 46 Bert, C. W and Reddy, V. S., "Cylindrical Shells of Bimodulus Composite Material," ASCE Journal of the Engineering Mechanics Division, Vol. 108, 1982, pp. 675-688.
- 47 Reissner, E., "On The Theory of Bending of Elastic Plates," Journal of Mathematics and Physics, Vol. 23, No 4, 1944, pp. 184-191.
- 48 Basset, A. B., "On the Extension and Flexure of Cylindrical and Spherical Thin Elastic Shells," Phil. Trans. Royal Soc., (London), Serial A, Vol 6, 1890, pp. 433-480.
- 49 Hildebrand, F. B., Reissner, E., and Thomas, G. B. "Notes on the Foundations of the Theory of Small Displacements of Orthotropic Shells," NACA TN-1833, Washington, D. C., 1949.

- 50 Yang, P., Norris, C. H. and Stavsky, Y., "Elastic Wave Propagation in Heterogeneous Plates," *International Journal of Solids and Structures*, Vol. 2, 1966, pp. 655-684.
- 51 Dong, S. B. and Tso, F. K. W., "On a Laminated Orthotropic Shell Theory Including Transverse Shear Deformation," *Journal of Applied Mechanics*, Vol. 39, 1972, pp. 1091-1097.
- 52 Reddy, J. N., "Exact Solutions of Moderately Thick Laminated Shells," *ASCE Journal of the Engineering Mechanics Division*, Vol. 110, 1983, pp. 794-809.
- 53 Di Sciuva, M., "A Improved Shear-Deformable Theory for Moderate Thick Multilayered Anisotropic Shells and Plates," *Journal of Applied Mechanics* 54, 1987, pp. 589-596.
- 54 Librescu, L. and Schmidt, R., "Substantiation of a Shear-Deformable Theory for Anisotropic Laminated Shells Accounting for the Interlaminae Continuity Conditions," *International Journal of Engineering Science* 29, 1991, 669-683.
- 55 Librescu, L., Khdeir, A., and Frederick, D., "A Shear Deformable Theory of Laminated Composite Shallow Shell-Type Panels and Their Response Analysis, I: Free Vibration and Buckling," *Acta Mech*, Vol. 76, 1989, pp. 1-33.
- 56 Murthy, M. V. V., "An Improved Transverse Shear Deformable Theory for Laminated Anisotropic Shells and Plates," *NASA Technical Paper* 1903, November 1981, pp. 1-37.
- 57 Librescu, L., "Substantiation of a Theory of Elastic and Anisotropic Shells and Plates," *St. Cerc. Mech. Appl.*, Vol. 1, 1968, pp. 105-128.
- 58 Bhimaraddi, A., "A Higher Order Theory for Free Vibration Analysis of Circular Cylindrical Shells," *International Journal of Solids and Structures*, Vol. 20, 1984, pp. 623-630.

- 59 Reddy, J. N. and Liu, C. F., "A Higher-order Shear Deformation Theory of Laminated Elastic Shells," *International Journal of Engineering Science*, Vol. 23, 1985, pp. 319-330.
- 60 Soldatos, K. P., "A Refined Laminated Plate and Shell Theory with Applications," *Journal of Sound and Vibrations*, Vol. 144, 1991, pp. 109-129.
- 61 Soldatos, K. P., "Stability and Vibration of Thick Shear Deformable Cross-ply Laminated Non-circular Cylindrical Shells," in D. Hui, J. C. Duke, Jr., and H. Chung (eds.) *Nonlinear Analysis and NDE of Composite Material Vessels and Components*, ASME PVP-115, 1986, pp. 23-24.
- 62 Soldatos, K. P., "Buckling of Axially Compressed Angle-ply Laminated Circular Panels According to a Refined Shear Deformable Theory," in H. Chung and H. D. Fisher (eds.), *Recent Advances in Structural Dynamics*, ASME PVP-124, 1987, pp. 63-71.
- 63 Dennis, S. T. and Palazotto, A. N., "Transverse Shear Deformation in Orthotropic Cylindrical Pressure Vessels Using a Higher Order Shell Theory," *AIAA Journal*, Vol. 27, 1989, pp. 1441-1447.
- 64 Dennis, S. T. and Palazotto, A. N., "Large Displacement and Rotational Formulation for Laminated Shells Including Parabolic Transverse Shear," *International Journal of Non-Linear Mechanics*, Vol. 25, 1990, pp. 67-85.
- 65 Librescu, L. and Schmidt, R., "Refined Theories of Elastic Anisotropic Shells Accounting for Small Strains and Moderate Rotations," *International Journal of Non-Linear Mechanics*, Vol. 23, 1988, pp. 217-229.
- 66 Zukas, J. A. and Vinson, J. R., "Laminate Transversal Isotropic Cylindrical Shells," *Journal of Applied Mechanics*, Vol. 38, 1971, pp. 400-407.

- 67 Whitney, J. M. and Sun, C. T., "A Refined Theory for Laminated Anisotropic Cylindrical Shells," *Journal of Applied Mechanics*, Vol. 41, 1974, pp. 471-476.
- 68 Mirsky, I. and Herrmann, G., "Nonaxially Symmetric Motions of Cylindrical Shells," *The Journal of the Acoustical Society of America*, Vol. 29, 1956, pp. 1116-1124.
- 69 Voyiadjis, G. Z. and Shi, G., "A Refined Two-Dimensional Theory for Thick Cylindrical Shells," *International Journal of Solids and Structures*, Vol. 27, 1991, pp. 261-282.
- 70 Lorenz, R., "Die nichtachsensymmetrische Knickung dünnwandiger Hohlzylinder," *Phys. Z.*, Vol. 13, pp. 241-260, 1911.
- 71 Southwell, R. V., "On the Collapse of Tubes by External Pressure," *Phil. Mag.*, Vol. 25, pp. 687-698, 1913.
- 72 Flugge, W., "Die Stabilität der Kreiszyllinderschale," *Ing. Archiv*, Vol. 3, December 1932, pp. 463-506.
- 73 Batdorf, S. B., "A Simplified Method of Elastic Stability Analysis for Thin Cylindrical Shells, I - Donnell Equations," NACA, TN 1341, 1947.
- 74 Ho, B. P. C. and Cheng, S., "Some Problems in Stability of Heterogeneous Anisotropic Cylindrical Shells Under Combined Loading," *AIAA Journal*, Vol. 1, 1963, pp. 1603-1607.
- 75 Seide, P., and Weingarten, V. I., "On the Buckling of Circular Cylindrical Shells Under Pure Bending," *Journal of Applied Mechanics*, Vol. 28, 1961, pp. 112-116.
- 76 Holston, A., Jr., "Buckling of Inhomogeneous Anisotropic Cylindrical Shells by Bending," *AIAA Journal*, Vol. 6, October 1968, pp. 1837-1841.
- 77 von Karman, T. and Tsien, H. S., "The Buckling of Thin Cylinders Under Axial Compression," *Journal of Aero. Sciences*, Vol. 8, 1941, pp. 302-312.

- 78 Kiciman, O. K. and Popov, E. P., "Post-Buckling Analysis of Cylindrical Shells,"
Journal of Engineering Mechanics Division, ASCE, Vol. 104, 1978, pp. 751-762.
- 79 Naghdi, P. M., "On the Theory of Thin Elastic Shells," Quarterly of Applied
Mechanics, Vol. 14, 1957, pp. 369-380.
- 80 Koiter, W. T., "The Stability of Elastic Equilibrium," Ph. D. Dissertation, Delft,
Netherlands, 1945.
- 81 Hutchinson, J. W., "Axial Buckling of Pressurized Imperfect Cylindrical Shells,"
AIAA Journal, Vol. 3, 1965, pp. 1461-1466.
- 82 Budiansky, B. and Hutchinson, J. W., "Buckling of Circular Cylindrical Shells
Under Axial Compression," Contribution to the Theory of Aircraft Structures,
Delft University Press, Holland, 1972.
- 83 Arbocz, J. and Babcock, C. D., "The Effect of General Imperfections on the
Buckling of Cylindrical Shells," Journal of Applied Mechanics, Vol. 36, 1969, pp.
23-38.
- 84 Schmit, L. A. and Monforton, G. R., "Finite Element Analysis of Sandwich Plate
and Laminated Shells with Laminated Faces," AIAA Journal, Vol. 8, 1970, pp.
1453-1461.
- 85 Panda, S. C. and Natarajan, R., "Finite Element Analysis of Laminated Shells of
Revolution," Computers and Structures, Vol. 6, 1976, pp. 61-64.
- 86 Shivakumar, K. N. and Krishna Murty, A. V., "A High Precision Ring Element for
Vibrations of Laminated Shells," Journal of Sound and Vibration, Vol. 58, No. 3,
1978, pp. 311-318.
- 87 Rao, K. P., "A Rectangular Laminated Anisotropic Shallow Thin Shell Finite
Element," Computer Methods in Applied Mechanics and Engineering, Vol. 15,
1978, pp. 13-33.

- 88 Seide, P. and Chang, P. H. H., "Finite Element Analysis of Laminated Plates and Shells," NASA CR-157106, 1978.
- 89 Hsu, Y. S., Reddy, J. N., and Bert, C. W., "Thermoelasticity of Circular Cylindrical Shells Laminated of Bimodulus Composite Materials," *Journal of Thermal Stresses*, Vol. 4, No. 2, 1981, pp. 115-177.
- 90 Reddy, J. N., "Bending of Laminated Anisotropic Shells by a Shear Deformable Finite Element," *Fiber Science and Technology*, Vol. 17, 1982, pp. 2-24.
- 91 Venkatesh, A. and Rao, K. P., "A Doubly Curved Quadrilateral Finite Element for the Analysis of Laminated Anisotropic Thin Shells of Revolution," *Computers and Structures*, Vol. 12, 1980, pp. 825-832.
- 92 Venkatesh, A. and Rao, K. P., "Analysis of Laminated Shells with Laminated Stiffeners Using Rectangular Shell Finite Elements," *Computer Methods in Applied Mechanics and Engineering*, Vol. 38, 1983, pp. 255-272.
- 93 Sharifi, P. and Popov, E., "Nonlinear Buckling Analysis of Sandwich Arches," *ASCE Journal of the Engineering Mechanics Division*, Vol. 97, 1971, pp. 1397-1412.
- 94 Walker, A. C., "A Nonlinear Finite Element Analysis of Shallow Circular Arches," *International Journal of Solids and Structures*, Vol. 5, 1969, pp. 97-107.
- 95 Noor, A. K., and Peters, J. M., "Mixed Models and Reduced/Selective Integration Displacement Models for Nonlinear Analysis of Curved Beams," *International Journal for Numerical Methods in Engineering*, Vol. 17, 1981, pp. 615-631.
- 96 Riks, E., "An Incremental Approach to the Solution of Snapping and Buckling Problems," *International Journal of Solids and Structures*, Vol. 15, 1979, pp. 529-551.

- 97 Ramm, E., "Strategies for Tracing the Nonlinear Response Near Limit Point," Nonlinear Finite Element Analysis in Structural Mechanics, edited by Stein, M., Bathe, K. J., Berlin, 1981, pp. 63-89.
- 98 Crisfield, M. A., "A Fast Incremental Iterative Solution Procedure that Handles Snap-through," Computers and Structures, Vol. 13, 1981, pp. 55-62.
- 99 Reissner, E., "Memorandum on Effect of Soft Solid Core on Buckling of Axially Loaded Circular Cylindrical shells," Structures Study 64, Aug. 12, 1957, Lockheed Aircraft Corp., Missile Systems Div., Sunnyvale, California.
- 100 Zak, A. R. and Bollard, R. J. H., "Elastic Buckling of Cylindrical Thin Shells Filled with an Elastic Core," Am. Rocket Soc. Journal, Vol. 32, No. 4, April 1962, pp. 588-593.
- 101 Seide, P., "The Stability Under Axial Compression and Lateral Pressure of Circular-Cylindrical Shells with a Soft Elastic Core," Journal of The Aerospace Sciences, Vol. 29, No. 7, July 1962, pp. 851-862.
- 102 Yao, J. C., "Buckling of an Axially Compressed Long Cylindrical Shell with an Elastic Core," Journal of Applied Mechanics, Vol. 29, No. 2, June 1962, pp. 329-334.
- 103 Winkler, E., "Die Lehre von der Elastizitaet und Festigkeit," Prague, Dominicaus, 1867.
- 104 Myint, U. T., "Stability of Axially Compressed Core-Filled Cylinders," AIAA Journal, Vol. 4, No. 3, March 1966, pp. 552-553.
- 105 Seide, P. and Weingarten, V. I., "Buckling of Circular Rings and Long Cylinders Enclosing an Elastic Materialnder Uniform External Pressure," Am. Rocket Soc. Journal, Vol.32, 1962, pp. 680-688.

- 106 Herrmann, G. and Forrestal, M. J., "Buckling of a Long Cylindrical Shell Containing an Elastic Core," AIAA Journal, Vol. 3, 1965, pp. 1710-1715.
- 107 Korbut, B. A. and Saksonov, S. G., Prikl. Mekhan, 1, no. 6, 199, 1965.
- 108 Yao, J. C., "Bending due to ring loading of a cylindrical shell with an elastic core," Journal of Applied Mechanics, vol. 32, 1965, pp. 99-103.
- 109 Brush, D. O. and Almroth, B. O., "Buckling of Core-stabilized Cylinders under Axisymmetric External Loads," Journal of Aerospace Science, Vol. 29, 1962, pp. 1164-1170.
- 110 Vlasov, V. V., "Stability of Cylindrical Shells Containing a Filler on Being Subjected to Axial Compression and External Pressure," Prikl. Mekh., Vol. 9, No. 1, pp. 117-121.
- 111 Yabuta, T., "Effects of Elastic Supports on the Buckling of Circular Cylindrical Shells under Bending," Journal of Applied Mechanics, Vol. 47, 1980, pp. 866-870.
- 112 Weingarten, V. I., "The Stability Under Torsion of Circular-Cylindrical Shells with an Elastic Core," Am. Rocket Soc. Journal, Vol.32, No. 4, 1962.
- 113 Kachman, D. R., "Test Report on Buckling of Propellant Cylinders under Compressive Loads," Space Technology Lab.,Inc., GM-59-7520.6-24, Nov. 30, 1959.
- 114 Fitzgibbon, D. P., "Preliminary Results of Sub-Scale Tests on Cylinders Filled with an Elastic Core," Space Technology Lab.,Inc., GM-60-7520.6-11, April 25, 1960.
- 115 Goree, W. S., and Nash, W. A., "Elastic Stability of Circular Cylindrical Shells Stabilized by a Soft Elastic Core," Department of Engineering and Mechanics,

- Eng. and Ind. Exp. Sta., University of Florida, Interim Tech. Report No. 4 for Office of Ordnance Research, U. S. Army, May 1960.
- 116 Karam, G. N. and Gibson, L. J., "Elastic Buckling of Cylindrical Shells with Elastic Cores - II. Experiments," *Int. J. of Solids and Structures*, Vol. 32, No8/9, 1995, pp. 1259-1283.
- 117 Lemke, D. G., "Buckling of a Composite Orthotropic Cylinder Containing an Elastic Foundation," *AIAA Paper 63-233*, Los Angeles, Calif., 1963.
- 118 Holston, A., Jr., "Stability of Inhomogeneous Anisotropic Cylindrical Shells Containing Elastic Cores," *AIAA Journal*, Vol. 5, No. 6, June 1967, pp. 1135-1138.
- 119 Tarnopol'skii, Y. M., and Rose, A. V., "Distortion of Cross Sections During Deformation of Oriented Glass-Reinforced Plastics," *Polymer Mechanics*, Vol. 1, No. 5, Sept.-Oct. 1965, pp. 69-75.
- 120 Bert, C. W., "Buckling of Axially Compressed, Core-Filled Cylinders with Transverse Shear Flexibility," *Journal of Spacecraft*, Vol. 8, 1971, pp. 546-548.
- 121 Vlasov, V. V., "Stability of Composite Shells with an Elastic Core," *Mekh. Polimerov*, Vol 3, 1975, pp. 544-547.
- 122 Malyutin, I. S., Pilipenko, P. B., Georgievskii, V. P. and Smykov, V. I., "Experimental and Theoretical Study of the Stability in Axial Compression, of Cylindrical Shells Reinforced with an Elastic Filler," *Prikl. Mekh*, Vol. 16, 1980, pp. 56-60.
- 123 Babich, I. Y. and Cherevko, M. A., "Stability of Cylindrical shells with an Elastic-Plastic Filler under Axial Compression," *Prikl. Mekh*, Vol. 20, 1984, pp. 60-64.
- 124 Zimmermann, H., "Die Berechnung des Eisenbahnoberbaues," 2nd Edition, Berlin, 1930.

- 125 Hetenyi, M, "Beams on Elastic Foundations," The University of Michigan Press, Ann Arbor, Michigan, 1946.
- 126 Hetenyi, M, "A General Solution for the Bending of Beams on an Elastic Foundation of Arbitrary Continuity," Journal of Applied Physics, Vol. 21, pp. 55-58, 1950.
- 127 Pasternak, P. J., "On a New Method of Analysis of an Elastic Foundation by Means of Two Foundation Constants," Gosuedarstvennoe Izadatesvo Literaturi po Stroitelstvuri Arkhitekture, Moscow, 1954 (in Russian).
- 128 Vlasov, V. Z. and Leont'ev, N., "Beams and Plates and Shells on Elastic Foundation," Israel Program for Scientific Translation, Jerusalem, 1966 (translated from Russian).
- 129 Vallabhan, C. V. and Das, Y. C., "Modified Vlasov Model for Beams on Elastic Foundation, " J. Geotech. Engng. ASCE, Vol. 117, pp. 956-966, 1991.
- 130 Vallabhan, C. V., Straughan, W. T., and Das, Y. C., "Refined Model for Analysis of Plates on Elastic Foundation, " J. Geotech. Engng. ASCE, Vol. 117, pp. 2830-2844, 1991.
- 131 Amazigo, J. C., Budiansky, B. and Carrier, G. F., "Asymptotic Analysis of the Buckling of Imperfect Columns on Nonlinear Elastic Foundation," Int. J. Solids Structures, Vol. 6, 1970.
- 132 Fraser, W. B. and Budiansky, B., "The Buckling of a Column with Random Initial Deflections," J. Appl. Mech., Vol. 36, 1969.
- 133 Hui, D. and Hansen, J. S., "Two-Mode Buckling of an Elastically Supported Plate and its Relation to Catastrophe Theory," J. Appl. Mech., Vol. 47, 1980.

- 134 Hui, D., "Imperfection Sensitivity of Elastically Supported Beams and its Relation to the Double-Cusp Instability Model," Proc. R. Soc., London, Vol. A405, 1986.
- 135 Keener, J. P., "Buckling Imperfection Sensitivity of Columns and Spherical Caps," Q. Appl. Math., Vol. 32, 1974.
- 136 Tvergaard, V. and Needleman, "On the Development of Localized Buckling Patterns," In Collapse: the Buckling of Structures in Theory and Practice, Edited by J. M. T. Thompson and G. W. Hunt, Cambridge University Press, pp. 1-17, 1983.
- 137 Mahrenholtz, O., Nath, Y. and Varma, K. K., "Nonlinear Dynamic Response of Doubly Curved Shallow Shells on Nonlinear Elastic Subgrade," Z. Angew. Math. Mech., Vol. 64, No. 4, 1987.
- 138 Reissner, E., "A Note on Imperfection Sensitivity of Thin Plates on a Nonlinear Elastic Foundation," In Instability of Continuous Systems, Proc. IUTAM Symp. held at Herrenalb, Edited by H. E. Leipholz, Springer, Berlin, pp. 15-18, 1969.
- 139 Reissner, E., "On Postbuckling Behavior and Imperfection Sensitivity of Thin Elastic Plates on a Nonlinear Elastic Foundation," In Studies in Applied Mathematics, Vol. XIIX, No. 1, pp. 45-57, 1970.
- 140 von Karman, T., "Festigkeitsprobleme in Maschinenbau," Encyklopadie der Mathematischen Wissenschaften, Vol. 4, 1910, pp. 348-351.
- 141 Jones, R. M., "Mechanics of Composite Materials," McGraw-Hill, 1975.
- 142 Vinson, J. R. and Sierakowski, R. L., "The Behavior of Structures Composed of Composite Materials," Martinus Nijhoff Publishers, 1986.
- 143 Sloan, J. G., "The Behavior of Rectangular Composite Material Plates Under Lateral and Hygrothermal Loads," MMAE Thesis, University of Delaware, 1979.

- 144 Cowper, G. R., "The Shear Coefficient in Timoshenko's Beam Theory," *Journal of Applied Mechanics*, March 1966, Vol. 33, pp. 335-340.
- 145 Reddy, J. N. , "Exact Solutions of Moderately Thick Laminated Shells," *Journal of Engineering Mechanics*, Vol. 110, No. 5, May 1984, pp. 794-809.
- 146 Reddy, J. N., "Energy and Variational Methods in Applied Mechanics", Wiley-Interscience Publication, 1984.
- 147 Warren, J. E., "Nonlinear Stability Analysis of Frame-type Structures with Random Geometric Imperfections Using a Total-Lagrangian Finite Element Formulation," Ph. D. Dissertation, Virginia Tech, Blacksburg, VA, January, 1997.
- 148 Crisfield, M. A., "Nonlinear Finite Element Analysis of Solids and Structures," John Wiley and Sons, England, Vol. I, 1991.
- 149 Fellipa, C. A., "Solution of Nonlinear Equations," *Finite Element Analysis for Engineering Design*, Reddy, J. N., Krishnamoorthy, C. S., and Seetharamu, K. N. (Eds.), Springer-Verlag, New York, Vol. 37, 1988, pp. 274-309.
- 150 Wriggers, P. and Simo, J. C., "A General Procedure for the Direct Computation of Turning and Bifurcation Points," *International Journal for Numerical Methods in Engineering*, Vol. 30, 1990, pp. 155-176.
- 151 Sorem, R. M. and Surana, K. S., "p-Version Plate and Curved Shell Element for Geometrically Non-linear Analysis," *International Journal for Numerical Methods in Engineering*, Vol. 33, 1992, pp. 1681-1701.
- 152 Bodner, S. R., "On the Conservativeness of Various Distributed Force Systems," *Journal of the Aeronautical Sciences*, Vol. 25, No. 1, 1958, pp. 132-133.
- 153 Dym, C. L., "Buckling and Postbuckling Behavior of Steep Compressible Arches," *International Journal of Solids and Structures* , Vol. 9, 1973, pp. 129-140.

- 154 Rao, K. P., "A Rectangular Laminated Anisotropic Shallow Thin Shell Finite Element," *Comput. Methods Appl. Mech. Eng.*, Vol. 15, 1978, pp. 13-33.
- 155 Timoshenko, S. and Woinowsky-Krieger, S., "Theory of Plates and Shells," 2nd Edition, McGraw-Hill, New York, 1959.
- 156 Rao, K. P. and Tripathy, B., "Composite Cylindrical Panels - Optimum Lay-up for Buckling by Ranking," *Computers and Structures*, Vol. 38, No. 2, 1991, pp. 217-225.
- 157 Kassegne, S. K., "Layerwise Theory for Discretely Stiffened Laminated Cylindrical Shells," Ph. D. Dissertation, Virginia Tech, Blacksburg, VA, December 1992.
- 158 Liao, C. L., "An Incremental Total Lagrangian Formulation for General Anisotropic Shell-Type Structures," Ph. D. Dissertation, Virginia Tech, Blacksburg, VA, June, 1987.
- 159 Palmerio, A. F., "On a Moderate Rotation Theory for Anisotropic Shells," Ph. D. Dissertation, Virginia Tech, Blacksburg, VA, September, 1987.

APPENDIX A
COEFFICIENTS OF ELEMENT STIFFNESS MATRIX AND FORCE
VECTOR FOR A RING ELEMENT

A.1 COEFFICIENTS OF LINEAR ELEMENT STIFFNESS MATRIX AND FORCE VECTOR

The components of the element stiffness matrix $[k^{(e)}]_L$, which were shown in equations (3.31) and (3.32), can be expressed as:

$$[k_{ij}^{11}] = \int_{y_A}^{y_B} b \left\{ A_{22} \frac{d\phi_i^{(1)}}{dy} \frac{d\phi_j^{(1)}}{dy} + \frac{K_s A_{44}}{R^2} \phi_i^{(1)} \phi_j^{(1)} \right\} dy \quad (A.1)$$

$$[k_{ij}^{12}] = \int_{y_A}^{y_B} b \left\{ \frac{A_{22}}{R} \frac{d\phi_i^{(1)}}{dy} \phi_j^{(2)} - \frac{K_s A_{44}}{R} \phi_i^{(1)} \frac{d\phi_j^{(2)}}{dy} \right\} dy \quad (A.2)$$

$$[k_{ij}^{13}] = \int_{y_A}^{y_B} b \left\{ B_{22} \frac{d\phi_i^{(1)}}{dy} \frac{d\phi_j^{(3)}}{dy} - \frac{K_s A_{44}}{R} \phi_i^{(1)} \phi_j^{(3)} \right\} dy \quad (A.3)$$

$$[k_{ij}^{21}] = [k_{ij}^{12}]^T \quad (A.4)$$

$$[k_{ij}^{22}] = \int_{y_A}^{y_B} b \left\{ \frac{A_{22}}{R^2} \phi_i^{(2)} \phi_j^{(2)} + K_s A_{44} \frac{d\phi_i^{(2)}}{dy} \frac{d\phi_j^{(2)}}{dy} \right\} dy \quad (A.5)$$

$$[k_{ij}^{23}] = \int_{y_A}^{y_B} b \left\{ \frac{B_{22}}{R} \phi_i^{(2)} \frac{d\phi_j^{(3)}}{dy} + K_s A_{44} \frac{d\phi_i^{(2)}}{dy} \phi_j^{(3)} \right\} dy \quad (A.6)$$

$$\left[k_{ij}^{31} \right] = \left[k_{ij}^{13} \right]^T \quad (\text{A.7})$$

$$\left[k_{ij}^{32} \right] = \left[k_{ij}^{23} \right]^T \quad (\text{A.8})$$

$$\left[k_{ij}^{33} \right] = \int_{y_A}^{y_B} b \left\{ D_{22} \frac{d\phi_i^{(3)}}{dy} \frac{d\phi_j^{(3)}}{dy} + K_s A_{44} \phi_i^{(3)} \phi_j^{(3)} \right\} dy \quad (\text{A.9})$$

The components of the element force vector $\{f^{(e)}\}$, which were shown in equations (3.31) and (3.32), also can be given by

$$F_i^{(1)} = Q_4^{(e)} - Q_1^{(e)} \quad (\text{A.10})$$

$$F_i^{(2)} = \int_{y_A}^{y_B} q_{\text{total}} \cdot \phi_i^{(2)} dy + Q_5^{(e)} - Q_2^{(e)} \quad (\text{A.11})$$

$$F_i^{(3)} = Q_6^{(e)} - Q_3^{(e)} \quad (\text{A.12})$$

where $Q_i^{(e)}$ denotes the nodal contributions of the boundary forces of the element, which were shown in equation (3.25).

A.2 COEFFICIENTS OF NONLINEAR ELEMENT STIFFNESS MATRIX

The components of the element stiffness matrix $\left[k^{(e)} \right]_{\text{NL}}$, which were shown in equation (3.33), can be obtained as follows:

$$\begin{aligned} [k_{ij}^{11}]_{NL} = & \int_{y_A}^{y_B} b \left\{ -\frac{A_{22}}{2R} \left(\frac{dw_0}{dy} - \frac{v_0}{R} \right) \frac{d\phi_i^{(1)}}{dy} \phi_j^{(1)} - \frac{A_{22}}{R} \left(\frac{dw_0}{dy} - \frac{v_0}{R} \right) \phi_i^{(1)} \frac{d\phi_j^{(1)}}{dy} \right. \\ & \left. + \frac{A_{22}}{2R^2} \left(\frac{dw_0}{dy} - \frac{v_0}{R} \right)^2 \phi_i^{(1)} \phi_j^{(1)} \right\} dy \end{aligned} \quad (A.13)$$

$$\begin{aligned} [k_{ij}^{12}]_{NL} = & \int_{y_A}^{y_B} b \left\{ \frac{A_{22}}{2} \left(\frac{dw_0}{dy} - \frac{v_0}{R} \right) \frac{d\phi_i^{(1)}}{dy} \frac{d\phi_j^{(2)}}{dy} - \frac{A_{22}}{R^2} \left(\frac{dw_0}{dy} - \frac{v_0}{R} \right) \phi_i^{(1)} \phi_j^{(2)} \right. \\ & \left. - \frac{A_{22}}{2R} \left(\frac{dw_0}{dy} - \frac{v_0}{R} \right)^2 \phi_i^{(1)} \frac{d\phi_j^{(2)}}{dy} \right\} dy \end{aligned} \quad (A.14)$$

$$[k_{ij}^{13}]_{NL} = \int_{y_A}^{y_B} b \left\{ -\frac{B_{22}}{R} \left(\frac{dw_0}{dy} - \frac{v_0}{R} \right) \phi_i^{(1)} \frac{d\phi_j^{(3)}}{dy} \right\} dy \quad (A.15)$$

$$\begin{aligned} [k_{ij}^{21}]_{NL} = & \int_{y_A}^{y_B} b \left\{ A_{22} \left(\frac{dw_0}{dy} - \frac{v_0}{R} \right) \frac{d\phi_i^{(2)}}{dy} \frac{d\phi_j^{(1)}}{dy} - \frac{A_{22}}{2R^2} \left(\frac{dw_0}{dy} - \frac{v_0}{R} \right) \phi_i^{(2)} \phi_j^{(1)} \right. \\ & \left. - \frac{A_{22}}{2R} \left(\frac{dw_0}{dy} - \frac{v_0}{R} \right)^2 \frac{d\phi_i^{(2)}}{dy} \phi_j^{(1)} \right\} dy \end{aligned} \quad (A.16)$$

$$\begin{aligned} [k_{ij}^{22}]_{NL} = & \int_{y_A}^{y_B} b \left\{ \frac{A_{22}}{2R} \left(\frac{dw_0}{dy} - \frac{v_0}{R} \right) \frac{d\phi_i^{(1)}}{dy} \frac{d\phi_j^{(2)}}{dy} + \frac{A_{22}}{R} \left(\frac{dw_0}{dy} - \frac{v_0}{R} \right) \frac{d\phi_i^{(2)}}{dy} \phi_j^{(2)} \right. \\ & \left. + \frac{A_{22}}{2} \left(\frac{dw_0}{dy} - \frac{v_0}{R} \right)^2 \frac{d\phi_i^{(2)}}{dy} \frac{d\phi_j^{(2)}}{dy} \right\} dy \end{aligned} \quad (A.17)$$

$$[k_{ij}^{23}]_{NL} = \int_{y_A}^{y_B} b \left\{ B_{22} \left(\frac{dw_0}{dy} - \frac{v_0}{R} \right) \frac{d\phi_i^{(2)}}{dy} \frac{d\phi_j^{(3)}}{dy} \right\} dy \quad (A.18)$$

$$[k_{ij}^{31}]_{NL} = \int_{y_A}^{y_B} b \left\{ -\frac{B_{22}}{2R} \left(\frac{dw_0}{dy} - \frac{v_0}{R} \right) \frac{d\phi_i^{(3)}}{dy} \phi_j^{(1)} \right\} dy \quad (A.19)$$

$$\left[k_{ij}^{32} \right]_{NL} = \int_{y_A}^{y_B} b \left\{ \frac{B_{22}}{2} \left(\frac{dw_0}{dy} - \frac{v_0}{R} \right) \frac{d\phi_i^{(3)}}{dy} \frac{d\phi_j^{(2)}}{dy} \right\} dy \quad (A.20)$$

$$\left[k_{ij}^{33} \right]_{NL} = 0 \quad (A.21)$$

APPENDIX B
COEFFICIENTS OF ELEMENT TANGENT STIFFNESS MATRIX
FOR A RING ELEMENT

The components of the tangent stiffness matrix for a nonlinear, perfect ring element are given below.

$$\begin{aligned}
 [(\mathbf{k}_T)_{ij}^{11}] &= [\mathbf{k}_{ij}^{11}]_L + [\mathbf{k}_{ij}^{11}]_{NL} \\
 &+ \int_{y_A}^{y_B} b \left\{ -\frac{A_{22}}{2R} \left(\frac{dw_0}{dy} - \frac{v_0}{R} \right) \frac{d\phi_i^{(1)}}{dy} \phi_j^{(1)} \right. \\
 &\left. + \left[\frac{A_{22}}{R^2} \left(\frac{dv_0}{dy} + \frac{w_0}{R} + \left(\frac{dw_0}{dy} - \frac{v_0}{R} \right)^2 \right) + \frac{B_{22}}{R^2} \left(\frac{d\psi_y}{dy} \right) \right] \phi_i^{(1)} \phi_j^{(1)} \right\} dy
 \end{aligned} \tag{B.1}$$

$$\begin{aligned}
 [(\mathbf{k}_T)_{ij}^{12}] &= [\mathbf{k}_{ij}^{12}]_L + [\mathbf{k}_{ij}^{12}]_{NL} \\
 &+ \int_{y_A}^{y_B} b \left\{ \frac{A_{22}}{2} \left(\frac{dw_0}{dy} - \frac{v_0}{R} \right) \frac{d\phi_i^{(1)}}{dy} \frac{d\phi_j^{(2)}}{dy} \right. \\
 &\left. - \left[\frac{A_{22}}{R} \left(\frac{dv_0}{dy} + \frac{w_0}{R} + \left(\frac{dw_0}{dy} - \frac{v_0}{R} \right)^2 \right) + \frac{B_{22}}{R} \left(\frac{d\psi_y}{dy} \right) \right] \phi_i^{(1)} \frac{d\phi_j^{(2)}}{dy} \right\} dy
 \end{aligned} \tag{B.2}$$

$$[(\mathbf{k}_T)_{ij}^{13}] = [\mathbf{k}_{ij}^{13}]_L + [\mathbf{k}_{ij}^{13}]_{NL} \tag{B.3}$$

$$\begin{aligned}
\left[(\mathbf{k}_T)_{ij}^{21} \right] &= \left[\mathbf{k}_{ij}^{21} \right]_L + \left[\mathbf{k}_{ij}^{21} \right]_{NL} \\
&+ \int_{y_A}^{y_B} \mathbf{b} \left\{ -\frac{A_{22}}{2R^2} \left(\frac{dw_0}{dy} - \frac{v_0}{R} \right) \phi_i^{(2)} \phi_j^{(1)} \right. \\
&- \left. \left[\frac{A_{22}}{R} \left(\frac{dv_0}{dy} + \frac{w_0}{R} + \left(\frac{dw_0}{dy} - \frac{v_0}{R} \right)^2 \right) + \frac{B_{22}}{R} \left(\frac{d\psi_y}{dy} \right) \right] \frac{d\phi_i^{(2)}}{dy} \phi_j^{(1)} \right\} dy
\end{aligned} \tag{B.4}$$

$$\begin{aligned}
\left[(\mathbf{k}_T)_{ij}^{22} \right] &= \left[\mathbf{k}_{ij}^{22} \right]_L + \left[\mathbf{k}_{ij}^{22} \right]_{NL} \\
&+ \int_{y_A}^{y_B} \mathbf{b} \left\{ \frac{A_{22}}{2R} \left(\frac{dw_0}{dy} - \frac{v_0}{R} \right) \phi_i^{(2)} \frac{d\phi_j^{(2)}}{dy} \right. \\
&+ \left. \left[A_{22} \left(\frac{dv_0}{dy} + \frac{w_0}{R} + \left(\frac{dw_0}{dy} - \frac{v_0}{R} \right)^2 \right) + B_{22} \left(\frac{d\psi_y}{dy} \right) \right] \frac{d\phi_i^{(2)}}{dy} \frac{d\phi_j^{(2)}}{dy} \right\} dy
\end{aligned} \tag{B.5}$$

$$\left[(\mathbf{k}_T)_{ij}^{23} \right] = \left[\mathbf{k}_{ij}^{23} \right]_L + \left[\mathbf{k}_{ij}^{23} \right]_{NL} \tag{B.6}$$

$$\begin{aligned}
\left[(\mathbf{k}_T)_{ij}^{31} \right] &= \left[\mathbf{k}_{ij}^{31} \right]_L + \left[\mathbf{k}_{ij}^{31} \right]_{NL} \\
&+ \int_{y_A}^{y_B} \mathbf{b} \left\{ -\frac{B_{22}}{2R} \left(\frac{dw_0}{dy} - \frac{v_0}{R} \right) \frac{d\phi_i^{(3)}}{dy} \phi_j^{(1)} \right\} dy
\end{aligned} \tag{B.7}$$

$$\left[(\mathbf{k}_T)_{ij}^{32} \right] = \left[\mathbf{k}_{ij}^{32} \right]_L + \left[\mathbf{k}_{ij}^{32} \right]_{NL} \tag{B.8}$$

$$+ \int_{y_A}^{y_B} \mathbf{b} \left\{ \frac{B_{22}}{2} \left(\frac{dw_0}{dy} - \frac{v_0}{R} \right) \frac{d\phi_i^{(3)}}{dy} \frac{d\phi_j^{(2)}}{dy} \right\} dy$$

$$\begin{aligned}
\left[(\mathbf{k}_T)_{ij}^{33} \right] &= \left[\mathbf{k}_{ij}^{33} \right]_L + \left[\mathbf{k}_{ij}^{33} \right]_{NL} \\
&= \left[\mathbf{k}_{ij}^{33} \right]_L
\end{aligned} \tag{B.9}$$

APPENDIX C
COEFFICIENTS OF ELEMENT STIFFNESS MATRIX AND FORCE
VECTOR FOR A CYLINDRICAL SHELL ELEMENT

C.1 COEFFICIENTS OF LINEAR ELEMENT STIFFNESS MATRIX AND FORCE VECTOR

The components of the element stiffness matrix $[k^{(e)}]_L$, which were shown in equations (4.22) and (4.23), can be expressed as:

$$[k_{ij}^{11}] = \int_{\Omega} \left\{ A_{11} \frac{\partial \phi_i^{(1)}}{\partial x} \frac{\partial \phi_j^{(1)}}{\partial x} + (A_{16} + C_0 B_{16}) \left(\frac{\partial \phi_i^{(1)}}{\partial x} \frac{\partial \phi_j^{(1)}}{\partial y} + \frac{\partial \phi_i^{(1)}}{\partial y} \frac{\partial \phi_j^{(1)}}{\partial x} \right) + (A_{66} + 2C_0 B_{66} + C_0^2 D_{66}) \frac{\partial \phi_i^{(1)}}{\partial y} \frac{\partial \phi_j^{(1)}}{\partial y} \right\} dA \quad (C.1)$$

$$[k_{ij}^{12}] = \int_{\Omega} \left\{ A_{12} \frac{\partial \phi_i^{(1)}}{\partial x} \frac{\partial \phi_j^{(2)}}{\partial y} + (A_{16} - C_0 B_{16}) \frac{\partial \phi_i^{(1)}}{\partial x} \frac{\partial \phi_j^{(2)}}{\partial x} + (A_{26} + C_0 B_{16}) \frac{\partial \phi_i^{(1)}}{\partial y} \frac{\partial \phi_j^{(2)}}{\partial y} + (A_{66} - C_0^2 D_{66}) \frac{\partial \phi_i^{(1)}}{\partial y} \frac{\partial \phi_j^{(2)}}{\partial x} \right\} dA \quad (C.2)$$

$$[k_{ij}^{13}] = \int_{\Omega} \left\{ \frac{A_{12}}{R} \frac{\partial \phi_i^{(1)}}{\partial x} \phi_j^{(3)} + \left(\frac{A_{26} + C_0 B_{26}}{R} \right) \frac{\partial \phi_i^{(1)}}{\partial y} \phi_j^{(3)} \right\} dA \quad (C.3)$$

$$[k_{ij}^{14}] = \int_{\Omega} \left\{ B_{11} \frac{\partial \phi_i^{(1)}}{\partial x} \frac{\partial \phi_j^{(4)}}{\partial x} + (B_{16} + C_0 D_{16}) \left(\frac{\partial \phi_i^{(1)}}{\partial x} \frac{\partial \phi_j^{(4)}}{\partial y} + \frac{\partial \phi_i^{(1)}}{\partial y} \frac{\partial \phi_j^{(4)}}{\partial x} \right) + (B_{66} + C_0 D_{66}) \frac{\partial \phi_i^{(1)}}{\partial y} \frac{\partial \phi_j^{(4)}}{\partial y} \right\} dA \quad (C.4)$$

$$\begin{aligned}
\left[k_{ij}^{15} \right] = \int_{\Omega} \left\{ B_{12} \frac{\partial \phi_i^{(1)}}{\partial x} \frac{\partial \phi_j^{(5)}}{\partial y} + B_{16} \frac{\partial \phi_i^{(1)}}{\partial x} \frac{\partial \phi_j^{(5)}}{\partial x} \right. \\
\left. + (B_{26} + C_0 D_{26}) \frac{\partial \phi_i^{(1)}}{\partial y} \frac{\partial \phi_j^{(5)}}{\partial y} + (B_{66} + C_0 D_{66}) \frac{\partial \phi_i^{(1)}}{\partial y} \frac{\partial \phi_j^{(5)}}{\partial x} \right\} dy
\end{aligned} \tag{C.5}$$

$$\left[k_{ij}^{21} \right] = \left[k_{ij}^{12} \right]^T \tag{C.6}$$

$$\begin{aligned}
\left[k_{ij}^{22} \right] = \int_{\Omega} \left\{ A_{22} \frac{\partial \phi_i^{(2)}}{\partial y} \frac{\partial \phi_j^{(2)}}{\partial y} + (A_{26} - C_0 B_{26}) \left(\frac{\partial \phi_i^{(2)}}{\partial y} \frac{\partial \phi_j^{(2)}}{\partial x} + \frac{\partial \phi_i^{(2)}}{\partial x} \frac{\partial \phi_j^{(2)}}{\partial y} \right) \right. \\
\left. + (A_{66} - 2C_0 B_{66} + C_0^2 D_{66}) \frac{\partial \phi_i^{(2)}}{\partial x} \frac{\partial \phi_j^{(2)}}{\partial x} + \frac{K_s A_{44}}{R^2} \phi_i^{(2)} \phi_j^{(2)} \right\} dA
\end{aligned} \tag{C.7}$$

$$\begin{aligned}
\left[k_{ij}^{23} \right] = \int_{\Omega} \left\{ \frac{A_{22}}{R} \frac{\partial \phi_i^{(2)}}{\partial y} \phi_j^{(3)} + \left(\frac{A_{26} - C_0 B_{26}}{R} \right) \frac{\partial \phi_i^{(2)}}{\partial x} \phi_j^{(3)} \right. \\
\left. - \frac{K_s A_{44}}{R} \phi_i^{(2)} \frac{\partial \phi_j^{(3)}}{\partial y} - \frac{K_s A_{45}}{R} \phi_i^{(2)} \frac{\partial \phi_j^{(3)}}{\partial x} \right\} dA
\end{aligned} \tag{C.8}$$

$$\begin{aligned}
\left[k_{ij}^{24} \right] = \int_{\Omega} \left\{ B_{12} \frac{\partial \phi_i^{(2)}}{\partial y} \frac{\partial \phi_j^{(4)}}{\partial x} + (B_{16} - C_0 D_{16}) \frac{\partial \phi_i^{(2)}}{\partial x} \frac{\partial \phi_j^{(4)}}{\partial x} + B_{26} \frac{\partial \phi_i^{(2)}}{\partial y} \frac{\partial \phi_j^{(4)}}{\partial y} \right. \\
\left. + (B_{66} - C_0 D_{66}) \frac{\partial \phi_i^{(2)}}{\partial x} \frac{\partial \phi_j^{(4)}}{\partial y} - \frac{K_s A_{45}}{R} \phi_i^{(2)} \phi_j^{(4)} \right\} dA
\end{aligned} \tag{C.9}$$

$$\begin{aligned}
\left[k_{ij}^{25} \right] = \int_{\Omega} \left\{ B_{22} \frac{\partial \phi_i^{(2)}}{\partial y} \frac{\partial \phi_j^{(5)}}{\partial y} + (B_{26} - C_0 D_{26}) \left(\frac{\partial \phi_i^{(2)}}{\partial x} \frac{\partial \phi_j^{(5)}}{\partial y} \right) \right. \\
\left. + B_{26} \left(\frac{\partial \phi_i^{(2)}}{\partial y} \frac{\partial \phi_j^{(5)}}{\partial x} \right) + (B_{66} - C_0 D_{66}) \frac{\partial \phi_i^{(2)}}{\partial x} \frac{\partial \phi_j^{(5)}}{\partial x} - \frac{K_s A_{44}}{R} \phi_i^{(2)} \phi_j^{(5)} \right\} dA
\end{aligned} \tag{C.10}$$

$$\left[k_{ij}^{31} \right] = \left[k_{ij}^{13} \right]^T \tag{C.11}$$

$$[k_{ij}^{32}] = [k_{ij}^{23}]^T \quad (C.12)$$

$$[k_{ij}^{33}] = \int_{\Omega} \left\{ \frac{A_{22}}{R^2} \phi_i^{(3)} \phi_j^{(3)} + K_S A_{44} \frac{\partial \phi_i^{(3)}}{\partial y} \frac{\partial \phi_j^{(3)}}{\partial y} + K_S A_{55} \frac{\partial \phi_i^{(3)}}{\partial x} \frac{\partial \phi_j^{(3)}}{\partial x} \right. \\ \left. + K_S A_{45} \left(\frac{\partial \phi_i^{(3)}}{\partial x} \frac{\partial \phi_j^{(3)}}{\partial y} + \frac{\partial \phi_i^{(3)}}{\partial y} \frac{\partial \phi_j^{(3)}}{\partial x} \right) \right\} dA \quad (C.13)$$

$$[k_{ij}^{34}] = \int_{\Omega} \left\{ \frac{B_{12}}{R} \phi_i^{(3)} \frac{\partial \phi_j^{(4)}}{\partial x} + \frac{B_{26}}{R} \phi_i^{(3)} \frac{\partial \phi_j^{(4)}}{\partial y} \right. \\ \left. + K_S A_{55} \frac{\partial \phi_i^{(3)}}{\partial x} \phi_j^{(4)} + K_S A_{45} \frac{\partial \phi_i^{(3)}}{\partial y} \phi_j^{(4)} \right\} dA \quad (C.14)$$

$$[k_{ij}^{35}] = \int_{\Omega} \left\{ \frac{B_{22}}{R} \phi_i^{(3)} \frac{\partial \phi_j^{(5)}}{\partial y} + \frac{B_{26}}{R} \phi_i^{(3)} \frac{\partial \phi_j^{(5)}}{\partial x} \right. \\ \left. + K_S A_{44} \frac{\partial \phi_i^{(3)}}{\partial y} \phi_j^{(5)} + K_S A_{45} \frac{\partial \phi_i^{(3)}}{\partial x} \phi_j^{(5)} \right\} dA \quad (C.15)$$

$$[k_{ij}^{41}] = [k_{ij}^{14}]^T \quad (C.16)$$

$$[k_{ij}^{42}] = [k_{ij}^{24}]^T \quad (C.17)$$

$$[k_{ij}^{43}] = [k_{ij}^{34}]^T \quad (C.18)$$

$$[k_{ij}^{44}] = \int_{\Omega} \left\{ D_{11} \frac{\partial \phi_i^{(4)}}{\partial x} \frac{\partial \phi_j^{(4)}}{\partial x} + D_{16} \left(\frac{\partial \phi_i^{(4)}}{\partial y} \frac{\partial \phi_j^{(4)}}{\partial x} + \frac{\partial \phi_i^{(4)}}{\partial x} \frac{\partial \phi_j^{(4)}}{\partial y} \right) \right. \\ \left. + D_{66} \frac{\partial \phi_i^{(4)}}{\partial y} \frac{\partial \phi_j^{(4)}}{\partial y} + K_S A_{55} \phi_i^{(4)} \phi_j^{(4)} \right\} dA \quad (C.19)$$

$$\begin{aligned} \left[k_{ij}^{45} \right] = \int_{\Omega} \left\{ D_{12} \frac{\partial \phi_i^{(4)}}{\partial x} \frac{\partial \phi_j^{(5)}}{\partial y} + D_{16} \frac{\partial \phi_i^{(4)}}{\partial x} \frac{\partial \phi_j^{(5)}}{\partial x} + D_{26} \frac{\partial \phi_i^{(4)}}{\partial y} \frac{\partial \phi_j^{(5)}}{\partial y} \right. \\ \left. + D_{66} \frac{\partial \phi_i^{(4)}}{\partial y} \frac{\partial \phi_j^{(5)}}{\partial x} + K_s A_{45} \phi_i^{(4)} \phi_j^{(5)} \right\} dA \end{aligned} \quad (C.20)$$

$$\left[k_{ij}^{51} \right] = \left[k_{ij}^{15} \right]^T \quad (C.21)$$

$$\left[k_{ij}^{52} \right] = \left[k_{ij}^{25} \right]^T \quad (C.22)$$

$$\left[k_{ij}^{53} \right] = \left[k_{ij}^{35} \right]^T \quad (C.23)$$

$$\left[k_{ij}^{54} \right] = \left[k_{ij}^{45} \right]^T \quad (C.24)$$

$$\begin{aligned} \left[k_{ij}^{55} \right] = \int_{\Omega} \left\{ D_{22} \frac{\partial \phi_i^{(5)}}{\partial y} \frac{\partial \phi_j^{(5)}}{\partial y} + D_{26} \left(\frac{\partial \phi_i^{(5)}}{\partial y} \frac{\partial \phi_j^{(5)}}{\partial x} + \frac{\partial \phi_i^{(5)}}{\partial x} \frac{\partial \phi_j^{(5)}}{\partial y} \right) \right. \\ \left. + D_{66} \frac{\partial \phi_i^{(5)}}{\partial x} \frac{\partial \phi_j^{(5)}}{\partial x} + K_s A_{44} \phi_i^{(5)} \phi_j^{(5)} \right\} dA \end{aligned} \quad (C.25)$$

The components of the element force vector $\{f^{(e)}\}$, which were shown in equations (4.22) and (4.23), can be also given by

$$F_i^{(1)} = Q_6^{(e)} - Q_1^{(e)} \quad (C.26)$$

$$F_i^{(2)} = Q_7^{(e)} - Q_2^{(e)} \quad (C.27)$$

$$F_i^{(3)} = \int_{\Omega} p_{\text{total}} \cdot \phi_i^{(3)} dA + Q_8^{(e)} - Q_3^{(e)} \quad (C.28)$$

$$F_i^{(4)} = Q_9^{(e)} - Q_4^{(e)} \quad (C.29)$$

$$F_i^{(5)} = Q_{10}^{(e)} - Q_5^{(e)} \quad (C.30)$$

where $Q_i^{(e)}$ denotes the nodal contributions of the boundary forces of the element, which were shown in equation (4.12).

C.2 COEFFICIENTS OF NONLINEAR ELEMENT STIFFNESS MATRIX

The components of the element stiffness matrix $[k^{(e)}]_{NL}$, which were shown in equation (4.26), can be written as follows:

$$[k_{ij}^{11}]_{NL} = 0 \quad (C.31)$$

$$[k_{ij}^{12}]_{NL} = \int_{\Omega} \left\{ -\frac{1}{2R} \left(\frac{\partial w_0}{\partial x} \right) \left[A_{16} \frac{\partial \phi_i^{(1)}}{\partial x} \phi_j^{(2)} + (A_{66} + C_0 B_{66}) \frac{\partial \phi_i^{(1)}}{\partial y} \phi_j^{(2)} \right] \right. \\ \left. - \frac{1}{2R} \left(\frac{\partial w_0}{\partial y} - \frac{v_0}{R} \right) \left[A_{12} \frac{\partial \phi_i^{(1)}}{\partial x} \phi_j^{(2)} + (A_{26} + C_0 B_{26}) \frac{\partial \phi_i^{(1)}}{\partial y} \phi_j^{(2)} \right] \right\} dA \quad (C.32)$$

$$[k_{ij}^{13}]_{NL} = \int_{\Omega} \left\{ \frac{1}{2} \left(\frac{\partial w_0}{\partial x} \right) \left[A_{11} \frac{\partial \phi_i^{(1)}}{\partial x} \frac{\partial \phi_j^{(3)}}{\partial x} + (A_{16} + C_0 B_{16}) \frac{\partial \phi_i^{(1)}}{\partial y} \frac{\partial \phi_j^{(3)}}{\partial x} \right] \right. \\ \left. + A_{16} \frac{\partial \phi_i^{(1)}}{\partial x} \frac{\partial \phi_j^{(3)}}{\partial y} + (A_{66} + C_0 B_{66}) \frac{\partial \phi_i^{(1)}}{\partial y} \frac{\partial \phi_j^{(3)}}{\partial y} \right] \\ \left. + \frac{1}{2} \left(\frac{\partial w_0}{\partial y} - \frac{v_0}{R} \right) \left[A_{12} \frac{\partial \phi_i^{(1)}}{\partial x} \frac{\partial \phi_j^{(3)}}{\partial y} + (A_{26} + C_0 B_{26}) \frac{\partial \phi_i^{(1)}}{\partial y} \frac{\partial \phi_j^{(3)}}{\partial y} \right] \right. \\ \left. + A_{16} \frac{\partial \phi_i^{(1)}}{\partial y} \frac{\partial \phi_j^{(3)}}{\partial x} + (A_{66} + C_0 B_{66}) \frac{\partial \phi_i^{(1)}}{\partial x} \frac{\partial \phi_j^{(3)}}{\partial x} \right] \right\} dA \quad (C.33)$$

$$\left[\mathbf{k}_{ij}^{14} \right]_{\text{NL}} = 0 \quad (\text{C.34})$$

$$\left[\mathbf{k}_{ij}^{15} \right]_{\text{NL}} = 0 \quad (\text{C.35})$$

$$\begin{aligned} \left[\mathbf{k}_{ij}^{21} \right]_{\text{NL}} = \int_{\Omega} \left\{ -\frac{1}{R} \left(\frac{\partial w_0}{\partial x} \right) \left[A_{16} \phi_i^{(2)} \frac{\partial \phi_j^{(1)}}{\partial x} + (A_{66} + C_0 B_{66}) \phi_i^{(2)} \frac{\partial \phi_j^{(1)}}{\partial y} \right] \right. \\ \left. - \frac{1}{R} \left(\frac{\partial w_0}{\partial y} - \frac{v_0}{R} \right) \left[A_{12} \phi_i^{(2)} \frac{\partial \phi_j^{(1)}}{\partial x} + (A_{26} + C_0 B_{26}) \phi_i^{(2)} \frac{\partial \phi_j^{(1)}}{\partial y} \right] \right\} dA \end{aligned} \quad (\text{C.36})$$

$$\begin{aligned} \left[\mathbf{k}_{ij}^{22} \right]_{\text{NL}} = \int_{\Omega} \left\{ \frac{1}{2R^2} \left[A_{66} \left(\frac{\partial w_0}{\partial x} \right)^2 + 2A_{26} \left(\frac{\partial w_0}{\partial x} \right) \left(\frac{\partial w_0}{\partial y} - \frac{v_0}{R} \right) \right. \right. \\ \left. \left. + A_{22} \left(\frac{\partial w_0}{\partial y} - \frac{v_0}{R} \right)^2 \right] \phi_i^{(2)} \phi_j^{(2)} \right. \\ \left. - \left[\frac{A_{26}}{R} \left(\frac{\partial w_0}{\partial x} \right) + \frac{A_{22}}{R} \left(\frac{\partial w_0}{\partial y} - \frac{v_0}{R} \right) \right] \left(\phi_i^{(2)} \frac{\partial \phi_j^{(2)}}{\partial y} + \frac{1}{2} \frac{\partial \phi_i^{(2)}}{\partial y} \phi_j^{(2)} \right) \right. \\ \left. - \left[\left(\frac{A_{26} - C_0 B_{26}}{R} \right) \left(\frac{\partial w_0}{\partial y} - \frac{v_0}{R} \right) + \left(\frac{A_{66} - C_0 B_{66}}{R} \right) \left(\frac{\partial w_0}{\partial x} \right) \right] \right. \\ \left. \left(\phi_i^{(2)} \frac{\partial \phi_j^{(2)}}{\partial x} + \frac{1}{2} \frac{\partial \phi_i^{(2)}}{\partial x} \phi_j^{(2)} \right) \right\} dA \end{aligned} \quad (\text{C.37})$$

$$\begin{aligned} \left[\mathbf{k}_{ij}^{23} \right]_{\text{NL}} = \int_{\Omega} \left\{ \frac{1}{2} \left(\frac{\partial w_0}{\partial x} \right) \left[A_{12} \frac{\partial \phi_i^{(2)}}{\partial y} \frac{\partial \phi_j^{(3)}}{\partial x} + (A_{16} - C_0 B_{16}) \frac{\partial \phi_i^{(2)}}{\partial x} \frac{\partial \phi_j^{(3)}}{\partial x} \right. \right. \\ \left. \left. + A_{26} \frac{\partial \phi_i^{(2)}}{\partial y} \frac{\partial \phi_j^{(3)}}{\partial y} + (A_{66} - C_0 B_{66}) \frac{\partial \phi_i^{(2)}}{\partial x} \frac{\partial \phi_j^{(3)}}{\partial y} \right] \right. \\ \left. + \frac{1}{2} \left(\frac{\partial w_0}{\partial y} - \frac{v_0}{R} \right) \left[A_{22} \frac{\partial \phi_i^{(2)}}{\partial y} \frac{\partial \phi_j^{(3)}}{\partial y} + (A_{26} - C_0 B_{26}) \frac{\partial \phi_i^{(2)}}{\partial x} \frac{\partial \phi_j^{(3)}}{\partial y} \right. \right. \\ \left. \left. + A_{26} \frac{\partial \phi_i^{(2)}}{\partial y} \frac{\partial \phi_j^{(3)}}{\partial x} + (A_{66} - C_0 B_{66}) \frac{\partial \phi_i^{(2)}}{\partial x} \frac{\partial \phi_j^{(3)}}{\partial x} \right] \right. \\ \left. - \frac{1}{2R} \left[A_{66} \left(\frac{\partial w_0}{\partial x} \right)^2 + 2A_{26} \left(\frac{\partial w_0}{\partial x} \right) \left(\frac{\partial w_0}{\partial y} - \frac{v_0}{R} \right) \right. \right. \end{aligned} \quad (\text{C.38})$$

$$\begin{aligned}
& + A_{22} \left(\frac{\partial w_0}{\partial y} - \frac{v_0}{R} \right)^2 \phi_i^{(2)} \frac{\partial \phi_j^{(3)}}{\partial y} \\
& - \frac{1}{2R} \left[A_{16} \left(\frac{\partial w_0}{\partial x} \right)^2 + (A_{66} + A_{12}) \left(\frac{\partial w_0}{\partial x} \right) \left(\frac{\partial w_0}{\partial y} - \frac{v_0}{R} \right) \right. \\
& + A_{26} \left(\frac{\partial w_0}{\partial y} - \frac{v_0}{R} \right)^2 \left. \right] \phi_i^{(2)} \frac{\partial \phi_j^{(3)}}{\partial x} \\
& - \frac{1}{R^2} \left[A_{26} \left(\frac{\partial w_0}{\partial x} \right) + A_{22} \left(\frac{\partial w_0}{\partial y} - \frac{v_0}{R} \right) \right] \phi_i^{(2)} \phi_j^{(3)} \} dA
\end{aligned} \tag{C.38}$$

$$\begin{aligned}
\left[k_{ij}^{24} \right]_{NL} = \int_{\Omega} \left\{ -\frac{1}{R} \left(\frac{\partial w_0}{\partial x} \right) \left[B_{16} \phi_i^{(2)} \frac{\partial \phi_j^{(4)}}{\partial x} + B_{66} \phi_i^{(2)} \frac{\partial \phi_j^{(4)}}{\partial y} \right] \right. \\
\left. - \frac{1}{R} \left(\frac{\partial w_0}{\partial y} - \frac{v_0}{R} \right) \left[B_{12} \phi_i^{(2)} \frac{\partial \phi_j^{(4)}}{\partial x} + B_{26} \phi_i^{(2)} \frac{\partial \phi_j^{(4)}}{\partial y} \right] \right\} dA
\end{aligned} \tag{C.39}$$

$$\begin{aligned}
\left[k_{ij}^{25} \right]_{NL} = \int_{\Omega} \left\{ -\frac{1}{R} \left(\frac{\partial w_0}{\partial x} \right) \left[B_{26} \phi_i^{(2)} \frac{\partial \phi_j^{(5)}}{\partial y} + B_{66} \phi_i^{(2)} \frac{\partial \phi_j^{(5)}}{\partial x} \right] \right. \\
\left. - \frac{1}{R} \left(\frac{\partial w_0}{\partial y} - \frac{v_0}{R} \right) \left[B_{22} \phi_i^{(2)} \frac{\partial \phi_j^{(4)}}{\partial y} + B_{26} \phi_i^{(2)} \frac{\partial \phi_j^{(4)}}{\partial x} \right] \right\} dA
\end{aligned} \tag{C.40}$$

$$\begin{aligned}
\left[k_{ij}^{31} \right]_{NL} = \int_{\Omega} \left\{ \left(\frac{\partial w_0}{\partial x} \right) \left[A_{11} \frac{\partial \phi_i^{(3)}}{\partial x} \frac{\partial \phi_j^{(1)}}{\partial x} + (A_{16} + C_0 B_{16}) \frac{\partial \phi_i^{(3)}}{\partial x} \frac{\partial \phi_j^{(1)}}{\partial y} \right. \right. \\
+ A_{16} \frac{\partial \phi_i^{(3)}}{\partial y} \frac{\partial \phi_j^{(1)}}{\partial x} + (A_{66} + C_0 B_{66}) \frac{\partial \phi_i^{(3)}}{\partial y} \frac{\partial \phi_j^{(1)}}{\partial y} \left. \right] \\
+ \left(\frac{\partial w_0}{\partial y} - \frac{v_0}{R} \right) \left[A_{12} \frac{\partial \phi_i^{(3)}}{\partial y} \frac{\partial \phi_j^{(1)}}{\partial x} + (A_{26} + C_0 B_{26}) \frac{\partial \phi_i^{(3)}}{\partial y} \frac{\partial \phi_j^{(1)}}{\partial y} \right. \\
\left. + A_{16} \frac{\partial \phi_i^{(3)}}{\partial x} \frac{\partial \phi_j^{(1)}}{\partial x} + (A_{66} + C_0 B_{66}) \frac{\partial \phi_i^{(3)}}{\partial x} \frac{\partial \phi_j^{(1)}}{\partial y} \right] \} dA
\end{aligned} \tag{C.41}$$

$$\left[k_{ij}^{32} \right]_{NL} = \int_{\Omega} \left\{ \left(\frac{\partial w_0}{\partial x} \right) \left[A_{12} \frac{\partial \phi_i^{(3)}}{\partial x} \frac{\partial \phi_j^{(2)}}{\partial y} + (A_{16} - C_0 B_{16}) \frac{\partial \phi_i^{(3)}}{\partial x} \frac{\partial \phi_j^{(2)}}{\partial x} \right. \right.$$

$$\begin{aligned}
& + A_{26} \frac{\partial \phi_i^{(3)}}{\partial y} \frac{\partial \phi_j^{(2)}}{\partial y} + (A_{66} - C_0 B_{66}) \frac{\partial \phi_i^{(3)}}{\partial y} \frac{\partial \phi_j^{(2)}}{\partial x}] \\
& + \left(\frac{\partial w_0}{\partial y} - \frac{v_0}{R} \right) \left[A_{22} \frac{\partial \phi_i^{(3)}}{\partial y} \frac{\partial \phi_j^{(2)}}{\partial y} + (A_{26} - C_0 B_{26}) \frac{\partial \phi_i^{(3)}}{\partial y} \frac{\partial \phi_j^{(2)}}{\partial x} \right. \\
& + A_{26} \frac{\partial \phi_i^{(3)}}{\partial x} \frac{\partial \phi_j^{(2)}}{\partial y} + (A_{66} - C_0 B_{66}) \frac{\partial \phi_i^{(3)}}{\partial x} \frac{\partial \phi_j^{(2)}}{\partial x}] \\
& - \frac{1}{2R} \left[A_{66} \left(\frac{\partial w_0}{\partial x} \right)^2 + 2A_{26} \left(\frac{\partial w_0}{\partial x} \right) \left(\frac{\partial w_0}{\partial y} - \frac{v_0}{R} \right) \right. \\
& + A_{22} \left(\frac{\partial w_0}{\partial y} - \frac{v_0}{R} \right)^2] \frac{\partial \phi_i^{(3)}}{\partial y} \phi_j^{(2)} \\
& - \frac{1}{2R} \left[A_{16} \left(\frac{\partial w_0}{\partial x} \right)^2 + (A_{66} + A_{12}) \left(\frac{\partial w_0}{\partial x} \right) \left(\frac{\partial w_0}{\partial y} - \frac{v_0}{R} \right) \right. \\
& + A_{26} \left(\frac{\partial w_0}{\partial y} - \frac{v_0}{R} \right)^2] \frac{\partial \phi_i^{(3)}}{\partial x} \phi_j^{(2)} \\
& - \frac{1}{2R^2} \left[A_{26} \left(\frac{\partial w_0}{\partial x} \right) + A_{22} \left(\frac{\partial w_0}{\partial y} - \frac{v_0}{R} \right) \right] \phi_i^{(3)} \phi_j^{(2)} \} dA
\end{aligned} \tag{C.42}$$

$$\begin{aligned}
\left[k_{ij}^{33} \right]_{NL} & = \int_{\Omega} \left\{ \left[\frac{A_{11}}{2} \left(\frac{\partial w_0}{\partial x} \right)^2 + A_{16} \left(\frac{\partial w_0}{\partial x} \right) \left(\frac{\partial w_0}{\partial y} - \frac{v_0}{R} \right) \right. \right. \\
& + \frac{A_{66}}{2} \left(\frac{\partial w_0}{\partial y} - \frac{v_0}{R} \right)^2] \frac{\partial \phi_i^{(3)}}{\partial x} \frac{\partial \phi_j^{(3)}}{\partial x} \\
& + \left[\frac{A_{16}}{2} \left(\frac{\partial w_0}{\partial x} \right)^2 + \left(\frac{A_{12}}{2} + \frac{A_{66}}{2} \right) \left(\frac{\partial w_0}{\partial x} \right) \left(\frac{\partial w_0}{\partial y} - \frac{v_0}{R} \right) \right. \\
& + \frac{A_{26}}{2} \left(\frac{\partial w_0}{\partial y} - \frac{v_0}{R} \right)^2] \left(\frac{\partial \phi_i^{(3)}}{\partial x} \frac{\partial \phi_j^{(3)}}{\partial y} + \frac{\partial \phi_i^{(3)}}{\partial y} \frac{\partial \phi_j^{(3)}}{\partial x} \right) \\
& + \left[\frac{A_{66}}{2} \left(\frac{\partial w_0}{\partial x} \right)^2 + A_{26} \left(\frac{\partial w_0}{\partial x} \right) \left(\frac{\partial w_0}{\partial y} - \frac{v_0}{R} \right) \right. \\
& + \frac{A_{22}}{2} \left(\frac{\partial w_0}{\partial y} - \frac{v_0}{R} \right)^2] \frac{\partial \phi_i^{(3)}}{\partial y} \frac{\partial \phi_j^{(3)}}{\partial y} \\
& + \left[\frac{A_{26}}{R} \left(\frac{\partial w_0}{\partial x} \right) + \frac{A_{22}}{R} \left(\frac{\partial w_0}{\partial y} - \frac{v_0}{R} \right) \right] \left(\frac{\partial \phi_i^{(3)}}{\partial y} \phi_j^{(3)} + \frac{1}{2} \phi_i^{(3)} \frac{\partial \phi_j^{(3)}}{\partial y} \right)
\end{aligned} \tag{C.43}$$

$$\begin{aligned}
& + \left[\left(\frac{A_{26}}{R} \right) \left(\frac{\partial w_0}{\partial y} - \frac{v_0}{R} \right) + \left(\frac{A_{12}}{R} \right) \left(\frac{\partial w_0}{\partial x} \right) \right] \\
& \left(\frac{\partial \phi_i^{(3)}}{\partial x} \phi_j^{(3)} + \frac{1}{2} \phi_i^{(3)} \frac{\partial \phi_j^{(3)}}{\partial x} \right) \} dA
\end{aligned} \tag{C.43}$$

$$\begin{aligned}
\left[k_{ij}^{34} \right]_{NL} &= \int_{\Omega} \left\{ \left(\frac{\partial w_0}{\partial x} \right) \left[B_{11} \frac{\partial \phi_i^{(3)}}{\partial x} \frac{\partial \phi_j^{(4)}}{\partial x} + B_{16} \frac{\partial \phi_i^{(3)}}{\partial x} \frac{\partial \phi_j^{(4)}}{\partial y} \right. \right. \\
& + B_{16} \frac{\partial \phi_i^{(3)}}{\partial y} \frac{\partial \phi_j^{(4)}}{\partial x} + B_{66} \frac{\partial \phi_i^{(3)}}{\partial y} \frac{\partial \phi_j^{(4)}}{\partial y} \left. \right] \\
& + \left(\frac{\partial w_0}{\partial y} - \frac{v_0}{R} \right) \left[B_{12} \frac{\partial \phi_i^{(3)}}{\partial y} \frac{\partial \phi_j^{(4)}}{\partial x} + B_{26} \frac{\partial \phi_i^{(3)}}{\partial y} \frac{\partial \phi_j^{(4)}}{\partial y} \right. \\
& \left. \left. + B_{16} \frac{\partial \phi_i^{(3)}}{\partial x} \frac{\partial \phi_j^{(4)}}{\partial x} + B_{66} \frac{\partial \phi_i^{(3)}}{\partial x} \frac{\partial \phi_j^{(4)}}{\partial y} \right] \right\} dA
\end{aligned} \tag{C.44}$$

$$\begin{aligned}
\left[k_{ij}^{35} \right]_{NL} &= \int_{\Omega} \left\{ \left(\frac{\partial w_0}{\partial x} \right) \left[B_{12} \frac{\partial \phi_i^{(3)}}{\partial x} \frac{\partial \phi_j^{(5)}}{\partial y} + B_{16} \frac{\partial \phi_i^{(3)}}{\partial x} \frac{\partial \phi_j^{(5)}}{\partial x} \right. \right. \\
& + B_{26} \frac{\partial \phi_i^{(3)}}{\partial y} \frac{\partial \phi_j^{(5)}}{\partial y} + B_{66} \frac{\partial \phi_i^{(3)}}{\partial y} \frac{\partial \phi_j^{(5)}}{\partial x} \left. \right] \\
& + \left(\frac{\partial w_0}{\partial y} - \frac{v_0}{R} \right) \left[B_{22} \frac{\partial \phi_i^{(3)}}{\partial y} \frac{\partial \phi_j^{(5)}}{\partial y} + B_{26} \frac{\partial \phi_i^{(3)}}{\partial y} \frac{\partial \phi_j^{(5)}}{\partial x} \right. \\
& \left. \left. + B_{26} \frac{\partial \phi_i^{(3)}}{\partial x} \frac{\partial \phi_j^{(5)}}{\partial y} + B_{66} \frac{\partial \phi_i^{(3)}}{\partial x} \frac{\partial \phi_j^{(5)}}{\partial x} \right] \right\} dA
\end{aligned} \tag{C.45}$$

$$\left[k_{ij}^{41} \right]_{NL} = 0 \tag{C.46}$$

$$\begin{aligned}
\left[k_{ij}^{42} \right]_{NL} &= \int_{\Omega} \left\{ -\frac{1}{2R} \left(\frac{\partial w_0}{\partial x} \right) \left[B_{16} \frac{\partial \phi_i^{(4)}}{\partial x} \phi_j^{(2)} + B_{66} \frac{\partial \phi_i^{(4)}}{\partial y} \phi_j^{(2)} \right] \right. \\
& \left. - \frac{1}{2R} \left(\frac{\partial w_0}{\partial y} - \frac{v_0}{R} \right) \left[B_{12} \frac{\partial \phi_i^{(4)}}{\partial x} \phi_j^{(2)} + B_{26} \frac{\partial \phi_i^{(4)}}{\partial y} \phi_j^{(2)} \right] \right\} dA
\end{aligned} \tag{C.47}$$

$$\begin{aligned}
\left[k_{ij}^{43} \right]_{NL} = & \int_{\Omega} \left\{ \frac{1}{2} \left(\frac{\partial w_0}{\partial x} \right) \left[B_{11} \frac{\partial \phi_i^{(4)}}{\partial x} \frac{\partial \phi_j^{(3)}}{\partial x} + B_{16} \frac{\partial \phi_i^{(4)}}{\partial y} \frac{\partial \phi_j^{(3)}}{\partial x} \right. \right. \\
& + B_{16} \frac{\partial \phi_i^{(4)}}{\partial x} \frac{\partial \phi_j^{(3)}}{\partial y} + B_{66} \frac{\partial \phi_i^{(4)}}{\partial y} \frac{\partial \phi_j^{(3)}}{\partial y} \left. \right] \\
& + \frac{1}{2} \left(\frac{\partial w_0}{\partial y} - \frac{v_0}{R} \right) \left[B_{12} \frac{\partial \phi_i^{(4)}}{\partial x} \frac{\partial \phi_j^{(3)}}{\partial y} + B_{26} \frac{\partial \phi_i^{(4)}}{\partial y} \frac{\partial \phi_j^{(3)}}{\partial y} \right. \\
& \left. \left. + B_{16} \frac{\partial \phi_i^{(4)}}{\partial x} \frac{\partial \phi_j^{(3)}}{\partial x} + B_{66} \frac{\partial \phi_i^{(4)}}{\partial y} \frac{\partial \phi_j^{(3)}}{\partial x} \right] \right\} dA
\end{aligned} \tag{C.48}$$

$$\left[k_{ij}^{44} \right]_{NL} = 0 \tag{C.49}$$

$$\left[k_{ij}^{45} \right]_{NL} = 0 \tag{C.50}$$

$$\left[k_{ij}^{51} \right]_{NL} = 0 \tag{C.51}$$

$$\begin{aligned}
\left[k_{ij}^{52} \right]_{NL} = & \int_{\Omega} \left\{ -\frac{1}{2R} \left(\frac{\partial w_0}{\partial x} \right) \left[B_{26} \frac{\partial \phi_i^{(5)}}{\partial y} \phi_j^{(2)} + B_{66} \frac{\partial \phi_i^{(5)}}{\partial x} \phi_j^{(2)} \right] \right. \\
& \left. - \frac{1}{2R} \left(\frac{\partial w_0}{\partial y} - \frac{v_0}{R} \right) \left[B_{22} \frac{\partial \phi_i^{(5)}}{\partial y} \phi_j^{(2)} + B_{26} \frac{\partial \phi_i^{(5)}}{\partial x} \phi_j^{(2)} \right] \right\} dA
\end{aligned} \tag{C.52}$$

$$\begin{aligned}
\left[k_{ij}^{53} \right]_{NL} = & \int_{\Omega} \left\{ \frac{1}{2} \left(\frac{\partial w_0}{\partial x} \right) \left[B_{12} \frac{\partial \phi_i^{(5)}}{\partial y} \frac{\partial \phi_j^{(3)}}{\partial x} + B_{16} \frac{\partial \phi_i^{(5)}}{\partial x} \frac{\partial \phi_j^{(3)}}{\partial x} \right. \right. \\
& + B_{26} \frac{\partial \phi_i^{(5)}}{\partial y} \frac{\partial \phi_j^{(3)}}{\partial y} + B_{66} \frac{\partial \phi_i^{(5)}}{\partial x} \frac{\partial \phi_j^{(3)}}{\partial y} \left. \right] \\
& + \frac{1}{2} \left(\frac{\partial w_0}{\partial y} - \frac{v_0}{R} \right) \left[B_{22} \frac{\partial \phi_i^{(5)}}{\partial y} \frac{\partial \phi_j^{(3)}}{\partial y} + B_{26} \frac{\partial \phi_i^{(5)}}{\partial x} \frac{\partial \phi_j^{(3)}}{\partial y} \right. \\
& \left. \left. + B_{26} \frac{\partial \phi_i^{(5)}}{\partial y} \frac{\partial \phi_j^{(3)}}{\partial x} + B_{66} \frac{\partial \phi_i^{(5)}}{\partial x} \frac{\partial \phi_j^{(3)}}{\partial x} \right] \right\}
\end{aligned} \tag{C.53}$$

$$\left[\mathbf{k}_{ij}^{54} \right]_{\text{NL}} = 0 \quad (\text{C.54})$$

$$\left[\mathbf{k}_{ij}^{55} \right]_{\text{NL}} = 0 \quad (\text{C.55})$$

APPENDIX D
COEFFICIENTS OF ELEMENT TANGENT STIFFNESS MATRIX
FOR A CYLINDRICAL SHELL ELEMENT

The components of the tangent stiffness matrix for a nonlinear, perfect, cylindrical shell element are given below.

$$\left[(k_T)_{ij}^{11} \right] = \left[k_{ij}^{11} \right]_L + \left[k_{ij}^{11} \right]_{NL} \quad (D.1)$$

$$\left[(k_T)_{ij}^{12} \right] = \left[k_{ij}^{12} \right]_L + 2 \left[k_{ij}^{12} \right]_{NL} \quad (D.2)$$

$$\left[(k_T)_{ij}^{13} \right] = \left[k_{ij}^{13} \right]_L + 2 \left[k_{ij}^{13} \right]_{NL} \quad (D.3)$$

$$\left[(k_T)_{ij}^{14} \right] = \left[k_{ij}^{14} \right]_L + \left[k_{ij}^{14} \right]_{NL} \quad (D.4)$$

$$\left[(k_T)_{ij}^{15} \right] = \left[k_{ij}^{15} \right]_L + \left[k_{ij}^{15} \right]_{NL} \quad (D.5)$$

$$\left[(k_T)_{ij}^{21} \right] = \left[k_{ij}^{21} \right]_L + \left[k_{ij}^{21} \right]_{NL} \quad (D.6)$$

$$\begin{aligned} \left[(k_T)_{ij}^{22} \right] &= \left[k_{ij}^{22} \right]_L + \left[k_{ij}^{22} \right]_{NL} \\ &+ \int_{\Omega} \left\{ - \left[\frac{A_{26}}{R} \left(\frac{\partial w_0}{\partial x} \right) + \frac{A_{22}}{R} \left(\frac{\partial w_0}{\partial y} - \frac{v_0}{R} \right) \right] \left(\frac{1}{2} \frac{\partial \phi_i^{(2)}}{\partial y} \phi_j^{(2)} \right) \right. \\ &\left. - \left[\left(\frac{A_{26} - C_0 B_{26}}{R} \right) \left(\frac{\partial w_0}{\partial y} - \frac{v_0}{R} \right) + \left(\frac{A_{66} - C_0 B_{66}}{R} \right) \left(\frac{\partial w_0}{\partial x} \right) \right] \left(\frac{1}{2} \frac{\partial \phi_i^{(2)}}{\partial x} \phi_j^{(2)} \right) \right\} \end{aligned}$$

$$\begin{aligned}
& + \frac{1}{R^2} \{ A_{12} [\frac{\partial u_0}{\partial x} + \frac{1}{2} (\frac{\partial w_0}{\partial x})^2] + A_{22} [\frac{\partial v_0}{\partial y} + \frac{w_0}{R} + (\frac{\partial w_0}{\partial y} - \frac{v_0}{R})^2] \\
& \quad + A_{26} [\frac{\partial u_0}{\partial y} + \frac{\partial v_0}{\partial x} + 2 (\frac{\partial w_0}{\partial x}) (\frac{\partial w_0}{\partial y} - \frac{v_0}{R})] + \frac{A_{66}}{2} (\frac{\partial w_0}{\partial x})^2 \\
& \quad + B_{12} (\frac{\partial \psi_x}{\partial x}) + B_{22} (\frac{\partial \psi_y}{\partial y}) + B_{26} [\frac{\partial \psi_x}{\partial y} + \frac{\partial \psi_y}{\partial x} \\
& \quad - C_0 (\frac{\partial v_0}{\partial x} - \frac{\partial u_0}{\partial y})] \} \phi_i^{(2)} \phi_j^{(2)} \} dA
\end{aligned} \tag{D.7}$$

$$\begin{aligned}
\left[(k_T)_{ij}^{23} \right] &= \left[k_{ij}^{23} \right]_L + \left[k_{ij}^{23} \right]_{NL} \\
& + \int_{\Omega} \left\{ \frac{1}{2} \left(\frac{\partial w_0}{\partial x} \right) \left[A_{12} \frac{\partial \phi_i^{(2)}}{\partial y} \frac{\partial \phi_j^{(3)}}{\partial x} + (A_{16} - C_0 B_{16}) \frac{\partial \phi_i^{(2)}}{\partial x} \frac{\partial \phi_j^{(3)}}{\partial x} \right. \right. \\
& + A_{26} \frac{\partial \phi_i^{(2)}}{\partial y} \frac{\partial \phi_j^{(3)}}{\partial y} + (A_{66} - C_0 B_{66}) \frac{\partial \phi_i^{(2)}}{\partial x} \frac{\partial \phi_j^{(3)}}{\partial y} \left. \right] \\
& + \frac{1}{2} \left(\frac{\partial w_0}{\partial y} - \frac{v_0}{R} \right) \left[A_{22} \frac{\partial \phi_i^{(2)}}{\partial y} \frac{\partial \phi_j^{(3)}}{\partial y} + (A_{26} - C_0 B_{26}) \frac{\partial \phi_i^{(2)}}{\partial x} \frac{\partial \phi_j^{(3)}}{\partial y} \right. \\
& + A_{26} \frac{\partial \phi_i^{(2)}}{\partial y} \frac{\partial \phi_j^{(3)}}{\partial x} + (A_{66} - C_0 B_{66}) \frac{\partial \phi_i^{(2)}}{\partial x} \frac{\partial \phi_j^{(3)}}{\partial x} \left. \right] \\
& - \frac{1}{R} \left\{ A_{16} \left[\frac{\partial u_0}{\partial x} + \left(\frac{\partial w_0}{\partial x} \right)^2 \right] + A_{26} \left[\frac{\partial v_0}{\partial y} + \frac{w_0}{R} + \left(\frac{\partial w_0}{\partial y} - \frac{v_0}{R} \right)^2 \right] \right. \\
& \quad + A_{66} \left[\frac{\partial u_0}{\partial y} + \frac{\partial v_0}{\partial x} + \left(\frac{\partial w_0}{\partial x} \right) \left(\frac{\partial w_0}{\partial y} - \frac{v_0}{R} \right) \right] \\
& \quad + \left(\frac{A_{12} + A_{66}}{2} \right) \left(\frac{\partial w_0}{\partial x} \right) \left(\frac{\partial w_0}{\partial y} - \frac{v_0}{R} \right) \\
& \quad + B_{16} \left(\frac{\partial \psi_x}{\partial x} \right) + B_{26} \left(\frac{\partial \psi_y}{\partial y} \right) + B_{66} \left[\frac{\partial \psi_x}{\partial y} + \frac{\partial \psi_y}{\partial x} \right. \\
& \quad \left. - C_0 \left(\frac{\partial v_0}{\partial x} - \frac{\partial u_0}{\partial y} \right) \right] \} \phi_i^{(2)} \frac{\partial \phi_j^{(3)}}{\partial x} \\
& - \frac{1}{R} \left\{ A_{12} \left[\frac{\partial u_0}{\partial x} + \frac{1}{2} \left(\frac{\partial w_0}{\partial x} \right)^2 \right] + \frac{A_{66}}{2} \left(\frac{\partial w_0}{\partial x} \right)^2 \right. \\
& \quad + A_{22} \left[\frac{\partial v_0}{\partial y} + \frac{w_0}{R} + \left(\frac{\partial w_0}{\partial y} - \frac{v_0}{R} \right)^2 \right]
\end{aligned} \tag{D.8}$$

$$\begin{aligned}
& + A_{26} \left[\frac{\partial u_0}{\partial y} + \frac{\partial v_0}{\partial x} + 2 \left(\frac{\partial w_0}{\partial x} \right) \left(\frac{\partial w_0}{\partial y} - \frac{v_0}{R} \right) \right] \\
& + B_{12} \left(\frac{\partial \psi_x}{\partial x} \right) + B_{22} \left(\frac{\partial \psi_y}{\partial y} \right) + B_{26} \left[\frac{\partial \psi_x}{\partial y} + \frac{\partial \psi_y}{\partial x} \right. \\
& \left. - C_0 \left(\frac{\partial v_0}{\partial x} - \frac{\partial u_0}{\partial y} \right) \right] \} \phi_i^{(2)} \frac{\partial \phi_j^{(3)}}{\partial y} \} dA
\end{aligned}$$

$$\left[(k_T)_{ij}^{24} \right] = \left[k_{ij}^{24} \right]_L + \left[k_{ij}^{24} \right]_{NL} \quad (D.9)$$

$$\left[(k_T)_{ij}^{25} \right] = \left[k_{ij}^{25} \right]_L + \left[k_{ij}^{25} \right]_{NL} \quad (D.10)$$

$$\left[(k_T)_{ij}^{31} \right] = \left[k_{ij}^{31} \right]_L + \left[k_{ij}^{31} \right]_{NL} \quad (D.11)$$

$$\begin{aligned}
\left[(k_T)_{ij}^{32} \right] &= \left[k_{ij}^{32} \right]_L + \left[k_{ij}^{32} \right]_{NL} \\
& + \int_{\Omega} \left\{ -\frac{1}{2R^2} \left[A_{26} \left(\frac{\partial w_0}{\partial x} \right) + A_{22} \left(\frac{\partial w_0}{\partial y} - \frac{v_0}{R} \right) \right] \phi_i^{(3)} \phi_j^{(2)} \right. \\
& - \frac{1}{R} \left\{ A_{16} \left[\frac{\partial u_0}{\partial x} + \left(\frac{\partial w_0}{\partial x} \right)^2 \right] + A_{26} \left[\frac{\partial v_0}{\partial y} + \frac{w_0}{R} + \left(\frac{\partial w_0}{\partial y} - \frac{v_0}{R} \right)^2 \right] \right. \\
& + A_{66} \left[\frac{\partial u_0}{\partial y} + \frac{\partial v_0}{\partial x} + \left(\frac{\partial w_0}{\partial x} \right) \left(\frac{\partial w_0}{\partial y} - \frac{v_0}{R} \right) \right] \\
& + \left(\frac{A_{12} + A_{66}}{2} \right) \left(\frac{\partial w_0}{\partial x} \right) \left(\frac{\partial w_0}{\partial y} - \frac{v_0}{R} \right) \\
& + B_{16} \left(\frac{\partial \psi_x}{\partial x} \right) + B_{26} \left(\frac{\partial \psi_y}{\partial y} \right) + B_{66} \left[\frac{\partial \psi_x}{\partial y} + \frac{\partial \psi_y}{\partial x} \right. \\
& \left. - C_0 \left(\frac{\partial v_0}{\partial x} - \frac{\partial u_0}{\partial y} \right) \right] \} \frac{\partial \phi_i^{(3)}}{\partial x} \phi_j^{(2)} \\
& - \frac{1}{R} \left\{ A_{12} \left[\frac{\partial u_0}{\partial x} + \frac{1}{2} \left(\frac{\partial w_0}{\partial x} \right)^2 \right] + \frac{A_{66}}{2} \left(\frac{\partial w_0}{\partial x} \right)^2 \right. \\
& \left. + A_{22} \left[\frac{\partial v_0}{\partial y} + \frac{w_0}{R} + \left(\frac{\partial w_0}{\partial y} - \frac{v_0}{R} \right)^2 \right] \right\}
\end{aligned} \quad (D.12)$$

$$\begin{aligned}
& + A_{26} \left[\frac{\partial u_0}{\partial y} + \frac{\partial v_0}{\partial x} + 2 \left(\frac{\partial w_0}{\partial x} \right) \left(\frac{\partial w_0}{\partial y} - \frac{v_0}{R} \right) \right] \\
& + B_{12} \left(\frac{\partial \psi_x}{\partial x} \right) + B_{22} \left(\frac{\partial \psi_y}{\partial y} \right) + B_{26} \left[\frac{\partial \psi_x}{\partial y} + \frac{\partial \psi_y}{\partial x} \right. \\
& \left. - C_0 \left(\frac{\partial v_0}{\partial x} - \frac{\partial u_0}{\partial y} \right) \right] \} \frac{\partial \phi_i^{(3)}}{\partial y} \phi_j^{(2)} \} dA
\end{aligned}$$

$$\left[(k_T)_{ij}^{33} \right] = \left[k_{ij}^{33} \right]_L + \left[k_{ij}^{33} \right]_{NL}$$

$$\begin{aligned}
& + \int_{\Omega} \left\{ \frac{1}{R} \left[A_{26} \left(\frac{\partial w_0}{\partial x} \right) + A_{22} \left(\frac{\partial w_0}{\partial y} - \frac{v_0}{R} \right) \right] \left(\frac{1}{2} \phi_i^{(3)} \frac{\partial \phi_j^{(3)}}{\partial y} \right) \right. \\
& + \frac{1}{R} \left[A_{26} \left(\frac{\partial w_0}{\partial y} - \frac{v_0}{R} \right) + A_{12} \left(\frac{\partial w_0}{\partial x} \right) \right] \left(\frac{1}{2} \phi_i^{(3)} \frac{\partial \phi_j^{(3)}}{\partial x} \right) \\
& + \left\{ A_{11} \left[\frac{\partial u_0}{\partial x} + \left(\frac{\partial w_0}{\partial x} \right)^2 \right] + \frac{A_{66}}{2} \left(\frac{\partial w_0}{\partial y} - \frac{v_0}{R} \right)^2 \right. \\
& + A_{12} \left[\frac{\partial v_0}{\partial y} + \frac{w_0}{R} + \frac{1}{2} \left(\frac{\partial w_0}{\partial y} - \frac{v_0}{R} \right)^2 \right] \\
& + A_{16} \left[\frac{\partial u_0}{\partial y} + \frac{\partial v_0}{\partial x} + 2 \left(\frac{\partial w_0}{\partial x} \right) \left(\frac{\partial w_0}{\partial y} - \frac{v_0}{R} \right) \right] \\
& + B_{11} \left(\frac{\partial \psi_x}{\partial x} \right) + B_{12} \left(\frac{\partial \psi_y}{\partial y} \right) + B_{16} \left[\frac{\partial \psi_x}{\partial y} + \frac{\partial \psi_y}{\partial x} \right. \\
& \left. - C_0 \left(\frac{\partial v_0}{\partial x} - \frac{\partial u_0}{\partial y} \right) \right] \} \frac{\partial \phi_i^{(3)}}{\partial x} \frac{\partial \phi_j^{(3)}}{\partial x} \\
& + \left\{ A_{12} \left[\frac{\partial u_0}{\partial x} + \frac{1}{2} \left(\frac{\partial w_0}{\partial x} \right)^2 \right] + \frac{A_{66}}{2} \left(\frac{\partial w_0}{\partial x} \right)^2 \right. \\
& + A_{22} \left[\frac{\partial v_0}{\partial y} + \frac{w_0}{R} + \left(\frac{\partial w_0}{\partial y} - \frac{v_0}{R} \right)^2 \right] \\
& + A_{26} \left[\frac{\partial u_0}{\partial y} + \frac{\partial v_0}{\partial x} + 2 \left(\frac{\partial w_0}{\partial x} \right) \left(\frac{\partial w_0}{\partial y} - \frac{v_0}{R} \right) \right] \\
& + B_{12} \left(\frac{\partial \psi_x}{\partial x} \right) + B_{22} \left(\frac{\partial \psi_y}{\partial y} \right) + B_{26} \left[\frac{\partial \psi_x}{\partial y} + \frac{\partial \psi_y}{\partial x} \right. \\
& \left. - C_0 \left(\frac{\partial v_0}{\partial x} - \frac{\partial u_0}{\partial y} \right) \right] \} \frac{\partial \phi_i^{(3)}}{\partial y} \frac{\partial \phi_j^{(3)}}{\partial y}
\end{aligned}$$

(D.13)

$$\begin{aligned}
& + \{ A_{16} \left[\frac{\partial u_0}{\partial x} + \left(\frac{\partial w_0}{\partial x} \right)^2 \right] + A_{26} \left[\frac{\partial v_0}{\partial y} + \frac{w_0}{R} + \left(\frac{\partial w_0}{\partial y} - \frac{v_0}{R} \right)^2 \right] \right. \\
& + A_{66} \left[\frac{\partial u_0}{\partial y} + \frac{\partial v_0}{\partial x} + \left(\frac{\partial w_0}{\partial x} \right) \left(\frac{\partial w_0}{\partial y} - \frac{v_0}{R} \right) \right] \\
& + \left(\frac{A_{12} + A_{66}}{2} \right) \left(\frac{\partial w_0}{\partial x} \right) \left(\frac{\partial w_0}{\partial y} - \frac{v_0}{R} \right) \\
& + B_{16} \left(\frac{\partial \psi_x}{\partial x} \right) + B_{26} \left(\frac{\partial \psi_y}{\partial y} \right) + B_{66} \left[\frac{\partial \psi_x}{\partial y} + \frac{\partial \psi_y}{\partial x} \right. \\
& \left. - C_0 \left(\frac{\partial v_0}{\partial x} - \frac{\partial u_0}{\partial y} \right) \right] \left. \left(\frac{\partial \phi_i^{(3)}}{\partial x} \frac{\partial \phi_j^{(3)}}{\partial y} + \frac{\partial \phi_i^{(3)}}{\partial y} \frac{\partial \phi_j^{(3)}}{\partial x} \right) \right\} dA
\end{aligned}$$

$$[(k_T)_{ij}^{34}] = [k_{ij}^{34}]_L + [k_{ij}^{34}]_{NL} \quad (D.14)$$

$$[(k_T)_{ij}^{35}] = [k_{ij}^{35}]_L + [k_{ij}^{35}]_{NL} \quad (D.15)$$

$$[(k_T)_{ij}^{41}] = [k_{ij}^{41}]_L + [k_{ij}^{41}]_{NL} \quad (D.16)$$

$$[(k_T)_{ij}^{42}] = [k_{ij}^{42}]_L + 2 [k_{ij}^{42}]_{NL} \quad (D.17)$$

$$[(k_T)_{ij}^{43}] = [k_{ij}^{43}]_L + 2 [k_{ij}^{43}]_{NL} \quad (D.18)$$

$$[(k_T)_{ij}^{44}] = [k_{ij}^{44}]_L + [k_{ij}^{44}]_{NL} \quad (D.19)$$

$$[(k_T)_{ij}^{45}] = [k_{ij}^{45}]_L + [k_{ij}^{45}]_{NL} \quad (D.20)$$

$$[(k_T)_{ij}^{51}] = [k_{ij}^{51}]_L + [k_{ij}^{51}]_{NL} \quad (D.21)$$

$$[(k_T)_{ij}^{52}] = [k_{ij}^{52}]_L + 2 [k_{ij}^{52}]_{NL} \quad (D.22)$$

$$\left[(k_T)_{ij}^{53} \right] = \left[k_{ij}^{53} \right]_L + 2 \left[k_{ij}^{53} \right]_{NL} \quad (\text{D.23})$$

$$\left[(k_T)_{ij}^{54} \right] = \left[k_{ij}^{54} \right]_L + \left[k_{ij}^{54} \right]_{NL} \quad (\text{D.24})$$

$$\left[(k_T)_{ij}^{55} \right] = \left[k_{ij}^{55} \right]_L + \left[k_{ij}^{55} \right]_{NL} \quad (\text{D.25})$$

APPENDIX E

COEFFICIENTS OF ELEMENT STIFFNESS MATRIX FOR AN

INITIALLY IMPERFECT RING ELEMENT

The additional components of the element stiffness matrix for a ring type of element involving the initial imperfection function $\bar{w}_0(y)$ are expressed as below.

$$\begin{aligned} \left[k_{ij}^{14} \right]_{\text{Imperfect}} &= \int_{y_A}^{y_B} b \left\{ A_{22} \left(\frac{dw_0}{dy} - \frac{v_0}{R} \right) \frac{d\phi_i^{(1)}}{dy} \frac{d\phi_j^{(4)}}{dy} \right. \\ &\quad - \left[\frac{A_{22}}{R} \left(\frac{dv_0}{dy} + \frac{w_0}{R} + \frac{3}{2} \left(\frac{dw_0}{dy} - \frac{v_0}{R} \right)^2 + \left(\frac{dw_0}{dy} - \frac{v_0}{R} \right) \left(\frac{d\bar{w}_0}{dy} \right) \right) \right. \\ &\quad \left. \left. + \frac{B_{22}}{R} \left(\frac{d\psi_y}{dy} \right) \right] \phi_i^{(1)} \frac{d\phi_j^{(4)}}{dy} \right\} dy \end{aligned} \quad (\text{E.1})$$

$$\begin{aligned} \left[k_{ij}^{24} \right]_{\text{Imperfect}} &= \int_{y_A}^{y_B} b \left\{ \frac{A_{22}}{R} \left(\frac{dw_0}{dy} - \frac{v_0}{R} \right) \phi_i^{(2)} \frac{d\phi_j^{(4)}}{dy} \right. \\ &\quad + \left[A_{22} \left(\frac{dv_0}{dy} + \frac{w_0}{R} + \frac{3}{2} \left(\frac{dw_0}{dy} - \frac{v_0}{R} \right)^2 + \left(\frac{dw_0}{dy} - \frac{v_0}{R} \right) \left(\frac{d\bar{w}_0}{dy} \right) \right) \right. \\ &\quad \left. \left. + B_{22} \left(\frac{d\psi_y}{dy} \right) \right] \frac{d\phi_i^{(2)}}{dy} \frac{d\phi_j^{(4)}}{dy} \right\} dy \end{aligned} \quad (\text{E.2})$$

$$\left[k_{ij}^{34} \right]_{\text{Imperfect}} = \int_{y_A}^{y_B} b \left\{ B_{22} \left(\frac{dw_0}{dy} - \frac{v_0}{R} \right) \frac{d\phi_i^{(3)}}{dy} \frac{d\phi_j^{(4)}}{dy} \right\} dy \quad (\text{E.3})$$

$$\left[k_{ij}^{41} \right]_{\text{Imperfect}} = \left[k_{ij}^{42} \right]_{\text{Imperfect}} = \left[k_{ij}^{43} \right]_{\text{Imperfect}} = \left[k_{ij}^{44} \right]_{\text{Imperfect}} = \left\{ f^4 \right\} = 0 \quad (\text{E.4})$$

APPENDIX F
COEFFICIENTS OF ELEMENT TANGENT STIFFNESS MATRIX
FOR A NONLINEAR RING ELEMENT WITH INITIAL
IMPERFECTIONS

The components of the tangent stiffness matrix for a nonlinear ring element containing prescribed initial imperfections are given below.

$$\begin{aligned} \left[(k_T)_{ij}^{11} \right]_{\text{imperfect}} &= \left[(k_T)_{ij}^{11} \right]_{\text{perfect}} \\ &+ \int_{y_A}^{y_B} \mathbf{b} \left\{ -\frac{A_{22}}{R} \left(\frac{d\bar{w}_0}{dy} \right) \left(\frac{d\phi_i^{(1)}}{dy} \phi_j^{(1)} + \phi_i^{(1)} \frac{d\phi_j^{(1)}}{dy} \right) \right. \\ &+ \left. \frac{A_{22}}{R^2} \left(\frac{d\bar{w}_0}{dy} \right) \left[\frac{d\bar{w}_0}{dy} + 3 \left(\frac{dw_0}{dy} - \frac{v_0}{R} \right) \right] \phi_i^{(1)} \phi_j^{(1)} \right\} dy \end{aligned} \quad (\text{F.1})$$

where the components of $\left[(k_T)_{ij}^{11} \right]_{\text{perfect}}$ were shown in equation (B.1).

$$\begin{aligned} \left[(k_T)_{ij}^{12} \right]_{\text{imperfect}} &= \left[(k_T)_{ij}^{12} \right]_{\text{perfect}} \\ &+ \int_{y_A}^{y_B} \mathbf{b} \left\{ A_{22} \left(\frac{d\bar{w}_0}{dy} \right) \frac{d\phi_i^{(1)}}{dy} \frac{d\phi_j^{(2)}}{dy} - \frac{A_{22}}{R^2} \left(\frac{d\bar{w}_0}{dy} \right) \phi_i^{(1)} \phi_j^{(2)} \right. \\ &- \left. \frac{A_{22}}{R} \left(\frac{d\bar{w}_0}{dy} \right) \left[\frac{d\bar{w}_0}{dy} + 3 \left(\frac{dw_0}{dy} - \frac{v_0}{R} \right) \right] \phi_i^{(1)} \frac{d\phi_j^{(2)}}{dy} \right\} dy \end{aligned} \quad (\text{F.2})$$

where the components of $\left[(k_T)_{ij}^{12} \right]_{\text{perfect}}$ were shown in equation (B.2).

$$\begin{aligned} \left[(k_T)_{ij}^{13} \right]_{\text{imperfect}} &= \left[(k_T)_{ij}^{13} \right]_{\text{perfect}} \\ &- \int_{y_A}^{y_B} \mathbf{b} \left\{ \frac{B_{22}}{R} \left(\frac{d\bar{w}_0}{dy} \right) \phi_i^{(1)} \frac{d\phi_j^{(3)}}{dy} \right\} dy \end{aligned} \quad (\text{F.3})$$

where the components of $\left[(k_T)_{ij}^{13} \right]_{\text{perfect}}$ were shown in equation (B.3).

$$\begin{aligned} \left[(k_T)_{ij}^{21} \right]_{\text{imperfect}} &= \left[(k_T)_{ij}^{21} \right]_{\text{perfect}} \\ &+ \int_{y_A}^{y_B} b \left\{ A_{22} \left(\frac{d\bar{w}_0}{dy} \right) \frac{d\phi_i^{(2)}}{dy} \frac{d\phi_j^{(1)}}{dy} - \frac{A_{22}}{R^2} \left(\frac{d\bar{w}_0}{dy} \right) \phi_i^{(2)} \phi_j^{(1)} \right. \\ &\left. - \frac{A_{22}}{R} \left(\frac{d\bar{w}_0}{dy} \right) \left[\frac{d\bar{w}_0}{dy} + 3 \left(\frac{dw_0}{dy} - \frac{v_0}{R} \right) \right] \frac{d\phi_i^{(2)}}{dy} \phi_j^{(1)} \right\} dy \end{aligned} \quad (\text{F.4})$$

where the components of $\left[(k_T)_{ij}^{21} \right]_{\text{perfect}}$ were shown in equation (B.4).

$$\begin{aligned} \left[(k_T)_{ij}^{22} \right]_{\text{imperfect}} &= \left[(k_T)_{ij}^{22} \right]_{\text{perfect}} \\ &+ \int_{y_A}^{y_B} b \left\{ \frac{A_{22}}{R} \left(\frac{d\bar{w}_0}{dy} \right) \left[\phi_i^{(2)} \frac{d\phi_j^{(2)}}{dy} + \frac{d\phi_i^{(2)}}{dy} \phi_j^{(2)} \right] \right. \\ &\left. + A_{22} \left(\frac{d\bar{w}_0}{dy} \right) \left(\frac{d\bar{w}_0}{dy} + 3 \left(\frac{dw_0}{dy} - \frac{v_0}{R} \right) \right) \frac{d\phi_i^{(2)}}{dy} \frac{d\phi_j^{(2)}}{dy} \right\} dy \end{aligned} \quad (\text{F.5})$$

where the components of $\left[(k_T)_{ij}^{22} \right]_{\text{perfect}}$ were shown in equation (B.5).

$$\begin{aligned} \left[(k_T)_{ij}^{23} \right]_{\text{imperfect}} &= \left[(k_T)_{ij}^{23} \right]_{\text{perfect}} \\ &+ \int_{y_A}^{y_B} b \left\{ B_{22} \left(\frac{d\bar{w}_0}{dy} \right) \frac{d\phi_i^{(2)}}{dy} \frac{d\phi_j^{(3)}}{dy} \right\} dy \end{aligned} \quad (\text{F.6})$$

where the components of $\left[(k_T)_{ij}^{23} \right]_{\text{perfect}}$ were shown in equation (B.6).

$$\begin{aligned} \left[(k_T)_{ij}^{31} \right]_{\text{imperfect}} &= \left[(k_T)_{ij}^{31} \right]_{\text{perfect}} \\ &- \int_{y_A}^{y_B} b \left\{ \frac{B_{22}}{R} \left(\frac{d\bar{w}_0}{dy} \right) \frac{d\phi_i^{(3)}}{dy} \phi_j^{(1)} \right\} dy \end{aligned} \quad (\text{F.7})$$

where the components of $\left[(k_T)_{ij}^{31} \right]_{\text{perfect}}$ were shown in equation (B.7).

$$\begin{aligned} \left[(k_T)_{ij}^{32} \right]_{\text{imperfect}} &= \left[(k_T)_{ij}^{32} \right]_{\text{perfect}} \\ &+ \int_{y_A}^{y_B} \mathbf{b} \left\{ B_{22} \left(\frac{d\bar{w}_0}{dy} \right) \frac{d\phi_i^{(3)}}{dy} \frac{d\phi_j^{(2)}}{dy} \right\} dy \end{aligned} \quad (\text{F.8})$$

where the components of $\left[(k_T)_{ij}^{32} \right]_{\text{perfect}}$ were shown in equation (B.8).

$$\left[(k_T)_{ij}^{33} \right]_{\text{imperfect}} = \left[(k_T)_{ij}^{33} \right]_{\text{perfect}} \quad (\text{F.9})$$

where the components of $\left[(k_T)_{ij}^{33} \right]_{\text{perfect}}$ were shown in equation (B.9).

APPENDIX G

COEFFICIENTS OF ELEMENT STIFFNESS MATRIX FOR AN INITIALLY IMPERFECT, CYLINDRICAL SHELL ELEMENT

The additional components of the element stiffness matrix for a cylindrical shell type of element involving the initial imperfection function $\bar{w}_0(x, y)$ are expressed as below.

$$\begin{aligned}
 [k_{ij}^{16}]_{\text{Imperfect}} = \int_{\Omega} \{ & \left(\frac{\partial w_0}{\partial x} \right) \left[A_{11} \frac{\partial \phi_i^{(1)}}{\partial x} \frac{\partial \phi_j^{(6)}}{\partial x} + A_{16} \frac{\partial \phi_i^{(1)}}{\partial x} \frac{\partial \phi_j^{(6)}}{\partial y} \right. \\
 & + (A_{16} + C_0 B_{16}) \frac{\partial \phi_i^{(1)}}{\partial y} \frac{\partial \phi_j^{(6)}}{\partial x} + (A_{66} + C_0 B_{66}) \frac{\partial \phi_i^{(1)}}{\partial y} \frac{\partial \phi_j^{(6)}}{\partial y} \left. \right] \\
 & + \left(\frac{\partial w_0}{\partial y} - \frac{v_0}{R} \right) \left[A_{16} \frac{\partial \phi_i^{(1)}}{\partial x} \frac{\partial \phi_j^{(6)}}{\partial x} + A_{12} \frac{\partial \phi_i^{(1)}}{\partial x} \frac{\partial \phi_j^{(6)}}{\partial y} \right. \\
 & \left. + (A_{66} + C_0 B_{66}) \frac{\partial \phi_i^{(1)}}{\partial y} \frac{\partial \phi_j^{(6)}}{\partial x} + (A_{26} + C_0 B_{26}) \frac{\partial \phi_i^{(1)}}{\partial y} \frac{\partial \phi_j^{(6)}}{\partial y} \right] \} dA
 \end{aligned} \tag{G.1}$$

$$\begin{aligned}
 [k_{ij}^{26}]_{\text{Imperfect}} = \int_{\Omega} \{ & \left(\frac{\partial w_0}{\partial x} \right) \left[(A_{16} - C_0 B_{16}) \frac{\partial \phi_i^{(2)}}{\partial x} \frac{\partial \phi_j^{(6)}}{\partial x} \right. \\
 & + (A_{66} - C_0 B_{66}) \frac{\partial \phi_i^{(2)}}{\partial x} \frac{\partial \phi_j^{(6)}}{\partial y} + A_{12} \frac{\partial \phi_i^{(2)}}{\partial y} \frac{\partial \phi_j^{(6)}}{\partial x} + A_{26} \frac{\partial \phi_i^{(2)}}{\partial y} \frac{\partial \phi_j^{(6)}}{\partial y} \left. \right] \\
 & + \left(\frac{\partial w_0}{\partial y} - \frac{v_0}{R} \right) \left[(A_{66} - C_0 B_{66}) \frac{\partial \phi_i^{(2)}}{\partial x} \frac{\partial \phi_j^{(6)}}{\partial x} \right. \\
 & + (A_{26} - C_0 B_{26}) \frac{\partial \phi_i^{(2)}}{\partial x} \frac{\partial \phi_j^{(6)}}{\partial y} + A_{26} \frac{\partial \phi_i^{(2)}}{\partial y} \frac{\partial \phi_j^{(6)}}{\partial x} + A_{22} \frac{\partial \phi_i^{(2)}}{\partial y} \frac{\partial \phi_j^{(6)}}{\partial x} \left. \right] \\
 & - \frac{1}{R} \left\{ A_{16} \left[\frac{\partial u_0}{\partial x} + \frac{3}{2} \left(\frac{\partial w_0}{\partial x} \right)^2 + \left(\frac{\partial w_0}{\partial x} \right) \left(\frac{\partial \bar{w}_0}{\partial x} \right) \right] \right. \\
 & + A_{26} \left[\frac{\partial v_0}{\partial y} + \frac{w_0}{R} + \frac{3}{2} \left(\frac{\partial w_0}{\partial y} - \frac{v_0}{R} \right)^2 + \left(\frac{\partial w_0}{\partial y} - \frac{v_0}{R} \right) \left(\frac{\partial \bar{w}_0}{\partial y} \right) \right] \\
 & \left. + A_{26} \left[\frac{\partial u_0}{\partial y} + \frac{\partial v_0}{\partial x} + 2 \left(\frac{\partial w_0}{\partial x} \right) \left(\frac{\partial w_0}{\partial y} - \frac{v_0}{R} \right) + \left(\frac{\partial w_0}{\partial x} \right) \left(\frac{\partial \bar{w}_0}{\partial y} \right) \right] \right\} dA
 \end{aligned} \tag{G.2}$$

$$\begin{aligned}
& + \left(\frac{\partial w_0}{\partial y} - \frac{v_0}{R} \right) \left(\frac{\partial \bar{w}_0}{\partial x} \right)] + A_{12} \left(\frac{\partial w_0}{\partial x} \right) \left(\frac{\partial w_0}{\partial y} - \frac{v_0}{R} \right) \\
& + B_{16} \left(\frac{\partial \psi_x}{\partial x} \right) + B_{26} \left(\frac{\partial \psi_y}{\partial y} \right) + B_{66} \left[\frac{\partial \psi_x}{\partial y} + \frac{\partial \psi_y}{\partial x} - C_0 \left(\frac{\partial v_0}{\partial x} - \frac{\partial u_0}{\partial y} \right) \right] \} \phi_i^{(2)} \frac{\partial \phi_j^{(6)}}{\partial x} \\
& - \frac{1}{R} \left\{ A_{12} \left[\frac{\partial u_0}{\partial x} + \frac{1}{2} \left(\frac{\partial w_0}{\partial x} \right)^2 + \left(\frac{\partial w_0}{\partial x} \right) \left(\frac{\partial \bar{w}_0}{\partial x} \right) \right] + A_{66} \left(\frac{\partial w_0}{\partial x} \right)^2 \right. \\
& + A_{22} \left[\frac{\partial v_0}{\partial y} + \frac{w_0}{R} + \frac{3}{2} \left(\frac{\partial w_0}{\partial y} - \frac{v_0}{R} \right)^2 + \left(\frac{\partial w_0}{\partial y} - \frac{v_0}{R} \right) \left(\frac{\partial \bar{w}_0}{\partial y} \right) \right] \\
& + A_{26} \left[\frac{\partial u_0}{\partial y} + \frac{\partial v_0}{\partial x} + 3 \left(\frac{\partial w_0}{\partial x} \right) \left(\frac{\partial w_0}{\partial y} - \frac{v_0}{R} \right) + \left(\frac{\partial w_0}{\partial x} \right) \left(\frac{\partial \bar{w}_0}{\partial y} \right) \right. \\
& \left. + \left(\frac{\partial w_0}{\partial y} - \frac{v_0}{R} \right) \left(\frac{\partial \bar{w}_0}{\partial x} \right) \right] \\
& \left. + B_{12} \left(\frac{\partial \psi_x}{\partial x} \right) + B_{22} \left(\frac{\partial \psi_y}{\partial y} \right) + B_{26} \left[\frac{\partial \psi_x}{\partial y} + \frac{\partial \psi_y}{\partial x} - C_0 \left(\frac{\partial v_0}{\partial x} - \frac{\partial u_0}{\partial y} \right) \right] \right\} \\
& \phi_i^{(2)} \frac{\partial \phi_j^{(6)}}{\partial y} \} dA \tag{G.2}
\end{aligned}$$

$$\begin{aligned}
\left[k_{ij}^{36} \right]_{\text{Imperfect}} & = \int_{\Omega} \left\{ \left(A_{11} \left[\frac{\partial u_0}{\partial x} + \frac{3}{2} \left(\frac{\partial w_0}{\partial x} \right)^2 + \left(\frac{\partial w_0}{\partial x} \right) \left(\frac{\partial \bar{w}_0}{\partial x} \right) \right] \right. \right. \\
& + A_{12} \left[\frac{\partial v_0}{\partial y} + \frac{w_0}{R} + \frac{1}{2} \left(\frac{\partial w_0}{\partial y} - \frac{v_0}{R} \right)^2 + \left(\frac{\partial w_0}{\partial y} - \frac{v_0}{R} \right) \left(\frac{\partial \bar{w}_0}{\partial y} \right) \right] \\
& + A_{16} \left[\frac{\partial u_0}{\partial y} + \frac{\partial v_0}{\partial x} + 3 \left(\frac{\partial w_0}{\partial x} \right) \left(\frac{\partial w_0}{\partial y} - \frac{v_0}{R} \right) + \left(\frac{\partial w_0}{\partial x} \right) \left(\frac{\partial \bar{w}_0}{\partial y} \right) \right. \\
& \left. + \left(\frac{\partial w_0}{\partial y} - \frac{v_0}{R} \right) \left(\frac{\partial \bar{w}_0}{\partial x} \right) \right] + A_{66} \left(\frac{\partial w_0}{\partial y} - \frac{v_0}{R} \right)^2 \\
& \left. + B_{11} \left(\frac{\partial \psi_x}{\partial x} \right) + B_{12} \left(\frac{\partial \psi_y}{\partial y} \right) + B_{16} \left[\frac{\partial \psi_x}{\partial y} + \frac{\partial \psi_y}{\partial x} - C_0 \left(\frac{\partial v_0}{\partial x} - \frac{\partial u_0}{\partial y} \right) \right] \right) \frac{\partial \phi_i^{(3)}}{\partial x} \frac{\partial \phi_j^{(6)}}{\partial x} \\
& + \left(A_{12} \left[\frac{\partial u_0}{\partial x} + \frac{1}{2} \left(\frac{\partial w_0}{\partial x} \right)^2 + \left(\frac{\partial w_0}{\partial x} \right) \left(\frac{\partial \bar{w}_0}{\partial x} \right) \right] + A_{66} \left(\frac{\partial w_0}{\partial x} \right)^2 \right. \\
& + A_{22} \left[\frac{\partial v_0}{\partial y} + \frac{w_0}{R} + \frac{3}{2} \left(\frac{\partial w_0}{\partial y} - \frac{v_0}{R} \right)^2 + \left(\frac{\partial w_0}{\partial y} - \frac{v_0}{R} \right) \left(\frac{\partial \bar{w}_0}{\partial y} \right) \right] \\
& \left. + A_{26} \left[\frac{\partial u_0}{\partial y} + \frac{\partial v_0}{\partial x} + 3 \left(\frac{\partial w_0}{\partial x} \right) \left(\frac{\partial w_0}{\partial y} - \frac{v_0}{R} \right) + \left(\frac{\partial w_0}{\partial x} \right) \left(\frac{\partial \bar{w}_0}{\partial y} \right) \right] \right) \frac{\partial \phi_i^{(3)}}{\partial x} \frac{\partial \phi_j^{(6)}}{\partial y} \} dA \tag{G.3}
\end{aligned}$$

$$\begin{aligned}
& + \left(\frac{\partial w_0}{\partial y} - \frac{v_0}{R} \right) \left(\frac{\partial \bar{w}_0}{\partial x} \right)] + B_{12} \left(\frac{\partial \psi_x}{\partial x} \right) + B_{22} \left(\frac{\partial \psi_y}{\partial y} \right) \\
& + B_{26} \left[\frac{\partial \psi_x}{\partial y} + \frac{\partial \psi_y}{\partial x} - C_0 \left(\frac{\partial v_0}{\partial x} - \frac{\partial u_0}{\partial y} \right) \right] \frac{\partial \phi_i^{(3)}}{\partial y} \frac{\partial \phi_j^{(6)}}{\partial y} \\
& + \left(A_{16} \left[\frac{\partial u_0}{\partial x} + \frac{3}{2} \left(\frac{\partial w_0}{\partial x} \right)^2 + \left(\frac{\partial w_0}{\partial x} \right) \left(\frac{\partial \bar{w}_0}{\partial x} \right) \right] \right. \\
& + A_{26} \left[\frac{\partial v_0}{\partial y} + \frac{w_0}{R} + \frac{3}{2} \left(\frac{\partial w_0}{\partial y} - \frac{v_0}{R} \right)^2 + \left(\frac{\partial w_0}{\partial y} - \frac{v_0}{R} \right) \left(\frac{\partial \bar{w}_0}{\partial y} \right) \right] \\
& + A_{66} \left[\frac{\partial u_0}{\partial y} + \frac{\partial v_0}{\partial x} + 2 \left(\frac{\partial w_0}{\partial x} \right) \left(\frac{\partial w_0}{\partial y} - \frac{v_0}{R} \right) + \left(\frac{\partial w_0}{\partial x} \right) \left(\frac{\partial \bar{w}_0}{\partial y} \right) \right. \\
& + \left. \left. \left(\frac{\partial w_0}{\partial y} - \frac{v_0}{R} \right) \left(\frac{\partial \bar{w}_0}{\partial x} \right) \right] + B_{12} \left(\frac{\partial \psi_x}{\partial x} \right) + B_{22} \left(\frac{\partial \psi_y}{\partial y} \right) \right. \\
& + B_{26} \left[\frac{\partial \psi_x}{\partial y} + \frac{\partial \psi_y}{\partial x} - C_0 \left(\frac{\partial v_0}{\partial x} - \frac{\partial u_0}{\partial y} \right) \right] + A_{12} \left(\frac{\partial w_0}{\partial x} \right) \left(\frac{\partial w_0}{\partial y} - \frac{v_0}{R} \right) \right) \\
& \quad \left(\frac{\partial \phi_i^{(3)}}{\partial x} \frac{\partial \phi_j^{(6)}}{\partial y} + \frac{\partial \phi_i^{(3)}}{\partial y} \frac{\partial \phi_j^{(6)}}{\partial x} \right) \\
& + \frac{1}{R} \left[A_{12} \left(\frac{\partial w_0}{\partial x} \right) + A_{26} \left(\frac{\partial w_0}{\partial y} - \frac{v_0}{R} \right) \right] \phi_i^{(3)} \frac{\partial \phi_j^{(6)}}{\partial x} \\
& + \frac{1}{R} \left[A_{26} \left(\frac{\partial w_0}{\partial x} \right) + A_{22} \left(\frac{\partial w_0}{\partial y} - \frac{v_0}{R} \right) \right] \phi_i^{(3)} \frac{\partial \phi_j^{(6)}}{\partial y} \} dA
\end{aligned} \tag{G.3}$$

$$\begin{aligned}
\left[k_{ij}^{46} \right]_{\text{Imperfect}} & = \int_{\Omega} \left\{ \left(\frac{\partial w_0}{\partial x} \right) \left[B_{11} \frac{\partial \phi_i^{(4)}}{\partial x} \frac{\partial \phi_j^{(6)}}{\partial x} + B_{16} \frac{\partial \phi_i^{(4)}}{\partial x} \frac{\partial \phi_j^{(6)}}{\partial y} \right. \right. \\
& + B_{16} \frac{\partial \phi_i^{(4)}}{\partial y} \frac{\partial \phi_j^{(6)}}{\partial x} + B_{66} \frac{\partial \phi_i^{(4)}}{\partial y} \frac{\partial \phi_j^{(6)}}{\partial y} \left. \right] \\
& + \left(\frac{\partial w_0}{\partial y} - \frac{v_0}{R} \right) \left[B_{16} \frac{\partial \phi_i^{(4)}}{\partial x} \frac{\partial \phi_j^{(6)}}{\partial x} + B_{12} \frac{\partial \phi_i^{(4)}}{\partial x} \frac{\partial \phi_j^{(6)}}{\partial y} \right. \\
& + B_{66} \frac{\partial \phi_i^{(4)}}{\partial y} \frac{\partial \phi_j^{(6)}}{\partial x} + B_{26} \frac{\partial \phi_i^{(4)}}{\partial y} \frac{\partial \phi_j^{(6)}}{\partial y} \left. \right] \} dA
\end{aligned} \tag{G.4}$$

$$\begin{aligned}
\left[\mathbf{k}_{ij}^{56} \right]_{\text{Imperfect}} &= \int_{\Omega} \left\{ \left(\frac{\partial w_0}{\partial x} \right) \left[B_{16} \frac{\partial \phi_i^{(5)}}{\partial x} \frac{\partial \phi_j^{(6)}}{\partial x} + B_{66} \frac{\partial \phi_i^{(5)}}{\partial x} \frac{\partial \phi_j^{(6)}}{\partial y} \right. \right. \\
&\quad + B_{12} \frac{\partial \phi_i^{(5)}}{\partial y} \frac{\partial \phi_j^{(6)}}{\partial x} + B_{26} \frac{\partial \phi_i^{(5)}}{\partial y} \frac{\partial \phi_j^{(6)}}{\partial y} \left. \right] \\
&\quad + \left(\frac{\partial w_0}{\partial y} - \frac{v_0}{R} \right) \left[B_{66} \frac{\partial \phi_i^{(5)}}{\partial x} \frac{\partial \phi_j^{(6)}}{\partial x} + B_{26} \frac{\partial \phi_i^{(5)}}{\partial x} \frac{\partial \phi_j^{(6)}}{\partial y} \right. \\
&\quad \left. \left. + B_{26} \frac{\partial \phi_i^{(5)}}{\partial y} \frac{\partial \phi_j^{(6)}}{\partial x} + B_{22} \frac{\partial \phi_i^{(5)}}{\partial y} \frac{\partial \phi_j^{(6)}}{\partial y} \right] \right\} dA
\end{aligned} \tag{G.5}$$

$$\begin{aligned}
&\left[\mathbf{k}_{ij}^{61} \right]_{\text{Imperfect}} \\
&= \left[\mathbf{k}_{ij}^{62} \right]_{\text{Imperfect}} \\
&= \left[\mathbf{k}_{ij}^{63} \right]_{\text{Imperfect}} \\
&= \left[\mathbf{k}_{ij}^{64} \right]_{\text{Imperfect}} \\
&= \left[\mathbf{k}_{ij}^{65} \right]_{\text{Imperfect}} \\
&= \left[\mathbf{k}_{ij}^{66} \right]_{\text{Imperfect}} \\
&= \left\{ \mathbf{f}^6 \right\} = 0
\end{aligned} \tag{G.6}$$

APPENDIX H

COEFFICIENTS OF ELEMENT TANGENT STIFFNESS MATRIX

FOR A NONLINEAR, CYLINDRICAL SHELL ELEMENT WITH

INITIAL IMPERFECTIONS

The components of the tangent stiffness matrix for a nonlinear cylindrical shell element containing prescribed initial imperfections are given below.

$$\left[(k_T)_{ij}^{11} \right]_{\text{Imperfect}} = \left[(k_T)_{ij}^{11} \right]_{\text{perfect}} \quad (\text{H.1})$$

where the components of $\left[(k_T)_{ij}^{11} \right]_{\text{perfect}}$ were shown in equation (D.1).

$$\begin{aligned} \left[(k_T)_{ij}^{12} \right]_{\text{Imperfect}} &= \left[(k_T)_{ij}^{12} \right]_{\text{perfect}} \\ &+ \int_{\Omega} -\frac{1}{R} \left\{ \left[A_{16} \left(\frac{\partial \bar{w}_0}{\partial x} \right) + A_{12} \left(\frac{\partial \bar{w}_0}{\partial y} \right) \right] \frac{\partial \phi_i^{(1)}}{\partial x} \phi_j^{(2)} \right. \\ &\left. + \left[(A_{66} + C_0 B_{66}) \left(\frac{\partial \bar{w}_0}{\partial x} \right) + (A_{26} + C_0 B_{26}) \left(\frac{\partial \bar{w}_0}{\partial y} \right) \right] \frac{\partial \phi_i^{(1)}}{\partial y} \phi_j^{(2)} \right\} dA \end{aligned} \quad (\text{H.2})$$

where the components of $\left[(k_T)_{ij}^{12} \right]_{\text{perfect}}$ were shown in equation (D.2).

$$\begin{aligned} \left[(k_T)_{ij}^{13} \right]_{\text{Imperfect}} &= \left[(k_T)_{ij}^{13} \right]_{\text{perfect}} \\ &+ \int_{\Omega} \left\{ \left(\frac{\partial \bar{w}_0}{\partial x} \right) \left[A_{11} \frac{\partial \phi_i^{(1)}}{\partial x} \frac{\partial \phi_j^{(3)}}{\partial x} + A_{16} \frac{\partial \phi_i^{(1)}}{\partial x} \frac{\partial \phi_j^{(3)}}{\partial y} \right. \right. \\ &\left. \left. + (A_{16} + C_0 B_{16}) \frac{\partial \phi_i^{(1)}}{\partial y} \frac{\partial \phi_j^{(3)}}{\partial x} + (A_{66} + C_0 B_{66}) \frac{\partial \phi_i^{(1)}}{\partial y} \frac{\partial \phi_j^{(3)}}{\partial y} \right] \right\} dA \end{aligned} \quad (\text{H.3})$$

$$\begin{aligned}
& + \left(\frac{\partial \bar{w}_0}{\partial y} \right) \left[A_{16} \frac{\partial \phi_i^{(1)}}{\partial x} \frac{\partial \phi_j^{(3)}}{\partial x} + A_{12} \frac{\partial \phi_i^{(1)}}{\partial x} \frac{\partial \phi_j^{(3)}}{\partial y} \right. \\
& \left. + (A_{66} + C_0 B_{66}) \frac{\partial \phi_i^{(1)}}{\partial y} \frac{\partial \phi_j^{(3)}}{\partial x} + (A_{26} + C_0 B_{26}) \frac{\partial \phi_i^{(1)}}{\partial y} \frac{\partial \phi_j^{(3)}}{\partial y} \right] \} dA
\end{aligned} \tag{H.3}$$

where the components of $\left[(k_T)_{ij}^{13} \right]_{\text{perfect}}$ were shown in equation (D.3).

$$\left[(k_T)_{ij}^{14} \right]_{\text{imperfect}} = \left[(k_T)_{ij}^{14} \right]_{\text{perfect}} \tag{H.4}$$

where the components of $\left[(k_T)_{ij}^{14} \right]_{\text{perfect}}$ were shown in equation (D.4).

$$\left[(k_T)_{ij}^{15} \right]_{\text{imperfect}} = \left[(k_T)_{ij}^{15} \right]_{\text{perfect}} \tag{H.5}$$

where the components of $\left[(k_T)_{ij}^{15} \right]_{\text{perfect}}$ were shown in equation (D.5).

$$\begin{aligned}
& \left[(k_T)_{ij}^{21} \right]_{\text{imperfect}} = \left[(k_T)_{ij}^{21} \right]_{\text{perfect}} \\
& + \int_{\Omega} -\frac{1}{R} \left\{ \left[A_{16} \left(\frac{\partial \bar{w}_0}{\partial x} \right) + A_{12} \left(\frac{\partial \bar{w}_0}{\partial y} \right) \right] \phi_i^{(2)} \frac{\partial \phi_j^{(1)}}{\partial x} \right. \\
& \left. + \left[(A_{66} + C_0 B_{66}) \left(\frac{\partial \bar{w}_0}{\partial x} \right) + (A_{26} + C_0 B_{26}) \left(\frac{\partial \bar{w}_0}{\partial y} \right) \right] \phi_i^{(2)} \frac{\partial \phi_j^{(1)}}{\partial y} \right\} dA
\end{aligned} \tag{H.6}$$

where the components of $\left[(k_T)_{ij}^{21} \right]_{\text{perfect}}$ were shown in equation (D.6).

$$\begin{aligned}
& \left[(k_T)_{ij}^{22} \right]_{\text{imperfect}} = \left[(k_T)_{ij}^{22} \right]_{\text{perfect}} \\
& + \int_{\Omega} \left\{ -\frac{1}{R} \left[(A_{66} - C_0 B_{66}) \left(\frac{\partial \bar{w}_0}{\partial x} \right) + (A_{26} - C_0 B_{26}) \left(\frac{\partial \bar{w}_0}{\partial y} \right) \right] \right.
\end{aligned} \tag{H.7}$$

$$\begin{aligned}
& \left(\frac{\partial \phi_i^{(2)}}{\partial x} \phi_j^{(2)} + \phi_i^{(2)} \frac{\partial \phi_j^{(2)}}{\partial x} \right) \\
& - \frac{1}{R} \left[A_{26} \left(\frac{\partial \bar{w}_0}{\partial x} \right) + A_{22} \left(\frac{\partial \bar{w}_0}{\partial y} \right) \right] \left(\frac{\partial \phi_i^{(2)}}{\partial y} \phi_j^{(2)} + \phi_i^{(2)} \frac{\partial \phi_j^{(2)}}{\partial y} \right) \\
& + \frac{1}{R^2} \left\{ \left(\frac{\partial \bar{w}_0}{\partial x} \right) \left[A_{66} \left[\left(\frac{\partial \bar{w}_0}{\partial x} \right) + (2A_{66} + A_{12}) \left(\frac{\partial w_0}{\partial x} \right) \right] \right. \right. \\
& + A_{26} \left[\left(\frac{\partial \bar{w}_0}{\partial y} \right) + 3 \left(\frac{\partial w_0}{\partial y} - \frac{v_0}{R} \right) \right] \\
& + \left. \left(\frac{\partial \bar{w}_0}{\partial y} \right) \left[A_{26} \left[\left(\frac{\partial \bar{w}_0}{\partial x} \right) + 3 \left(\frac{\partial w_0}{\partial x} \right) \right] \right. \right. \\
& + \left. \left. A_{22} \left[\left(\frac{\partial \bar{w}_0}{\partial y} \right) + 3 \left(\frac{\partial w_0}{\partial y} - \frac{v_0}{R} \right) \right] \right] \right\} \phi_i^{(2)} \phi_j^{(2)} \} dA
\end{aligned} \tag{H.7}$$

where the components of $\left[(k_T)_{ij}^{22} \right]_{\text{perfect}}$ were shown in equation (D.7).

$$\begin{aligned}
\left[(k_T)_{ij}^{23} \right]_{\text{imperfect}} &= \left[(k_T)_{ij}^{23} \right]_{\text{perfect}} \\
& + \int_{\Omega} \left\{ \left(\frac{\partial \bar{w}_0}{\partial x} \right) \left[(A_{16} - C_0 B_{16}) \frac{\partial \phi_i^{(2)}}{\partial x} \frac{\partial \phi_j^{(3)}}{\partial x} + (A_{66} - C_0 B_{66}) \frac{\partial \phi_i^{(2)}}{\partial x} \frac{\partial \phi_j^{(3)}}{\partial y} \right. \right. \\
& + A_{12} \frac{\partial \phi_i^{(2)}}{\partial y} \frac{\partial \phi_j^{(3)}}{\partial x} + A_{26} \frac{\partial \phi_i^{(2)}}{\partial y} \frac{\partial \phi_j^{(3)}}{\partial y} \\
& + \left. \left(\frac{\partial \bar{w}_0}{\partial y} \right) \left[(A_{66} - C_0 B_{66}) \frac{\partial \phi_i^{(2)}}{\partial x} \frac{\partial \phi_j^{(3)}}{\partial x} + (A_{26} - C_0 B_{26}) \frac{\partial \phi_i^{(2)}}{\partial x} \frac{\partial \phi_j^{(3)}}{\partial y} \right. \right. \\
& + A_{26} \frac{\partial \phi_i^{(2)}}{\partial y} \frac{\partial \phi_j^{(3)}}{\partial x} + A_{22} \frac{\partial \phi_i^{(2)}}{\partial y} \frac{\partial \phi_j^{(3)}}{\partial y} \\
& - \frac{1}{R} \left\{ \left(\frac{\partial \bar{w}_0}{\partial x} \right) \left[A_{16} \left[\left(\frac{\partial \bar{w}_0}{\partial x} \right) + 3 \left(\frac{\partial w_0}{\partial x} \right) \right] \right. \right. \\
& + \left. \left[A_{66} \left(\frac{\partial \bar{w}_0}{\partial y} \right) + (2A_{66} + A_{12}) \left(\frac{\partial w_0}{\partial y} - \frac{v_0}{R} \right) \right] \right\} \\
& + \left. \left(\frac{\partial \bar{w}_0}{\partial y} \right) \left[\left[A_{12} \left(\frac{\partial \bar{w}_0}{\partial x} \right) + (2A_{66} + A_{12}) \left(\frac{\partial w_0}{\partial x} \right) \right] \right. \right. \\
& + \left. \left. A_{26} \left[\left(\frac{\partial \bar{w}_0}{\partial y} \right) + 3 \left(\frac{\partial w_0}{\partial y} - \frac{v_0}{R} \right) \right] \right] \right\} \phi_i^{(2)} \frac{\partial \phi_j^{(3)}}{\partial x}
\end{aligned} \tag{H.8}$$

$$\begin{aligned}
& -\frac{1}{R} \left\{ \left(\frac{\partial \bar{w}_0}{\partial x} \right) \left[A_{66} \left(\frac{\partial \bar{w}_0}{\partial x} \right) + (2A_{66} + A_{12}) \left(\frac{\partial w_0}{\partial x} \right) \right] \right. \\
& + A_{26} \left[\left(\frac{\partial \bar{w}_0}{\partial y} \right) + 3 \left(\frac{\partial w_0}{\partial y} - \frac{v_0}{R} \right) \right] \\
& + \left(\frac{\partial \bar{w}_0}{\partial y} \right) \left[A_{26} \left[\left(\frac{\partial \bar{w}_0}{\partial x} \right) + 3 \left(\frac{\partial w_0}{\partial x} \right) \right] \right. \\
& \left. \left. + A_{22} \left[\left(\frac{\partial \bar{w}_0}{\partial y} \right) + 3 \left(\frac{\partial w_0}{\partial y} - \frac{v_0}{R} \right) \right] \right] \right\} \phi_i^{(2)} \frac{\partial \phi_j^{(3)}}{\partial y} \\
& - \frac{1}{R^2} \left[A_{26} \left(\frac{\partial \bar{w}_0}{\partial x} \right) + A_{22} \left(\frac{\partial \bar{w}_0}{\partial y} \right) \right] \phi_i^{(2)} \phi_j^{(3)} \} dA
\end{aligned} \tag{H.8}$$

where the components of $\left[(k_T)_{ij}^{23} \right]_{\text{perfect}}$ were shown in equation (D.8).

$$\begin{aligned}
\left[(k_T)_{ij}^{24} \right]_{\text{imperfect}} &= \left[(k_T)_{ij}^{24} \right]_{\text{perfect}} \\
& + \int_{\Omega} -\frac{1}{R} \left\{ \left[B_{16} \left(\frac{\partial \bar{w}_0}{\partial x} \right) + B_{12} \left(\frac{\partial \bar{w}_0}{\partial y} \right) \right] \phi_i^{(2)} \frac{\partial \phi_j^{(4)}}{\partial x} \right. \\
& \left. + \left[B_{66} \left(\frac{\partial \bar{w}_0}{\partial x} \right) + B_{26} \left(\frac{\partial \bar{w}_0}{\partial y} \right) \right] \phi_i^{(2)} \frac{\partial \phi_j^{(4)}}{\partial y} \right\} dA
\end{aligned} \tag{H.9}$$

where the components of $\left[(k_T)_{ij}^{24} \right]_{\text{perfect}}$ were shown in equation (D.9).

$$\begin{aligned}
\left[(k_T)_{ij}^{25} \right]_{\text{imperfect}} &= \left[(k_T)_{ij}^{25} \right]_{\text{perfect}} \\
& + \int_{\Omega} -\frac{1}{R} \left\{ \left[B_{66} \left(\frac{\partial \bar{w}_0}{\partial x} \right) + B_{26} \left(\frac{\partial \bar{w}_0}{\partial y} \right) \right] \phi_i^{(2)} \frac{\partial \phi_j^{(5)}}{\partial x} \right. \\
& \left. + \left[B_{26} \left(\frac{\partial \bar{w}_0}{\partial x} \right) + B_{22} \left(\frac{\partial \bar{w}_0}{\partial y} \right) \right] \phi_i^{(2)} \frac{\partial \phi_j^{(5)}}{\partial y} \right\} dA
\end{aligned} \tag{H.10}$$

where the components of $\left[(k_T)_{ij}^{25} \right]_{\text{perfect}}$ were shown in equation (D.10).

$$\begin{aligned}
\left[(k_T)_{ij}^{31} \right]_{\text{imperfect}} &= \left[(k_T)_{ij}^{31} \right]_{\text{perfect}} \\
&+ \int_{\Omega} \left\{ \left(\frac{\partial \bar{w}_0}{\partial x} \right) \left[A_{11} \frac{\partial \phi_i^{(3)}}{\partial x} \frac{\partial \phi_j^{(1)}}{\partial x} + A_{16} \frac{\partial \phi_i^{(3)}}{\partial y} \frac{\partial \phi_j^{(1)}}{\partial x} \right. \right. \\
&+ (A_{16} + C_0 B_{16}) \frac{\partial \phi_i^{(3)}}{\partial x} \frac{\partial \phi_j^{(1)}}{\partial y} + (A_{66} + C_0 B_{66}) \frac{\partial \phi_i^{(3)}}{\partial y} \frac{\partial \phi_j^{(1)}}{\partial y} \left. \right] \\
&+ \left(\frac{\partial \bar{w}_0}{\partial y} \right) \left[A_{16} \frac{\partial \phi_i^{(3)}}{\partial x} \frac{\partial \phi_j^{(1)}}{\partial x} + A_{12} \frac{\partial \phi_i^{(3)}}{\partial y} \frac{\partial \phi_j^{(1)}}{\partial x} \right. \\
&\left. \left. + (A_{66} + C_0 B_{66}) \frac{\partial \phi_i^{(3)}}{\partial y} \frac{\partial \phi_j^{(1)}}{\partial x} + (A_{26} + C_0 B_{26}) \frac{\partial \phi_i^{(3)}}{\partial y} \frac{\partial \phi_j^{(1)}}{\partial y} \right] \right\} dA
\end{aligned} \tag{H.11}$$

where the components of $\left[(k_T)_{ij}^{31} \right]_{\text{perfect}}$ were shown in equation (D.11).

$$\begin{aligned}
\left[(k_T)_{ij}^{32} \right]_{\text{imperfect}} &= \left[(k_T)_{ij}^{32} \right]_{\text{perfect}} \\
&+ \int_{\Omega} \left\{ \left(\frac{\partial \bar{w}_0}{\partial x} \right) \left[(A_{16} - C_0 B_{16}) \frac{\partial \phi_i^{(3)}}{\partial x} \frac{\partial \phi_j^{(2)}}{\partial x} + (A_{66} - C_0 B_{66}) \frac{\partial \phi_i^{(3)}}{\partial y} \frac{\partial \phi_j^{(2)}}{\partial x} \right. \right. \\
&+ A_{12} \frac{\partial \phi_i^{(3)}}{\partial x} \frac{\partial \phi_j^{(2)}}{\partial y} + A_{26} \frac{\partial \phi_i^{(3)}}{\partial y} \frac{\partial \phi_j^{(2)}}{\partial y} \left. \right] \\
&+ \left(\frac{\partial \bar{w}_0}{\partial y} \right) \left[(A_{66} - C_0 B_{66}) \frac{\partial \phi_i^{(3)}}{\partial x} \frac{\partial \phi_j^{(2)}}{\partial x} + (A_{26} - C_0 B_{26}) \frac{\partial \phi_i^{(3)}}{\partial y} \frac{\partial \phi_j^{(2)}}{\partial x} \right. \\
&+ A_{26} \frac{\partial \phi_i^{(3)}}{\partial x} \frac{\partial \phi_j^{(2)}}{\partial y} + A_{22} \frac{\partial \phi_i^{(3)}}{\partial y} \frac{\partial \phi_j^{(2)}}{\partial y} \left. \right] \\
&- \frac{1}{R} \left\{ \left(\frac{\partial \bar{w}_0}{\partial x} \right) \left[A_{16} \left[\left(\frac{\partial \bar{w}_0}{\partial x} \right) + 3 \left(\frac{\partial w_0}{\partial x} \right) \right] \right. \right. \\
&+ \left[A_{66} \left(\frac{\partial \bar{w}_0}{\partial y} \right) + (2A_{66} + A_{12}) \left(\frac{\partial w_0}{\partial y} - \frac{v_0}{R} \right) \right] \left. \right] \\
&+ \left(\frac{\partial \bar{w}_0}{\partial y} \right) \left[\left[A_{12} \left(\frac{\partial \bar{w}_0}{\partial x} \right) + (2A_{66} + A_{12}) \left(\frac{\partial w_0}{\partial x} \right) \right] \right. \\
&+ A_{26} \left[\left(\frac{\partial \bar{w}_0}{\partial y} \right) + 3 \left(\frac{\partial w_0}{\partial y} - \frac{v_0}{R} \right) \right] \left. \right] \left. \right\} \frac{\partial \phi_i^{(3)}}{\partial x} \phi_j^{(2)} \\
&- \frac{1}{R} \left\{ \left(\frac{\partial \bar{w}_0}{\partial x} \right) \left[A_{66} \left(\frac{\partial \bar{w}_0}{\partial x} \right) + (2A_{66} + A_{12}) \left(\frac{\partial w_0}{\partial x} \right) \right] \right.
\end{aligned} \tag{H.12}$$

$$\begin{aligned}
& + A_{26} \left[\left(\frac{\partial \bar{w}_0}{\partial y} \right) + 3 \left(\frac{\partial w_0}{\partial y} - \frac{v_0}{R} \right) \right] \\
& + \left(\frac{\partial \bar{w}_0}{\partial y} \right) \left[A_{26} \left[\left(\frac{\partial \bar{w}_0}{\partial x} \right) + 3 \left(\frac{\partial w_0}{\partial x} \right) \right] \right. \\
& \left. + A_{22} \left[\left(\frac{\partial \bar{w}_0}{\partial y} \right) + 3 \left(\frac{\partial w_0}{\partial y} - \frac{v_0}{R} \right) \right] \right] \frac{\partial \phi_i^{(3)}}{\partial y} \phi_j^{(2)} \\
& - \frac{1}{R^2} \left[A_{26} \left(\frac{\partial \bar{w}_0}{\partial x} \right) + A_{22} \left(\frac{\partial \bar{w}_0}{\partial y} \right) \right] \phi_i^{(3)} \phi_j^{(2)} \} dA
\end{aligned} \tag{H.12}$$

where the components of $\left[(k_T)_{ij}^{32} \right]_{\text{perfect}}$ were shown in equation (D.12).

$$\begin{aligned}
\left[(k_T)_{ij}^{33} \right]_{\text{Imperfect}} &= \left[(k_T)_{ij}^{33} \right]_{\text{perfect}} \\
& + \int_{\Omega} \left\{ \frac{1}{R} \left[A_{12} \left(\frac{\partial \bar{w}_0}{\partial x} \right) + A_{26} \left(\frac{\partial \bar{w}_0}{\partial y} \right) \right] \left(\frac{\partial \phi_i^{(3)}}{\partial x} \phi_j^{(3)} + \phi_i^{(3)} \frac{\partial \phi_j^{(3)}}{\partial x} \right) \right. \\
& + \frac{1}{R} \left[A_{26} \left(\frac{\partial \bar{w}_0}{\partial x} \right) + A_{22} \left(\frac{\partial \bar{w}_0}{\partial y} \right) \right] \left(\frac{\partial \phi_i^{(3)}}{\partial y} \phi_j^{(3)} + \phi_i^{(3)} \frac{\partial \phi_j^{(3)}}{\partial y} \right) \\
& + \left\{ \left(\frac{\partial \bar{w}_0}{\partial x} \right) \left[A_{11} \left[\left(\frac{\partial \bar{w}_0}{\partial x} \right) + 3 \left(\frac{\partial w_0}{\partial x} \right) \right] \right. \right. \\
& + A_{16} \left[\left(\frac{\partial \bar{w}_0}{\partial y} \right) + 3 \left(\frac{\partial w_0}{\partial y} - \frac{v_0}{R} \right) \right] \\
& + \left. \left. \left(\frac{\partial \bar{w}_0}{\partial y} \right) \left[A_{16} \left[\left(\frac{\partial \bar{w}_0}{\partial x} \right) + 3 \left(\frac{\partial w_0}{\partial x} \right) \right] \right. \right. \right. \\
& + \left. \left. \left. \left[A_{66} \left(\frac{\partial \bar{w}_0}{\partial y} \right) + (2A_{66} + A_{12}) \left(\frac{\partial w_0}{\partial y} - \frac{v_0}{R} \right) \right] \right] \right\} \frac{\partial \phi_i^{(3)}}{\partial x} \frac{\partial \phi_j^{(3)}}{\partial x} \\
& + \left\{ \left(\frac{\partial \bar{w}_0}{\partial x} \right) \left[A_{66} \left(\frac{\partial \bar{w}_0}{\partial x} \right) + (2A_{66} + A_{12}) \left(\frac{\partial w_0}{\partial x} \right) \right] \right. \\
& + A_{26} \left[\left(\frac{\partial \bar{w}_0}{\partial y} \right) + 3 \left(\frac{\partial w_0}{\partial y} - \frac{v_0}{R} \right) \right] \\
& + \left. \left. \left(\frac{\partial \bar{w}_0}{\partial y} \right) \left[A_{26} \left[\left(\frac{\partial \bar{w}_0}{\partial x} \right) + 3 \left(\frac{\partial w_0}{\partial x} \right) \right] \right. \right. \right. \\
& + \left. \left. \left. \left[A_{22} \left[\left(\frac{\partial \bar{w}_0}{\partial y} \right) + 3 \left(\frac{\partial w_0}{\partial y} - \frac{v_0}{R} \right) \right] \right] \right\} \frac{\partial \phi_i^{(3)}}{\partial y} \frac{\partial \phi_j^{(3)}}{\partial y}
\end{aligned} \tag{H.13}$$

$$\begin{aligned}
& + \left\{ \left(\frac{\partial \bar{w}_0}{\partial x} \right) \left[A_{16} \left[\left(\frac{\partial \bar{w}_0}{\partial x} \right) + 3 \left(\frac{\partial w_0}{\partial x} \right) \right] \right. \right. \\
& + \left. \left[A_{12} \left(\frac{\partial \bar{w}_0}{\partial y} \right) + (2A_{66} + A_{12}) \left(\frac{\partial w_0}{\partial y} - \frac{v_0}{R} \right) \right] \right\} \\
& + \left(\frac{\partial \bar{w}_0}{\partial y} \right) \left[\left[A_{66} \left(\frac{\partial \bar{w}_0}{\partial x} \right) + (2A_{66} + A_{12}) \left(\frac{\partial w_0}{\partial x} \right) \right] \right. \\
& \left. + A_{26} \left[\left(\frac{\partial \bar{w}_0}{\partial y} \right) + 3 \left(\frac{\partial w_0}{\partial y} - \frac{v_0}{R} \right) \right] \right] \left\{ \frac{\partial \phi_i^{(3)}}{\partial x} \frac{\partial \phi_j^{(3)}}{\partial y} + \frac{\partial \phi_i^{(3)}}{\partial y} \frac{\partial \phi_j^{(3)}}{\partial x} \right\} dA
\end{aligned} \tag{H.13}$$

where the components of $\left[(k_T)_{ij}^{33} \right]_{\text{perfect}}$ were shown in equation (D.13).

$$\begin{aligned}
\left[(k_T)_{ij}^{34} \right]_{\text{imperfect}} &= \left[(k_T)_{ij}^{34} \right]_{\text{perfect}} \\
& + \int_{\Omega} \left\{ \left(\frac{\partial \bar{w}_0}{\partial x} \right) \left[B_{11} \frac{\partial \phi_i^{(3)}}{\partial x} \frac{\partial \phi_j^{(4)}}{\partial x} + B_{16} \frac{\partial \phi_i^{(3)}}{\partial x} \frac{\partial \phi_j^{(4)}}{\partial y} \right. \right. \\
& + B_{16} \frac{\partial \phi_i^{(3)}}{\partial y} \frac{\partial \phi_j^{(4)}}{\partial x} + B_{66} \frac{\partial \phi_i^{(3)}}{\partial y} \frac{\partial \phi_j^{(4)}}{\partial y} \left. \right] \\
& + \left(\frac{\partial \bar{w}_0}{\partial y} \right) \left[B_{16} \frac{\partial \phi_i^{(3)}}{\partial x} \frac{\partial \phi_j^{(4)}}{\partial x} + B_{66} \frac{\partial \phi_i^{(3)}}{\partial x} \frac{\partial \phi_j^{(4)}}{\partial y} \right. \\
& \left. + B_{12} \frac{\partial \phi_i^{(3)}}{\partial y} \frac{\partial \phi_j^{(4)}}{\partial x} + B_{26} \frac{\partial \phi_i^{(3)}}{\partial y} \frac{\partial \phi_j^{(4)}}{\partial y} \right] \left. \right\} dA
\end{aligned} \tag{H.14}$$

where the components of $\left[(k_T)_{ij}^{34} \right]_{\text{perfect}}$ were shown in equation (D.14).

$$\begin{aligned}
\left[(k_T)_{ij}^{35} \right]_{\text{imperfect}} &= \left[(k_T)_{ij}^{35} \right]_{\text{perfect}} \\
& + \int_{\Omega} \left\{ \left(\frac{\partial \bar{w}_0}{\partial x} \right) \left[B_{16} \frac{\partial \phi_i^{(3)}}{\partial x} \frac{\partial \phi_j^{(5)}}{\partial x} + B_{12} \frac{\partial \phi_i^{(3)}}{\partial x} \frac{\partial \phi_j^{(5)}}{\partial y} \right. \right. \\
& + B_{66} \frac{\partial \phi_i^{(3)}}{\partial y} \frac{\partial \phi_j^{(5)}}{\partial x} + B_{26} \frac{\partial \phi_i^{(3)}}{\partial y} \frac{\partial \phi_j^{(5)}}{\partial y} \left. \right] \\
& + \left(\frac{\partial \bar{w}_0}{\partial y} \right) \left[B_{66} \frac{\partial \phi_i^{(3)}}{\partial x} \frac{\partial \phi_j^{(5)}}{\partial x} + B_{26} \frac{\partial \phi_i^{(3)}}{\partial x} \frac{\partial \phi_j^{(5)}}{\partial y} \right.
\end{aligned} \tag{H.15}$$

$$+ B_{26} \frac{\partial \phi_i^{(3)}}{\partial y} \frac{\partial \phi_j^{(5)}}{\partial x} + B_{22} \frac{\partial \phi_i^{(3)}}{\partial y} \frac{\partial \phi_j^{(5)}}{\partial y}] \} dA$$

where the components of $\left[(k_T)_{ij}^{35} \right]_{\text{perfect}}$ were shown in equation (D.15).

$$\left[(k_T)_{ij}^{41} \right]_{\text{imperfect}} = \left[(k_T)_{ij}^{41} \right]_{\text{perfect}} \quad (\text{H.16})$$

where the components of $\left[(k_T)_{ij}^{41} \right]_{\text{perfect}}$ were shown in equation (D.16).

$$\begin{aligned} \left[(k_T)_{ij}^{42} \right]_{\text{imperfect}} &= \left[(k_T)_{ij}^{42} \right]_{\text{perfect}} \\ &+ \int_{\Omega} -\frac{1}{R} \left\{ \left[B_{16} \left(\frac{\partial \bar{w}_0}{\partial x} \right) + B_{12} \left(\frac{\partial \bar{w}_0}{\partial y} \right) \right] \frac{\partial \phi_i^{(4)}}{\partial x} \phi_j^{(2)} \right. \\ &\left. + \left[B_{66} \left(\frac{\partial \bar{w}_0}{\partial x} \right) + B_{26} \left(\frac{\partial \bar{w}_0}{\partial y} \right) \right] \frac{\partial \phi_i^{(4)}}{\partial y} \phi_j^{(2)} \right\} dA \end{aligned} \quad (\text{H.17})$$

where the components of $\left[(k_T)_{ij}^{42} \right]_{\text{perfect}}$ were shown in equation (D.17).

$$\begin{aligned} \left[(k_T)_{ij}^{43} \right]_{\text{imperfect}} &= \left[(k_T)_{ij}^{43} \right]_{\text{perfect}} \\ &+ \int_{\Omega} \left\{ \left(\frac{\partial \bar{w}_0}{\partial x} \right) \left[B_{11} \frac{\partial \phi_i^{(4)}}{\partial x} \frac{\partial \phi_j^{(3)}}{\partial x} + B_{16} \frac{\partial \phi_i^{(4)}}{\partial x} \frac{\partial \phi_j^{(3)}}{\partial y} \right. \right. \\ &+ B_{16} \frac{\partial \phi_i^{(4)}}{\partial y} \frac{\partial \phi_j^{(3)}}{\partial x} + B_{66} \frac{\partial \phi_i^{(4)}}{\partial y} \frac{\partial \phi_j^{(3)}}{\partial y} \left. \right] \\ &+ \left(\frac{\partial \bar{w}_0}{\partial y} \right) \left[B_{16} \frac{\partial \phi_i^{(4)}}{\partial x} \frac{\partial \phi_j^{(3)}}{\partial x} + B_{66} \frac{\partial \phi_i^{(4)}}{\partial y} \frac{\partial \phi_j^{(3)}}{\partial x} \right. \\ &\left. \left. + B_{12} \frac{\partial \phi_i^{(4)}}{\partial x} \frac{\partial \phi_j^{(3)}}{\partial y} + B_{26} \frac{\partial \phi_i^{(4)}}{\partial y} \frac{\partial \phi_j^{(3)}}{\partial y} \right] \right\} dA \end{aligned} \quad (\text{H.18})$$

where the components of $\left[(k_T)_{ij}^{43} \right]_{\text{perfect}}$ were shown in equation (D.18).

$$\left[(k_T)_{ij}^{44} \right]_{\text{imperfect}} = \left[(k_T)_{ij}^{44} \right]_{\text{perfect}} \quad (\text{H.19})$$

where the components of $\left[(k_T)_{ij}^{44} \right]_{\text{perfect}}$ were shown in equation (D.19).

$$\left[(k_T)_{ij}^{45} \right]_{\text{imperfect}} = \left[(k_T)_{ij}^{45} \right]_{\text{perfect}} \quad (\text{H.20})$$

where the components of $\left[(k_T)_{ij}^{45} \right]_{\text{perfect}}$ were shown in equation (D.20).

$$\left[(k_T)_{ij}^{51} \right]_{\text{imperfect}} = \left[(k_T)_{ij}^{51} \right]_{\text{perfect}} \quad (\text{H.21})$$

where the components of $\left[(k_T)_{ij}^{51} \right]_{\text{perfect}}$ were shown in equation (D.21).

$$\begin{aligned} \left[(k_T)_{ij}^{52} \right]_{\text{imperfect}} &= \left[(k_T)_{ij}^{52} \right]_{\text{perfect}} \\ &+ \int_{\Omega} -\frac{1}{R} \left\{ \left[B_{66} \left(\frac{\partial \bar{w}_0}{\partial x} \right) + B_{26} \left(\frac{\partial \bar{w}_0}{\partial y} \right) \right] \frac{\partial \phi_i^{(5)}}{\partial x} \phi_j^{(2)} \right. \\ &\left. + \left[B_{26} \left(\frac{\partial \bar{w}_0}{\partial x} \right) + B_{22} \left(\frac{\partial \bar{w}_0}{\partial y} \right) \right] \frac{\partial \phi_i^{(5)}}{\partial y} \phi_j^{(2)} \right\} dA \end{aligned} \quad (\text{H.22})$$

where the components of $\left[(k_T)_{ij}^{52} \right]_{\text{perfect}}$ were shown in equation (D.22).

$$\begin{aligned} \left[(k_T)_{ij}^{53} \right]_{\text{imperfect}} &= \left[(k_T)_{ij}^{53} \right]_{\text{perfect}} \\ &+ \int_{\Omega} \left\{ \left(\frac{\partial \bar{w}_0}{\partial x} \right) \left[B_{16} \frac{\partial \phi_i^{(5)}}{\partial x} \frac{\partial \phi_j^{(3)}}{\partial x} + B_{12} \frac{\partial \phi_i^{(5)}}{\partial y} \frac{\partial \phi_j^{(3)}}{\partial x} \right. \right. \\ &\left. \left. + B_{66} \frac{\partial \phi_i^{(5)}}{\partial x} \frac{\partial \phi_j^{(3)}}{\partial y} + B_{26} \frac{\partial \phi_i^{(5)}}{\partial y} \frac{\partial \phi_j^{(3)}}{\partial y} \right] \right. \\ &\left. + \left(\frac{\partial \bar{w}_0}{\partial y} \right) \left[B_{66} \frac{\partial \phi_i^{(5)}}{\partial x} \frac{\partial \phi_j^{(3)}}{\partial x} + B_{26} \frac{\partial \phi_i^{(5)}}{\partial y} \frac{\partial \phi_j^{(3)}}{\partial x} \right] \right\} dA \end{aligned} \quad (\text{H.23})$$

$$+ B_{26} \frac{\partial \phi_i^{(5)}}{\partial x} \frac{\partial \phi_j^{(3)}}{\partial y} + B_{22} \frac{\partial \phi_i^{(5)}}{\partial y} \frac{\partial \phi_j^{(3)}}{\partial y}] \} dA$$

where the components of $\left[(k_T)_{ij}^{53} \right]_{\text{perfect}}$ were shown in equation (D.23).

$$\left[(k_T)_{ij}^{54} \right]_{\text{imperfect}} = \left[(k_T)_{ij}^{54} \right]_{\text{perfect}} \quad (\text{H.24})$$

where the components of $\left[(k_T)_{ij}^{54} \right]_{\text{perfect}}$ were shown in equation (D.24).

$$\left[(k_T)_{ij}^{55} \right]_{\text{imperfect}} = \left[(k_T)_{ij}^{55} \right]_{\text{perfect}} \quad (\text{H.25})$$

where the components of $\left[(k_T)_{ij}^{55} \right]_{\text{perfect}}$ were shown in equation (D.25).

VITA

Hung-Peng Li was born in Tachia Town, Taichung, Taiwan, Republic of China on February 10, 1963. After graduated from Taichung First High School in 1981, he began his undergraduate study at Chung-Yuan University later that same year. He obtained a degree of Bachelor of Science in Mechanical Engineering in June of 1985. After successfully serving in the Army for two years, he worked as a machine maintenance engineer in Chiu 9 Lun Machinery Company, Ltd. from June 1987 to July of 1988. In September of 1988, he entered the Mechanical Engineering Department at Auburn University as a graduate student, and successfully completed the requirements for a Mater of Science degree in August, 1991. After graduating from Auburn University, he was enrolled later in 1991 in the Department of Engineering Science and Mechanics at Virginia Polytechnic Institute and State University for pursuing a Ph.D. degree. He successfully fulfilled the requirements for a Ph.D. degree under the supervision of Professor Robert Heller in September of 1998.

Hung-Peng Li